The Use of 185 nm Radiation for Drinking Water Treatment

Influence of Major Solutes and Temperature on the Degradation of Trace Organic Contaminants

by

Laith Furatian

B.Sc., The University of Alberta, 1999
M.Sc., The University of New Hampshire, 2011

A THESIS SUBMITTED IN PARTIAL FULFILLMENT OF
THE REQUIREMENTS FOR THE DEGREE OF

DOCTOR OF PHILOSOPHY

in

The Faculty of Graduate and Postdoctoral Studies

(Chemical and Biological Engineering)

THE UNIVERSITY OF BRITISH COLUMBIA

(Vancouver)

June 2017

Abstract

The treatment of water via 185 nm radiation allows for the oxidative degradation of trace organic contaminants without the need for chemical addition. Critical information required for the practical application of such a process has been lacking. Carbamazepine was determined to be an ideal probe compound for study of the 185 nm regime due to negligible direct photolysis at 254 nm. An increase in probe degradation rate due to 185 nm is observed with increasing temperature when water is the only significant absorber of photons. A comparison with the temperature dependence of the 254 nm - H_2O_2 process is made and a fundamental explanation proposed. Experimental evidence reveals that probe degradation rate is strongly influenced by anionic composition at environmentally relevant concentrations, particularly chloride. Evidence for the role of the chlorine radical is obtained by kinetic studies involving select probes, radical scavengers, and ionic strength. Interactions between the major organic and inorganic solutes indicate that resulting degradation kinetics are highly sensitive to the composition of the water matrix, a fact that has been neglected from the literature. A method to quantify molar absorption coefficients is developed that is not prone to errors due to stray radiant energy or wavelength inaccuracies. A method to quantify the 185:254 nm output of a low pressure mercury lamp is presented with results in agreement with values reported in the literature. In addition to the hydroxyl radical ($^{\bullet}OH$), other radical species such as chlorine ($Cl^{\bullet}$) and sulphate ($SO_4^{\bullet -}$) are proposed to be involved in oxidative degradation of trace organics in the 185 nm regime. This suggests that the degradation rate of a given target contaminant depends on the composition of the water matrix, the second-order rate constants with the relevant radicals, and the relative reaction rate constants of the target and the matrix.

Lay Summary

Certain types of chemical impurities are difficult to remove from water. One method that may be useful in destroying certain chemicals is to split water molecules using ultraviolet radiation to produce an aggressive oxidant that will then attack impurities. However, this process is highly dependent on the types and amounts of naturally occurring substances also dissolved in water. A complex mixture of oxidants may be produced with potentially significant differences in their abilities to attack a given impurity. Thus, since the composition of water differs between places and over the seasons, the efficiency of this approach may differ substantially between locations and over time. An attempt to understand how the natural composition of water and its temperature influence the efficiency of this process were the goals of this research. This information could then be used to optimize the process and even determine under what conditions its use would be impractical.

Preface

This dissertation is original, unpublished, independent work by the author, Laith Furatian.

Table of Contents

List of Tables

List of Figures

Nomenclature

Symbols

α_i	Absorption coefficient of solute i	(cm^{-1})
$[C]_o$	Initial concentration of C	(M)
$[C]_t$	Concentration of C after elapsed time t	(M)
D	Absorbed photons per unit volume	($J\,m^{-3}$ or M)
ϵ_i	Molar absorption coefficient of solute i	($M^{-1}\,cm^{-1}$)
E	Activation energy	($kJ\,mol^{-1}$)
F	Fluence rate	($J\,m^{-2}$)
f_i	Fraction of photons absorbed by species i	
I_a	Photon absorption rate	($M\,s^{-1}$ or $J\,m^{-3}\,s^{-1}$)
I_o	Incident photon fluence rate	($mol\,m^{-2}\,s^{-1}$ or $J\,m^{-2}\,s^{-1}$)
k'	Pseudo-first order rate constant, time based	(s^{-1})
k''	Pseudo-first order rate constant, fluence based	(M^{-1} or $m^2\,J^{-1}$)
$k_{A,B}$	second order rate constant between species A and B	($M^{-1}\,s^{-1}$)
ℓ	Optical path length	(cm)
Φ	Quantum yield	
$[^{\bullet}OH]_{ss}$	Steady-state hydroxyl radical concentration	(M)
$[Cl^{\bullet}]_{ss}$	Steady-state chlorine radical concentration	(M)
$[SO_4^{\bullet -}]_{ss}$	Steady-state sulphate radical concentration	(M)
R	Universal gas constant	($J\,K^{-1}\,mol^{-1}$)
t	Exposure time	(s)
V	Volume	(L or cm^3)

Acronyms

AOP	Advanced Oxidation Process
AWWA	American Water Works Association
CBZ	Carbamazepine
DBP	Disinfection By-Product
DOC	Dissolved Organic Carbon
DOM	Dissolved Organic Matter
GAC	Granular Activated Carbon
HPLC	High-Performance Liquid Chromatography
IHSS	International Humic Substances Society
MIB	2-Methylisoborneol
NB	Nitrobenzene
NOM	Natural Organic Matter
PAC	Powdered Activated Carbon
pCBA	para-Chlorobenzoic Acid
THM	Trihalomethane
TOC	Total Organic Carbon

Acknowledgements

Doctoral studies are a very personal undertaking that can too often become a lonely pursuit. Yet, I was spared a completely solitary and ascetic existence during this work by the generous support of others.

I thank Dr. Madjid Mohseni for providing me an opportunity, his patience, and the autonomy to conduct scientific research at this level. I am also thankful for the support of my supervisory committee members Dr. Benoit Barbeau, Dr. Xiaotao Bi, and in particular Dr. Domenico Santoro for his genuine enthusiasm for the topic. Thanks to Dr. Naoko Ellis, Dr. Allan Bertram, and particularly Dr. Ron Hofmann for being motivated examiners. And thanks to Dr. Jim Malley for introducing me to the fields of UV disinfection and advanced oxidation back in New Hampshire, which set me on this path, as well as for his continued mentorship from afar.

Scientific research is a messy endeavour. Dialogue with others greatly assists both progress and avoiding dead ends. Several individuals have provided much valuable discussion and insight. I thank Doug Yuen for his assistance in the design and fabrication of the apparatus, Timothy Ma and Paula Parkinson for their advice regarding chemical analysis, Dr. Mike Thurman for sharing his wealth of experience as a researcher, and Dr. Jim Bolton for his erudite perspective on the topic.

As Titus Plautus wrote, "Where there are friends there are riches", and I have been fortunate to have had friends provide moral support, encouragement, curiosity in my work, technical advice, and above all companionship. I thank (in no particular order) Lee Hupka, Marv Clark, Ernest McCrank,

Chris Lawson, Bruce Haines, Lisa Jensen, Erin Ziegenfuss, Jennifer Cane, Anthony Kennedy, Sean McBeath, Herbert Hartshorn, Gregory Marshall, Madalena Santos, Aaron Dublenko, Cyrus Perron, Rajka Rada Jovic, Kosmas Panagiotidis, Wilson Wong, Hayder Salem, and Dr. Norman Epstein. Forgive me if I have forgotten you.

No greater support is possible than that of my family. The love and kindness of Anna, our daughter Muna, and Anna's parents David and Pamela, have given me the energy to complete this task. Anna and Muna are my reasons for living and have taught me things school never could. Yet, the greatest thanks are to my mother, who has supported me from my first breath, sacrificed so much, and asked for so little. Thank you.

Dedication

To Sonia, Anna, and Muna.

Chapter 1

Introduction

1.1 Public Drinking Water Supplies

The provision of safe drinking water supplies has been one of the triumphs of public health. The quality of life enjoyed in developed countries depends on this largely "invisible" service. Where it is absent, an additional burden is placed upon daily life. Yet, where such service is successful, it is often under appreciated. Success involves substantial technical, economic, and political organization. Criteria for success include adequate safety for human consumption, acceptable aesthetics, sufficient capacity to satisfy demand, reliability of service, and reasonable cost.

Water in the environment is often unfit to drink without sufficient treatment due to the presence of both naturally occurring and anthropogenic contaminants. Such contaminants include microbiological, chemical and radiological hazards that may pose an unacceptable risk to human health if consumed. The primary goal of water treatment is to lower the concentration of hazards such that the calculated risk from exposure is reduced to a level deemed acceptable. A secondary but fundamentally important goal of treatment is that water be rendered aesthetically adequate to consumers. A third goal is the protection of the distribution system integrity by adjustments of such parameters as pH, alkalinity and hardness, to produce a water that is neither corrosive nor scale forming.

Water for which the risk of harm from consumption is acceptable is considered "safe". However, such risk can never be reduced to zero, and the determination of what constitutes acceptable risk, and therefor the extent

of treatment, is ultimately an economic and political decision. Whether a water is deemed aesthetically acceptable or "palatable" is a determination made by consumers, and is generally independent of safety. Aesthetic issues have been reported as the most common complaint to utilities by consumers and historically have motivated additional treatment beyond that required to produce "safe" water. Consumers tend to associate poor aesthetics of water with poor quality, regardless of assurances to the contrary. Thus suppliers address aesthetics to maintain consumer confidence.

Water supply sources are usually selected to be of the best available quality, and thus require the least amount of treatment. Compared to groundwaters, surface waters harbour greater microbial hazards, are subject to greater fluctuations in quality and thus usually require greater treatment. Yet, when groundwater supplies are insufficient to meet demand, surface waters must be exploited. Consequently, large population centres tend to be served by treated surface water. A wide variety of treatment approaches have evolved in developed countries, depending on site specific challenges as well as cultural preferences. In North America, treatment by stages involving chemical coagulation and flocculation, clarification, and filtration is referred to as "conventional treatment", and has typically been followed with disinfection by chlorine. The adoption and spread of this process is associated with the disappearance of the once common waterborne outbreaks of typhoid and cholera (Logsdon and Lippy, 1982; Wolman and Gorman, 1931).

In regions where water is scarce, even sources of heavily impaired quality may be considered to supply drinking water. In some cases, it has been deemed feasible to recycle wastewater for domestic purposes. The City of Windhoek Namibia has been practicing direct potable reuse since 1958 (Du Pisani, 2006). Singapore and Orange County California are other early adopters that have found potable reuse expedient, and the numbers of such facilities are increasing. In arid yet heavily populated regions, raw sewage represents a reliable source, yet requires extensive processing beyond the capabilities of conventional treatment. Nevertheless, the alternative is often sea water de-

salination or importation via aqueducts over great distances, both of which requiring substantially higher expenditure of energy than that needed for the potabalization of municipal wastewater. At the current time, the energy consumption of reverse osmosis desalination of sea water is approximately $3 - 6\,\mathrm{kW\,h\,m^{-3}}$, compared to about $0.1\,\mathrm{kW\,h\,m^{-3}}$ required for conventional treatment (Howe et al., 2012). These values serve as useful references when considering the feasibility of alternative treatment technologies required for more challenging sources such as those of water reuse.

Water treatment is a constantly evolving field. It is far from being a solved problem, and there will likely never exist a unique solution able to address all situations adequately. With environmental changes, scientific developments, and shifting cultural attitudes, prevailing practices will continuously be subject to scrutiny and reevaluation. At the current time, the basic tools of water suppliers have not fundamentally changed over the past half century. Turbidity, chlorine residual, and filter backwash frequency are among the daily concerns of treatment plant personnel. Turbidity is used as a convenient measure of treated water quality, yet is essentially a surrogate for particulate matter. Where particle counters are used, such readings are significant as surrogates for the presence of microbes that are either planktonic or attached to particulates. Discreet measurements of microbial quality, requiring lengthy laboratory procedures, are still largely evaluated using indicator organisms as surrogates for the direct detection of pathogens (Gleeson and Gray, 1997). The deficiencies in these nested surrogates are well known. Even if the formidable technological challenge of direct pathogen detection is eventually achieved, the emergence of previously unknown pathogens will likely remain a possibility. And regardless of purity, the quality of the final product must satisfy the judgment of the consumer's palate. The unpredictability of health and aesthetic based risk has motivated a precautionary philosophy to treatment and the adoption of a multiple barrier approach. As new knowledge elucidates known risks and discovers new ones, the practice of water treatment will continue to adapt for the foreseeable future.

1.2 A Recent History of Water Treatment

The early twentieth century spread of water treatment practices, filtration and chlorine disinfection in particular, coincide with decreasing rates of infant mortality and longer life expectancies. Yet, with these successes, new challenges emerged. Environmental pollution strained the capabilities of water utilities to provide a product that was not only safe but also aesthetically acceptable. Chlorine, the very agent involved in eliminating the once frequent typhoid and cholera outbreaks, created nuisances when applied to waters impaired by industrial and urban pollution. Episodic algal blooms subjected to chlorine resulted in the sudden release of potent "earthy" and "musty" taste and odour compounds. Phenols from industrial discharges, primarily the coke furnace waste streams of iron production, reacted with chlorine to produce chlorophenols, imparting notoriously strong and unpleasant odour to treated water (Baker and Taras, 1981).

During the period spanning the 1920s to 1960s, drinking water suppliers struggled against the consequences of pollution before the sources themselves were mitigated. Alternative disinfectants that did not react with phenol were developed. In North America, the chloramination process, involving the sequential addition of ammonia followed by chlorine to form chloramines, gained popularity as it was found that chloramines are germicidal yet of negligible reactivity with phenols. Chlorine dioxide similarly did not react with phenols and was deemed an effective disinfectant. Its use, however, was limited due to cost and proprietary equipment requirements. Adsorption of contaminants by powdered activated carbon (PAC), while a costly material, was found to be effective and convenient for managing brief periodic events attributed to algae. To this day, many North American water treatment plants are equipped to deploy PAC for this same purpose.

In Europe the application of ozone, which had been superseded by inexpensive chlorine, experienced a resurgence in interest as it was able to degrade phenols while providing disinfection. Granular activated carbon (GAC)

was regularly used to improve continuous taste and odour issues as well as for dechlorination. Europe's heavily polluted rivers such as the Rhine, the Meuse, and the Seine carried elevated levels of ammonia that required substantial doses of chlorine for removal by break-point chlorination. A desirable alternative was found in the sequential combination of ozone and GAC. Ozonation increased dissolved oxygen and oxidized organics refractory to biodegradation into more biodegradable products. GAC, applied as packed beds, provided a high surface area that could be colonized by biofilms whose growth was supported by dissolved oxygen and the more bioavailable organic products of ozonation. The resulting process provided oxidation of phenols, biological nitrification of ammonia to nitrate, and the biological uptake of organics. The result is the production of a final effluent of low organic content with a typical chlorine demand on the order of $0.1\,\mathrm{mg\,L^{-1}}$. Such an effluent is considered biologically stable, as it inhibits the growth of bacterial slimes in the distribution system (Rice and Robson, 1982).

By the end of the 1960s, industrial and urban sources of water pollution were being addressed directly. In North America, chloramines and PAC were in common use in conjunction with conventional treatment. In Europe, alternatives to chlorine, particularly ozone, and biological treatment using GAC were established practices. Waterborne outbreaks, though drastically reduced, were not completely eliminated, with many instances of gastrointestinal illness still being reported and traced to drinking water. One of the main causes for this was believed to be the noncompliance of a large number of water utilities, particularly smaller systems with limited resources, to existing regulations and recommended practices. A large fraction of the reported outbreaks were of unknown etiology, and some suspected the existence of pathogens, most likely viruses, that were neither adequately removed by conventional treatment nor sufficiently susceptible to chlorine disinfection, as the culprit for the continued waterborne illness rates (Cookson Jr, 1974; Craun et al., 1976).

Meanwhile, technological advances in analytical instrumentation allowed the

detection and quantification of chemical contaminants in water at the level of parts-per-billion or less. Gas-chromatography coupled with the flame ionization detector (GC-FID) allowed sensitive detection of hydrocarbons, while the advent of the electron capture detector (GC-ECD) allowed very sensitive detection of halogenated organics (Bellar and Lichtenberg, 1974; Mieure, 1977). Mass spectrometry (GC-MS) facilitated identification via determination of molecular structure (Lingg et al., 1977). These instruments together with associated innovations in aqueous sample preparation would have a profound impact on water treatment practice.

In 1972, a now famous environmental investigation was conducted in the rapidly industrialized Mississippi Delta. Motivated by taste and odour complaints in the tap water of New Orleans, and using cutting edge instrumentation, 36 organic contaminants were detected and identified in both Mississippi River water and treated water from the Corrollton water treatment plant (USEPA, 1972). In 1974, J.J. Rook working at the water treatment plant of Rotterdam in the Netherlands, discovered that the addition of chlorine reacted with naturally occurring organic matter (NOM) to form halogenated organics, primarily trihalomethanes (THMs), mostly chloroform, none of which were detected in the raw water (Rook, 1974). Independent confirmation of Rook's findings in the USA by Bellar et al. (1974) further exacerbated the trace contaminant crisis as chloroform had recently been declared a carcinogen by the National Cancer Institute (Page, 1976). Controversy erupted from these discoveries and the belief prevailing at the time that cancer was primarily caused by environmental exposure to chemicals (i.e. extrinsic factors). In late 1974, President Ford signed the Safe Drinking Water Act (SDWA) into law, giving the recently formed US Environmental Protection Agency (USEPA) statutory responsibility over the safety of the nation's public drinking water systems, involving regulatory, monitoring and enforcement powers. Similar legislation was soon passed in other developed countries (Sayre, 1988).

Following the discovery of halogenated disinfection by-products (DBPs), in-

cluding THMs and others, the USEPA announced a nation wide survey of 80 cities to determine the extent of the THM phenomena. Completed in 1975, the National Organics Reconnaissance Survey (NORS) revealed THMs to be widespread in chlorinated drinking water (Symons et al., 1975). The discovery of industrial contaminants in New Orleans drinking water and the revelations of the NORS prompted the USEPA to initiate the National Organics Monitoring Survey (NOMS) covering 113 community water supplies during 1976 to 1977, including a range of source types and treatment processes (USEPA, 1978). The findings of both the NORS and NOMS identified over 700 distinct organic contaminants collectively present in US drinking water at the part-per-billion level or less, with THMs being the most widespread (Cotruvo and Wu, 1978). The USEPA and the drinking water industry in North America scrambled to investigate alternative methods of removing the newly discovered potential hazards from finished drinking water (Brodtmann Jr and Russo, 1979; LePage, 1981; Norman et al., 1980; Rice et al., 1981; Suffet, 1980).

In Europe, the discovery of chlorinated DBPs accelerated the spread of biological treatment using the combination of ozone and GAC and reduction in the use of chlorine disinfection, while North American interest in European practices increased (Heilker, 1979; Knoppert et al., 1980; Kühn et al., 1978; Rapinat, 1982; Schalekamp, 1979; Schulhof, 1979; Sontheimer et al., 1978). However, in North America, greater efforts were directed at modifying existing practices to prevent DBP formation. Chlorine disinfection kinetics involves a timescale of hours in the treatment plant, while the formation of halogenated DBPs occurs over a timescale of days in the distribution system. Thus, the further discovery that chloramines do not readily form THAs during distribution timescales prompted some utilities to convert chlorine to chloramines by ammonia addition following disinfection and before distribution. Such a conversion involved minimal capital cost, yet neglected the possibility that chloramines might produce other DBPs that were yet to be discovered. Another approach later used in North America to prevent the formation of DBPs was the augmentation of conventional treatment to re-

move NOM prior to chlorine addition. The process now known as "enhanced coagulation", involving higher coagulant doses, results in moderate increases in NOM removal, but is limited in coagulant dose by available alkalinity and results in an increase in residual sludge production and disposal cost (Crozes et al., 1995). The USEPA initially proposed a requirement for the use of GAC as a barrier against synthetic organic contaminants where utilities were vulnerable to industrial pollution. The requirement would have included a large fraction of the nation's treatment plants but was never implemented due in part to concern regarding cost (Symons, 1984). The ability of ozone to efficiently oxidize many organic compounds stimulated research in what would come to be known as advanced oxidation processes (AOPs), discussed below.

Much debate in the scientific and water treatment community concerned the significance of trace organic contaminants and their removal. Rice criticized the concept of the "alternative disinfection" approach to avoiding THM formation, arguing a change in disinfectant would simply result in formation of a different set of by-products, and that efforts should be concentrated on removing NOM prior to disinfection (Rice and Cotruvo, 1978). Rosen cautioned that the long list of trace organic contaminants that had been detected in drinking water using GC techniques were the most volatile compounds, perhaps representing less than 10% of the total, and that the use of methods such as liquid chromatography would reveal the presence of a much longer list of contaminants (Rosen, 1976). Regulations based on the health significance of trace contaminants was questioned by Pendygraft et al. (1979). Stumm et al. (1983) argued for a shift in thinking from measuring trace concentrations of contaminants in the environment and the widespread practice of single organism bioassays of toxicity, to a more rational and holistic ecotoxicology approach and risk analysis. After a long career in the drinking water field, Abel Wolman (1892-1989) gave a keynote address to the American Water Works Association (AWWA) annual conference of 1976 regarding the past and future of the field (Wolman, 1976). His lucid assessment of future challenges remains just as relevant four decades

later:

> The water field, as every other, will be the beneficiary of advancing scientific and technologic discovery. It will also be plagued by real and pseudo dangers. Managers are slowly becoming accustomed to the fact that water never was simply the H_2O of the laboratory, but is the receptacle into which all of the ingredients of nature and man has been poured. With ever increasing tools of detection, infinitesimal concentrations of everything will be recorded. Some of these will be hazardous in truth, others useful for television media, and still others grist for the courts and lawyers. Instead of succumbing to despair, the worker in the field will have to maintain an equilibrium between the real, the hypothetical and even the hysterical.

Wolman continues, urging rationalism and patience in the face of new challenges:

> Water, as a strong determinant of the health of its users, will be subjected to increasing scrutiny, simply because it is a universal ingredient in man's metabolism. The future will focus inevitably upon the infinitesimal concentrations of organic and inorganic materials, if for no other reason than that we can now detect them. In the past, our tools of detection were gross. Now, the time frame for possible effects is considered to be decades rather than days, insofar as carcinogenic, mutagenic and genetic potentials are concerned. The economic implications are many. Common sense, supported by epidemiologic, rigid scrutiny, will ultimately prevail, if we can remain patient.

In the case of by-products of chlorination, four decades of research, spanning more than 60 epidemiological studies, have failed to demonstrate harmful effects at typical exposures (Hrudey and Charrois, 2012). Research continues

to discover other halogenated DBPs, with hundreds of new compounds having been found at increasingly smaller concentrations in chlorinated drinking water (Hrudey and Charrois, 2012). Regarding trace organic contaminants, the absence of health significance aside, the changing nature of industrial manufacturing in North America have made the long list of contaminants detected in the 1970s largely an anachronism today, as the majority of those substances are no longer released to North American waters (Tchobanoglous et al., 2015). The development of liquid chromatography coupled with mass spectrometry (LC-MS), has indeed revealed the presence of a myriad of newly discovered contaminants in water at the part-per-trillion level or less, namely pharmaceuticals and their metabolites (Benotti et al., 2009). The human health significance of exposure to these contaminants at such low levels is unclear yet has gained media attention. Meanwhile, real threats to human health from waterborne outbreaks persist, due not to newly discovered contaminants, but to the banality of known hazards, existing treatment deficiencies and human error (Hrudey and Hrudey, 2004).

1.3 UV Disinfection

Among the most dramatic changes in drinking water practice in recent years has been the rapid adoption of UV disinfection, now a mature and accepted technology. This has enabled the development of other applications of UV to water treatment, namely UV based AOPs. The rise of UV disinfection is briefly reviewed.

By the 1960s, the germicidal effects of ultraviolet radiation at the molecular level where well understood (Jagger, 1967), and while a few water treatment facilities used UV in the early days of the twentieth century, virtually all such facilities seem to have vanished within a few years as the more convenient and inexpensive chlorination process spread. When the American Society of Civil Engineers (ASCE) and the AWWA published the first edition of *Water Treatment Plant Design* (ASCE, 1969), the technological

problem of disinfection was considered essentially solved. The chapter on disinfection, while briefly acknowledging the existence of UV and other disinfectants, was entirely devoted to methods of chlorination. To some extent this was justified, since the causative organisms of diseases such as typhoid and cholera were spread between humans, originated from sewage contamination, involved high infective doses, and were very sensitive to chlorine. The second and third editions acknowledged the need for new disinfectants, adding sections on ozone and chlorine dioxide (ASCE, 1990; AWWA, 1998). By the end of the 1990s, due to a growing body of UV research, drinking water disinfection by UV spread to hundreds of towns and cities in North America, Europe and elsewhere. Consequently, by the fifth edition of *Water Treatment Plant Design*, a chapter devoted entirely to UV disinfection was deemed necessary (AWWA, 2012). For a review of UV disinfection practices, the reader is also directed to the AWWA's *Ultraviolet Disinfection Handbook* (Bolton and Cotton, 2011).

Prior to this rise, UV disinfection of drinking water was an established practice in several European countries by the mid-1980s, yet absent from North American utilities. Motivation for use in Europe was driven by a desire for an alternative to chlorine for the disinfection of groundwater and biological filtrates (Kruithof et al., 1992). By the end of the 1990s, the rapid adoption of UV for drinking water treatment, in North America and elsewhere, can be understood on the basis of a few now well established facts. Two common pathogens were gradually associated with waterborne outbreaks that were not necessarily due to gross contamination of source water, treatment deficiencies, or recontamination in distribution. These were identified as the protozoan parasites *Giardia lamblia* and *Cryptosporidium parvum*. Giardia cysts and Cryptosporidium oocysts, the vegetative states of each organism, were found to be ubiquitous in the aquatic environment and common in raw surface water supplies (LeChevallier and Di Giovanni, 2002; LeChevallier and Norton, 1995; LeChevallier et al., 1991). Infective doses were determined to be low, on the order of ten (oo)cysts or less (DuPont et al., 1995; Rendtorff, 1954). They were found to be highly resistant to chlorine, partic-

ularly Cryptosporidium (Hibler, 1987; Korich et al., 1990). Contrary to prior understanding, Giardia and Cryptosporidium (oo)cysts are very sensitive to UV radiation when using assays to detect infectivity rather than viability (Bukhari et al., 1999; Campbell et al., 1995; Clancy et al., 1998, 2000; Craik et al., 2000; Linden et al., 2002). Lastly, UV irradiation of drinking water at typical disinfection doses does not produce significant by-products of concern nor increase formation of regulated DBPs upon subsequent chlorination (Liu et al., 2002; Malley et al., 1996; Reckhow et al., 2010).

Much of the research that motivated the discoveries mentioned above was prompted by the Cryptosporidium outbreak that occurred in Milwaukee WI in the spring of 1993. The largest known outbreak of waterborne illness in US history involved an estimated 400,000 individuals acquiring the infection (MacKenzie et al., 1994) and resulting in an estimated 100 deaths (Hrudey and Hrudey, 2004). The cause of the Milwaukee outbreak, though never fully determined, was associated with treatment plant deficiencies and challenging conditions (Fox and Lytle, 1996). Yet, Cryptosporidium outbreaks in Las Vegas NV (Roefer et al., 1996) and Waterloo ON (Pett et al., 1993) occurred during normal operation in the absence of any known deficiencies or challenging source water conditions, suggesting utilities were more vulnerable than previously thought. The magnitude of the Cryptosporidium threat revealed by the Milwaukee outbreak specifically lead to the USEPA promulgation of the Long-Term 2 Enhanced Surface Water Treatment Rule (LT2ESWTR) and the rapid adoption of UV disinfection in the USA and elsewhere. Large-scale early adopters of UV disinfection include Pittsburg PA (2001), Edmonton AB (2002), and Seattle WA (2003) (Hargy, 2002). By 2010, a North American survey revealed that 161 utilities in Canada and 148 utilities in the USA had installed or were planning to instal UV disinfection at treatment capacities greater than $2\,\mathrm{ML\,d^{-1}}$ (Wright et al., 2012). Several such facilities have installed UV treatment with the main objective of disinfection, yet with the capability of periodic treatment of taste and odour when operated in "advanced oxidation" mode. Such plants include those of the City of Cornwall and the Region of Peel, both in the Canadian province

of Ontario. The Andijk treatment plant in Holland uses UV for simultaneous disinfection and destruction of agricultural and industrial pollutants originating from the Rhine River. In Orange County California, UV is used as a final polishing step in the treatment of wastewater for indirect potable reuse, both as a disinfection barrier and for the destruction of contaminants poorly retained by reverse osmosis membranes.

1.4 Advanced Oxidation Processes

During the 1970s and 1980s, as the inventory of trace organic contaminants detectable in water expanded, new treatment technologies were investigated that could reduce their concentration. One approach for the removal of trace organic contaminants is oxidative degradation, with the most promising techniques involving ozone or ultraviolet radiation. Interest in the latter has recently increased, in part due to the maturity of UV technology developed for disinfection.

Both ozone decomposition promoted by H_2O_2 (O_3/H_2O_2) and UV photolysis of H_2O_2 (UV/H_2O_2) produce the hydroxyl radical ($^{\bullet}OH$). Reaction rate constants of $^{\bullet}OH$ with most organic solutes are high, spanning roughly three orders of magnitude ($10^8 - 10^{10}\,M^{-1}\,s^{-1}$) near the diffusion limit (Buxton et al., 1988; Haag and Yao, 1992). Elevated rate constants over a narrow range imply that $^{\bullet}OH$ is a highly reactive and nonselective oxidant. Because of these properties, treatment processes based on $^{\bullet}OH$ generation are referred to as Advanced Oxidation Processes (AOPs), a term first used by Glaze et al. (1987). While a variety of other AOPs have been proposed and studied, only those based on O_3 and UV have thus far shown promise in full-scale drinking water applications.

Unlike $^{\bullet}OH$, ozone is a very selective oxidant, in that its reaction rate constants with aqueous solutes span over ten orders of magnitude. For example, ozone is highly reactive with sulphide ($3 \times 10^9\,M^{-1}\,s^{-1}$) though practically

inert to tetrachloroethene ($< 0.1\,M^{-1}\,s^{-1}$) (Von Gunten, 2003). Decomposition of ozone is initiated by OH^- and is thus accelerated at elevated pH (Forni et al., 1982). This decomposition generates $^{\bullet}OH$ through a chain reaction mechanism with an experimentally observed yield of 0.5 mole $^{\bullet}OH$ per mole of O_3 (Forni et al., 1982; Staehelin and Hoigné, 1982). However, HCO_3^- and CO_3^{2-}, omnipresent in natural waters, react with $^{\bullet}OH$ to produce the much less reactive carbonate radical ($CO_3^{\bullet-}$), interrupting the chain reaction. Furthermore, since the $^{\bullet}OH$ rate constant of CO_3^{2-} ($4 \times 10^8\,M^{-1}\,s^{-1}$) is approximately 50 times greater than that of HCO_3^- ($8.5 \times 10^6\,M^{-1}\,s^{-1}$), the scavenging of $^{\bullet}OH$ increases significantly above pH 9 (Buxton et al., 1988). In waters of typical pH (6-9) and moderate to high alkalinity ($> 2\,mM$), ozone decomposition is inhibited. It is the relative stability of ozone in such waters that provides the required ozone lifetime for effective disinfection. Ozone decomposition, however, occurs rapidly over the usual pH range in the presence of a small amount of H_2O_2 (Staehelin and Hoigné, 1982). A typical H_2O_2:O_3 (mol/mol) dose ratio of 0.1-0.5 is sufficient to initiate rapid conversion to $^{\bullet}OH$, with the optimum site-specific ratio determined by experiment (Acero and Von Gunten, 2001). The O_3/H_2O_2 AOP is a simple augmentation in a plant that already uses ozone, with the point of H_2O_2 addition delayed sufficiently so as not to interfere with ozone disinfection. Ozone is commonly followed by biological filtration, which further enhances removal of the more biodegradable AOP products and provides quenching of residual H_2O_2. Where ozone is not currently used, considerable infrastructure must be installed for generation, use, and disposal of ozone (Langlais et al., 1991; Rakness, 2011). A problem with the O_3/H_2O_2 AOP, as with O_3 disinfection, is the generation of the by-product bromate (BrO_3^-) in bromide containing waters (Haag and Hoigné, 1983). A current limit on bromate in drinking water of $10\,\mu g\,L^{-1}$ is suggested or required in North America and Europe (Kristiana et al., 2012). This value is partly based on detection limits of existing analytical methods. Methods to avoid bromate formation involve additional process complexity and cost (Von Gunten, 2003). Future implementation of the O_3/H_2O_2 AOP depends largely on regulatory limits for bromate in treated waters.

The UV/H_2O_2 AOP generates $^{\bullet}$OH by the photolysis of H_2O_2 that has been added upstream of UV reactors. Photolysis of H_2O_2 to $^{\bullet}$OH involves a quantum yield of unity at 254 nm(Baxendale and Wilson, 1957). However, H_2O_2 is a poor absorber of UV with a molar absorption coefficient at 254 nm of only $20\,M^{-1}\,cm^{-1}$. Thus higher concentrations of H_2O_2 must be applied for sufficient photolysis to take place, with typical doses of H_2O_2 in the range of 5 to $15\,mg\,L^{-1}$. Also, the dose or fluence of UV energy required is high, approximately $1000\,mJ\,cm^{-2}$ or more, compared to the $40\,mJ\,cm^{-2}$ typically applied in UV disinfection (Bolton and Cotton, 2011; Dotson et al., 2012). Another significant challenge is the undesirability of residual H_2O_2 in treated effluent and its quenching prior to distribution. Negligible reduction in H_2O_2 occurs during passage through UV reactors, thus virtually the full amount dosed must be quenched. Benefits of UV include simultaneous disinfection, absence of by-products of concern, and a compact footprint.

The choice between implementing the O_3/H_2O_2 or UV/H_2O_2 AOP will depend on many site-specific conditions. The electrical energy per order or EE_O concept (Bolton et al., 1996) has been used to compare the two AOPs in general, with the H_2O_2 converted to an energy equivalent based on chemical and electrical costs (Rosenfeldt et al., 2006). Such a comparison has suggested that the O_3/H_2O_2 AOP involves a lower operating cost. However, the optimal choice in general depends on such site-specific factors as the existing treatment process and layout (if any), space availability, water chemistry, treatment objectives, and electrical, chemical, and capital costs. Both selection of an AOP and its placement in an overall treatment system must consider a few features common to both processes.

Due to the relatively nonselective reactivity of $^{\bullet}$OH, the oxidation of trace organic contaminants by AOP generally results in a mixture of daughter products, the complete mineralization of contaminants to CO_2 requiring an impractical amount of energy. Even if the concentration of the target contaminant is reduced to below detection, the merit of treatment by AOP

depends on the desirability of the mixture produced. For example, treatment by AOP of the herbicide atrazine creates a mixture of dozens of triazine daughter products (Acero et al., 2000). The health relevance of human exposure to such trace mixtures, relative to that of the parent compound, is generally unknown. If the daughter products of such a mixture are more biodegradable than the parent compound, subsequent biological filtration may be suggested. However, the selection of an AOP should be made only after a comparison with alternative treatment processes.

UV/H_2O_2 is the more appropriate AOP in cases where avoiding bromate formation is essential, where the direct photolysis of the target contaminant is significant, and where continuous terminal UV disinfection may be briefly augmented to an AOP. This last case has often been motivated by the seasonal occurrence of taste and odour events due to the naturally occurring compounds geosmin and 2-methylisoborneol (MIB).

Both geosmin and MIB are produced by cyanobacteria and actinomycetes, causing taste and odours detectable in water by most humans at concentrations on the order of $10\,\mathrm{ng\,L^{-1}}$ or less (Persson, 1980; Young et al., 1996). Geosmin is described as "earthy", and MIB as "musty", and together they have been a major cause of consumer complaints (McGuire, 1995). Their detection often causes public concern regarding the safety of the water supply despite posing no health risk (Dionigi et al., 1993). Occurrence is typically unpredictable and seasonal, and conventional treatment ineffective (Suffet, 1995). Both molecules are tertiary aliphatic alcohols. Consequently, they are poorly sorbed to activated carbon (Chowdhury et al., 2013). They have been found to be relatively inert to the conventional oxidants Cl_2, ClO_2, $KMnO_4$, H_2O_2, and O_3, yet their $^{\bullet}OH$ reaction rates are reported to be between $10^9 - 10^{10}\,\mathrm{M^{-1}\,s^{-1}}$ (Glaze et al., 1990; Lalezary et al., 1986; Peter and Von Gunten, 2007). Though the identity of the AOP by-products of geosmin and MIB have not been reported, the success of treatment suggests that none have a lower odour threshold than the parent compounds. One possible daughter product of MIB is camphor, which has an odour thresh-

old 6 orders of magnitude greater than MIB (Amoore and Hautala, 1983). Episodes of geosmin and MIB have typically involved concentrations in the range of 50 to 100 ng L^{-1}, with extreme cases as high as 500 ng L^{-1} or more (Suffet, 1995). The increased occurrence of eutrophication associated with population growth and climate change may increase the frequency of problems related to geosmin and MIB.

Redundancy is a common engineering practice in water treatment, including UV disinfection. Redundant UV capacity may be fully employed to provide the required UV fluence for AOP treatment when geosmin or MIB are detected. The usual disinfection dose of about 40 mJ cm^{-2} may be instantly increased many fold by maximizing lamp outputs, the ignition of additional lamps, and possibly a reduction in flow. This can be done with a relatively small footprint, particularly when medium pressure mercury lamps are used. This approach requires the continuous on-site storage of H_2O_2, often in a 50% w/w solution, an additional plant hazard. Lastly, the requirement to quench residual H_2O_2 presents a major cost to the process.

Many North American treatment plants add chlorine, as a secondary disinfectant, upstream of UV reactors (Dotson et al., 2012). It was discovered that this practice resulted in the UV photolysis of HOCl and OCl^- with the generation of $^{\bullet}OH$ (Feng et al., 2007; Watts and Linden, 2007). This UV/Cl_2 AOP eliminates the need for H_2O_2 and its quenching, though may require higher chlorine doses than used in disinfection. However, this process is pH dependent, due to differences in the relevant properties of the two species HOCl and OCl^-. Molar absorption coefficients, photolysis quantum yields, and $^{\bullet}OH$ rate constants of HOCl and OCl^- are such that UV/Cl_2 is much less efficient than UV/H_2O_2 when treating water above pH 6 (Jin et al., 2011; Wang et al., 2012; Watts et al., 2007). Requirement for pH adjustments before and after the UV/Cl_2, as well as additional dechlorination to trim the final residual, would negate the benefits of avoiding H_2O_2 addition.

Both ozone and UV based AOPs involve the added complexity of chemical

addition and control. A new AOP approach that is able to generate $^{\bullet}OH$ from water itself would eliminate such complexity and is the subject of this study.

1.5 185 nm Advanced Oxidation

In addition to the germicidal radiation emitted at 254 nm, the conventional low pressure mercury lamp also emits at a wavelength of 185 nm. The 185 nm radiation is capable of generating $^{\bullet}OH$ from the photolysis of water. This fact forms the basis of using conventional UV lamps, in a suitably designed reactor, as an AOP that does not require chemical addition.

Low pressure mercury lamps emit virtually all radiation at two wavelengths, 254 and 185 nm. The atomic energy levels of mercury are such that the emittance at 254 nm is always greater than that at 185 nm, with a 185 nm to 254 nm ratio reported between 0.12 to 0.34 (Barnes, 1960; Johnson, 1971). Increased lamp temperatures and arc currents have been found necessary for higher ratios of 185 nm. More recently this ratio has been reported to be 0.08 (Masschelein and Rice, 2002), without any indication of how it was measured.

An envelope encloses the lamp to contain the mercury vapour within which radiation is generated, while a sleeve with an air gap surrounds the lamp and provides isolation from water in a reactor. High purity silica (SiO_2) is the material of choice for lamp envelopes and sleeves. Two general types are fused quartz, obtained from SiO_2 containing minerals, and fused silica, produced from the particulates of high purity $SiCl_4$ vapour combustion with O_2 (Koller, 1965; Phillips, 1983). Optical transmission of both materials is high at 254 nm, while fused silica is superior at 185 nm, making fused silica the optimal material for lamp envelopes and sleeves in a 185 nm AOP reactor.

At the scale of optical path lengths typical of UV reactors, the absorbance by water at 254 nm is negligible ($< 0.01\,\mathrm{cm}^{-1}$) (Quickenden and Irvin, 1980). At 185 nm, absorbance is significant, often cited as $\alpha_w = 1.8 \pm 0.1\,\mathrm{cm}^{-1}$ at 25 °C (Weeks et al., 1963). A temperature coefficient for α_w was found by Weeks et al. (1963) to be $0.05\,\mathrm{cm}^{-1}\,^{\circ}\mathrm{C}^{-1}$ over the range 20 to 35 °C, in agreement with that found between 25 to 50 °C by Barrett and Mansell (1960). More recent work has reported $\alpha_w = 1.60 \pm 0.03\,\mathrm{cm}^{-1}$ at 25 °C (Kröckel and Schmidt, 2014). Furthermore, the measurements of $\alpha_w(\lambda)$ by Kröckel and Schmidt (2014) over the range of 187 to 181 nm reveals a strong increase in absorbance with decreasing wavelength, confirming the substantial error in α_w at 185 nm due to small wavelength errors.

Photons of 185 nm have sufficient energy (6.7 eV) to photolyze water to $H^{\bullet}$ and $^{\bullet}OH$ with a quantum yield of approximately 0.3 (Getoff and Schenck, 1968). In the presence of dissolved oxygen, the $H^{\bullet}$ formed will react with O_2 at a diffusion limited rate to form the perhydroxyl radical ($HO_2^{\bullet}$). At typical water pH of 6 - 9, $HO_2^{\bullet}$ disproportionates to the superoxide radical anion $O_2^{\bullet-}$ with $pK_a = 4.8$ (Bielski et al., 1985). Both $HO_2^{\bullet}$ and $O_2^{\bullet-}$ will react with $^{\bullet}OH$ at diffusion limited rates, but have low reactivities with organic solutes. The net result is to provide a source of $^{\bullet}OH$. In pure water, $^{\bullet}OH$ recombination results in the accumulation of H_2O_2. However, the presence of major solutes will greatly reduce the likelihood of such a reaction and H_2O_2 accumulation will be negligible. A summary of key reactions with quantum yield and rate constants (Buxton et al., 1988) resulting in net $^{\bullet}OH$ production is as follows:

$$H_2O \xrightarrow{185\,nm} H^{\bullet} + {}^{\bullet}OH \qquad \Phi = 0.3 \tag{1.1}$$

$$H^{\bullet} + O_2 \longrightarrow HO_2^{\bullet} \qquad k = 2 \times 10^{10}\,\mathrm{M}^{-1}\,\mathrm{s}^{-1} \tag{1.2}$$

$$HO_2^{\bullet} \rightleftharpoons O_2^{\bullet-} + H^{+} \qquad pK_a = 4.8 \tag{1.3}$$

$$O_2^{\bullet-} + {}^{\bullet}OH \longrightarrow O_2 + OH^{-} \qquad k = 7 \times 10^{9}\,\mathrm{M}^{-1}\,\mathrm{s}^{-1} \tag{1.4}$$

$$HO_2^{\bullet} + {}^{\bullet}OH \longrightarrow H_2O + O_2 \qquad k = 6 \times 10^{9}\,\mathrm{M}^{-1}\,\mathrm{s}^{-1} \tag{1.5}$$

Because of the high absorption coefficient of water, 90% of 185 nm photons are absorbed within a water layer approximately 5 mm thick. The lifetime of generated $^{\bullet}$OH is on the order of 1 µs in typical water matrices (Hoigné, 1997), thus confining oxidative degradation to the 185 nm irradiated volume. Achieving sufficient irradiation by 185 nm of the entire volume of flow imposes severe constraints on reactor geometry and mixing. The overall efficiency of the 185 nm AOP therefor depends critically on reactor design.

While direct photolysis at 254 nm is significant for some organic molecules, it is likely less so at 185 nm. Molar absorption coefficients of molecules in solution rarely exceed $10^5\,\mathrm{M}^{-1}\,\mathrm{cm}^{-1}$ (Wayne, 1988). Trace organic contaminant concentrations in surface waters are usually much less than $1\,\mu\mathrm{g\,L}^{-1}$. For a molecular weight of $100\,\mathrm{g\,mol}^{-1}$, an upper value for the fraction of photons absorbed by the compound in pure water will be on the order of 10^{-3}, and much less than this in the presence of major solutes that also absorb. The quantum yield (Φ) of direct photolysis in solution is typically much less than unity due to the influence of the solvent (Wayne, 1988). In a typical drinking water matrix, the contribution of direct photolysis at 185 nm to contaminant degradation is thus expected to be negligible relative to $^{\bullet}$OH oxidation.

A recent review of 185 nm water treatment (Zoschke et al., 2014) includes a discussion of research on photochemical reactions of some solutes in the 185 nm regime. Based on the work cited therein, several comments can be made. Removal of NOM, as measured by DOC, using 185 nm radiation is unfeasible based on energy requirements. In general, the biodegradability of NOM will be increased by 185 nm irradiation, to an extent dependent on total exposure. Nitrate may be converted to nitrite under certain conditions, but the chemistry involved is complex. No other degradation pathways for trace organic contaminants have been considered other than $^{\bullet}$OH oxidation. Fundamental mechanistic studies are lacking. Most research has involved qualitative studies or produced quantitative results specific to a particular apparatus and water matrix, often insufficiently described. Few attempts

have been made to measure the extent of reaction, not by time, but on the basis of photons or energy absorbed by the system. Comparison of results from different equipment and scales is therefore difficult. A recommendation made in a review of photochemical water treatment more than two decades earlier, that researchers adopt an energy based approach to describe the extent of treatment, remains relevant (Legrini et al., 1993). This deficiency may in part be due to the absence of convenient 185 nm detectors, either reliable electronic radiometers or chemical actinometers. Unlike the KI-KIO_3 actinometer for quantification of radiation at 254 nm (Bolton et al., 2011; Rahn, 1997; Rahn et al., 2003), extant actinometric methods at 185 nm are time consuming, require gas-tight assemblies and sophisticated techniques to achieve sufficient precision and accuracy (see Kuhn et al. (2004) and references therein).

1.6 Knowledge Gaps

Many details essential for successful application of the 185 nm AOP are not currently available, imprecise, or in dispute. The process relies on the generation of 185 nm radiation, yet the efficiency of this process has not been reported in the open literature for modern lamps. The absorbance value of water below 20 °C is not known, nor is any information available regarding the temperature dependence of the quantum yield for the photolysis of water.

Studies of the influence of the major inorganic solutes on the 185 nm AOP are absent. Several studies have investigated nitrate, motivated by concern for nitrite generation. However, nitrate is not a major ion in surface waters, often present at concentrations less than $1\,mg\,L^{-1}$. Chloride, sulphate, bicarbonate and carbonate are present in some waters from 10 to $100\,mg\,L^{-1}$(Wetzel, 2001) or more. These solutes are known to be relatively strong absorbers of 185 nm radiation (Barrett et al., 1965; Fox, 1970; Hayon and McGarvey, 1967; Jortner et al., 1964; Weeks et al., 1963). Upon such absorption, an excited state is created in which an electron is shared be-

tween the anion and several surrounding water molecules in what is known as a charge transfer to solvent (CTTS) excited state (Blandamer and Fox, 1970). A fraction of these electrons dissociate and escape the solvent cage to leave behind a radical:

$$Cl^- \xrightarrow{185\,nm} Cl^\bullet + e^-_{aq} \tag{1.6}$$

$$SO_4^{2-} \xrightarrow{185\,nm} SO_4^{\bullet -} + e^-_{aq} \tag{1.7}$$

The solvated electron (e^-_{aq}) produced is efficiently scavenged in the presence of dissolved oxygen to produce the superoxide anion radical which may then proceeds as in reaction 1.4 above (Buxton et al., 1988):

$$e^-_{aq} + O_2 \longrightarrow O_2^{\bullet -} \qquad k = 2 \times 10^{10}\,M^{-1}\,s^{-1} \tag{1.8}$$

Photochemical generation of $Cl^\bullet$ and $SO_4^{\bullet -}$ depends on the molar absorption coefficients (ϵ) and quantum yields (Φ) at 185 nm of their respective anions (see Table 1.1).

Table 1.1: Molar absorption coefficient (ϵ) and quantum yield (Φ) for Cl^- and SO_4^{2-} at 185 nm

$\epsilon(M^{-1}\,cm^{-1})$		Φ^a		Ref.
Cl^-	SO_4^{2-}	Cl^-	SO_4^{2-}	
3800 ± 300	260 ± 30	0.43 ± 0.02	0.64	Dainton and Fowles (1965)
ca. 3500	190			Weeks et al. (1963)
	200		0.67[a]	Barrett et al. (1965)
		0.49		Jortner et al. (1964)

[a] Corrected by Fox (1970) using $\Phi(H_2) = 0.4$ for 5 M ethanol actinometer

The value of $\epsilon_{185}(CO_3^{2-})$ is reported to be approximately $10^3\,M^{-1}\,cm^{-1}$ (Hayon and McGarvey, 1967; Weeks et al., 1963). No information is found

regarding $\epsilon_{185}(HCO_3^-)$, nor the quantum yield of HCO_3^-/CO_3^{2-} (reaction 1.9).

$$HCO_3-/CO_3^{2-} \xrightarrow{185\,nm} CO_3^{\bullet-} + e_{aq}^- \tag{1.9}$$

Only $CO_3^{\bullet-}$ is expected under the usual pH conditions, since $pK_a < 0$ for $HCO_3^{\bullet}/CO_3^{\bullet-}$ (Czapski et al., 1999). If it were to be found that the 185 nm absorbances of HCO_3^- and CO_3^{2-} are similar, then at a typical total carbonate concentration of 1 mM, the contribution to absorption by the carbonate system would be comparable to that of water itself even at pH < 8, since $pK_a = 10.3$ for HCO_3-/CO_3^{2-} (Butler, 1982). The reactivity of $CO_3^{\bullet-}$ is relatively low, with a few exceptions such as aniline derivatives (Chen et al., 1975; Larson and Zepp, 1988). Hence, HCO_3-/CO_3^{2-} is expected to be a scavenger of both $^{\bullet}OH$ and 185 nm photons, exhibiting a parasitic effect on process efficiency by two distinct phenomena.

The second-order reaction rate constants of the three species $^{\bullet}OH$,$Cl^{\bullet}$, and $SO_4^{\bullet-}$ with a few organic and inorganic solutes have been reported, allowing a comparison of their values. In many cases, the reactivity of $^{\bullet}OH$ and $Cl^{\bullet}$ are similar (Buxton et al., 2000), both with $6 \times 10^8\,M^{-1}\,s^{-1}$ for 2-methyl-2-propanol (tert-butanol). Available data for $SO_4^{\bullet-}$ show a wider range of second order reaction rate constants for substituted benzenes than for $^{\bullet}OH$, suggesting an electron-transfer mechanism (Neta et al., 1977). For small aliphatic alcohols, carboxylic acids, aldehydes and ketones, $SO_4^{\bullet-}$ rate constants are typically two orders of magnitude less than those of $^{\bullet}OH$ and $Cl^{\bullet}$ (Buxton et al., 2000).

As mentioned above, the carbonate system is known to be a significant scavenger of $^{\bullet}OH$. Reaction rate constants with $Cl^{\bullet}$ and $SO_4^{\bullet-}$ reported in the literature are displayed in Table 1.2.

Unlike $^{\bullet}OH$, no information can be found on the reactivities of $Cl^{\bullet}$ and $SO_4^{\bullet-}$

Table 1.2: Comparison of rate constants for $^{\bullet}OH$, $Cl^{\bullet}$, and $SO_4^{\bullet-}$ with HCO_3^- and CO_3^{2-}

	$k(M^{-1}\,s^{-1})$		Ref.
Radical	HCO_3^-	CO_3^{2-}	
$^{\bullet}OH$	8.5×10^6	3.9×10^8	Buxton et al. (1988)
$Cl^{\bullet}$	2.4×10^9	-	Buxton et al. (2000)
	2.2×10^8	5.0×10^8	Mertens and von Sonntag (1995)
$SO_4^{\bullet-}$	3.5×10^6	-	Buxton et al. (2000)
	9.1×10^6	-	Ross and Neta (1979)

with NOM nor any of its fractions, such as humic and fulvic acids. Furthermore, no information is available regarding the contribution by NOM to the absorption of 185 nm photons. Strong absorbance on a molecular basis is expected due to the substantial aromaticity of humic and fulvic acids. Yet due to the colloidal nature of such macromolecules, often with molecular weights of several thousand dalton, the relative contribution of absorption at 185 nm is likely to be highly dependent on molecular size distribution, pH-dependent spacial conformation, and complexation with other solutes.

The photo-generated $Cl^{\bullet}$ reacts with Cl^- to form $Cl_2^{\bullet-}$, the dichloride radical anion. This reaction and the reverse decay of $Cl_2^{\bullet-}$ result in the equilibrium $Cl^{\bullet} + Cl^- \rightleftharpoons Cl_2^{\bullet-}$ which lies far to the right (Buxton et al., 1998). Both $Cl^{\bullet}$ and $Cl_2^{\bullet-}$ react with water via several postulated equilibria terminating in formation of $^{\bullet}OH$. At neutral pH with $[Cl^-] < 0.1\,M$, an overall equilibrium is reported to lie far to the right (Buxton et al., 1998):

$$Cl^{\bullet}/Cl_2^{\bullet-} + H_2O \rightleftharpoons H^+ + HOCl^{\bullet-} \rightleftharpoons Cl^- + {}^{\bullet}OH + H^+ \tag{1.10}$$

In the presence of solutes reacting with $^{\bullet}OH$ at diffusion limited rates, the

above equilibrium will not be established and the reactions with water will be first order (Buxton et al., 1998). The resulting $Cl_2^{\bullet-}$ exhibits low reactivity with organic solutes (Hasegawa and Neta, 1978). Photogenerated $SO_4^{\bullet-}$ reacts with Cl^-, producing $Cl^\bullet$ (Gilbert et al., 1988). The reverse reaction of $Cl^\bullet$ and SO_4^{2-} is competitive resulting in an equilibrium with a constant near unity (Buxton et al., 1999). The reaction of $SO_4^{\bullet-}$ with water may also leads to formation of $^\bullet OH$. What information exists regarding these reactions is available from fundamental research in radiation chemistry and more recent investigations relating to the atmospheric chemistry of cloud droplets. Important reactions and their reported rate constants are listed in Table 1.3. Reactions with tert-butanol are included for comparison.

Table 1.3: Important reactions involving $Cl^\bullet$, $Cl_2^{\bullet-}$, and $SO_4^{\bullet-}$

Reaction	Rate Constant
$Cl^\bullet + Cl^- \longrightarrow Cl_2^{\bullet-}$	$8.5 \times 10^9\,M^{-1}\,s^{-1}$
$Cl_2^{\bullet-} \longrightarrow Cl^\bullet + Cl^-$	$6.0 \times 10^4\,s^{-1}$
$Cl^\bullet + H_2O \longrightarrow$	$2.5 \times 10^5\,s^{-1}$
$Cl_2^{\bullet-} + H_2O \longrightarrow$	$1.3 \times 10^3\,s^{-1}$
$Cl^\bullet + SO_4^{2-} \longrightarrow Cl^- + SO_4^{\bullet-}$	$2.1 \times 10^8\,M^{-1}\,s^{-1}$
$SO_4^{\bullet-} + Cl^- \longrightarrow SO_4^{2-} + Cl^\bullet$	$6.1 \times 10^8\,M^{-1}\,s^{-1}$
$SO_4^{\bullet-} + H_2O \longrightarrow$	$\sim 700\,s^{-1}$
$Cl^\bullet + t{-}BuOH \longrightarrow$	$6.2 \times 10^8\,M^{-1}\,s^{-1}$
$Cl_2^{\bullet-} + t{-}BuOH \longrightarrow$	$< 10^3\,M^{-1}\,s^{-1}$
$SO_4^{\bullet-} + t{-}BuOH \longrightarrow$	$7.8 \times 10^5\,M^{-1}\,s^{-1}$
$^\bullet OH + t{-}BuOH \longrightarrow$	$6.0 \times 10^8\,M^{-1}\,s^{-1}$

Rate constants from Buxton et al. (1998, 1999, 2000)

It can be seen from the above that the identity and concentrations of inorganic and organic solutes should impart a strong influence on the radical chemistry of 185 nm irradiated water, and therefore 185 nm AOP efficiency. A fraction of the absorbed 185 nm photons may be lost to those species that

do not contribute reactive radicals upon absorption. All three radicals ($^{\bullet}$OH, $Cl^{\bullet}$, and $SO_4^{\bullet-}$) may be generated at comparable rates depending on the fraction of photons absorbed by water and the respective anions. The reactivity of these radicals with scavengers such as NOM and HCO_3-/CO_3^{2-}, as well as reactions among the radicals and anions will determine their steady-state concentrations and thus their contribution to the rate of oxidative degradation of specific organic contaminants. The overall rate will also depend on the rate constants of a specific contaminant with each radical. For example, if $Cl^{\bullet}$ has a higher rate constant with a target contaminant, but is also more reactive with the matrix, a smaller steady-state concentration would be available and the contribution to removal would be smaller. Conversely, if $SO_4^{\bullet-}$ had a lower rate constant with the target but was much less reactive with the matrix, a higher steady-state concentration and thus greater contribution to removal could result. In general, the observed degradation rate will depend on the relative distribution of absorbed photons by components of the matrix, and the relative reactivites of the generated radicals to the target contaminant and the scavengers. In such a system, a small change in one of the components of the matrix may result in a dramatic change in the observed degradation rate. The dependence of the 185 nm AOP on these potential influences requires confirmation and a minimal set of parameters to characterize the process should be identified.

While it is a straight forward matter to measure the molar absorbance coefficients of compounds above 190 nm, below this wavelength commercial spectrophotometers exhibit substantial error due to stray radiant energy. This stems from the use of a broad spectrum deuterium lamp as the UV source of such instruments, the amount of power emitted below 190 nm being very small relative to longer wavelengths extending to 300 nm. If imperfections in grating monochrometers result in even a small amount of longer wavelength stray radiation entering an aqueous sample, such longer wavelength radiation will emerge from the sample with negligible attenuation relative to 185 nm, reaching the detector as a significant contribution to the detected signal. Thus, the effect of stray radiant energy results in

the detected absorbance signal appearing to have a lower magnitude than the actual value. Furthermore, errors due to finite slit widths compound the inaccuracies of measurement when the magnitude of absorption varies strongly with wavelength. Ideally, dedicated instruments would employ a low pressure mercury lamp, which would provide a powerful source of 185 nm radiation that is easily isolated by a monochrometer. No such instrument is currently commercially available, and unless methods of compensating for or reducing the effect of stray radiant energy are explicitly described, any absorbance measurements reported using commercial instruments are suspect of substantial error. Alternative methods of measuring absorbance coefficients are needed. For further discussion of this topic, see Burgess and Frost (1999) and Sommer (1989).

Lastly, the by-products of aqueous reactions of $Cl^{\bullet}$ and $SO_4^{\bullet -}$ are virtually unknown. In particular, the possibility of $Cl^{\bullet}$ reacting by addition to aromatic rings, such as those that abound in humic and fulvic acids, should be investigated in order to determine whether the 185 nm AOP generates halogenated organics in the presence of Cl^- and DOM.

1.7 Research Objectives

The design of a practical 185 nm AOP depends critically on proper hydraulic mixing, optimal use of radiation, and an accurate reaction model. A reliable model of a reacting system requires the identities of the reacting species, the elementary reactions in which they participate, and the kinetic rate constants of these reactions. The specific objectives of this work focus on fundamental information required for a useful reaction model of the 185 nm AOP. These are:

Temperature: Investigation of the impact of water temperature on the 185 nm AOP. Given the potential effects of temperature over the typical range of operation, and the unknown influence on water absorbance at low

temperatures and photolysis quantum yield, a quantitative observation of these effects are desired to assess their significance.

Dissolved Organic Matter: Investigation of the influence of DOM, both as an absorber of 185 nm and as a scavenger of radicals formed. The DOM to be studied includes well characterized NOM reference materials from the International Humic Substances Society (IHSS), as well as pure organic substances used as model compounds. Interactions of DOM and Cl^-, SO_4^{2-}, and HCO_3^- on the kinetics are included.

Inorganic Anions: Evidence of the role of $Cl^\bullet$ and $SO_4^{\bullet-}$ as reactive species and significant contributors to oxidative degradation is gathered. The dual influence of HCO_3^- as an absorber of photons and a radical scavenger is studied. Interactions between Cl^-, SO_4^{2-}, and HCO_3^- are investigated.

Molar Absorption Coefficients at 185 nm: Alternative methods of quantifying the molar absorption coefficients (ϵ_{185}) of major solutes are required that do not suffer from errors associated with stray radiant energy or finite monochrometer slit widths. An alternative indirect method is investigated.

In order to achieve these goals, a suitable bench-scale apparatus is developed that will allow photochemical kinetic experiments to be conducted quantitatively. An important element of this approach is the identification and characterization of appropriate probe compounds and the ability to eliminate, compensate or correct for the presence of 254 nm radiation.

Chapter 2

Experimental Approach

2.1 General Approach

In order to study the influences of temperature and major solutes systematically, it is expedient to do so at bench-scale with as many variables controlled as possible. This is facilitated by using a quasi-collimated beam apparatus for the continuous irradiation of a well mixed sample of precisely known composition. The influence of the variables of interest on the kinetics of the system may then be measured using a suitably selected probe compound. The precise composition of the irradiated systems is ensured by assembly of the solutions using ultrapure water and analytical grade reagents, with verification by instrumental analysis. Lastly, before the experiments of primary interest are conducted, key assumptions and experimental conditions should be tested. The theoretical approach, experimental techniques, and preliminary tests are reviewed in this chapter.

2.2 The Probe Compound and the Observable k'

A probe compound is a compound added to a water matrix being studied prior to irradiation and in a sufficiently small quantity so as to have negligible impact on the relevant properties of the solution. Upon irradiation, photochemically induced degradation of the probe occurs. Samples of the solution, after various amounts of irradiation, are obtained and analyzed for the remaining probe concentration.

Under 185 nm irradition, the apparent reduction in probe concentration may

occur by several mechanisms. One mechanism involves probe oxidation by radicals generated in solution subsequent to the absorption of 185 nm photons, primarily $^{\bullet}$OH as a product of water photolysis. A second mechanism involves the direct photolysis of probe molecules by absorption of 254 nm photons, which are simultaneously emitted from the low pressure mercury lamp at a much higher proportion relative to 185 nm. Other significant mechanisms may include volatilization and hydrolysis. With regard to direct photolysis of trace contaminants at 185 nm, as discussed in Chapter 1, this process is considered negligible.

Since, only mechanisms involving 185 nm radiation are of interest, other mechanisms may be avoided by the selection of an appropriate probe compound and proper experimental techniques. Criteria for a suitable probe include ease of analysis, low limit of detection, sufficient aqueous solubility and stability, and negligible rate of direct 254 nm photolysis. Probe selection and characterization is discussed in detail in a subsequent section.

Photogenerated $^{\bullet}$OH reacts with the probe compound C, typically producing a mixture of oxidized products:

$$C + {}^{\bullet}\mathrm{OH} \longrightarrow C'_{ox} + C''_{ox} + C'''_{ox} + ... \tag{2.1}$$

The reaction occurs with a second-order rate constant $k_{\mathrm{OH},C}$, which if unknown may be determined experimentally by competitive kinetics relative to a reference compound for which the rate constant is known. The degradation rate of C is given by the Law of Mass Action as:

$$\frac{d[C]}{dt} = -k_{\mathrm{OH},C}[^{\bullet}\mathrm{OH}][C] \tag{2.2}$$

Due to the high reactivity of $^{\bullet}$OH with many solutes, it is usually a reasonable assumption that once irradiation of the sample has begun, the $^{\bullet}$OH concentration rapidly increases until the rate of generation equals the rate of consumption by reaction. At this point, a steady-state $^{\bullet}$OH concentration is achieved, typically very small ($< 10^{-9}$ M), within a time period very short relative to the total time of irradiation (i.e. $\ll 1$ s). With a constant value of $[^{\bullet}\mathrm{OH}]_{ss}$ in equation 2.2, integration yields the solution:

$$ln([C]_t/[C]_o) = -k_{\mathrm{OH},C}[^{\bullet}\mathrm{OH}]_{ss}\, t \tag{2.3}$$

where $[C]_t$ is the probe concentration remaining after an irradiation time of t, and $[C]_o$ is the initial probe concentration. If the steady-state assumption is indeed valid, then a plot of $ln([C]_t/[C]_o)$ vs. t will appear first-order and produce a straight line, with a slope equal to $k_{\mathrm{OH},C}[^{\bullet}\mathrm{OH}]_{ss}$. Equation 2.3 may then be simplified to:

$$ln([C]_t/[C]_o) = -k'\, t \tag{2.4}$$

with k' as the pseudo-first order rate constant with dimensions of reciprocal time (T^{-1}). If k' is measured experimentally, and $k_{\mathrm{OH},C}$ is known, then an

estimate of $[^{\bullet}OH]_{ss}$ may be calculated.

The single term k' contains the dependences of temperature and solution composition. If controlled changes in solution conditions induce an increase or decrease in k', such relationships may be investigated quantitatively and further insight possibly deduced. The pseudo-first order rate constant k' is thus the main experimental response used as the observable for this study.

2.3 Expressing the Extent of Reaction

Equations 2.3 and 2.4 imply that the extent of reaction is measured by the exposure time t, or time of irradiation. However, the extent of photochemical reactions are not determined by the exposure time in general, but by the number or amount of photons absorbed per unit of absorbing material D. This fact may be considered a consequence of what are often referred to as the first and second laws of photochemistry. Quoting from Calvert and Pitts (1966), the first law, formulated by Grotthus and Drapper, states:

"*Only the light which is absorbed by a molecule can be effective in producing photochemical change in the molecule.* "

The first law implies that before any photochemical reaction can occur, photons must be absorbed.

Again, quoting from Calvert and Pitts (1966), the second law, deduced by Stark, Einstein, and Bodenstein, states:

"*The absorption of light by a molecule is a one-quantum process so that the sum of primary process quantum yields* Φ_i *must be unity* (*i.e.* $\Sigma\Phi_i = 1$). "

The second law applies in the absence of chain reactions, biphotonic processes, and composite reactions that involve photon absorption in more than

a single step. During the UV irradiation of aqueous solutions, the lifetimes of photogenerated radicals are sufficiently short, and the products of reaction sufficiently nonreactive in general, that no chain reactions are expected to occur. Furthermore, no evidence of such chain reactions has been reported in the literature. Biphotonic processes involve the sequential absorption of two photons by a single molecule. While this may readily occur in the case of high intensity radiation provided by a laser, under irradiation via an incoherent source, such as the low pressure mercury lamp, the population of molecules excited by an initial photon is sufficiently small, and their lifetimes sufficiently short, that the probability of an excited state molecule absorbing a second photon is assumed to be negligible. Lastly, while the 185 nm based degradation of trace organics is certainly a composite reaction, only a single photon absorption is assumed involved per molecule degraded.

Thus, under continuous incoherent irradiation, the extent of reaction may be determined if both the exposure time, t, and the rate of photon absorption per unit of absorbing material, I_a, are known. The product given by:

$$D = I_a\, t \tag{2.5}$$

provides the number or amount of photons absorbed per unit of absorbing material upon a given exposure time. For a given solution, any combination of I_a and t that produces a given value of D will yield the identical extent of reaction. The comparison of two photochemical reaction systems, therefore, should be based on D, and not on t alone, since in general I_a will differ. Furthermore, it is the cumulative value of D that dictates reaction extent, regardless of whether irradiation is continuous or intermittent. This detail is important for nearly opaque fluids such as water at 185 nm. Adopting a Lagrangian description of a fluid, during mixing the microscopic volume

elements of fluid will absorb photons primarily while passing near irradiated interfaces but not while further away. Since, in such a volume element, I_a varies with time, D for a given element will be obtained by an integral, $D = \int I_a(t)dt$, of the element's $I_a(t)$ history.

For highly absorbing fluids, the local value of I_a at each spatial point in the fluid will drastically decrease with distance from the irradiated interface. This is the case for water under 185 nm and optical path lengths on the order of a few centimetres. The spatial profile of I_a may thus involve a very high value near the interface, attenuating to vanishingly small values further inside the fluid. The value of I_a accessible to measurement is the average over the irradiated volume. It is shown by Calvert and Pitts (1966) that if a filled sample cell is uniformly irradiated by a parallel beam, and if the diffusion (or lifetime) of radicals can be neglected, the measured and local rates will be identical if I_a appears in the rate law to the first power (i.e. $d[C]/dt \propto {I_a}^n$, with $n = 1$). The first-order assumption of I_a in the rate expressions of the 185 nm AOP is based on the assumptions that the composite reactions involve only a single photon absorbing step, and that chain reactions and biphotonic processes are absent. Considering equation 2.2, this is equivalent to assuming $[^{\bullet}\mathrm{OH}]_{ss} \propto I_a$.

Equation 2.4 can be rewritten in terms of D rather than t:

$$ln([C]_D/[C]_o) = -k'' D \tag{2.6}$$

If D is expressed in units of $\mathrm{mol\,L^{-1}}$, then k'' must have the reciprocal units of $\mathrm{L\,mol^{-1}}$. Alternatively, D and k'' may be expressed in energy units using the molar photon energy of $6.47 \times 10^5\,\mathrm{J\,mol^{-1}}$ at 185 nm. Then I_a may be expressed in units of $\mathrm{mol\,L^{-1}\,s^{-1}}$ (or $\mathrm{J\,m^{-3}\,s^{-1}}$). Furthermore, k' and k'' are

simply related by $k' = k'' I_a$, and thus interconversion between equations 2.4 and 2.6 requires only that I_a be known.

If an irradiated fluid is well mixed, the absorbed photons are evenly distributed throughout the entire fluid volume. If the fluid is nearly opaque (i.e. $> 99\%$ photon absorption), the rate of photon absorption per unit volume I_a may be calculated from:

$$I_a = \frac{I_o\, S}{V} \tag{2.7}$$

where I_o is the incident photon fluence rate ($\mathrm{mol\,m^{-2}\,s^{-1}}$), S is the surface area through which the incident radiation enters the fluid ($\mathrm{m^2}$), and V is the volume of absorbing solution under irradiation ($\mathrm{m^3}$). Again, using the molar photon energy at 185 nm, the fluence rate may be expressed with units of $\mathrm{J\,m^{-2}\,s^{-1}}$. If the incident irradiation is nearly collimated, the incident fluence rate is approximately equal to the incident irradiance. The incident photon fluence, F ($\mathrm{mol\,m^{-2}}$), is obtained from the product $I_o\, t$. Alternative expressions for D are thus given by:

$$D = \frac{I_o S t}{V} = \frac{F}{\ell} \tag{2.8}$$

where ℓ is the optical path length or depth of the uniformly irradiated solution. Using chemical actinometry or a calibrated electronic radiometer, I_o may be measured.

Note that to make absolute kinetic measurements and quantitative compar-

isons between different UV reaction systems, D should be used and the value of I_o, or its equivalent, must be known. If making comparative kinetic measurements of different opaque solutions using the identical reaction system, then t may be used, as I_o will be identical between cases and I_a approximately so.

2.4 A 185 nm Kinetic Model

For comparative investigations of the temperature and major solute effects on 185 nm kinetics, an equation for the observable, k', in terms of parameters that are either known or can be measured is useful. A model is proposed based on the relation of $[^{\bullet}\mathrm{OH}]_{ss}$ to such parameters, and is obtained by invoking the steady-state assumption. Implicit in the steady-state assumption is that the rate of $^{\bullet}$OH generation equals the rate of its consumption. The rate of $^{\bullet}$OH generation by photolysis of water is given by:

$$\frac{d[^{\bullet}\mathrm{OH}]}{dt} = \Phi_{\mathrm{H_2O}}\, f_{\mathrm{H_2O}}\, I_a \tag{2.9}$$

where $\Phi_{\mathrm{H_2O}}$ is the quantum yield for water photolysis at 185 nm, approximately equal to 0.3 (equation 1.1), and $f_{\mathrm{H_2O}}$ is the fraction of photons absorbed by water.

In a solution composed of multiple solute species $S_1, S_2, ...$, each species S_i reacts with $^{\bullet}$OH with a second-order rate constant of k_{OH,S_i}. The rate of $^{\bullet}$OH consumption is given by the Law of Mass Action and may be written as a summation of all reactions $^{\bullet}\mathrm{OH} + S_i$:

$$\frac{d[^{\bullet}\mathrm{OH}]}{dt} = \sum_i k_{\mathrm{OH},S_i}\,[^{\bullet}\mathrm{OH}]_{ss}\,[S_i] \tag{2.10}$$

Under steady-state conditions $d[^{\bullet}\mathrm{OH}]/dt = 0$, and by equating equations 2.9 and 2.10, the expression for $[^{\bullet}\mathrm{OH}]_{ss}$ may be written as:

$$[^{\bullet}\mathrm{OH}]_{ss} = \frac{\Phi_{\mathrm{H_2O}}\, f_{\mathrm{H_2O}}\, I_a}{\sum k_{\mathrm{OH},S_i}\,[S_i]} \tag{2.11}$$

As discussed above, I_a on the right-hand side of equation 2.10 is the average value over the volume. Consequently, the value of $[^{\bullet}\mathrm{OH}]_{ss}$ on the left-hand side is also the volume averaged value. Yet, it is acknowledged that, like I_a, the local value of $[^{\bullet}\mathrm{OH}]_{ss}$ is greatest at the irradiated interface and attenuates rapidly deeper into the fluid. As the lifetime of $^{\bullet}$OH is sufficiently short, on the order of microseconds, diffusion is negligible and each microscopic volume element will receive varying amounts of $^{\bullet}$OH as it travels, depending on the local value of I_a along its trajectory.

The combinations of equations 2.3, 2.4, and 2.11 yields the following:

$$k' = \frac{k_{\mathrm{OH},C}\,\Phi_{\mathrm{H_2O}}\, f_{\mathrm{H_2O}}\, I_a}{\sum k_{\mathrm{OH},S_i}\,[S_i]} \tag{2.12}$$

The right-hand side of equation 2.12 is the observable obtained from experiment, calculated from the diminishing concentration of C with increasing

t. Note that if the initial concentration of the probe compound $[C]_o$ is sufficiently small, then it will contribute negligibly to the sum $\sum k_{\mathrm{OH},S_i}\,[S_i]$. The value of $[^{\bullet}\mathrm{OH}]_{ss}$ (equation 2.11) and k' (equation 2.12) will therefore be independent of the probe compound concentration $[C]_o$. This condition is satisfied when $k_{\mathrm{OH},C}[C]_o \ll \sum k_{\mathrm{OH},S_i}\,[S_i]$. A value for $[C]_o$ has been selected throughout this work such that $k_{\mathrm{OH},C}[C]_o$ is at least ten times less than the value of $\sum k_{\mathrm{OH},S_i}\,[S_i]$ for all other scavengers.

If comparative studies are conducted, say between two temperatures or two concentrations of a particular solute S_i, the relative values of the resulting k'_1 and k'_2 may be related using 2.12 without the knowledge of I_a, provided it is common to both cases. However, if a solution is obtained for which all the terms of the left-hand side are known, except I_a, then I_a may be determined once k' is measured. Subsequently, I_a may be used to calculate I_o, or convert the abscissa coordinate of kinetic plots from a t-scale to a D-scale. By this approach, a method of measuring I_o, as an alternative to chemical actinometry and electronic radiometry, is made available.

The discussion thus far is predicated on the assumption that water is an opaque solution at 185 nm, and this is approximately true for optical path lengths of 1 cm or more. However, for shorter depths water may be considered either semitransparent or transparent, and the calculation of absorbed energy must be modified accordingly. For such cases, a useful discussion is provided by Harm (1980).

In the case that 185 nm photons are absorbed by other solutes, and generate other radicals able to react with the probe compound C, the observed rate constant k' may be expanded to include additional contributions. Based on the discussion from Chapter 1, it is known a priori that in addition to $^{\bullet}\mathrm{OH}$, the radicals $\mathrm{Cl}^{\bullet}$ and $\mathrm{SO}_4^{\bullet-}$ may also be significant oxidants of C. The expression for k' may thus be expanded to:

$$k' = k_{\mathrm{OH},C}\,[^{\bullet}\mathrm{OH}]_{ss} + k_{\mathrm{Cl},C}\,[\mathrm{Cl}^{\bullet}]_{ss} + k_{\mathrm{SO_4^-},C}\,[\mathrm{SO_4^{\bullet -}}]_{ss} \tag{2.13}$$

If the generation of each of these radicals is assumed to be independent, with negligible interconversion between them, the steady-state radical terms may be expressed in the general form:

$$[R^{\cdot}]_{ss} = \frac{\Phi_R f_R I_a}{\sum k_{R,S_i}[S_i]} \tag{2.14}$$

where Φ_R is the quantum yield of the photochemical generation of the radical at 185 nm, and f_R is the fraction of 185 nm photons absorbed by the parent species generating $R^{\cdot}$. The sum of the f_R values may not equal unity if other solutes exist that also absorb a significant fraction of 185 nm photons, yet do not contribute to the radicals included in equation 2.14. The contribution of each of the terms of k' will depend on the distribution of absorbed photons (f_R), the overall reactivity of the solution with each radical ($\sum k_{R,S_i}[S_i]$), and the reactivity of the probe compound with each radical ($k_{R,C}$). The key assumption in using equation 2.14 in the equation 2.13 is that interconversion between radical species is negligible. This assumption is tested experimentally in subsequent chapters. While discrepancies between observations and predictions using equations 2.13 and 2.14 will require modification of the model, the details of the discrepancies themselves may shed mechanistic insights. Lastly, additional terms may be added to the above to incorporate additional radical species other than the three considered thus far.

The fractions f_R of absorbed photons by each absorbing solute of the solution are given by:

$$f_R = \frac{\alpha_R}{\alpha_{tot}} \tag{2.15}$$

where α_R is the absorption coefficient for solute R, and α_{tot} is the absorption coefficient for the entire solution, both with units of cm^{-1}. The value of $\alpha_{tot} = \alpha_{R_1} + \alpha_{R_2} + ... = \Sigma\alpha_{R_i}$. For a given solute S_i, the value of α_i is related by $\alpha_i = \epsilon_i[S_i]$, where ϵ_i is the molar absorption coefficient for solute S_i, with typical units of $\mathrm{M}^{-1}\,\mathrm{cm}^{-1}$.

2.5 Experimental Apparatus

Two collimated beam apparatus were used for this study and are described here. As true collimation requires the absence of divergence of radiation, with the electromagnetic wavefront forming a plane normal to the direction of propagation (i.e. optical path), the apparatus used here are understood to imply quasi-collimated devices designed to sufficiently approximate true collimation. One of the collimated beams was dedicated to studies of the 185 nm regime, and a second for 254 nm - H_2O_2 regime (UV/H_2O_2) studies. The former is described in detail below and illustrated in Figure 2.1. The latter is similar but without nitrogen gas purging capabilities or the emission of 185 nm radiation.

The 185 nm collimated beam used a low pressure mercury lamp with an envelope made of undoped quartz (LightSources Inc, Orange CT USA) and a copper ballast. Such lamps are often referred to as “ozone generating” by lamp manufacturers. The odour of ozone is readily detected when these

lamps are ignited in ambient air. The lamp was mounted in a tubular aluminum housing with an aperture for fitting of a collimation tube and two ports for purging air from the optical path with nitrogen gas. The interior of the aluminum housing was polished to increase reflectance of radiation above the collimation tube. The collimation tube used in all 185 nm experiments was composed of black teflon, measured 18 cm in length and 3.2 cm inner diameter, and had an inside surface roughened to reduce reflection. The sample cells (i.e reaction vessels) were commercially available precision cylindrical cells made of fused silica (Starna, Atascadero CA USA), either 1.0 cm or 2.0 cm in path length, with teflon stoppers and miniature teflon coated magnetic stir bars placed inside. These cells had an inner diameter of 1.9 cm, ensuring complete cross-sectional illumination of the sample under the collimation tube. For irradiation, a sample filled cell was placed atop a small stir plate, mounted upon an x-y stage fastened to a laboratory jack stand, and aligned beneath the collimation tube with the shutter closed. The vertical position of the top of the cell was adjusted with the jack stand to a common height used in all experiments. A wide shutter housing was fastened to the bottom of the collimation tube. A transparent curtain of plastic, extending approximately 3 cm below the bottom of the shutter housing, and overlapping the sample, was used to ensure an uninterrupted flow of nitrogen gas down the collimation tube and over the sample. Nitrogen flow around the sample was tested using a smoke pen. The nitrogen gas ports of the lamp housing were located on opposite ends of the housing to reduce dead zones and used barbed brass fittings to accept plastic tubing carrying nitrogen gas from a standard cylinder. A regulator on the cylinder was set to a nominal pressure of 5 psi and a rotameter was used to measure and regulate the flow of nitrogen into the lamp housing to $\sim 5\,\mathrm{L\,min^{-1}}$. For temperature control, a custom made mount was fabricated (Quantum Northwest, Liberty Lake WA USA) and is described in more detail in Chapter 3. A shutter of thick card was used via a slot in the shutter housing and operated manually in coordination with a stop-watch to measure exposure times. During daily initial use, nitrogen flushing was initiated, followed by the ignition of the lamp, and the system allowed to stabilize for at least

twenty minutes prior to any sample irradiations.

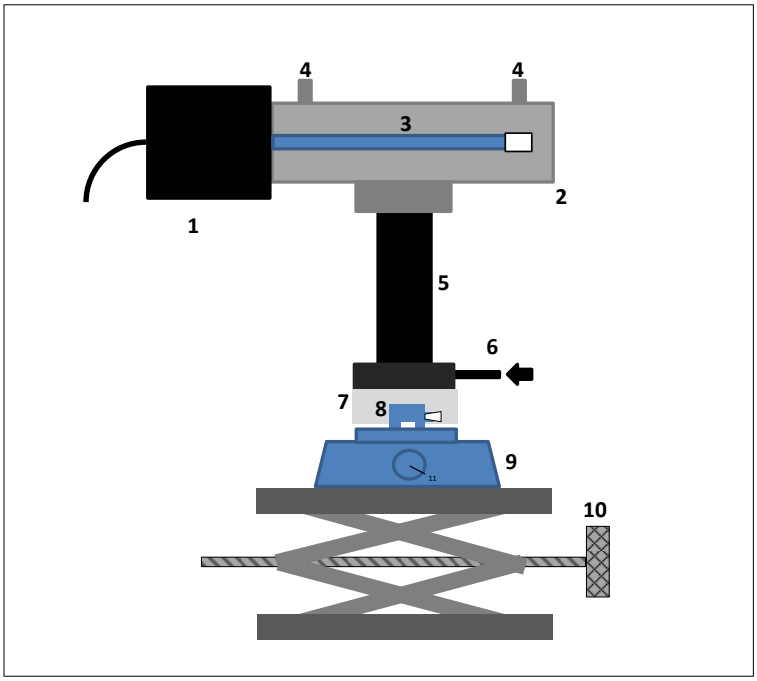

Figure 2.1: The 185 nm Collimated Beam Apparatus: 1. copper ballast and lamp socket, 2. aluminum lamp housing, 3. low pressure mercury lamp (inside housing), 4. nitrogen gas ports, 5. teflon collimation tube, 6. shutter (in open position), 7. plastic curtain, 8. fused silica sample cell with teflon stir bar and stopper, 9. magnetic stir plate, 10. laboratory jack stand

The 254 nm collimated beam used for UV/H_2O_2 experiments also used a low pressure mercury lamp (LightSources Inc, Orange CT USA), which as mentioned above prevents the emission of 185 nm radiation and is often described by lamp manufacturers as "germicidal" and "non-ozone generating". The lamp was cooled using ambient air via fans to push air through the lamp housing. A collimation tube, painted black, provided a distance from lamp to liquid sample surface of at least 30 cm with an inner diameter of 6 cm. Samples were held in 50 mL dishes of less than 5 cm inner diameter, placed upon a stir plate and used teflon coated stir-bars. The stir plate was

placed upon a laboratory jack stand for accurate vertical position control. For temperature controlled experiments, this dish was replaced by a custom fabricated water jacketed miniature borosilicate glass beaker (Cansci Glass Products Ltd, Richmond BC Canada) through which water flowed from an external recirculating chiller (Thermo Fischer Scientific, Waltham MA USA) via plastic tubing. Additional details on temperature control are found in Chapter 3.

2.6 Materials

All solutions were made using ultrapure water (18.2 MΩ cm). Analytical grade reagents (Sigma-Aldrich, St. Louis MO USA) were used for all chemicals, other than Natural Organic Matter (NOM). Well characterized NOM reference materials were obtained from the International Humic Substances Society (IHSS) as reverse osmosis isolates in freeze dried powder form. Both Suwannee River and Nordic Lake NOM stock solutions were made by dissolving NOM powder in water acidified with H_2SO_4, neutralizing the solutions with NaOH, and filtering by pre-washed 0.45 µm filters into glass bottles for storage at 4 °C until use. Ultrahigh purity nitrogen gas (Praxair Canada Inc, Mississauga ON Canada) was used for purging air from the optical path of the 185 nm enabled collimated beam.

2.7 Probe Compound Selection and Characterization

The two probe compounds used in this work were carbamazepine (CAS Number 298-46-4) and nitrobenzene (CAS Number 98-95-3). The primary criteria used for selecting the probe compounds were: (1) ease of quantification by HPLC with UV detection and (2) negligible direct photolysis at 254 nm relative to $^{\bullet}OH$ oxidation under experimental conditions. The latter

criteria obviates the need to eliminate 254 nm radiation from the 185 nm collimated beam, or correct for its effect. An additional criteria was that compounds be of practical interest as environmental contaminants. Carbamazepine, a common and persistent pharmaceutical, is a useful indicator and tracer of wastewater influences in the environment remote from the point of discharge (Clara et al., 2004; Tixier et al., 2003), while nitrobenzene is a well known industrial contaminant.

The direct photolysis rate at 254 nm is proportional to the product of the molar absorption coefficient (ϵ_{254}) and the quantum yield (Φ_{254}) at 254 nm. If either of these parameters are sufficiently low, then direct photolysis will be negligible. To ensure this was the case for both carbamazepine and nitrobenzene, these parameters were measured. Additionally, the second-order $^{\bullet}$OH rate constants ($k_{\mathrm{OH},C}$) of each are required, and may be determined by competitive kinetics with a reference compound. The reference compound used was para-chlorobenzoic acid or pCBA (CAS Number 74-11-3). The experimentally determined values of ϵ_{254}, Φ_{254}, and $k_{\mathrm{OH},C}$ are listed in Table 2.1.

Table 2.1: Photochemical reaction parameters for probe compounds at 254 nm

Compound	ϵ_{254} $(\mathrm{M^{-1}\,cm^{-1}})$	Φ_{254}	$k_{\mathrm{OH},C}$ $(\mathrm{M^{-1}\,s^{-1}})$
carbamazepine	6759 ± 190	0.00067 ± 0.00002	$6.8 \pm 0.6 \times 10^9$
nitrobenzene	6240 ± 130	0.007 ± 0.001	3.9×10^9 [a]
pCBA	3410 ± 75	0.011 ± 0.003	5.0×10^9 [b]

[a] Reference rate constants from Buxton et al. (1988)
[b] Reference rate constants from Neta and Dorfman (1968)

It can be seen that it is the low value of Φ_{254} for carbamazepine that ensure negligible 254 nm photolysis relative to the reference pCBA. Furthermore, both carbamazepine and nitrobenzene probes are superior to pCBA based on chromatographability, producing larger HPLC peaks with larger dynamic

ranges and lower limits of detection due to higher ϵ_λ values in the UV. Also, their peaks are more symmetric as a result of negligible acidity of either molecule. Organic acids, such as pCBA ($pK_a \sim 4$), are generally more prone to peak asymmetry and are highly sensitive to mobile phase pH when within approximately two pH units of the pK_a. While pCBA has been a popular probe in AOP literature, its replacement by carbamazepine would improve results. Unlike nitrobenzene, carbamazepine is of negligible volatility, simplifying experimental techniques and analysis.

2.7.1 Molar Absorption Coefficients at 254 nm

For the determinations of ϵ_{254}, a series of solutions were made by dilution of a stock of known concentration prepared gravimetrically. The absorbance of each solution was then measured at 254 nm in a 1.0 cm path length quartz cuvette using a UVmini-1240 Spectrophotometer (Shimadzu, Kyoto Japan). The slope of the concentration versus the absorbance was calculated by linear regression, then used to calculate ϵ_{254} based on the Beer-Lambert law. Triplicate determinations were made using three separate gravimetric preparations of stock solutions. The final results are averages of three determinations. See Appendix - Table A.2 for data.

2.7.2 Photolysis Quantum Yields at 254 nm

For determinations of Φ_{254}, solutions of each probe alone in ultrapure water at a concentration of approximately 1 µM were irradiated by 254 nm collimated beam for a range of exposure times, with the remaining concentrations quantified by HPLC. The incident fluence rate I_o at 254 nm, for these exposures, was determined by KI-KIO_3 actinometry. Since such solutions are nearly transparent at 254 nm, the incident and volume averaged fluence rates are approximately equal. The measured I_o was used to convert the observed time-based direct photolysis rate constant k'_d, with units s^{-1}, to fluence-based rate units of $m^2\,J^{-1}$. Then, values of Φ_{254} were calculated

from the fluence-based expression for k'_d given by (Bolton and Stefan, 2002):

$$k'_d = \frac{\Phi_{254}\,\epsilon_{254}\,ln(10)}{10\,U_{254}} \tag{2.16}$$

where ϵ_{254} has units of $\mathrm{M^{-1}\,cm^{-1}}$, and U_{254} is the molar photon energy $4.72 \times 10^5\,\mathrm{J\,mol^{-1}}$, using the more precise wavelength of 253.7 nm. Dark controls are essential for nitrobenzene to correct for volatilization, unless a sealed irradiation cell is used. See Appendix - Tables A.3 to A.7 for data.

2.7.3 Second-order $^{\bullet}$OH Rate Constants

The second-order rate constants of the probe carbamazepine with $^{\bullet}$OH ($k_{\mathrm{OH},C}$) was determined using competitive kinetics in the UV/H_2O_2 system, with pCBA as the reference compound, using $k_{\mathrm{OH},pCBA} \equiv 5.0 \times 10^9\,\mathrm{M^{-1}\,s^{-1}}$ (Neta and Dorfman, 1968). A H_2O_2 concentration of $5.0\,\mathrm{mg\,L^{-1}}$ was used. 2-methyl-2-propanol (CAS Number 75-65-0), commonly known also as tert-butanol, was used as an $^{\bullet}$OH scavenger at a concentration of approximately $10\,\mathrm{mg\,L^{-1}}$. This scavenger was used to ensure that the value of $[^{\bullet}\mathrm{OH}]_{ss}$ remains constant over the time of irradiation and that the contribution of the probe compounds to the $^{\bullet}$OH scavenging in solution is negligible (i.e. $k_{\mathrm{OH},C}[C] \ll \Sigma k_{\mathrm{OH},S}[S]$ for each). Absorbance of 254 nm by tert-butanol is negligible ($\epsilon_{254} < 10\,\mathrm{M^{-1}\,cm^{-1}}$). Tert-Butanol has been widely used as a scavenger in pulse radiolysis studies (Schuchmann and Von Sonntag, 1979), often in competitive kinetics determinations of rate constants. See Appendix - Tables A.8 to A.11 for data.

2.8 Analytical Methods

HPLC Analysis: The quantification of the probe compounds, carbamazepine and nitrobenzene, and the reference compound pCBA, were performed by high-performance liquid chromatography (HPLC) using a Dionex UltiMate 3000 System (Thermo Fisher Scientific, Waltham MA USA). The autosampler withdrew a 100 µL sample volume from each vial, injecting it into a 15 mm C18 column maintained at 35 °C in isocratic mode. A mobile phase flow of 1.0 mL min^{-1} was used and composed of 30% acetonitrile and 70% water acidified to pH 2.5 with approximately 10 mM of phosphoric acid. UV detection was performed using one of three wavelengths 211, 239, and 265 nm. Use of 211 nm allowed the greatest dynamic range, while in the presence of NOM interference required use of longer wavelengths. Stock solutions were prepared gravimetrically using 5 mL volumetric flasks and a small amount of methanol as a cosolvent. The stock solutions were then either diluted using ultrapure water to form working intermediate stock solutions or diluted to a set of standards using the HPLC mobile phase as diluent. The dynamic range was found to span concentrations from 2 µM down to 0.01 µM with the %RSD always less than 2.5% (see Appendix - Table A.1).

DOC Analysis: All dissolved organic carbon (DOC) measurements were performed by a GE Sievers M9 TOC Analyzer (GE Analytical Instruments, Boulder CO USA), using the UV-persulfate method. Standard solutions of potassium hydrogen phthalate (CAS Number 877-24-7) were used for instrument calibration, and to verify DOC measurements of gravimetrically prepared solutions of tert-butanol, methanol, acetate, and acetone, as well as the reference materials Suwannee River and Nordic Reservoir NOM. Note that all samples analyzed were either filtered with sub-micron pore size filters or composed of particle free pure solutions. Thus the measurements made by TOC are equivalent to the operationally defined DOC.

Ion Exchange Chromatography: The anionic composition of all solu-

tions assembled from analytical grade reagents and ultrapure water were verified in concentration against prepared standards and checked for contaminants using ion exchange chromatography, A Dionex Ion Chromatography system (Thermo Fisher Scientific, Waltham MA USA) was used.

KI-KIO_3 Actinometry at 254 nm: Quantification of 254 nm fluence rates were performed using the KI-KIO_3 actinometer (Bolton et al., 2011; Rahn, 1997; Rahn et al., 2003). Quantification of I_3^- was performed spectrophotometrically at 350 nm, using a UVmini-1240 spectrophotometer (Shimadzu, Koyoto Japan).

Quantification and Quenching of Hydrogen Peroxide: The H_2O_2 concentration applied in UV/H_2O_2 experiments, both prior to and following irradiations was performed using the I_3^- method (Klassen et al., 1994). Samples were quenched of remaining H_2O_2 using bovine catalase (Sigma Aldrich) prior to HPLC analysis. Quenching used a 10 µL droplet of 100 µg L^{-1} of catalase, placed at the bottom of an HPLC vial before a 1 mL sample of solution was added. Quantification of I_3^- was measured spectrophotometrically at 350 nm using a UVmini-1240 spectrophotometer (Shimadzu, Koyoto Japan).

pH: An Oakton pH meter calibrated at pH 4, 7, and 10 was used for all pH measurements using a disposable type gel filled probe.

2.9 Initial Testing of 185 nm Experimental Methods

This section describes the preliminary investigations and due diligence performed regarding the performance of the 185 nm collimated beam experiments.

Mixing Conditions: Among the requirements of the collimated beam approach is the need for the irradiated sample volume to be well mixed. To ensure that the extent of reaction was not influenced by the mixing speed, the degradation rate of carbamazepine was measured at three speeds of the stir plate (approximately 500, 1000, 1500 rpm) during 10 minute irradiations. No effect was found, and circa 1000 rpm was used for all subsequent experiments, due to greater stability of the stir bar operation at that speed.

Dissolved Oxygen: While the presence of dissolved O_2 creates oxidative conditions in the 185 nm regime by scavenging $H^{\bullet}/e^{\bullet-}_{aq}$, the absence of dissolved O_2 may induce reductive conditions. In the presence of pure nitrogen gas flowing over an irradiated sample, O_2 in solution is stripped and ultimately depleted if the solution is not covered. Tests using ultrapure water saturated with air, in both open 10 mL beakers and teflon stoppered fused silica cuvettes (i.e. cells), were tested for dissolved O_2 following irradiations in the 185 nm collimated beam. During irradiations, N_2 flowed at $5\,L\,min^{-1}$ over the beakers or cells, mixed with miniature stir bars. A modified iodometric method based on Winkler's titration revealed that approximately half the dissolved O_2 was depleted within ten minutes in the open beakers, whereas depletion was negligible when sealed cuvettes were used instead. Thus, cylindrical cuvettes of 1.0 cm were used for all subsequent experiments. A small air bubble was left in the cell next to the teflon stopper and the portion of the cell arm above painted black. The iodometric test for dissolved O_2 miniaturized the quantities of reagents required, and in place of adding starch indicator and titrating with thiosulfate ($S_2O_3^{2-}$), the absorbance at 350 nm was measured, with a calibration curve created from air saturated solutions, N_2 saturated solutions, and mixtures of the two.

Influence of Phosphate Buffer: Ideally, the pH of irradiated solutions should not drift during experiments. Some researchers have used phosphate buffers ($H_2PO_4^-/HPO_4^{2-}$) composed of sodium salts. However, studying the influence of water composition is complicated if the pH buffer itself participates in photochemical reactions. Thus, the use of phosphate buffers

was tested in the 185 nm regime. It was found that orthophosphates do participate in the removal of the probe compound carbamazepine, likely by absorption of photons and formation of phosphate radicals (Maruthamuthu and Neta, 1977). Solutions containing carbamazepine (0.25 µM) and tert-butanol (7.0 mg L^{-1} as C), with phosphate buffer strength of 10 mM at pH 6.0, 7.0 and 8.0, were irradiated. The degradation rate increased with pH, suggesting a greater influence of HPO_4^{2-} relative to $H_2PO_4^-$ (See Appendix - Table A.13 for data). When such solutions at pH 7.0 are tested with increasing buffer strength of 0, 1, 10, and 100 mM, again the degradation rate increases significantly (See Appendix - Table A.13 for data). Thus, phosphate buffers were not used in this work, and the pH of solutions was monitored before and after irradiation to detect significant change. Drifting of pH during irradiations was not observed.

Influence of Fluoride: Kinetic studies often use ionic strength effects to elucidate mechanistic aspects of reacting systems in aqueous solutions. The activity of ionic reactants will be more strongly influenced by changes in ionic strength than neutral molecules. However, if neutral reactants (e.g. $Cl^\bullet$) are in equilibrium with ionic species (e.g. $Cl^\bullet + Cl^- \rightleftharpoons Cl_2^{\bullet-}$), a so-called secondary-salt effect may manifest when ionic strength is varied (Moore and Pearson, 1981). Modifying the ionic strength for this purpose requires a species that will be photochemically inert, neither absorbing radiation nor participating in radical reactions. Sodium fluoride (NaF) was considered for this purpose. The influence of NaF was found to be negligible on the 185 nm system, using carbamazepine (0.25 µM) and tert-butanol (7.0 mg L^{-1} as C), with F^- concentrations of 1, 10, and 100 mg L^{-1} (See Appendix - Table A.14 for data).

Opaque Assumption of Water at 185 nm: The absorbance coefficient of water at 185 nm is relatively high, and in this work is assumed to be 1.8 cm^{-1} (Weeks et al., 1963). Thus, approximately 98% of the radiation entering pure water will be absorbed within a path length of 1.0 cm, with approximately 60% absorbed within a path length of 0.2 cm. Unlike the

optical absorption of water at longer wavelengths, the substantial attenuation of 185 nm radiation over short path length relative to typical lamp and reactor dimensions implies that water is essentially an opaque fluid at that wavelength. As discussed earlier, this fact has important implications on how the absorbed energy dose of a 185 nm AOP is described and imposes severe geometrical constraints on reactor design.

To verify the assumption that water is effectively opaque at 185 nm, two precision cylindrical fused silica cells of path length 1.0 cm and 2.0 cm were filled with the same solution of carbamazepine (0.25 µM) and tert-butanol (7.0 mg L^{-1} as C), irradiated for several exposure times t, and analyzed for the remaining carbamazepine. The results reveal that when $ln([C]_t/[C]_o)$ is plotted, not versus t, but versus t normalized by volume V of sample (i.e. t/V), the slopes of the two curves are in excellent agreement (See Appendix - Table A.15 for data). This supports the description of the extent of reaction using $D = I_o S t/V$ (equation 2.8) and the associated assumptions. While the product $I_o S$ is the same in both cases above, the same value of D is delivered to the two systems only when both terms t/V also equal. Since the volume of the smaller cell is half that of the larger, an exposure time of half as long in the smaller cell, relative to the larger, is required to provide identical values of D to both cells. This result confirms the opacity assumption of water under the conditions used.

$KI-KIO_3$ Actinometry and 185 nm: As discussed above, expressing the extent of reaction in the 185 nm regime requires knowledge of I_a, which can be obtained from I_o in a collimated beam, and used to calculate D via equations 2.5 and 2.7. Measurement of I_o by chemical actinometry at 185 nm with actinometers described in the literature (Kuhn et al., 2004) is difficult, generally requiring gas-tight assemblies and gas chromatography analysis. In contrast, actinometry at 254 nm is a relatively simple determination using the $KI-KIO_3$ actinometer (Bolton et al., 2011; Rahn, 1997; Rahn et al., 2003). Given the high absorbance of I^- expected at 185 nm (Weeks et al., 1963), and the charge-transfer-to-solvent mechanisms involved, it is

reasonable to suspect that 185 nm photons may contribute to the response of the KI−KIO_3 actinometer. If so, then 185 nm radiation would interfere with a 254 nm measurement, causing a spurious response. However, such a condition would allow 185 nm radiation itself to be measured by KI−KIO_3 actinometry using a difference method. Two irradiations would be required. In the first, the full amount of both 185 and 254 nm radiation reach the actinometer. In the second, 185 nm radiation is eliminated before reaching the actinometer, while 254 nm radiation is unchanged from the first case. Under such conditions, any difference in response between the two measurements would be due to the contribution of 185 nm.

To selectively block only 185 nm, while transmitting 254 nm radiation unchanged, a properly design interference filter (Heavens, 1991) or fused silica window doped with titanium may be applied. However, an adequate alternative of much lower cost was used, involving a 12 mm thick optical window of high purity natural quartz (Esco Optics, Oak Ridge NJ USA). It was assumed, and supported by manufacturer information, that 185 nm radiation is attenuated by approximately 40%, due to absorption, over a path length of 2 mm in natural quartz, while negligible absorption occurs for 254 nm radiation over the same distance. Over the 12 mm thick distance of the natural quartz window, therefore, it is calculated that approximately 0.4% of 185 nm radiation entering the window reaches the opposite end. In contrast, full transmission is assumed at 254 nm, minus reflection losses of approximately 4%, estimated using Fresnel's equation at normal incidence (Born and Wolf, 1999), and an estimate of the refractive index at 185 nm (Kitamura et al., 2007).

To test this approach, the actinometer solution was placed in a sealed fused silica cell of 2.0 cm path length, under both the 254 nm and 185 nm collimated beam apparatus, with replicate determinations made at the same exposure time. The resulting apparent incident 254 nm fluence rates I_o were subsequently calculated.

In the case of the 254 nm radiation alone, I_o was determined to be $0.501 \pm 0.013\,\mathrm{mJ\,cm^{-2}}$ without the quartz window, and $0.486 \pm 0.008\,\mathrm{mJ\,cm^{-2}}$ with the quartz window, each averaged over ten replicate irradiations (see data in Appendix - Table A.15). The ratio of the latter to the former is 0.97 ± 0.03, which is in agreement, within experimental error, for what would be expected if only reflection losses from the quartz window are significant. In the case of the 185 nm collimated beam, I_o was found to be $0.872 \pm 0.026\,\mathrm{mJ\,cm^{-2}}$ without the quartz window, and $0.842 \pm 0.017\,\mathrm{mJ\,cm^{-2}}$ with the quartz window, averaged over five replicate irradiations (See Appendix - Tables A.17 for data). The ratio of the latter to the former is 0.97 ± 0.03, identical with that obtained using 254 nm radiation alone.

The conclusion is that the $KI-KIO_3$ actinometer does not respond to the 185 nm radiation present. While this actinometer cannot be used to quantify 185 nm radiation in the present apparatus, neither does 185 nm interfere with 254 nm measurements. Given the reactions proposed to be involved in generation of I_3^- by this actinometer (Rahn, 1997), the absorption of 185 nm by I^- (Fox, 1970) and subsequent generation of $I^\bullet$ is expected. The lack of significance may be due to absorption of 185 nm by other components of the actinometer solution, such as IO_3^-, without contribution to the measured response. The development of a convenient actinometer for use at 185 nm, that is also insensitive to 254 nm radiation, would be useful.

Chapter 3

Temperature

3.1 Temperature and Water Treatment

Seasonal fluctuations in surface water temperature span a wide range at latitudes far from the equator, often from 0 to 20 °C or more. Treatment processes in such locations must ensure adequate performance regardless of temperature. Cold temperatures generally present a greater challenge. The higher viscosity of cold water reduces the particle removal efficiency of solid-liquid separation processes. Depressed reaction rates of chemical disinfection necessitate increased contact time. While UV disinfection is relatively insensitive to water temperature, the influence of temperature on UV based AOPs is not well documented.

3.2 Temperature Dependence of UV AOPs

The $^{\bullet}$OH driven treatment of UV based AOPs involves composite chemical reactions. Component steps include photolytic generation of $^{\bullet}$OH, reaction with target contaminants, and competition reactions with major solutes that act as radical scavengers. These component steps themselves are composed of multiple elementary reactions. Despite this complexity, the net reaction rate of many composite reactions may be represented by a single Arrhenius expression, involving an overall activation energy.

$$k = Ae^{-E/RT} \tag{3.1}$$

where k is an overall reaction rate constant, A is the pre-exponential factor, E is the activation energy, R is the universal gas constant $8.314\,46\,\mathrm{J\,K^{-1}\,mol^{-1}}$, and T is the absolute temperature. If a plot of $ln(k)$ vs. $1/T$ produces a straight line, then E may be extracted from the slope.

Component steps may have individual activation energies. Whether $^{\bullet}$OH is generated by 185 nm photolysis of H_2O, or 254 nm photolysis of H_2O_2, the experimentally observed pseudo-first order rate constant k' for the $^{\bullet}$OH degradation of a trace organic contaminant C, in a solution containing a much larger concentration of the scavenger S, may be expressed with a modified version of equation 2.12 as:

$$k' = \frac{k_{\mathrm{OH},C}}{k_{\mathrm{OH},S}}\,\Phi\,\Theta \tag{3.2}$$

where $k_{\mathrm{OH},C}$ and $k_{\mathrm{OH},S}$ are the second order rate constants of $^{\bullet}$OH with a target C and scavenger S respectively, Φ is either the quantum yield of water photolysis at 185 nm or the 254 nm photolysis of H_2O_2, and Θ contains all temperature independent terms. This expression can be rewritten in terms of the Arrhenius expressions for the three components as:

$$k' = A_{tot}e^{-E_{tot}/RT}\Theta = \frac{A_C e^{-E_C/RT}\,A_\Phi e^{-E_\Phi/RT}}{A_S e^{-E_S/RT}}\Theta \tag{3.3}$$

from which the overall Arrhenius activation energy may be related to the component activation energies by:

$$E_{tot} = E_C + E_\Phi - E_S \tag{3.4}$$

with E_{tot} found from the experimental Arrhenius plot given by

$$ln(k') = ln(A_{tot}\,\Theta) - E_{tot}/RT \tag{3.5}$$

If the term Θ does in fact posses a significant temperature dependence, then an Arrhenius plot of $ln(k')$ vs. $1/T$ will reveal curvature. The absence of curvature allows the estimation of one of the component activation energies if the others are known. For diffusion limited reactions, such as those involving $^{\bullet}$OH, E_a is often in the range of 10 to 20 kJ mol^{-1} (Buxton et al., 1988). Examples of E for $^{\bullet}$OH reactions include 21 kJ mol^{-1} for HCO_3^- and 10 kJ mol^{-1} for tert-butanol (Buxton et al., 1988). It is important to note that, in the context of this discussion, an activation energy is not necessarily associated with an elementary reaction nor a transient intermediate. Interpretation at the molecular level is difficult. Even the reaction rate constants, in particular $k_{OH,S}$ for scavengers, represents an effective reaction rate, as the scavenger is generally not a pure substance but a complex mixture of organic matter. The activation energy concept may nevertheless be useful in gaining mechanistic insights.

In the case of 185 nm radiation, the term Θ contains the absorption coefficient of water α_{H_2O}, which varies with temperature and may contribute to the temperature sensitivity of the observed reaction rate. A temperature coefficient of 0.05 cm^{-1} °C^{-1} has been reported between 20 and 50 °C (Barrett and Mansell, 1960; Weeks et al., 1963). This gives a value for α_{H_2O} of 1.55 cm^{-1} at 20 °C and 2.30 cm^{-1} at 35 °C. The behaviour at lower tem-

peratures is not known, but a value for α_{H_2O} at 5 °C of between 0.80 and 1.00 cm^{-1} is reasonable. The impact of α_{H_2O} on the process depends on reactor design. For designs that rely on the total absorption of radiation within a short distance ($\leq$ 1 cm) operation at lower temperatures may result in a 5 to 10% reduction in absorbed radiation. For reactors that utilize larger optical path lengths, mixing requirements may become slightly relaxed at lower temperatures, and the overall effect less significant.

Once 185 nm photons are absorbed by water, $^{\bullet}OH$ are generated with a quantum yield Φ_{H_2O} of approximately 0.3 (Getoff and Schenck, 1968). The temperature dependence of Φ_{H_2O} is not known, but may follow an Arrhenius type relation with an activation energy dependent on competing rates of radical recombination k_r and escape k_e from the solvent cage.

$$H_2O \underset{k_r}{\overset{185\,nm}{\rightleftharpoons}} [H^{\bullet},{}^{\bullet}OH]_{aq} \xrightarrow{k_e} H^{\bullet} + {}^{\bullet}OH \tag{3.6}$$

The effective activation energy E_Φ will depend on k_r and k_e, which are not directly accessible by experimental methods used in this work. The situation is similar for 254 nm photolysis of H_2O_2, though more information is available on the temperature dependence of the quantum yield $\Phi_{H_2O_2}$, which is approximately unity at 25 °C.

$$H_2O_2 \underset{k_r}{\overset{254\,nm}{\rightleftharpoons}} [HO^{\bullet},{}^{\bullet}OH]_{aq} \xrightarrow{k_e} HO^{\bullet} + {}^{\bullet}OH \tag{3.7}$$

Based on limited temperature dependence data reported for 254 nm photol-

ysis of H_2O_2, an activation energy E_Φ for equation 3.7 is estimated to be in the range of 11 to 13 kJ mol^{-1} (Baxendale and Wilson, 1957; Hunt and Taube, 1952; Volman and Chen, 1959).

3.3 Experimental Approach

Experimental investigations of temperature dependence employed solutions with identical compositions for the collimated beam studies of both the 185 nm and the 254 nm-H_2O_2 regimes, except for the addition of H_2O_2 in the latter.

Solutions were composed of approximately 0.25 µM of the probe compound carbamazepine, and 8 mg L^{-1} as C (0.2 µM) of tert-butanol in ultrapure water. For 254 nm-H_2O_2 studies, 3.5 mg L^{-1} (0.1 µM) was added prior to irradiation.

The 185 nm irradiations used a 1.0 cm path length cylindrical fused silica cell with miniature teflon coated stir bar and stopper, and was placed in a custom made temperature controlled cell holder (Quantum Northwest, Liberty Lake, WA USA). The cell holder, composed of a black anodized aluminum body and black teflon lid, was equipped with a precision Peltier cell, magnetic stirring motor, water circulation with external ice bath for removal of heat, and nitrogen gas ports for condensation prevention. Temperature control within 0.1 °C was verified using a fine gage thermocouple (Omega, Laval QC Canada) placed in contact with the cell.

The 254 nm irradiations used a custom water jacketed borosilicate beaker (Cansci, Richmond BC Canada) with temperature controlled by water flowing from a recirculating chiller (Thermo Fisher Scientific, Waltham MA USA). A miniature teflon stir bar was placed in the beaker and the beaker placed on a magnetic stir plate mounted to a jack stand beneath the 254 nm collimated beam described in Chapter 2.

For both types of collimated beams, a series of irradiations were performed with samples exposed for a range of exposure times. All exposures were performed in triplicate. Approximately 1 mL samples were taken and placed in 2 mL HPLC vials. In the case of 254 nm-H_2O_2 tests, a 10 µL droplet of 100 µg L^{-1} bovine catalase solution was placed at the bottom of each HPLC vial to quench residual H_2O_2 and avoid contributions to probe degradation from dark reactions between sampling and HPLC analysis. Dark controls for 254 nm-H_2O_2 tests were also included.

3.4 Results

3.4.1 Temperature Effects in the 254 nm - H_2O_2 Regime

The results for 254 nm - H_2O_2 tests are displayed in Figure 3.1 and Table 3.1. They reveal that the reaction rate observed increases with temperature from 5 °C to 35 °C.

The observed pseudo-first order rate constants k' are calculated from linear regression of the triplicate measurements for each irradiation time used, with the standard error of the slope used to express uncertainty $\sigma_{k'}$. The uncertainty of $ln(k')$ is calculated from the approximation $\sigma_{ln(k')} \approx \sigma_{k'}/k'$ (Harris, 2010). The calculated values are displayed in Table 3.1.

Table 3.1: Effect of temperature on removal rate of carbamazepine probe in 254 nm-H_2O_2 regime

T(°C)	5	20	35
$k' \times 10^3$ (min^{-1})	7.3 ± 0.3	11.4 ± 0.2	16.1 ± 0.5
$ln(k')$	-4.92 ± 0.04	-4.47 ± 0.02	-4.13 ± 0.03

$[H_2O_2] = 3.5$ mg L^{-1}, $[tBuOH] = 8$ mg L^{-1} as C, $[CBZ]_o \simeq 0.25$ µM

The Arrhenius plot for the 254 nm-H_2O_2 regime is displayed in Figure 3.2 using the data tabulated in Table 3.1 and the equation 3.4.

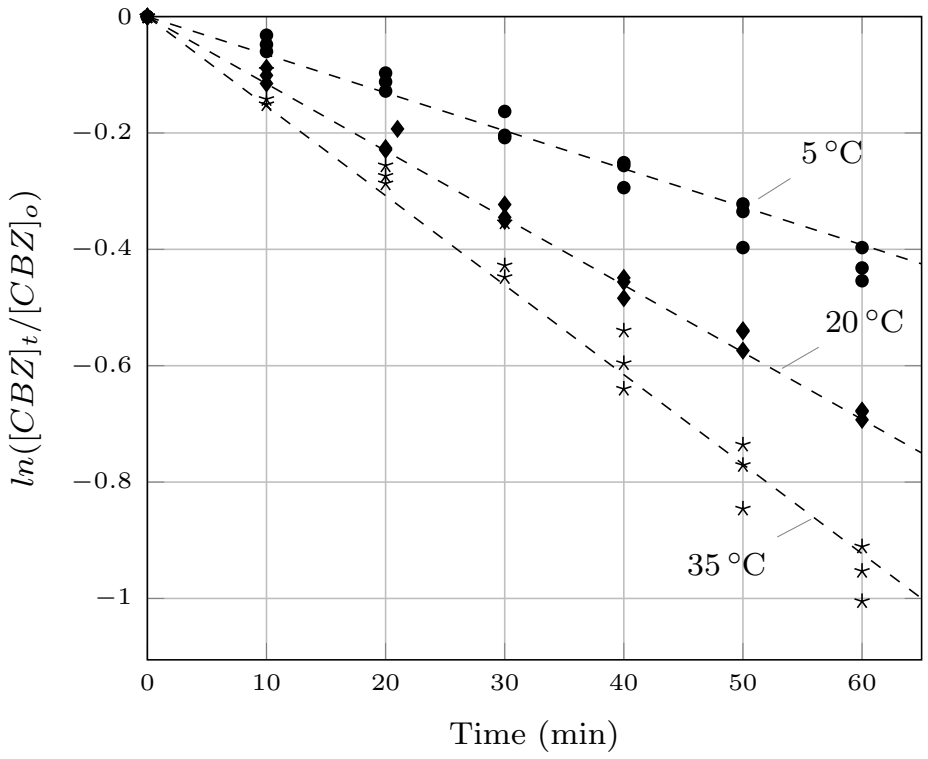

Figure 3.1: Temperature dependence in 254 nm - H_2O_2 regime. $[H_2O_2]$ = 3.5 mg L^{-1}. $[tBuOH]$ = 8 mg L^{-1} as C. $[CBZ]_o \simeq 0.25$ µM.

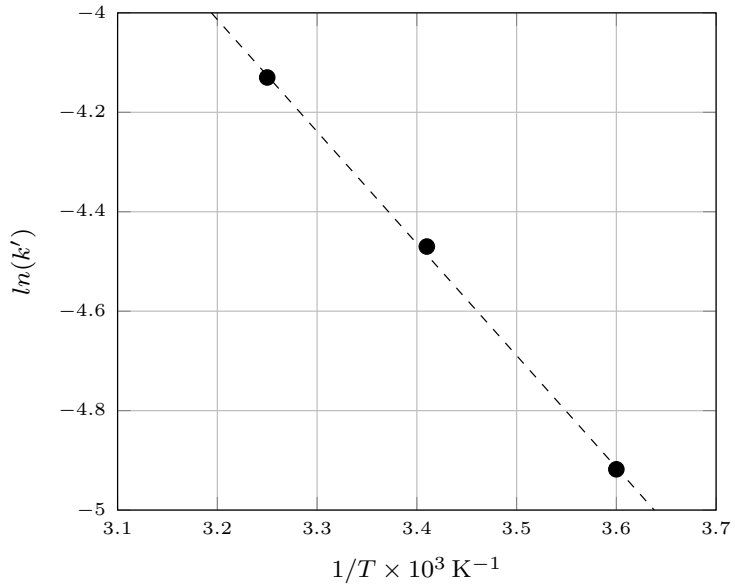

Figure 3.2: Arrhenius plots for 254 nm-H_2O_2 regime. $[H_2O_2] = 3.5\,\mathrm{mg\,L^{-1}}$. $[tBuOH] = 8\,\mathrm{mg\,L^{-1}}$ as C. $[CBZ]_o \simeq 0.25\,\mu\mathrm{M}$.

3.4.2 Temperature Effects in the 185 nm Regime

The results for 185 nm tests are displayed in Figure 3.3. As with the previous case, the reaction rate is observed to increase with temperature from 5 °C to 35 °C.

As with the 254 nm-H_2O_2 regime, the observed pseudo-first order rate constants k' are calculated from linear regression of the triplicate measurements for each irradiation time used, with the standard error of the slope used to express uncertainty $\sigma_{k'}$. As before, the uncertainty of $ln(k')$ is calculated from the approximation $\sigma_{ln(k')} \approx \sigma_{k'}/k'$. The calculated values are displayed in Table 3.2.

The Arrhenius plot for the 185 nm regime is displayed in Figure 3.4 using the data tabulated in Table 3.2.

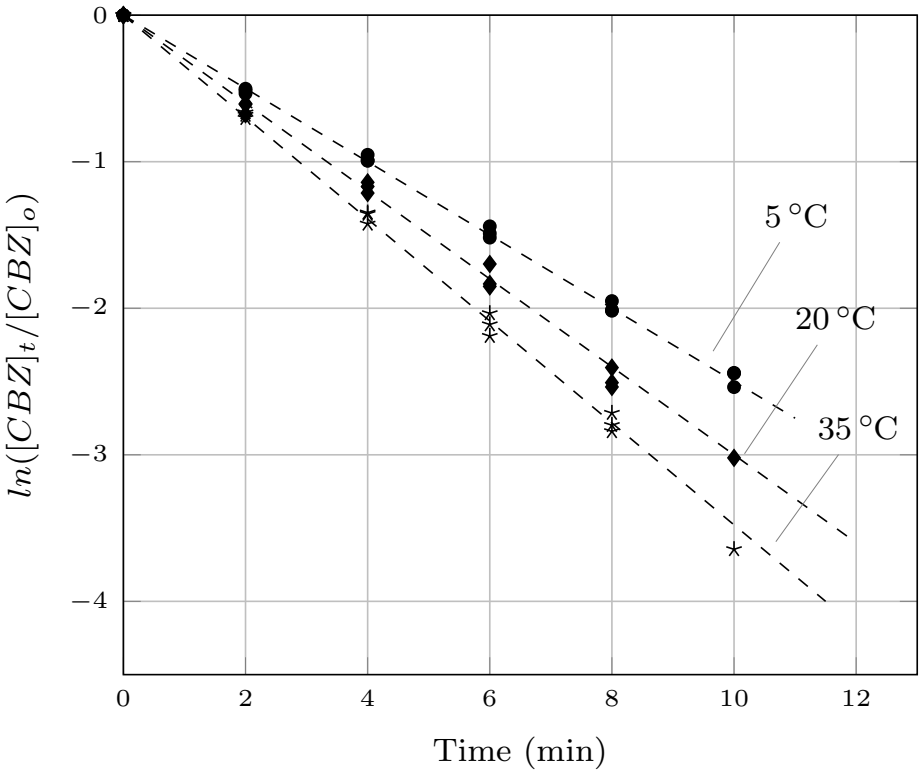

Figure 3.3: Temperature dependence in 185 nm regime. $[tBuOH]$ = $8\,\mathrm{mg\,L^{-1}}$ as C. $[CBZ]_o \simeq 0.25\,\mu\mathrm{M}$.

The slopes of both Arrhenius plots, as calculated by linear regression, allow the determination of the experimental activation energy for both the 185 nm and 254 nm-H_2O_2 regimes. The values are displayed in Table 3.3.

Table 3.2: Effect of temperature on removal rate of carbamazepine probe in 185 nm regime

$T(°C)$	5	20	35
$k' \times 10^2$ (min^{-1})	24.7 ± 0.2	30.5 ± 0.5	35.6 ± 0.5
$ln(k')$	-1.40 ± 0.01	-1.19 ± 0.02	-1.03 ± 0.01

$[tBuOH] = 8\,mg\,L^{-1}$ as C, $[CBZ]_o \simeq 0.25\,\mu M$

Table 3.3: Experimental (overall) activation energies for carbamazepine degradation in the presence of tert-butanol in 254 nm-H_2O_2 and 185 nm regimes

	254 nm-H_2O_2	185 nm
E_a $(kJ\,mol^{-1})$	18.7 ± 0.9	8.6 ± 0.5

NB: These values pertain to the composite reactions and not elementary steps.

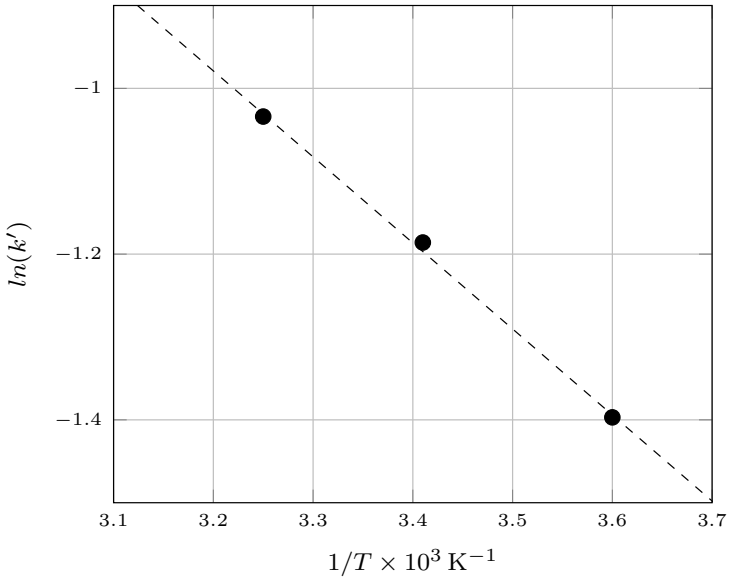

Figure 3.4: Arrhenius plots for 185 nm regime. $[tBuOH] = 8\,mg\,L^{-1}$ as C. $[CBZ]_o \simeq 0.25\,\mu M$.

3.5 Discussion

The results indicate that the 185 nm AOP is less temperature sensitive than the UV/H_2O_2 AOP under the conditions tested. This result is understood to apply to water matrices for which H_2O is the major absorber of 185 nm photons, where the scavenging term $\Sigma k_i[S_i]$ has a magnitude greater than $10^5\,s^{-1}$ and were the activation energy of the target contaminant is less than the effective activation energy for the scavenging term (i.e. $E_C < E_S$). If the last condition is reversed (i.e. $E_C > E_S$), the observed rate k' may follow an inverse relationship with temperature.

In the present case, the scavenger is the pure substance tert-butanol, with an $^{\bullet}OH$ activation energy E_S reported as $10 \pm 3\,kJ\,mol^{-1}$ (Ervens et al., 2003). Using an average of the reported values of the activation energy of H_2O_2 photolysis at 254 nm, $E_\Phi = 12 \pm 1\,kJ\,mol^{-1}$, allows the estimation of the activation energy of $^{\bullet}OH$ with carbamazepine, E_C, using equation 3.4. In this manner, the value $E_C = 17 \pm 5\,kJ\,mol^{-1}$ is obtained. Application of equation 3.4 for the 185 nm regime allows for the estimation of E_Φ, the activation energy of the 185 nm photolysis of water itself. A value of $E_\Phi \approx 0\,kJ\,mol^{-1}$ is obtained. The fundamental activation energies deduced from experimental data are listed in Table 3.4.

Table 3.4: Summary of fundamental activation energies estimated from this work

	$^{\bullet}OH + CBZ$	$H_2O \xrightarrow{185\,nm} H^{\bullet} + {}^{\bullet}OH$
E_a ($kJ\,mol^{-1}$)	17 ± 5	≈ 0

Explanation for the $E_\Phi \approx 0\,kJ\,mol^{-1}$ value of H_2O photolysis at 185 nm is provided by the proposed structure for H_2O in the liquid state. While the precise structure of liquid H_2O remains in dispute (Ball, 2008), the modern consensus based on evidence from X-ray and neutron diffraction supports the view that virtually all molecules of H_2O in the liquid state are dynamically

hydrogen bonded to an average of four neighbours in an ice-like tetrahedral motif with distorted bond angles (Frank, 1972; Franks, 2000). The existence of non-hydrogen bonded interstitial H_2O molecules (monomers) is supported by evidence from Raman and infrared spectroscopy, though the proportion of such molecules is interpreted to be small ($< 1\%$).

Evidence from far-UV absorption also supports the existence of interstitial H_2O monomers. Extensive measurements by Stevenson (1965) of 185 nm absorption of ultrapure water in both the vapour and liquid state confirm observations by others (Barrett and Mansell, 1960; Watanabe and Zelikoff, 1953; Weeks et al., 1963) that the molar absorption coefficient of H_2O vapour is three orders of magnitude greater than that of the liquid. Stevenson (1965) reported $\epsilon_v = 22.1\,\mathrm{M^{-1}\,cm^{-1}}$ and $\epsilon_\ell = 0.0274\,\mathrm{M^{-1}\,cm^{-1}}$ at 23.5 °C and made measurements of liquid absorption with increasing temperature. The ratio ϵ_ℓ/ϵ_v remained approximately 0.0012 between 23 and 27 °C, rising sharply above 30 °C to 0.0090 at 91.8 °C. Such observations are explained by the existence of monomers in the liquid state, representing a fraction of all molecules on the order of 10^{-3} in the vicinity of 20 °C, with such monomers responsible for virtually all 185 nm photon absorption. The temperature dependence reported by Stevenson is interpreted as an increase in monomer population with temperature that nevertheless remains a minority even near the boiling point. This is consistent with the considerable degree of hydrogen bonding remaining at the boiling point and the relatively high critical temperature of water.

Upon 185 nm excitation of an H_2O monomer, it is proposed that only a relatively weak van der Waals force must be overcome in order for the photoproducts to escape the solvent cage, since no hydrogen bonds are involved. Though the excited H_2O molecule may lose energy to the solvent by collision with a rate k_r proportional to $\sqrt{T}$, the excess energy of the excited molecules itself is likely sufficient to overcome a van der Waals energy of $\sim 5\,\mathrm{kJ\,mol^{-1}}$. The activation energy for the photolysis of an H_2O molecule, $E_\phi \approx 0$, applies to the excited-state molecule that has absorbed a 185 nm photon. Such pho-

tons possess an energy of 647 kJ mol^{-1} while the bond-dissociation energy between HO and H is approximately 494 kJ mol^{-1} (Darwent, 1970). The excess energy, equivalent to approximately two hydrogen bonds, is more than sufficient to overcome a postulated van der Waals force.

3.6 Summary

The temperature studies conducted indicate that, under the conditions tested, the 185 nm-AOP is relatively insensitive to temperature. An activation energy for the $^{\bullet}$OH reaction with carbamazepine has been estimated as 17 ± 5 kJ mol^{-1}. The activation energy for the 185 nm photolysis of H_2O has been estimated to be approximately 0 kJ mol^{-1} and supports the view that 185 nm photon absorption occurs in interstitial non-hydrogen bonded H_2O monomers present as an approximate 10^{-3} fraction of all molecules.

Additional temperature dependence studies should be investigated in water matrices for which H_2O is not the major absorber of 185 nm photons.

Chapter 4

Dissolved Organic Matter

4.1 Dissolved Organic Matter in Natural Waters

Wherever water is found in the environment, it will contain some amount of organic matter. Fractions of organic matter based on size may be categorized as particulate, colloidal or dissolved. Dissolved organic matter (DOM) is expressed quantitatively in terms of its carbon content in units of $\mathrm{mg\,L^{-1}}$ as C, and defined operationally as that fraction not retained by a 0.45 µm nominal pore size filter (APHA, 2012). The dissolved organic carbon (DOC), is measured by oxidizing all organic carbon in an aqueous sample to CO_2, then measuring the CO_2 generated. If unfiltered, the measurement represent the total organic carbon (TOC). The possibility of confusion exist when discussing DOM quantitatively, since DOC is measured and not DOM. The discrepancy between the two parameters is significant, since the proportion of carbon in DOM is approximately 50% in natural waters, and thus the value of DOC is typically half that of DOM when expressed in mass based concentration units.

In some cases, such as in rainwater, groundwater and the ocean, the DOC is relatively low, often $\leq 1\,\mathrm{mg\,L^{-1}}$ as C. In other cases, such as swamps, wetlands, and soil it is relatively high, often $\gg 10\,\mathrm{mg\,L^{-1}}$ as C (Thurman, 1985). In freshwater rivers and lakes, DOC values between 1 and $10\,\mathrm{mg\,L^{-1}}$ as C are typical. When groundwater is used as a source of drinking water, the impact of organic matter may often be negligible. However, when surface waters are used (i.e. rivers and lakes), organic matter has significant consequences to many practical aspects of treatment, storage and distribution.

Surface waters contain organic matter both of terrestrial origins received via drainage over the watershed (allochthonous), and of aquatic origins derived from photosynthetic and microbial activity (autochthonous) (Wetzel, 2001). The resulting material is a complex mixture in size and composition that defies simple descriptions. In surface waters, the DOC fraction represents the majority by mass, often 90% or more of the TOC (Wetzel, 2001). Yet, since the transition between colloidal and dissolved fractions is more a continuum than a sharply defined point, DOC will contain a colloidal contribution to some extent.

The chemical composition of DOM varies between watersheds and within them due to meteorological events and seasonal fluctuations. The majority of DOM typically consists of molecules with molecular weights from a few hundred to up to several tens of thousands of daltons. Due to long residence times in the environment, DOM is often heavily oxidized and of low biodegradability. The composition of DOM may be divided between non-humic and humic components. The non-humic portion includes well known types of compounds such as carbohydrates, proteins, amino acids, fatty acids, aldehydes, ketones, alcohols and carboxylic acids. These occupy the lower molecular weight fractions. The majority of naturally occurring DOM is composed of humic substances, a general category of unknown structure, which can be further classified as fulvic and humic acids. Fulvic acids tend to be smaller than humic acids, have higher oxygen content, and are soluble at all pH values. Humic acids are on average larger and precipitate at pH 2 or less. Based on ^{13}C NMR analysis and UV absorption spectra, the macromolecules of humic substances are known to posses, to varying extents, carboxyl, hydroxyl, and amine functional groups, as well as substantial conjugation and aromaticity. Such properties are likely to impart strong influences on the optical and chemical properties of the water matrix, in particular the absorption of photons and oxidant reactivity.

In addition to organic matter found in the pristine environment, other con-

tributions to DOM may be significant. Municipal wastewater discharges, and even gross industrial contamination, may contribute measurably to the DOC found in surface waters. Anthropogenic materials such as these differ substantially in chemical composition to those materials described above. In the case of biological wastewater effluent, for example, DOC will originate largely from the cellular debris of bacteria used in the activated sludge process, and the extracellular polymeric substances they excrete. Negligible humic material will be present. In order to distinguish the DOM from the pristine environment with materials from anthropogenic sources, the term "natural organic matter" or NOM is often used by engineers in the drinking water field.

In water treatment, DOM has several important influences. The modification of surface chemistry on particulates and larger colloids and the complexation of metal coagulants influence the efficiency of solid-liquid separation processes. Adsorption of DOM to activated carbon reduces removal efficiency of target organic contaminants by occupying adsorption sites. Reactions with DOM exert a demand on chlorine and other oxidants, usually increasing the dose of oxidant required to produce a residual concentration. Absorption of radiation interferes with UV disinfection, acting as a filter that reduces exposure of microbes and increases the required UV fluence or dose that must be applied to achieve a given degree of inactivation. Unintended reactions between oxidants and DOM generate by-products such as halogenated DBPs or smaller organic molecules that are more available as substrate for subsequent microbial regrowth in distribution and storage. Components of DOM itself may impart colour, taste and odour to finished water, reducing the aesthetic quality of the product.

4.2 The 185 nm AOP and Influence of Dissolved Organic Matter

The 185 nm AOP is influenced by DOM in at least two ways. First, photons that would otherwise contribute to the generation of $^{\bullet}$OH from water photolysis, may be absorbed by DOM without subsequent radical generation. Aromatic and carbonyl moieties offer sites of strong photon absorption due to π-bonds. Second, generated $^{\bullet}$OH will react with DOM molecules in competition with target contaminants often many orders of magnitude lower in concentration. The reactivity of DOM, quantified as an aggregate second order radical rate constant, is thus a measure of the strength of competition and expressed by the product $k_{\mathrm{OH},S}[S]$, where $[S]$ is the DOC in units of $\mathrm{mg\,L^{-1}}$ as C and $k_{\mathrm{OH},S}$ has units of $\mathrm{L\,mg^{-1}\,s^{-1}}$. The scavenging product for most waters is typically in the range of 10^4-$10^5\,\mathrm{s^{-1}}$ (Elovitz and von Gunten, 1999; Goldstone et al., 2002; Westerhoff et al., 1999, 2007).

As discussed earlier, under steady-state conditions, the removal rate of a compound C may be expressed as $ln(C/C_o) = -k't$, with the pseudo-first order rate constant k' expressed as:

$$k' = \frac{k_{\mathrm{OH},C}\,\Phi_{\mathrm{H_2O}}\,f_{\mathrm{H_2O}}\,I_a}{\sum\,k_{\mathrm{OH},S_i}\,[S_i]} \qquad \text{(2.12 revisited)}$$

where $k_{\mathrm{OH},C}$ is the second-order rate constants for the reaction of $^{\bullet}$OH with a target contaminant C, Φ is the quantum yield for 185 nm photolysis of H_2O, $f_{\mathrm{H_2O}}$ is the fraction of absorbed photons that are absorbed by H_2O, I_a is the 185 nm absorption rate per unit volume, and $\sum k_{\mathrm{OH},S}[S_i]$ represents the scavenging term. Scavenging is represented as a sum of individual contributions from compounds S_i, though these individual contributions are inaccessible and only the sum is typically quantified experimentally when

naturally occurring DOM is used.

In Equation 2.12 , the term f_{H_2O} may be significant if a substantial fraction of 185 nm photons are not absorbed by water but by other solutes. This term may be evaluated if the solution obeys the Beer-Lambert law and the component absorption coefficients are known. In this case, if the molar absorbance coefficient associated with DOC is known and the total absorbance of the solution is known, then the absorbance of water may be determined from $\alpha_{H_2O} = \alpha_{tot} - \alpha_{DOC}$, and $f_{H_2O} = \alpha_{H_2O}/\alpha_{tot}$. The value of α_{DOC} may be determined for any value of DOC, provided the absorption coefficient ϵ_{DOC} is known, via the expression $\alpha_{DOC} = \epsilon_{DOC}[DOC]$. At the wavelength of 254 nm, the absorption coefficient is referred to as Specific UV Absorbance or SUVA. This term is widely used to characterize DOM at 254 nm, with typical values of 1 to 4 $L\,mg^{-1}\,m^{-1}$ as C. Comparable values at 185 nm have not been reported to date.

4.3 Use of Reference Materials

Due to the variability and site-specific characteristics of organic matter, studies of the influence of DOM on treatment benefit from standardized materials. Use of such materials allows researchers to better compare results and more accurately verify the work of others. Such standard reference materials are available from the International Humic Substances Society (IHSS). This work uses two IHSS reference materials, namely Suwannee River and Nordic Reservoir NOM, obtained from preparative scale separation of the DOM from water, as described in detail by Serkiz and Perdue (1990) and Sun et al. (1995).

Stock solutions were made using each of the IHSS reference materials, prepared by quantitatively dissolving the freeze dried samples, filtration of solutions via pre-washed 0.45 µm filters, and pH neutralization with H_2SO_4. Determination of the stock solution DOC values was performed by analysis

of dilutions via TOC Analyzer calibrated with potassium hydrogen phthalate (KHP) standards. Aliquots of the stock solutions were then used to prepare a set of four solutions with a concentration of DOC in the range of 1 to 10 mg L^{-1} as C, also verified by TOC Analyzer. The final concentration of Cl^- and SO_4^{2-} was calculated to be < 1 mg L^{-1} and confirmed by ion chromatography. The solutions were then spiked with the probe compound carbamazepine (~ 0.25 µM), transferred to a 1.0 cm path length fused silica cell, and irradiated using the 185 nm collimated beam. Discrete irradiations were performed at exposure times scaled to produce at least one natural log unit removal of the probe compound in the solution with highest DOC at the longest exposure time, found to require approximately 5 min. All irradiations were replicated in triplicate.

Experimental results for 185 nm irradiations of NOM solutions are displayed in Figures 4.1 and 4.2, for Suwannee River and Nordic Reservoir NOM respectively. Excellent linearity is observed in all cases, and the corresponding pseudo-first order rate constants are tabulated in Table 4.1.

Table 4.1: The removal rate of probe for varying concentration and source of DOM in 185 nm regime

Reference DOM	[DOC] (mg L^{-1} as C)	k' (min^{-1})
Suwannee River	3.0	0.845 ± 0.018
	5.0	0.555 ± 0.007
	7.5	0.356 ± 0.004
	10.0	0.250 ± 0.004
Nordic Reservoir	1.8	1.09 ± 0.04
	2.7	0.82 ± 0.02
	5.2	0.416 ± 0.007
	9.8	0.202 ± 0.001

Reference materials from the IHSS.

A plot of k' vs. the reciprocal of the DOC is shown in Figure 4.3, and reveals a linear behaviour as expected from Equation 2.12. The absence of

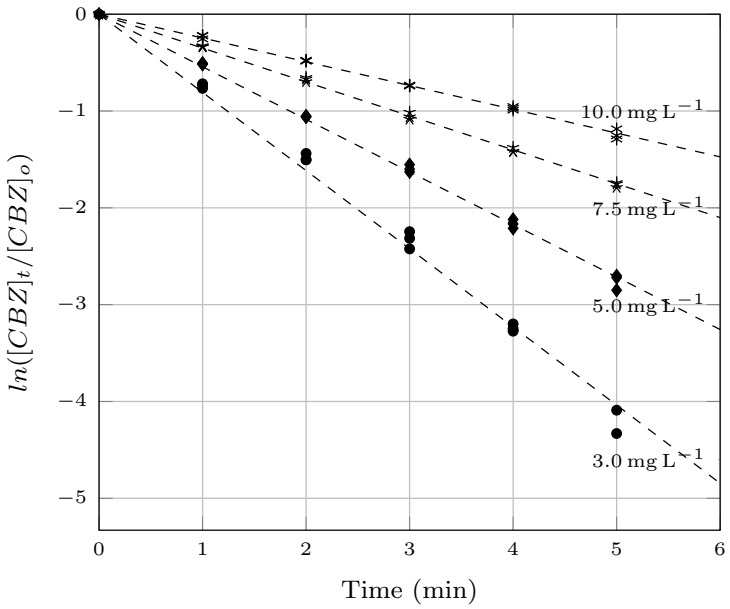

Figure 4.1: Suwannee River NOM in 185 nm regime. All concentrations are in units of mg L^{-1} as C. $[CBZ]_o \sim 0.25\,\mu M$. All solutions at pH 7.

significant curvature suggests that the influence of f_{H_2O} may be negligible under the conditions tested. Furthermore, the ratio of the slopes for the plots 4.3, obtained by linear regression, yields a value of 1.10 ± 0.07. If the effect of 185 nm absorbance is indeed negligible, this result suggests that the $^{\bullet}$OH reactivities of the two DOM reference material tested (i.e. $k_{OH,DOC}$) are comparable despite originating from distinct and disparate sources.

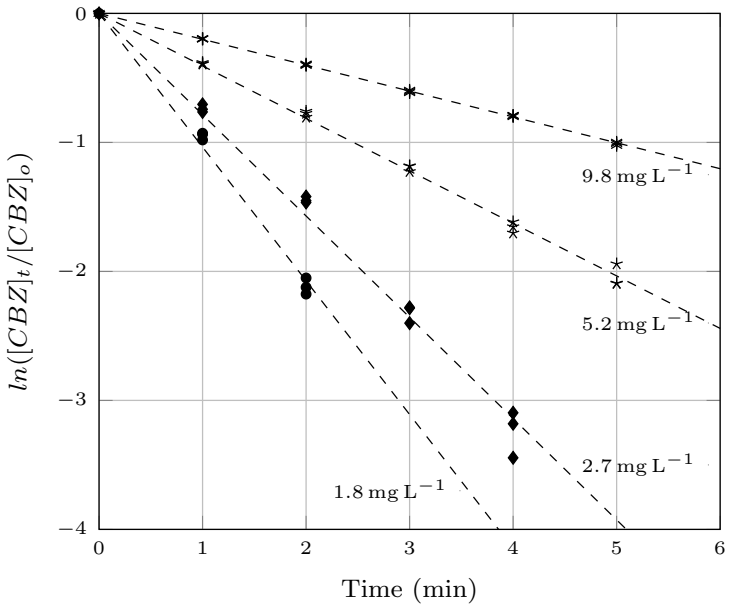

Figure 4.2: Nordic NOM in 185 nm regime. All concentrations are in units of mg L^{-1} as C. $[CBZ]_o \sim 0.25\,\mu$M. All solutions at pH 7.

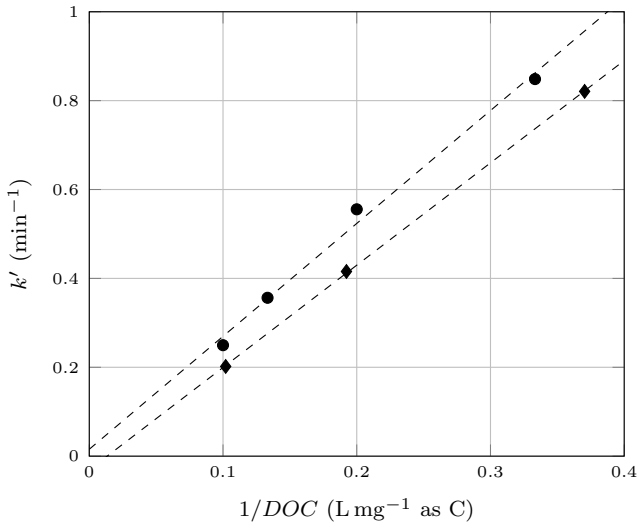

Figure 4.3: Removal rate of carbamazepine probe with DOM, Suwannee River (●), Nordic Reservoir (♦) NOM.

4.4 Pure Substances as Model Organic Matter

Due to the complex composition of naturally occurring organic matter, the use of pure compounds facilitate the study of the 185 nm AOP. Subsequent studies involved well characterized compounds used as a radical scavenger and model DOM.

Three pure compounds were selected for study. These are listed in the Table 4.2 with the corresponding second-order $^{\bullet}$OH rate constants. Compounds were selected based on (1) known $^{\bullet}$OH rate constant, (2) negligible absorption of 254 nm radiation, (3) high aqueous solubility, (4) relatively low vapour pressure. The last two criteria result in low volatility. The three compounds used are miscible with water.

Table 4.2: Selected pure compounds used as model organic matter in studies of 185 nm regime

Compound (S)	Formula	$k_{\mathrm{OH},S}$ ($\mathrm{M^{-1}\,s^{-1}}$)
tert-butanol (2-methyl-2-propanol)	$(CH_3)_3COH$	6.0×10^8
methanol	CH_3OH	9.7×10^8
acetone (2-propanone)	CH_3COCH_3	1.1×10^8

Rate constants taken from Buxton et al. (1988).

Stock solutions of the three compounds, tert-butanol, methanol, and acetone were prepared gravimetrically from neat HPLC grade reagents and ultrapure water, with the resulting concentrations measured by TOC Analyzer upon suitable dilution. Aliquots of the stock solution and spikes of the probe compound carbamazepine were then used to assemble solutions for irradiation. Concentrations of the model compounds, $[S]$, were selected to satisfy the

criteria $k_{\mathrm{OH},CBZ}[CBZ] \ll k_{\mathrm{OH},S}[S]$. Discreet irradiations were performed as before for exposure times sufficient to induce at least one natural log unit decrease in the probe compound concentration (typically 1 to 10 min). The results are plotted in Figures 4.4, 4.5, and 4.6.

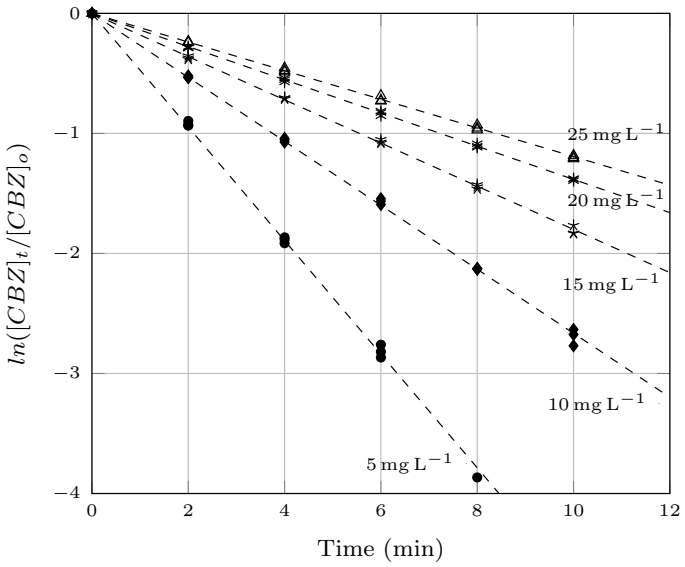

Figure 4.4: Tert-Butanol ($(CH_3)_3COH$) in 185 nm regime. All concentrations are in units of mg L^{-1} as C.

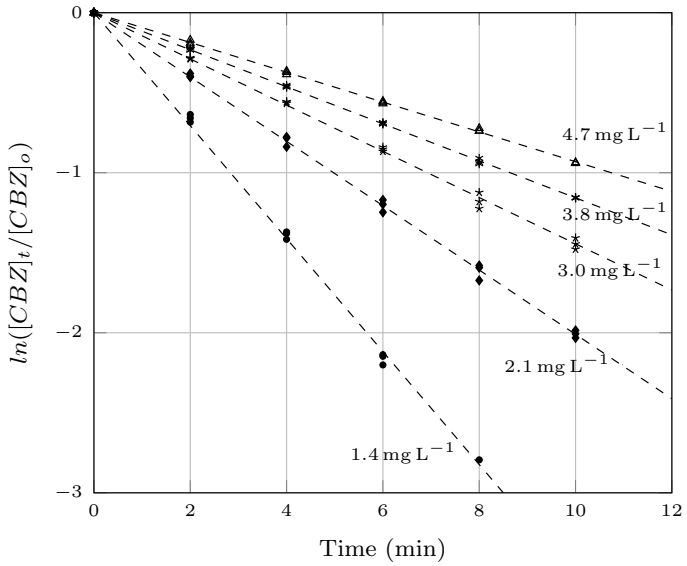

Figure 4.5: Methanol (CH_3OH) in 185 nm regime. All concentrations are in units of mg L^{-1} as C.

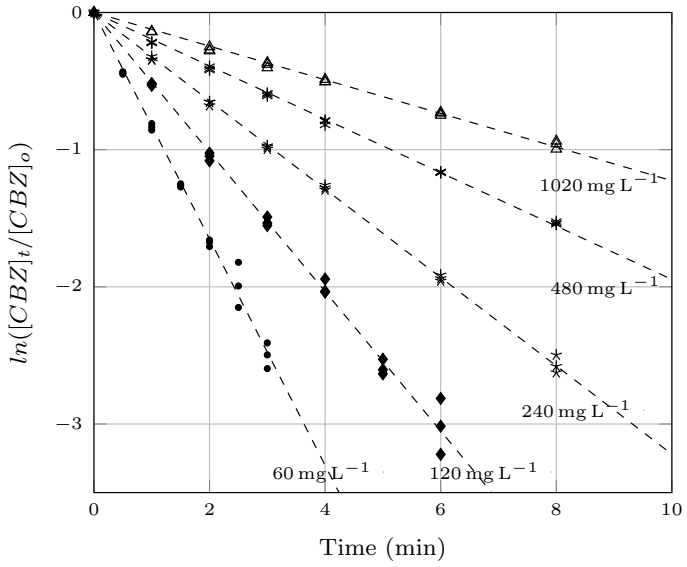

Figure 4.6: Acetone (CH_3COCH_3) in 185 nm regime. All concentrations are in units of mg L^{-1} as C.

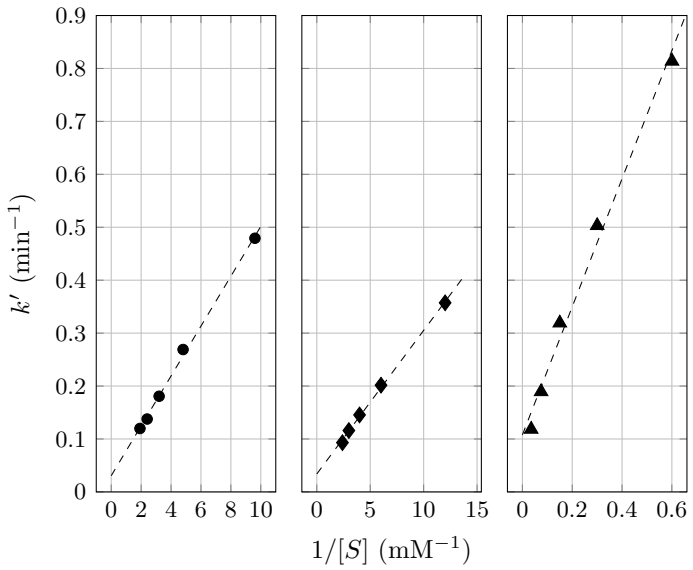

Figure 4.7: Removal rate of probe with pure compounds as model DOM: tert-butanol (●), methanol (♦), acetone (▲).

All plots reveal high linearity ($R^2 > 0.95$) for all values of $[S]$ and the values of k' are displayed in Table 4.3. Plots of k' vs. $1/[S]$, in Figure 4.7, reveal strong linearity, supporting the model expressed by Equation 2.12. In the case of methanol, in dilute solutions the molar absorption coefficient (ϵ) at 185 nm has been reported to be less than $10\,\mathrm{M}^{-1}\,\mathrm{cm}^{-1}$ (Weeks et al., 1963).

For the concentrations of methanol used in these experiments, the fraction f_{H_2O} in Equation 2.12 is calculated to be approximately unity. The same condition is expected for tert-butanol, given structural similarities between the two alcohols. However, the presence of a π-bond in the carbonyl group of acetone suggests that absorption at 185 nm may be significant. Furthermore, given the lower $^{\bullet}$OH reactivity of acetone, a higher concentration was required in these experiments to ensure the steady-state condition was satisfied (i.e. $k_{\mathrm{OH},CBZ}[CBZ] \ll k_{\mathrm{OH},S}[S]$). Thus, a value of f_{H_2O} less than unity is expected to yield detectable curvature in the corresponding plot displayed in Figure 4.7. Insufficient resolution is available for the conditions used to

Table 4.3: The removal rate of probe for pure scavengers tert-butanol, methanol, and acetone in 185 nm regime

Scavenger	Concentration ($mg\,L^{-1}$ as C)	Concentration (mM)	k' (min^{-1})
$(CH_3)_3COH$	5.0	0.104	0.479 ± 0.006
	10.0	0.208	0.269 ± 0.003
	15.0	0.312	0.181 ± 0.002
	20.0	0.416	0.138 ± 0.001
	20.0	0.521	0.120 ± 0.001
CH_3OH	1.0	0.083	0.357 ± 0.004
	2.0	0.167	0.202 ± 0.002
	3.0	0.250	0.145 ± 0.002
	4.0	0.333	0.116 ± 0.001
	5.0	0.416	0.093 ± 0.001
CH_3COCH_3	60	1.67	0.814 ± 0.019
	120	3.33	0.503 ± 0.010
	240	6.66	0.319 ± 0.003
	480	13.32	0.189 ± 0.001
	1020	28.31	0.118 ± 0.001

Uncertainties represent the standard errors in the slopes calculated by linear regression.

confirm the presence of such curvature. However, a comparison of the ratios of k' vs. $1/[S]$ from the three plots is useful. Modifying Equation 2.12 for a pure substance as scavenger S and incorporating all other terms in the parameter Ω:

$$k' = \frac{k_{OH,C}\,\Phi_{H_2O}\,f_{H_2O}\,I_a}{k_{OH,S}[S]} = \frac{\Omega}{[S]} \tag{4.1}$$

In the case of $f_{H_2O} \approx 1$, as is expected for tert-butanol and methanol, the ratio of the Ω values for two systems using pure scavengers S should approximate the inverse ratio of the corresponding rate constants $k_{OH,S}$:

$$\frac{k'_{S_1}}{k'_{S_2}} = \frac{\Omega_{S_1}}{\Omega_{S_2}} \approx \frac{k_{OH,S_2}}{k_{OH,S_1}} \tag{4.2}$$

Linear regression analysis of the data displayed in Table 4.3 and Figure 4.7 yield the values of $\Omega_{tBuOH} = 0.047 \pm 0.001\,\mathrm{mM\,min^{-1}}$ and $\Omega_{MeOH} = 0.027 \pm 0.001\,\mathrm{mM\,min^{-1}}$ for tert-butanol and methanol respectively. The experimentally determined ratio is thus:

$$\frac{\Omega_{tBuOH}}{\Omega_{MeOH}} \approx \frac{k_{OH,MeOH}}{k_{OH,tBuOH}} = 1.7 \pm 0.1 \tag{4.3}$$

The ratio evaluated from rate constants found in the widely cited compilation of Buxton et al. (1988) gives:

$$\frac{k_{OH,MeOH}}{k_{OH,tBuOH}} = \frac{9.7 \times 10^8\,\mathrm{M^{-1}\,s^{-1}}}{6.0 \times 10^8\,\mathrm{M^{-1}\,s^{-1}}} = 1.6 \tag{4.4}$$

The two values are in relatively good agreement, supporting the validity of the model expressed by Equation 2.12 and the assumption that $f_{H_2O} \approx 1$ for solutions of tert-butanol or methanol at the concentrations used.

However, in the case of acetone, $\Omega_{Acetone} = 1.21 \pm 0.07\,\mathrm{mM\,min^{-1}}$ was found,

resulting in ratios between acetone and tert-butanol and methanol that deviate substantially from those calculated from rate constants. The ratios $\Omega(Acetone : MeOH)$ and $\Omega(Acetone : tBuOH)$ are both approximately five fold greater than the corresponding inverse ratios of the rate constants:

$$\frac{\Omega_{Acetone}}{\Omega_{MeOH}} = 45 \qquad \frac{k_{\mathrm{OH},MeOH}}{k_{\mathrm{OH},Acetone}} = 8.8 \tag{4.5}$$

$$\frac{\Omega_{Acetone}}{\Omega_{tBuOH}} = 26 \qquad \frac{k_{\mathrm{OH},tBuOH}}{k_{\mathrm{OH},Acetone}} = 5.5 \tag{4.6}$$

It is likely that the assumption of $f_{\mathrm{H_2O}} \approx 1$ is not valid for acetone due to the possibility of strong absorption at 185 nm due to the π-bond of the carbonyl group of acetone. This would result in $f_{\mathrm{H_2O}} < 1$, which would induce a curvature to the plot in Figure 4.7 that deviates from the straight line towards the ordinate. This is opposite to the slight curvature that appears towards the abscissa. While it is possible the observation may be due to an experimental error, an impurity of acetone with a much lower $^{\bullet}$OH reactivity would tend to produce a similar effect. Such a contaminant may be oxalic acid or oxalate ($pK_a = 4.4$), with reaction rate constants $k_{\mathrm{OH},S} = 1.4 \times 10^6$ and $7.7 \times 10^6\,\mathrm{M^{-1}\,s^{-1}}$ respectively (Buxton et al., 1988). Oxalic acid/oxalate is reported to be an oxidative degradation product of acetone (Stefan and Bolton, 1999; Stefan et al., 1996), which may have been present in the neat solution at the start of irradiations. The irradiated solutions were unbuffered and any accidental drop in pH, while not having been detected, would have amplified the effect of such an impurity. A reexamination of acetone in the 185 nm regime would be useful. Regardless, the likely

non-transparency of acetone make it less ideal as a model scavenger in some cases.

4.5 Estimation of 185 nm Incident Fluence Rate

In the absence of a convenient chemical actinometer for the determination of the incident fluence rate at 185 nm, I_o, the experimental results obtained above for tert-butanol and methanol may be used to estimate its value. A comparison of its magnitude relative to the incident fluence rate at 254 nm, determined earlier by KI-KIO_3 actinometry, will yield an important parameter of low pressure mercury lamps.

Note that for non-absorbing pure scavengers S, a plot of the observed rate constant k' *vs.* $1/[S]$ yields a slope previously referred to as Ω. From Equation 4.1, the expression for Ω_S is given by:

$$\Omega_S = \frac{k_{\mathrm{OH},C}}{k_{\mathrm{OH},S}} \Phi_{\mathrm{H_2O}} f_{\mathrm{H_2O}} I_a \tag{4.7}$$

All the terms of the Equation 4.7 are known or measurable except for I_a, the rate of 185 nm photon absorption per unit volume. Thus, the experimentally determined values of Ω_S, known values of $k_{OH,C}$ for carbamazepine, and $k_{OH,S}$ for tert-butanol and methanol, $\Phi_{\mathrm{H_2O}} = 0.3$, and the assumption that $f_{\mathrm{H_2O}} \approx 1$, allow the calculation of I_a in units of $\mathrm{M\,s^{-1}}$. This value can then be converted to a fluence rate using the cross sectional area and volume of the irradiation cell, and the molar photon energy at 185 nm of $647\,\mathrm{kJ\,mol^{-1}}$.

Using an internal diameter of 1.90 cm and path length of 1.00 cm to deter-

mine the area and volume of the irradiation cell (neglecting the volume of the miniature stir bar), calculations of the 185 nm fluence rate $I_{o,185}$ yield the following values:

$$I_{o,185} = 0.15 \pm 0.01\,\mathrm{mW\,cm^{-2}} \qquad (via\ tert-butanol) \tag{4.8}$$

$$I_{o,185} = 0.14 \pm 0.01\,\mathrm{mW\,cm^{-2}} \qquad (via\ methanol) \tag{4.9}$$

Note the values from the different scavengers are in agreement. The value for the incident fluence rate at 254 nm for the same apparatus at the same position was determined using the KI-KIO_3 actinometer to be:

$$I_{o,254} = 0.87 \pm 0.03\,\mathrm{mW\,cm^{-2}} \qquad (via\ \mathrm{KI-KIO_3}) \tag{4.10}$$

as described in Chapter 2 in the section starting on page 48. While this value was obtained using a 2.0 cm path length cell, the liquid surface was at the same position as that of the 1.0 cm path length cell used in these determinations. The ratio of incident fluence rates at 185 to 254 nm is thus:

$$I_{o,185} : I_{o,254} = 0.16 \pm 0.01 \tag{4.11}$$

This value is within the range of 0.12 to 0.34 reported by Barnes (1960) and by Johnson (1971), who used different types of low pressure mercury lamps. Furthermore, according to those studies, the ratio may be increased by optimization of the diameter, current, temperature of lamps dedicated for 185 nm output. Additionally, the replacement of natural quartz with fused silica for the lamp material will further increase output.

4.6 Summary

From these studies it can be seen that the primary effect of DOM on the 185 nm AOP occurs via the scavenging of $^{\bullet}$OH, resulting in an inverse dependency of the observed psuedo-first order rate constant with the concentration. The two reference materials used, Suwannee River and Nordic Reservoir NOM obtained from the IHSS, induce a similar effect on the 185 nm AOP, suggesting that the aggregate reactivity, and potentially the absorption at 185 nm are comparable for the two materials.

Furthermore, additional support for a model expressed by Equation 2.12 is provided by the use of pure compounds tert-butanol and methanol as model DOM. Indirect experimental evidence supports the assumption that neither of these compounds are significant photon absorbers at 185 nm. However, the significance of photon absorption to the process in general remains unclear and requires further investigation.

Lastly, the use of a suitable probe compound (carbamazepine) and model scavenger (tert-butanol or methanol) allowed the estimation of 185 nm fluence rate in-lieu of a convenient chemical actinometer. This determination thus allowed the subsequent estimation of the 185:254 nm ratio of fluence rates emitted by the particular low pressure mercury lamp used in the collimated beam. A value of $16 \pm 1\%$ was obtained in agreement with literature

values for low pressure mercury lamps. This technique was possible because both the probe compound and the model scavengers used are effectively photochemically inert to 254 nm radiation, and of negligible absorbance at 185 nm at the concentrations used. However, as this method is tedious, a convenient chemical actinometer remains highly desirable. A comparison of such an actinometer with this kinetic method will be insightful.

Chapter 5

Chloride

5.1 Chloride in Natural Waters

The major inorganic solutes in surface waters include the cations Ca^{2+}, Mg^{2+}, Na^{+}, and K^{+}, as well as the anions SO_4^{2-}, Cl^{-}, HCO_3^{-}, and CO_3^{2-}, with other ionic species present at concentrations typically below $1\,mg\,L^{-1}$ (Wetzel, 2001). The typical concentration of Cl^{-} in surface waters ranges from 1 to $100\,mg\,L^{-1}$, with levels in more pristine waters commonly in the range of 5 to $10\,mg\,L^{-1}$ (Livingstone, 1963). The actual concentration depends strongly on the proximity of the corresponding watershed to the marine environment, as well as its underlying geology (Drever, 1988). Concentrations of Cl^{-} much higher than $100\,mg\,L^{-1}$ may occur in water bodies heavily impacted by human activities, such as extensive irrigation, urban runoff, and industrial pollution. A study of the composition of the Rhine river by Zorbist and Stumm (1981) showed that the Cl^{-} concentration was $1.1\,mg\,L^{-1}$ leaving the Swiss Alps, and $178.2\,mg\,L^{-1}$ crossing the border from Germany to the Netherlands. Using statistical techniques and historical data dating back to 1854, it was shown that more than 90% of the Cl^{-} in the lower Rhine was of anthropogenic origin. A maximum Cl^{-} concentration of $250\,mg\,L^{-1}$ is recommended by the WHO (2004), and is emulated by Canadian and other national standards. This recommendation is not based on health effects but rather aesthetics of the detectable salty taste of higher Cl^{-} levels. High Cl^{-} levels do not always impart a salty taste, and Cl^{-} levels as high as $1000\,mg\,L^{-1}$ may impart no salty taste when the dominant cations are Ca^{2+} and Mg^{2+} rather than Na^{+} (APHA, 2012). The results of studies on the involvement of Cl^{-} in the 185 nm AOP are presented here.

5.2 Impact of Chloride on AOPs

Based on the literature of advanced oxidation processes involving ozone or UV with H_2O_2, the influence of Cl^- on process efficiency is not generally considered and assumed to be negligible (Crittenden et al., 1999; Von Gunten, 2003). The radiation chemistry literature, however, shows that the aqueous radical chemistry of chloride is complex, with certain fundamental details in dispute.

Pulse radiolysis studies of aqueous chloride solutions by Anbar and Thomas (1964) found a transient species with a peak absorbance at 340 nm identified as the dichloride radical anion $Cl_2^{\bullet-}$. The formation of $Cl_2^{\bullet-}$ was observed at Cl^- concentrations of 0.2 to 10 mM and pH < 3. At pH 7, $Cl_2^{\bullet-}$ was not observed unless Cl^- concentrations were elevated above 0.1 M. In the presence of $^{\bullet}OH$ scavengers CH_3OH or $K_4[Fe(CN)_6]$, the extent of $Cl_2^{\bullet-}$ formation was found to be inhibited, but not its rate of decay. From these observations it was deduced that the formation of $Cl_2^{\bullet-}$ involves a two step process, first the reaction of $^{\bullet}OH$ with Cl^- to form $Cl^{\bullet}$, with subsequent reaction of $Cl^{\bullet}$ with Cl^- to form $Cl_2^{\bullet-}$. Irradiation of neutral solutions of H_2O_2 and Cl^- established that $Cl_2^{\bullet-}$ did not form, implying that $^{\bullet}OH$ does not react with Cl^- at neutral pH and that the $Cl_2^{\bullet-}$ observed at high Cl^- concentrations occurred in the spur region where pulse radiolysis energy is deposited and local radical concentrations are several orders of magnitude greater as compared to the bulk. Thus the reaction of $^{\bullet}OH$ with Cl^- to form $Cl_2^{\bullet-}$ requires the presence of H^+.

Jayson et al. (1973) investigated the pulse radiolysis of solutions containing NaCl at either neutral pH or acidified to pH<3 using $HClO_4$. Absorption of a transient at 240 nm was seen to decrease at the same rate as the absorption increased at 340 nm. Experimental evidence supported the identity of the species absorbing at 240 nm to be $^{\bullet}OH$ generated from the radiolysis of H_2O, while the species absorbing at 340 nm was proposed to be the $Cl_2^{\bullet-}$ reported by Anbar and Thomas (1964). Their observations were explained

by the net conversion of $^{\bullet}OH$ to $Cl_2^{\bullet-}$ by the following mechanism:

$$^{\bullet}OH + Cl^- \rightleftharpoons HOCl^{\bullet-} \tag{5.1}$$

$$HOCl^{\bullet-} + H^+ \rightleftharpoons Cl^{\bullet} + H_2O \tag{5.2}$$

$$Cl^- + Cl^{\bullet} \rightleftharpoons Cl_2^{\bullet-} \tag{5.3}$$

provided that the forward reaction of 5.3 is fast compared to the generation of $Cl^{\bullet}$ by 5.1 and 5.2 and that the equilibrium of 5.1 lies to the left. The overall rate of $Cl_2^{\bullet-}$ formation was found to depend on the concentrations of Cl^-, H^+ and ionic strength in a manner consistent with the above mechanism 5.1 to 5.3. Rate constants for all of the above forward and backward reactions, as well as equilibrium constants (K) were determined. The equilibrium constants were reported as $K_1 = 0.70\,M^{-1}$, $K_2 = 1.6 \times 10^7$ and $K_3 = 1.9 \times 10^5\,M^{-1}$ (uncertainties omitted). However, this work did not take into account the contribution of $Cl^{\bullet}$ to the absorption at 340 nm, though it has been reported by others that $Cl^{\bullet}$ has a peak absorbance at 320 nm and a molar absorption coefficient at 340 nm comparable to that of $Cl_2^{\bullet-}$ (Buxton et al., 1998; Kläning and Wolff, 1985; Nagarajan and Fessenden, 1985; Treinin and Hayon, 1975).

Gilbert et al. (1988) used electron spin resonance spectroscopy to study the products of organic molecules exposed to $Cl^{\bullet}$ and $Cl_2^{\bullet-}$ generated photochemically. Despite the equilibrium 5.3, when $[Cl^-]$ is sufficiently low, significant $Cl^{\bullet}$ reaction occurs via addition to unsaturated carbon bonds, H-abstraction,

or electron transfer at rates near the diffusion limit. It was deduced that $Cl_2^{\bullet-}$ is of relatively low reactivity compared to $Cl^{\bullet}$, consistent with the findings of Hasegawa and Neta (1978). Furthermore, it was postulated from these and previous findings by the same group that $Cl^{\bullet}$ is of higher reactivity and lower selectivity relative to $^{\bullet}OH$ for the alcohols and organic acids tested. Lastly, while $^{\bullet}OH$ reactions tend to favour H-abstraction from the α-carbon position, reactions with $Cl^{\bullet}$ tend to favour attack at the hydroxyl group via electron transfer.

Buxton et al. (1998) used both pulse radiolysis and laser flash photolysis at 193 nm to investigate equilibrium 5.3. They obtained a value of $1.4 \times 10^5\,M^{-1}$ in relatively close agreement with that of Jayson et al. (1973), the discrepancy attributed possibly to the previous study not taking $Cl^{\bullet}$ into account when measuring $Cl_2^{\bullet-}$. Deviations of reactions 5.3 from equilibrium were studied by the presence of the organic scavenger tert-butanol. The reactions of $Cl^{\bullet}$ and $Cl_2^{\bullet-}$ with water:

$$Cl^{\bullet} + H_2O \longrightarrow H^+ + HOCl^{\bullet-} \tag{5.4}$$

$$Cl_2^{\bullet-} + H_2O \longrightarrow H^+ + HOCl^{\bullet-} + Cl^- \tag{5.5}$$

were found to have rate constants of $2.5 \times 10^5\,s^{-1}$ (5.4) and $1.3 \times 10^3\,s^{-1}$ (5.5). The reaction 5.4 is equivalent to the reverse reaction of equilibrium 5.2 introduced by Jayson et al. (1973). In addition to the scavenging of $Cl^{\bullet}$ by Cl^- to form $Cl_2^{\bullet-}$, reactions with organic solutes and water itself are potentially significant sinks of $Cl^{\bullet}$.

Given the high reactivity of $Cl^{\bullet}$, a subsequent study by Buxton et al. (2000) used laser flash photolysis of chloroacetone at 243 nm to generate $Cl^{\bullet}$ in the absence of Cl^- and equilibrium 5.3. With temperature controlled photolysis cells, this approach was used to measure the second-order reaction rate constants for $Cl^{\bullet}$ with several simple organic compounds and inorganic anions at 25 °C, as well activation energies by varying the temperature from 5 to 35 °C. Relevant details from this study will be discussed below in relation to findings from this work.

As mentioned in Chapter 1, the Cl^- anion is transparent to UV radiation at wavelengths above 200 nm at the concentrations found in solution. In the vicinity of 185 nm, a strong absorption band occurs for aqueous Cl^- due to a charge-transfer-to-solvent mechanism discussed (Blandamer and Fox, 1970; Fox et al., 1978). As previously mentioned in Table 1.2, the molar absorption coefficient (ϵ_{185}) for Cl^- at 185 nm has been reported as $3800 \pm 300\ M^{-1}\ cm^{-1}$, and results in photodissociation to the radical $Cl^{\bullet}$ and a solvated electron e^-_{aq} with a quantum yield (Φ_{Cl^-}) of 0.43 ± 0.02 (Dainton and Fowles, 1965). This implies that at [Cl^-] between 15 and 20 $mg\,L^{-1}$, more than half the 185 nm photons absorbed by the water matrix are absorbed by Cl^- rather than H_2O. Thus, in the 185 nm regime, the presence of Cl^- results in the formation of $Cl^{\bullet}$ and decreased H_2O photolysis, possibly shifting the main reactive species from $^{\bullet}OH$ to $Cl^{\bullet}$. Experimental confirmation of this is one of the main objectives of the work presented in this chapter.

5.3 Chloride in the 254 nm - H_2O_2 Regime

The influence of Cl^- on the 254 nm photolysis of H_2O_2 was investigated using the UV/H_2O_2 collimated beam apparatus. Carbamazepine was used as a probe compound and the DOM used was either tert-butanol or Suwannee River NOM reference material obtained from the IHSS. The Cl^- concentration was varied between 0 and 100 $mg\,L^{-1}$ using NaCl. Solution pH was

neutralized using NaOH. The dose of H_2O_2 applied was $7\,mg\,L^{-1}$. Dark controls were used to verify the absence of significant thermal reactions. All solutions were reproduced in triplicate and irradiated. Following irradiations, residual H_2O_2 was quenched with a 10 µL droplet of approximately $100\,mg\,L^{-1}$ bovine catalase before analysis of carbamazepine by HPLC.

Results obtained using tert-butanol at $7\,mg\,L^{-1}$ as C are plotted in Figure 5.1, and reveal no detectable difference in degradation rate for any of the four Cl^- levels used.

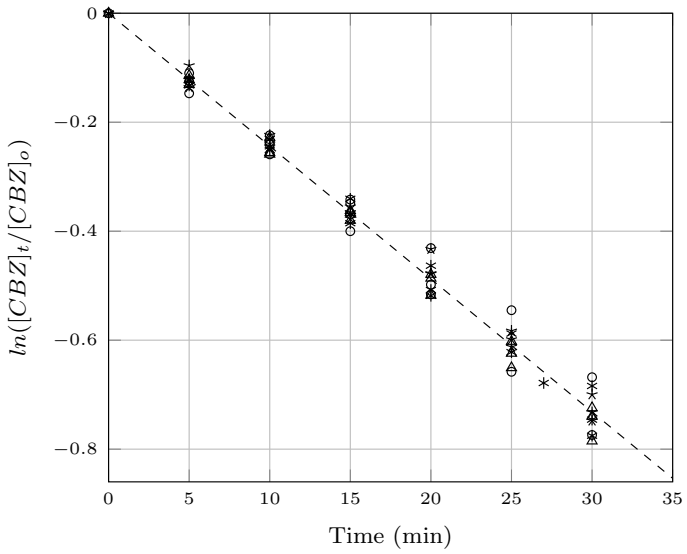

Figure 5.1: Tert-Butanol in the 254 nm - H_2O_2 regime and influence of chloride. $[H_2O_2]$ =7 $mg\,L^{-1}$. $[tBuOH] = 7\,mg\,L^{-1}$ as C. $[CBZ]_o \simeq 0.25$ µM. NaCl used as source of Cl^-. $[Cl^-] < 1\,mg\,L^{-1}$ (—○—), $[Cl^-] = 25\,mg\,L^{-1}$ (—∗—), $[Cl^-] = 40\,mg\,L^{-1}$ (—△—), $[Cl^-] = 100\,mg\,L^{-1}$ (—⋆—).

Subsequently, Suwannee River DOM at $7\,mg\,L^{-1}$ as C was tested, and the results plotted in Figure 5.2. Again, the observed degradation rates for 0 and $100\,mg\,L^{-1}$ of Cl^- show no statistically significant difference. Thus, under the conditions used and an environmentally meaningful range of Cl^- concentration, any influence of Cl^- on removal kinetics is undetectable.

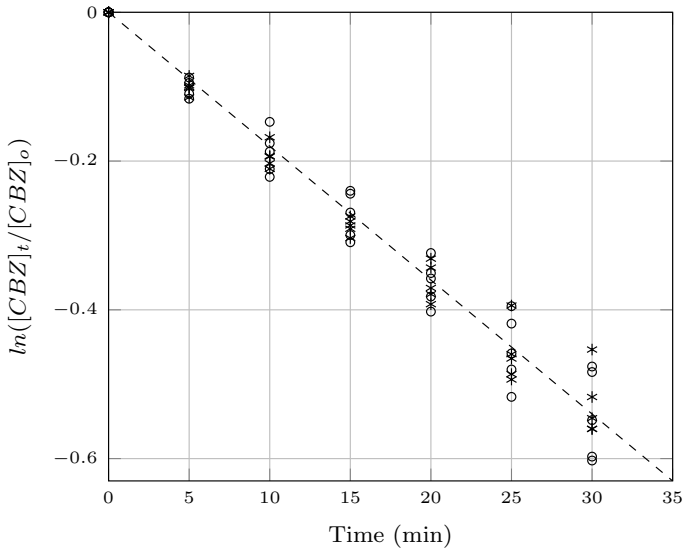

Figure 5.2: Suwannee River NOM in the 254 nm - H_2O_2 regime and influence of chloride. $[H_2O_2]$ =7 mg L^{-1}. $[DOC] = 7\,mg\,L^{-1}$ as C. $[CBZ]_o \simeq 0.25\,\mu M$. All solutions prepared at pH 7. NaCl used as source of Cl^-. $[Cl^-] < 1\,mg\,L^{-1}$ (—∘—), $[Cl^-] = 100\,mg\,L^{-1}$ (—∗—).

5.4 Chloride in the 185 nm Regime

When these same experiments are repeated in the 185 nm regime, a significant effect is observed, the results of which are plotted in Figure 5.3 whith tert-butanol used as DOM, and in Figure 5.4 with Suwannee River NOM.

When tert-butanol is used, an increase in $[Cl^-]$ results in a pronounced increase in the rate of degradation of the probe carbamazepine. In contrast, when tert-butanol is replaced by Suwannee River NOM, the opposite effect is observed, with an increase in $[Cl^-]$ corresponding to a decrease in the rate of probe degradation.

These observations may be explained by at least three independent aspects

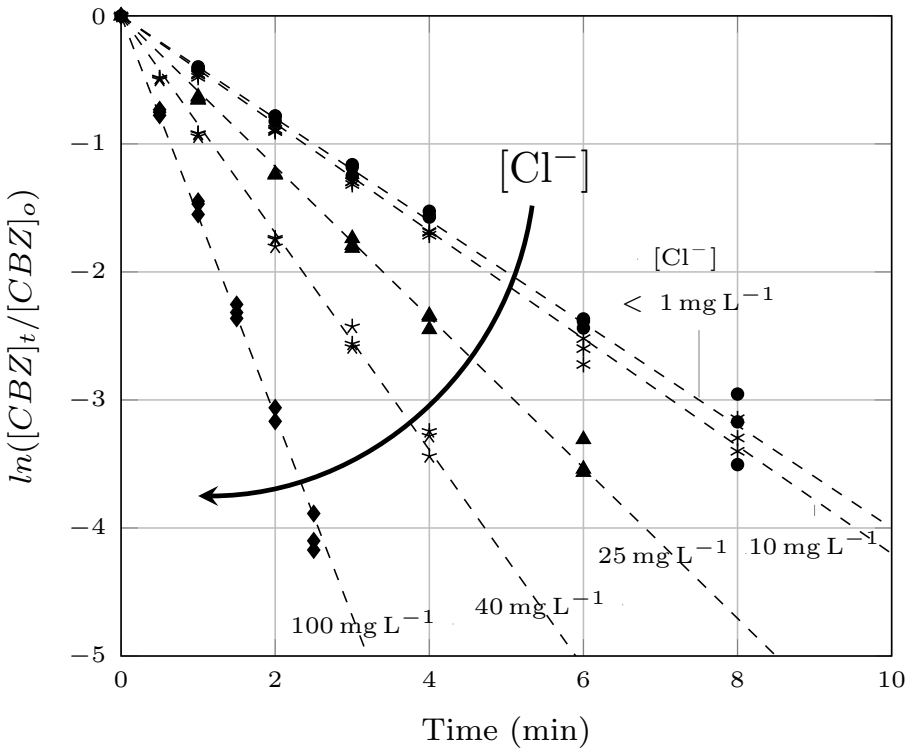

Figure 5.3: Tert-Butanol ($(CH_3)_3COH$) in the 185 nm regime and influence of chloride, using carbamazepine (CBZ) as a probe. $[(CH_3)_3COH] = 7\,\mathrm{mg\,L^{-1}}$ as C. $[CBZ]_o \simeq 0.25\,\mu\mathrm{M}$. NaCl used as source of Cl^-. Arrow indicates trend in observed degradation rate resulting from increased chloride concentration.

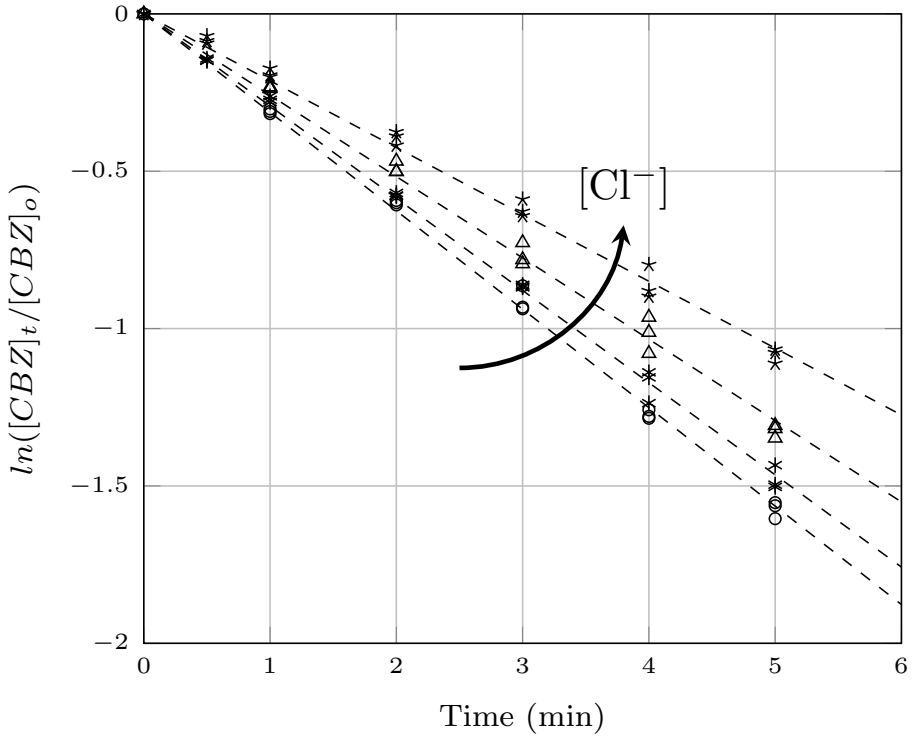

Figure 5.4: Suwannee River NOM in the 185 nm regime and influence of chloride, using carbamazepine (CBZ) as a probe. $[DOC] = 8\,\mathrm{mg\,L^{-1}}$ as C. $[CBZ]_o \simeq 0.25\,\mu\mathrm{M}$. NaCl used as source of Cl^-. $[Cl^-] < 1\,\mathrm{mg\,L^{-1}}$ (—○—), $[Cl^-] = 25\,\mathrm{mg\,L^{-1}}$ (—✶—), $[Cl^-] = 40\,\mathrm{mg\,L^{-1}}$ (—△—), $[Cl^-] = 100\,\mathrm{mg\,L^{-1}}$ (—⋆—). Arrow indicates trend in the observed probe degradation rate resulting from increased chloride concentration.

related to the increase in [Cl^-]. First, increased [Cl^-] results in a shift in 185 nm photon absorbance away from water and toward Cl^-, with corresponding changes in the generation rates of $^\bullet OH$ and $Cl^\bullet$. A second effect is the difference in $^\bullet OH$ and $Cl^\bullet$ reactivities towards the matrix, as measured by the second-order reaction rate constants with the major scavengers. The greater the reactivity, the lower the radical concentration should be under steady-state conditions. Lastly, differences in the reactivities of $^\bullet OH$ and $Cl^\bullet$ with the probe or target compound itself will contribute to changes in the observed degradation rate. An additional complication is the possibility that a portion of the $Cl^\bullet$ may be converted to $^\bullet OH$ (discussed below), though the converse is not expected to occur at circumneutral pH based on evidence presented earlier.

In general, using an expression based on Equation 2.13:

$$ln(C/C_o) = -k'\,t = -(k_{\mathrm{OH},C}[^\bullet\mathrm{OH}]_{ss} + k_{\mathrm{Cl},C}[\mathrm{Cl}^\bullet]_{ss})\,t \tag{5.6}$$

where k' is the experimentally observed pseudo first-order rate constant. This expression can be rewritten in terms of the quantum yields Φ, the fraction of absorbed photons f, the rate of 185 nm photon absorption per unit volume I_a, the second-order rate constant for the radical-scavenger reactions and the concentration of scavenger $[S]$. Grouping common terms, an expression for k' is given by:

$$k' = \left(\frac{k_{\mathrm{OH},C}}{k_{\mathrm{OH},S}}\,\Phi_{\mathrm{H_2O}} f_{\mathrm{H_2O}} + \frac{k_{\mathrm{Cl},C}}{k_{\mathrm{Cl},S}}\,\Phi_{\mathrm{Cl}^-} f_{\mathrm{Cl}^-}\right)\frac{I_a}{[S]} \tag{5.7}$$

Inspection of this expression reveals that the bracketed term controls the value of k' for a specific compound via four independent second-order rate constants. Each term in the sum will contribute to k' if both $^{\bullet}OH$ and $Cl^{\bullet}$ are present, and the contribution by each radical will further depend on the relative reactivities of the probe and the scavenger. It should be noted that the two quantum yields are of comparable magnitude, $\Phi_{H_2O} \simeq 0.3$, and $\Phi_{Cl^-} \simeq 0.4$. Furthermore, the rate constants involving $Cl^{\bullet}$ may be viewed as effective rate constants which incorporate the possible equilibrium with $Cl_2^{\bullet -}$. The second-order rate constants for $^{\bullet}OH$ and $Cl^{\bullet}$ with tert-butanol are essentially equal at $6 \times 10^8\,M^{-1}\,s^{-1}$ (Buxton et al., 2000). In general, $Cl^{\bullet}$ is expected to be more reactive than $^{\bullet}OH$, and increased reactivity of carbamazepine with $Cl^{\bullet}$ is consistent with the observations.

In the absence of pulse radiolysis or laser flash photolysis capabilities, whereby radical species may be directly detected and distinguished spectrophotometrically, indirect studies were conducted using probe compounds. The careful use of probe compounds may allow kinetic and mechanistic details to be deduced. A probe may be selected such that one of the two terms comprising k' in the right hand side of equation 5.7 is much smaller than the other. Ideally, two such probes would be available in order to alternately eliminate one of the terms experimentally. Based on the evidence from Figures 5.3 and 5.4, carbamazepine appears to be reactive to both $^{\bullet}OH$ and $Cl^{\bullet}$, with likely greater reactivity with the latter than the former.

No compound, both soluble in water and easily quantifiable by HPLC, is known to be highly reactive to $Cl^{\bullet}$ while negligibly reactive with $^{\bullet}OH$. However, a probe for the converse situation is suggested by the literature. During studies of solar processes in surface waters, it was suggested by Nowell and Hoigné (1992) that nitrobenzene would be relatively nonreactive to $Cl^{\bullet}$ based on structure-reactivity arguments and evidence from gas-phase reactions. Support for this assumption was provided by UV photolysis of aqueous chlorine at pH 1 containing two probe compounds, 1-chlorobutane and

nitrobenzene. Under these conditions, $Cl^{\bullet}$ would be formed in the absence of any Cl^{-}, and it was reported that the degradation of 1-chlorobutane was subsequently observed without detectable removal of nitrobenzene. The second-order reaction rate constant of nitrobenzene with $^{\bullet}OH$ is $3.0 \times 10^9\,M^{-1}\,s^{-1}$ (Buxton et al., 1988).

Thus, the use of nitrobenzene as a probe in the 185 nm regime should produce results discrepant with those observed in Figures 5.3 and 5.4 obtained using carbamazepine. Assuming equation 5.7 to be valid, the use of nitrobenzene as a probe, with either tert-butanol or Suwannee River NOM as the scavenger, should result in a decrease of k' with increasing $[Cl^{-}]$ in both cases. This is because as $[Cl^{-}]$ increases, the first term of equation 5.7 decreases due to the decreased absorption of photons by water (f_{H_2O}) resulting in a lower $[^{\bullet}OH]_{ss}$, while a presumed increase in $Cl^{\bullet}$ is ineffective due to a low $k_{Cl,NB}$ value. Experimental observations confirm the prediction that k' decreases in both cases, as plotted in Figures 5.5 and 5.6.

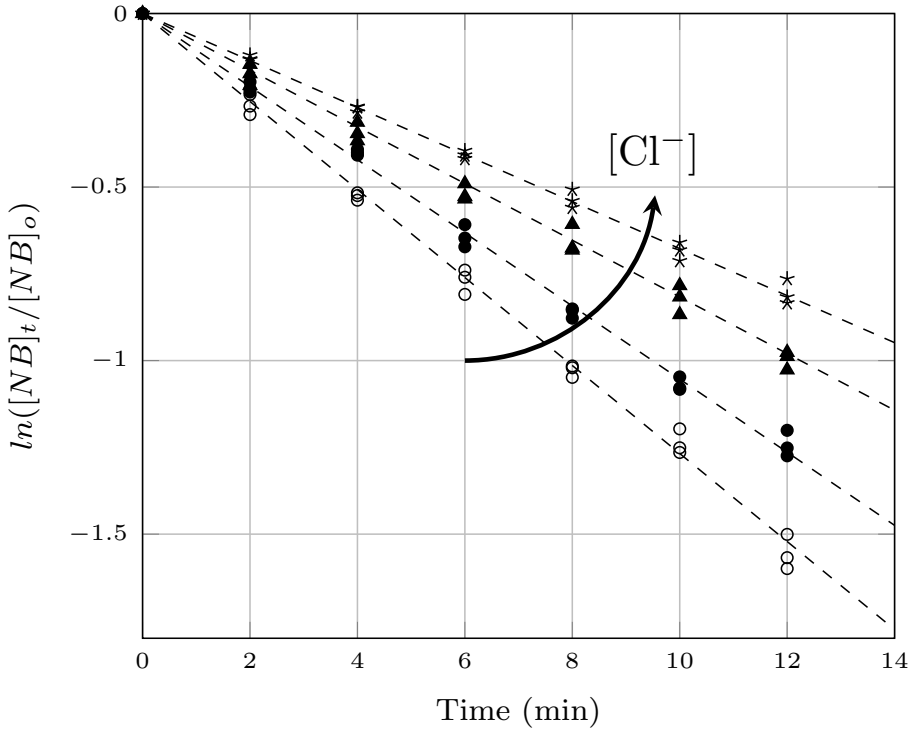

Figure 5.5: Tert-Butanol ($(CH_3)_3COH$) in the 185 nm regime and influence of chloride, using nitrobenzene (NB) as a probe. $[(CH_3)_3COH] = 8\,mg\,L^{-1}$ as C. $[NB]_o \simeq 1\,\mu M$. NaCl used as a source of Cl^-. $[Cl^-] < 1\,mg\,L^{-1}$ (—○—), $[Cl^-] = 25\,mg\,L^{-1}$ (—●—), $[Cl^-] = 40\,mg\,L^{-1}$ (—▲—), $[Cl^-] = 100\,mg\,L^{-1}$ (—⋆—). Arrow indicates trend in observed degradation rate resulting from increased chloride concentration.

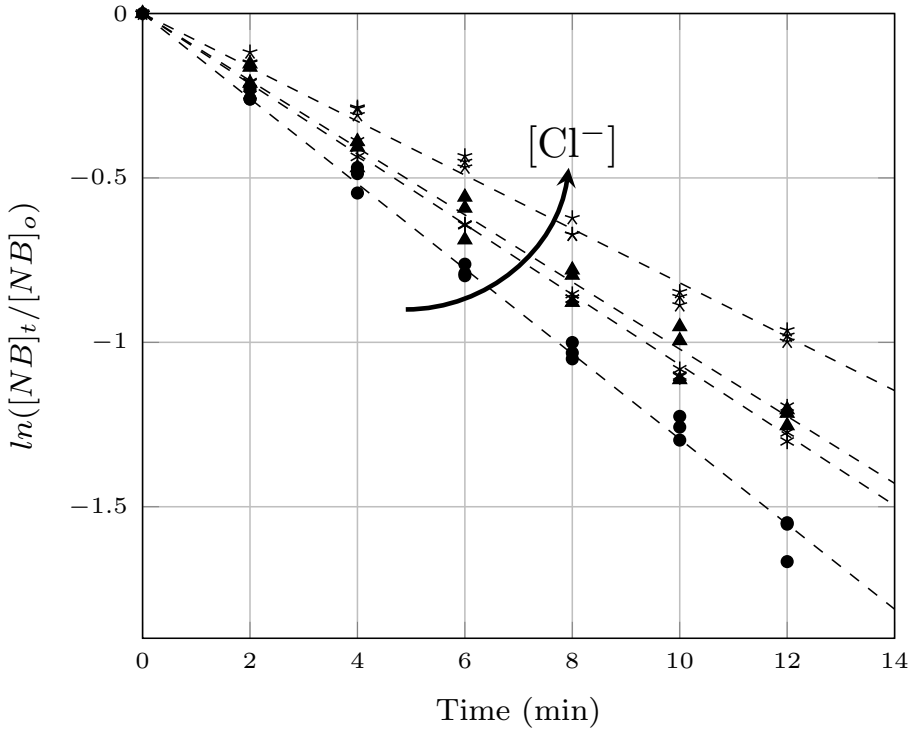

Figure 5.6: Suwannee River NOM in the 185 nm regime and influence of chloride, using nitrobenzene (NB) as a probe. $[DOC] = 8\,\mathrm{mg\,L^{-1}}$ as C. $[NB]_o \simeq 1\,\mu\mathrm{M}$. NaCl used as a source of Cl^-. $[Cl^-] < 1\,\mathrm{mg\,L^{-1}}$ (—●—), $[Cl^-] = 25\,\mathrm{mg\,L^{-1}}$ (—✶—), $[Cl^-] = 40\,\mathrm{mg\,L^{-1}}$ (—▲—), $[Cl^-] = 100\,\mathrm{mg\,L^{-1}}$ (—★—). Arrow indicates trend in observed degradation rate resulting from increased chloride concentration.

5.5 Relative Reactivity of •OH and Cl•

One of the difficulties with indirect kinetic studies of Cl^- in the 185 nm regime is the absence of suitable probe compounds that will allow the independent study of the •OH and Cl• contributions. However, either term of equation 5.7 may be isolated, regardless of the probe used, if a suitable scavenger compound S can be found such that the corresponding values of the second-order rate constants $k_{OH,S}$ and $k_{Cl,S}$ differ by several orders of magnitude. Very limited information on $k_{Cl,S}$ in the aqueous phase exists.

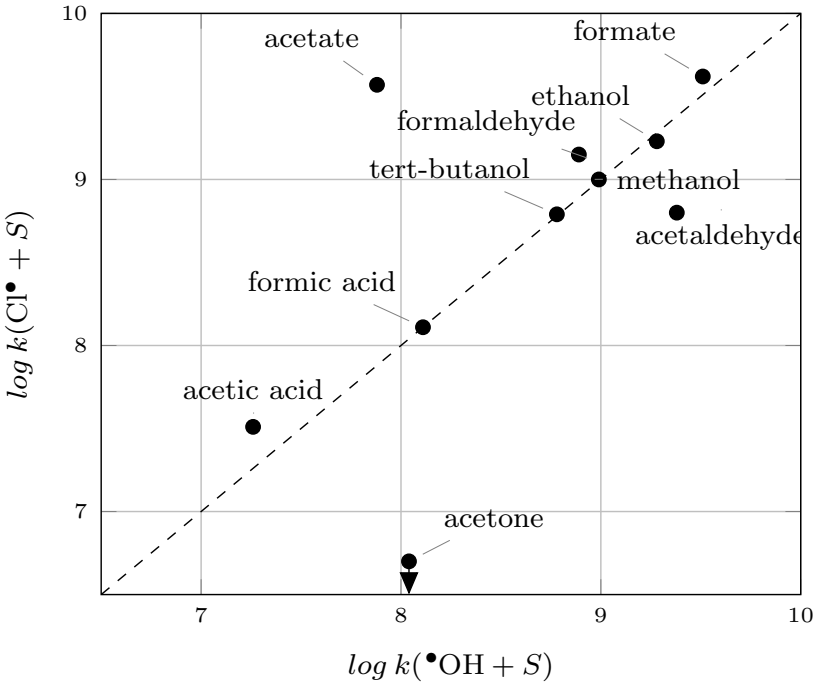

Figure 5.7: Comparison of second-order rate constants of select organic solutes with •OH and Cl• at 25 °C. Key features are the outliers, acetate and acetic acid, from the general trend. Adapted from Buxton et al. (2000)

The work by Buxton et al. (2000) reports values of $k_{Cl,S}$ for eleven small organic compounds. The plot of Figure 5.7 is adapted from that work and plots the values of $k_{OH,S}$ versus $k_{Cl,S}$ at 25 °C on log-log scales. It can be

seen that fairly good agreement between most of the compounds studied exists between the two rate constants. However, it is noted by the authors of that work that the activation energies, that were also measured for both •OH and Cl• reactions, differ and that the close correspondence observed at 25 °C will be weaker at other temperatures. Nevertheless, while compounds such as methanol and tert-butanol have virtually the same rate constants for both radicals, the two compounds, acetone (CH_3COCH_3) and acetate (CH_3COO^-) are prominent outliers from the general trend seen in Figure 5.7.

5.6 Evidence for Cl• from Probe-Scavenger Systems

An explanation for the observations of the chloride effect made using the probes carbamazepine (Figures 5.3 and 5.4) and nitrobenzene (Figures 5.5 and 5.6) is provided by a model described by Equation 5.7. In the absence of chloride and any other solutes absorbing at 185 nm (i.e. $f_{H_2O} \approx 1$), only •OH is involved and the expression is reduced to include only the first term of Equation 5.7. If the chloride level is sufficiently high (i.e. $f_{H_2O} \ll f_{Cl^-}$), the contribution of Cl• may dominate. Note, it is assumed thus far that any conversion of Cl• to•OH is negligible.

For low to moderate levels of chloride, an intermediate situation may prevail and potentially both radicals •OH and Cl• will contribute to an extent depending on relative reactivities to the probe (or target) compound and the scavenger (or matrix). In such a case, both terms of Equation 5.7 may contribute to the overall degradation rate. Table 5.1 displays the reaction rate constants plotted in Figure 5.7 of the four pure substances used as model scavengers in this work. The reaction rate ratios of the rightmost column contains the key information used in this study.

Table 5.1: Comparison of $^{\bullet}OH$ and $Cl^{\bullet}$ reactivities for pure compounds used as model organic matter in the 185 nm regime

Scavenger (S)	$k_{OH,S}$ $(M^{-1}\,s^{-1})\times10^{-8}$	$k_{Cl,S}$ $(M^{-1}\,s^{-1})\times10^{-8}$	$k_{OH,S}/k_{Cl,S}$
Methanol CH_3OH	9.7	10	0.97
tert-Butanol $(CH_3)_3COH$	6.0	6.2	0.97
Acetate CH_3COO^-	0.75	37	0.02
Acetone CH_3COCH_3	1.1	< 0.05	> 22

Rate constants taken from Buxton et al. (1988) and Buxton et al. (2000).

Since tert-butanol and methanol have essentially the same reaction rate constant for both $^{\bullet}OH$ and $Cl^{\bullet}$ ($k_{OH,S} \sim k_{Cl,S}$) and the quantum yields are comparable ($\Phi_{H_2O} \sim \Phi_{Cl^-}$), the effect of chloride depends largely on the relative reactivity of the probe compounds if Equation 5.7 is valid.

If acetate is used as the scavenger, the second-order reactivity with $Cl^{\bullet}$ is approximately 50 times greater than that for $^{\bullet}OH$. Thus, when Cl^- is present under 185 nm irradiation, the formation rate of $^{\bullet}OH$ will decrease, while that of $Cl^{\bullet}$ increases, and the $Cl^{\bullet}$ formed will be consumed more efficiently by acetate relative to $^{\bullet}OH$. This would have the effect of reducing the steady-state concentration of both radicals in question. In the case of carbamazepine, the second-order rate constants with both $^{\bullet}OH$ and $Cl^{\bullet}$ are assumed to be of the same order of magnitude ($k_{OH,C} \sim k_{Cl,C}$). However, a shift to $Cl^{\bullet}$ involves a shift to greater contribution from the second term in Equation 5.7. Since with acetate $k_{Cl,C}/k_{Cl,S} \ll k_{OH,C}/k_{OH,S}$, the observed pseudo-first order rate constant k' should decrease as $[Cl^-]$ increases. When nitrobenzene is

used as a probe, the same trend is expected, with the additional impact due to $k_{Cl,C} \ll k_{OH,C}$.

The experimental observations are in agreement with the above description. As can be seen in Figure 5.8, the observed rate constants k' for both probes, carbamazepine and nitrobenzene, decrease upon addition of chloride. Note that Figure 5.8 shows, that while k' for nitrobenzene is attenuated by the presence of Cl^-, a residual k' is measured and attributed to $^{\bullet}OH$ entirely. This is expected based on values of ϵ_{185} for Cl^- both reported in the literature and measured in this work (see Section 5.10). At $[Cl^-] = 100\,mg\,L^{-1}$, the fraction of 185 nm photons absorbed by water is approximately 25%. The k' for nitrobenzene, however, decreases by approximately 50%, suggesting the possibility that some $Cl^{\bullet}$ does indeed convert to $^{\bullet}OH$. Attempts to modify the model to account for such a conversion, using the reactions of $Cl^{\bullet}$ and $Cl_2^{\bullet-}$ with water (Equations 5.4 and 5.5 respectively), have been unsuccessful and indicate key mechanistic aspects are missing.

If acetone is used as the scavenger, the reverse situation is induced compared to that of acetate. Acetone reactivity with $Cl^{\bullet}$ is low relative to $^{\bullet}OH$, with $^{\bullet}OH$ being at least 22 times more reactive with acetone. In this case, the effect of chloride will depend more strongly on the reactivity of the probes with $Cl^{\bullet}$ ($k_{Cl,C}$). When chloride is sufficiently high and the $Cl^{\bullet}$ formation rate increases, the lower scavenging of $Cl^{\bullet}$ implies that those compounds with higher reactivities with $Cl^{\bullet}$ will degrade faster than when chloride is absent. For compounds of lower reactivity with $Cl^{\bullet}$, lower degradation rates are expected. Thus, with acetone as scavenger, the addition of chloride should cause the degradation rate of carbamazepine to increase, while that of nitrobenzene should decrease. This description is consistent with experimental observations, as can be seen from Figure 5.9, where k' increases for carbamazepine and decreases slightly for nitrobenzene. In the absence of actual values of $k_{Cl,C}$ for these probes, the description must remain semi-quantitative. However, if nitrobenzene is truly nonreactive with $Cl^{\bullet}$, as suggested by Nowell and Hoigné (1992), then the limited removal observed may

be due to another mechanism, such as the conversion of $Cl^{\bullet}$ to $^{\bullet}OH$ discussed above. Since direct photolysis at 254 nm is negligible, and volatilization is eliminated by using a sealed cell, a radical conversion process provides a plausible explanation.

Though conducted using pure compounds as scavengers, the results from acetate and acetone demonstrate that the net effect of chloride depends on several factors. Naturally occurring DOM contains carboxylic acid and ketone functional groups that may influence $Cl^{\bullet}$ reactivity. While the mechanisms of $Cl^{\bullet}$ are not well understood in the aqueous phase, it has been suggested by Gilbert et al. (1988) that $Cl^{\bullet}$ oxidation is more likely to occur via electron transfer at hydroxyl groups rather than H-abstraction commonly observed with $^{\bullet}OH$. Thus, the chemical details of site-specific NOM may have a substantial effect on observed degradation rates if the involvement of $Cl^{\bullet}$ is significant. Furthermore, while pH effects were not specifically studied in this work, it is worth noting that the radical reactivities of carboxylic acids, with both $^{\bullet}OH$ and $Cl^{\bullet}$, are strongly influenced by pH, as can be seen in Figure 5.7 for acetate/acetic acid and formate/formic acid.

The low reactivity of acetone with $Cl^{\bullet}$ was suggested by Buxton et al. (2000) as the result of the low extent of hydration of acetone. In aqueous solution, ketones react with water to form an equilibrium with the geminal diol (gem-diol). As electron transfer by $Cl^{\bullet}$ is preferred at the hydroxyl group, the position of the equilibrium towards the gem-diol will be related to the reactivity of the compound. In the case of acetone, the equilibrium is far to the non-hydrated ketone form, with only 0.1% of the molecules present as the hydrated gem-idol. In the case of formaldehyde, 99.9% is in the form of the gem-diol (McMurry, 1996). Acetaldehyde is approximately 55% hydrated (Kurz, 1967). The reactivities reported by Buxton et al. (2000) are in the order $formaldehyde > acetaldehyde > acetone$, matching the order of hydration.

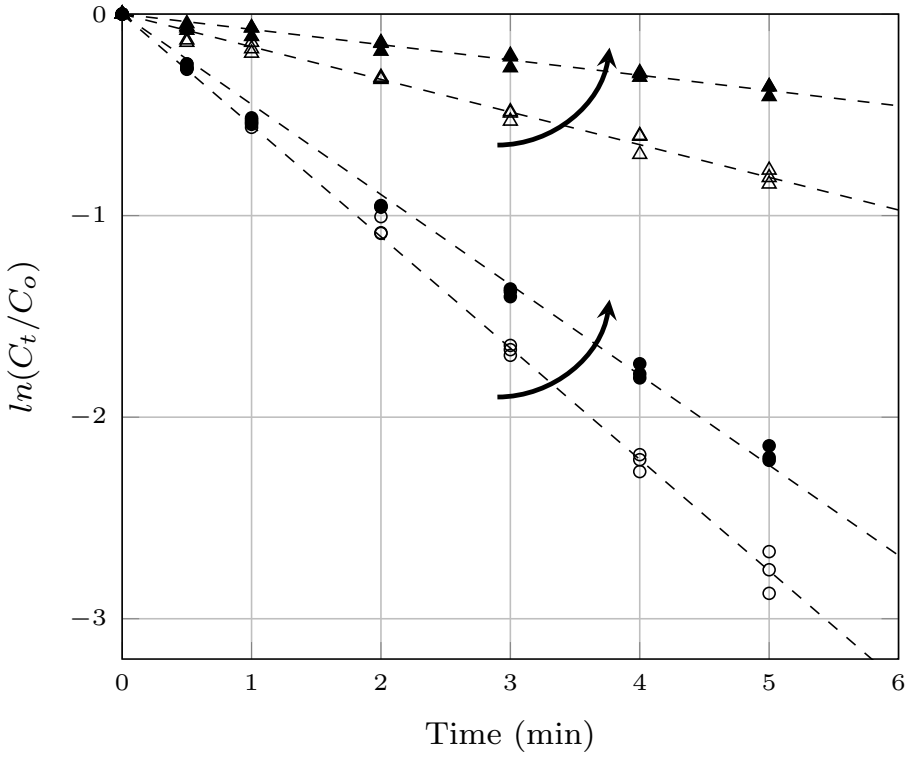

Figure 5.8: Acetate (CH_3COO^-) system (pH $\simeq$ 6) at 185 nm with both carbamazepine (CBZ) and nitrobenzene (NB) as probes. $[CH_3COO^-]$ = 8 mg L^{-1} as C. $[CBZ]_o \simeq 0.25\,\mu M$. $[NB]_o \simeq 1\,\mu M$. NaCl used as source of Cl^-. $[Cl^-] < 1$ mg L^{-1}-CBZ(—○—),NB(—△—); $[Cl^-] = 100$ mg L^{-1}-CBZ(—●—),NB(—▲—). Arrows indicate shift in degradation rate of the probe compound due to the presence of 100 mg L^{-1} of Cl^-.

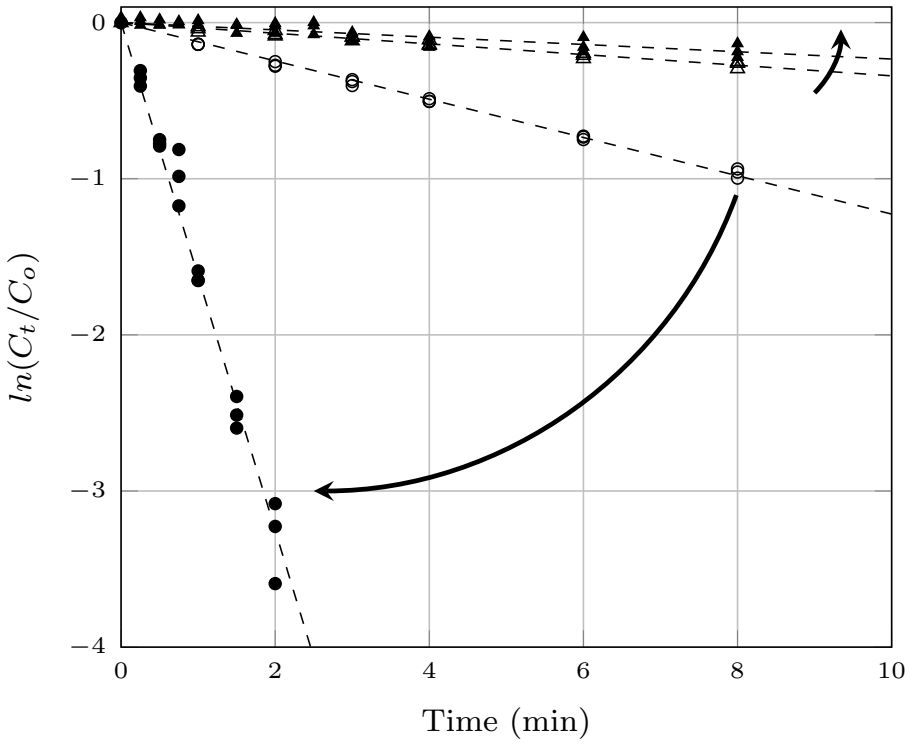

Figure 5.9: Acetone (CH_3COCH_3) system at 185 nm with both carbamazepine (CBZ) and nitrobenzene (NB) as probes. [(CH_3COCH_3] = $1000\,mg\,L^{-1}$ as C. $[CBZ]_o \simeq 0.25\,\mu M$. $[NB]_o \simeq 1\,\mu M$. NaCl used as source of Cl^-. [Cl^-] $< 1\,mg\,L^{-1}$-CBZ(—○—),NB(—△—); [Cl^-] = $100\,mg\,L^{-1}$-CBZ(—●—),NB(—▲—). Arrows indicate shift in degradation rate of the probe compound due to the presence of $100\,mg\,L^{-1}$ of Cl^-.

5.7 Evidence from Ionic Strength Effects

The dependence of reaction kinetics on ionic strength of the solution may yield insight on a process. By adjusting the ionic strength, most reaction rates will change. The Debye-Hückel theory predicts that for dilute solutions, the reaction rate k, between ions A and B will depend on ionic strength (μ), at 25 °C, according to:

$$log(k/k_o) = 1.02 z_A z_B \sqrt{\mu} \tag{5.8}$$

where z_A and z_B are the charges of the ions A and B, respectively (Laidler, 1987). This expression predicts no effect on reaction rate when one or both of the reactants are uncharged. However, an ionic strength effect is observed for many reactions involving neutral reactants and an empirical extension to the theory was made by Hückel to describe the activity of uncharged reactants. This leads to the expression for reactions between neutral molecules:

$$log(k/k_o) = b\mu \tag{5.9}$$

where b is a constant for which no theory is available to predict either its magnitude (Laidler, 1987) nor even its sign (Moore and Pearson, 1981).

Ionic strength studies are unable to establish a mechanism but may be useful in elaborating details regarding reactants. In the absence of charged reactants, an ionic strength effect may yet be substantial if one of the reactants is in equilibrium with charged species. In the case of $^{\bullet}$OH reacting with the

probe carbamazepine and the scavenger tert-butanol, no charged reactants are involved. However, when Cl^- is present and $Cl^\bullet$ is generated, the equilibrium 5.3 may induce a significant ionic strength effect on the reaction rate.

A semi-quantitative study was conducted whereby the ionic strength effect was investigated for the influence of chloride at 185 nm. Adjusting ionic strength with NaF, the degradation rate of carbamazepine in the presence of the scavenger tert-butanol, was studied with and without the addition of $100\,mg\,L^{-1}$ of chloride. The results in the absence of chloride are plotted in Figure 5.10, while those with chloride are plotted in Figure 5.11. The observed pseudo first-order rate constants k' are normalized to the rate at lowest ionic strength k'_o, and $log(k'/k'_o)$ is plotted against both μ and $\sqrt{\mu}$ for comparison in Figure 5.12.

It can be seen from Figures 5.10, 5.11, and 5.12, that the observed rate k' decreases with increasing ionic strength. Furthermore, it is apparent that the effect is significantly more pronounced in the presence of chloride. Note that in Figure 5.12, linear regression of rate data plotted both against μ (upper plot) and $\sqrt{\mu}$ (lower plot) indicates better agreement in the absence of chloride when plotted against μ, while the presence of chloride shows better agreement with $\sqrt{\mu}$ as the abscissa. The data points are limited, but supports the existence of a secondary salt effect when Cl^- is present, likely involving equilibrium 5.3. Additional studies conducted with greater resolution may be useful in elucidating the mechanisms involved.

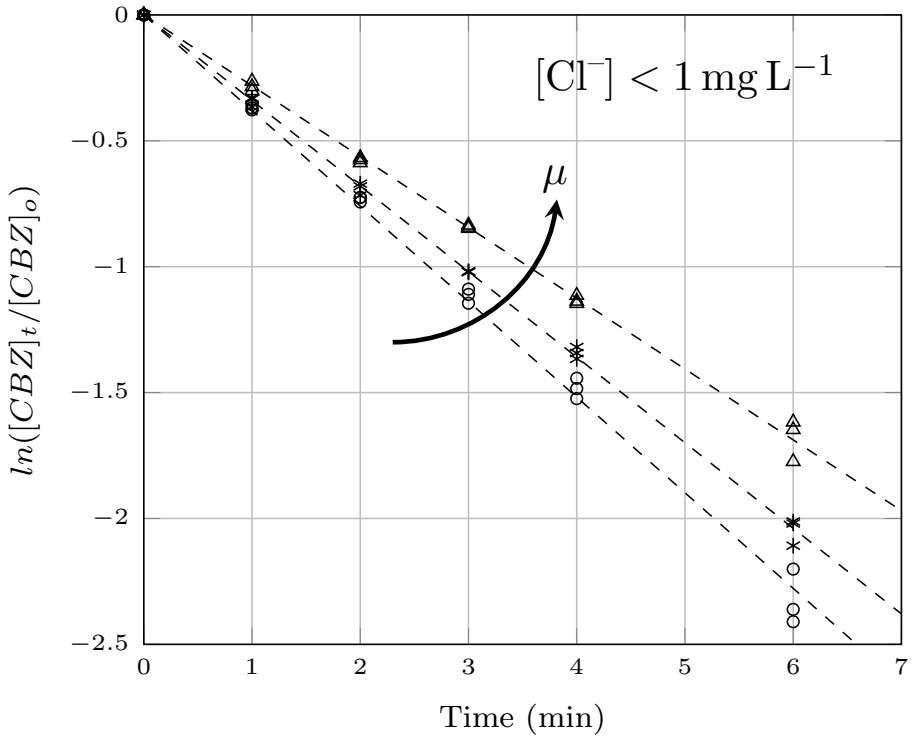

Figure 5.10: Influence of ionic strength (μ) in 185 nm regime on the degradation of carbamazepine (CBZ) in the presence of tert-butanol and no chloride. $[CBZ]_o \simeq 0.25\,\mu M$, $[(CH_3)_3COH] = 7\,mg\,L^{-1}$ as C. Ionic strength adjusted using NaF. $\mu =$ 0.00 M (—○—), 0.08 M(—∗—), 0.16 M (—△—). Arrow indicates shift in degradation rate of the probe compound due to increasing μ.

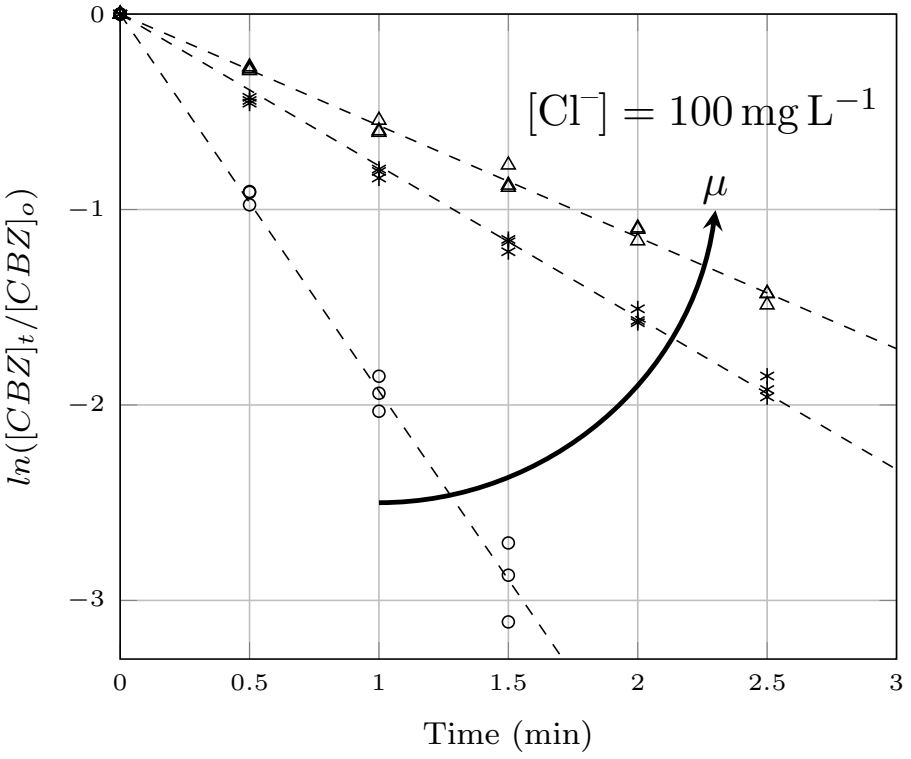

Figure 5.11: Influence of ionic strength (μ) in 185 nm regime on the degradation of carbamazepine (CBZ) in the presence of tert-butanol and chloride. $[CBZ]_o \simeq 0.25\,\mu M$. $[(CH_3)_3COH] = 7\,mg\,L^{-1}$ as C. $[Cl^-] = 100\,mg\,L^{-1}$. NaCl used as source of chloride. Ionic strength adjusted using NaF. $\mu = 0.00\,M$ (—○—), $0.08\,M$(—∗—), $0.16\,M$ (—△—). Arrow indicates shift in degradation rate of the probe compound due to increasing μ.

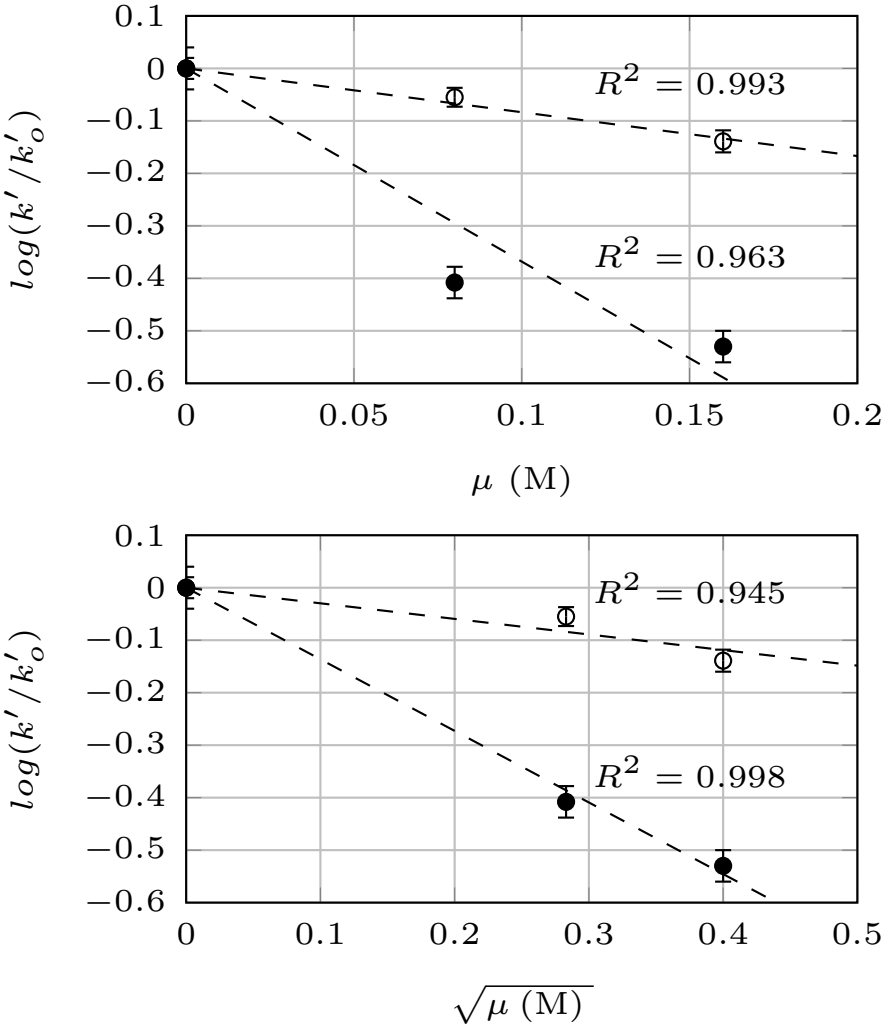

Figure 5.12: Influence of ionic strength (μ) on the degradation of carbamazepine with and without chloride. Ionic strength adjusted by NaF. Data obtained from slopes (k') of Figures 5.10 and 5.11. Upper plot with μ as abscissa. Lower plot with $\sqrt{\mu}$ as abscissa. Both plots use identical ordinates. Chloride obtained from NaCl. Tert-butanol used as a scavenger with $[(CH_3)_3COH] = 7\,mg\,L^{-1}$ as C. Carbamazepine used as probe with $[CBZ]_o \simeq 0.25\,\mu M$. $[Cl^-] < 1\,mg\,L^{-1}$ ($\circ$). $[Cl^-] = 100\,mg\,L^{-1}$ ($\bullet$). Error bars derive from the standard errors calculated for k' and the subsequent propagation of error calculation.

5.8 Product Studies of Phenol Degradation

Among the reaction mechanisms associated with $^{\bullet}OH$ is addition to an aromatic ring or unsaturated alkyl group. With the involvement of $Cl^{\bullet}$, an important question is whether analogous addition occurs. The potential formation of chlorinated organics is of practical significance in the field of drinking water treatment. Evidence of addition of $Cl^{\bullet}$ to alkenes in aqueous solution was reported by Gilbert et al. (1988) using electron spin resonance spectroscopy.

The first generation degradation products of $^{\bullet}OH$ with phenol include catechol and hydroquinone, which correspond to the addition of an OH group at the *ortho* and *para* positions, respectively. These are formed by an initial $^{\bullet}OH$ attack at the *ortho* or *para* positions to form a dihydroxycyclohexadienyl radical, or by $^{\bullet}OH$ attack and H-abstraction from the hydroxyl group to form a phenoxyl radical. The dihydoroxycyclohexanidenyl radicals convert to the resonance-stabilized phenoxyl radical by the elimination of H_2O. The phenoxyl radical then reacts with O_2, ultimately forming the final stable products (Mvula et al., 2001). In this case, no Cl-adducts should be observed, and a product comparison of phenol degradation by $^{\bullet}OH$ and $Cl^{\bullet}$ is suggested.

A series of 185 nm irradiations were conducted using solutions of phenol at approximately 1 µM, with tert-butanol at $7\,mg\,L^{-1}$ as C, both with and without $100\,mg\,L^{-1}$ of chloride. Samples were taken for HPLC analysis at irradiation times less than that required for 50% phenol degradation to prevent excessive oxidation of initial daughter products. The procedure used for HPLC analysis is identical to that of carbamazepine. Analytical grade standards were used to identify peaks by retention time and included catechol, hydroquinone, 2-chlorophenol, 3-chlorophenol, and 4-chlorophenol.

In the absence of chloride, the degradation products were identified as the earlier eluting catechol and hydroquinone. A third peak eluting earliest was

likely the common degradation product of catechol and hydroquinone, hydroxyquinol. In the presence of chloride, only catechol and hydroquinone were detected, with no detectable formation of any of the later eluting chlorophenols.

This observation is explained if, as reported by Gilbert et al. (1988), $Cl^{\bullet}$ reactions favour attack at the hydroxyl group to produce the phenoxyl radical and therefore the identical final products. Additional studies are required to confirm whether chlorinated species are formed to any significant extent in the 185 nm regime.

5.9 Bleaching of Dissolved Organic Matter in 185 nm Regime

The aromaticity of organic matter is largely responsible for the absorbance at 254 nm. Treatment by AOP is known to reduce this absorbance by reducing the amount of congugation in the carbon structure and possibly by ring openings induced by both $^{\bullet}OH$ attack and absorption of UV photons. This phenomena may be referred to as bleaching. It was desired to determine whether a significant difference could be observed between the bleaching occurring in the 185 nm regime with the presence or absence of chloride.

Solutions of Suwannee River NOM with $3.5\,mg\,L^{-1}$ as C, at pH 7, were irradiated with and without $100\,mg\,L^{-1}$ of chloride obtained from NaCl. Irradiations were conducted for exposure times of 5, 10, and 20 min, all in triplicate. An exposure time of 20 min, under the conditions used, would have been sufficient to induce an approximate 3-log reduction in carbamazepine, had the probe compound been used.

Consistent with previous studies, no reduction in DOC was observed, either with or without chloride. The 1 cm absorbance at 254 nm was found to be

reduced by approximately 50%, from 0.12 to 0.06 cm^{-1} in both cases. No statistically significant difference was observed for the bleaching of Suwannee River NOM in the 185 nm regime with or without chloride.

5.10 Molar Absorption Coefficient of Chloride at 185 nm

Accurate measurement of the 185 nm molar absorption coefficient of chloride is required, as it is likely to be the major absorber of photons at this wavelength and may shift the 185 nm regime from $^{\bullet}OH$ to $Cl^{\bullet}$ as the dominant oxidant.

Measurement of the absorbance of aqueous solutes at wavelengths below 200 nm is difficult using conventional UV-VIS spectrophotometers. Reasons for this include multiple factors that ultimately degrade the quality of the measurement, and are briefly reviewed here.

In a conventional spectrophotometer, the UV radiation source is a deuterium lamp, which emits a broad spectrum output in the UV, the majority of which is emitted at wavelengths greater than 200 nm. The small fraction of radiation produced below 200 nm is of relatively low power and higher noise. The absorbance of water itself is high ($\alpha_{H_2O} > 1\,cm^{-1}$), resulting in substantial attenuation of the signal of interest at typical path lengths of 1 cm. Thus, to measure the absorbance of a solute involves the subtraction of two weak signals, that of the test solution and the blank. Radiation that is not of interest reaches the sample due to limitations of the monochrometer slit and imperfections of the gratings. Such radiation is referred to as stray radiant energy and is overwhelmingly of longer wavelength. Such longer wavelength radiation experiences virtually no attenuation in water due to negligible absorbance, and thus reaches the detector to contribute to the signal of interest. The net effect of measuring a highly absorbing specimen

with such a weak signal in the presence of stray radiant energy is an apparent absorbance measurement that is lower than the actual absorbance. The greater the quantity of stray radiation present, the greater the discrepancy. It is difficult to measure, and therefore correct, for stray radiant energy at 185 nm. The influence of stray radiant energy may be reduced by minimizing the path length used for measurement. However, this also reduces the magnitude of a signal already prone to significant noise, and therefore does not improve precision. More extensive information regarding stray radiant energy may be found in Burgess and Frost (1999); Sommer (1989).

An alternative method to measuring ϵ_{185} for aqueous solutes exploits the convenience of the quasi-collimated beam and commercially available fused silica cells of precision thickness.

A double cell system was assembled, with an upper and lower cell placed in the quasi-collimated beam and in good optical contact with one another. The lower cell contained a standard reference solution to irradiate, with carbamazepine as probe and tert-butanol as scavenger. The upper cell was filled with either ultrapure water as a reference or the solution to be tested, such as a series of chloride solutions of known concentration. The precisely known path lengths are provided by standard commercially available spectrophotometer cells. The lower cell was of 10.0 mm path length, and the upper cell was of 1.0 mm path length.

A series of irradiations produced a set of pseudo first-order degradation curves, each with a slope of k' corresponding to the contents of the 1.0 mm cell, with ultrapure water as a reference giving k'_o. A plot of $log(k'/k'_o)$ vs. $[Cl^-]$ for probe compound degradation in the lower cell will have a slope equal to $0.1 \times \epsilon(M^{-1}\,cm^{-1})$ of the species in the upper cell. It is important that the probe be photochemically inert to 254 nm radiation by either a sufficiently low ϵ_{254} or Φ_{254}, a condition satisfied by carbamazepine.

Irradiations were performed in triplicate with fresh test solution placed in

the upper cell for each run. Data related to the calculation of k' is displayed in Figure 5.13. The series of values of $log(k'/k'_o)$ plotted against $[Cl^-]$ is displayed in Figure 5.14. The last value taken at $100\,mg\,L^{-1}$ of chloride was omitted from the linear regression calculation. While it was found to be reproducible, it was also found to involve significant deviation from Beer-Lambert behaviour. This may be due to ion-pair formation at the higher $[Cl^-]$ concentrations (Butler, 1964).

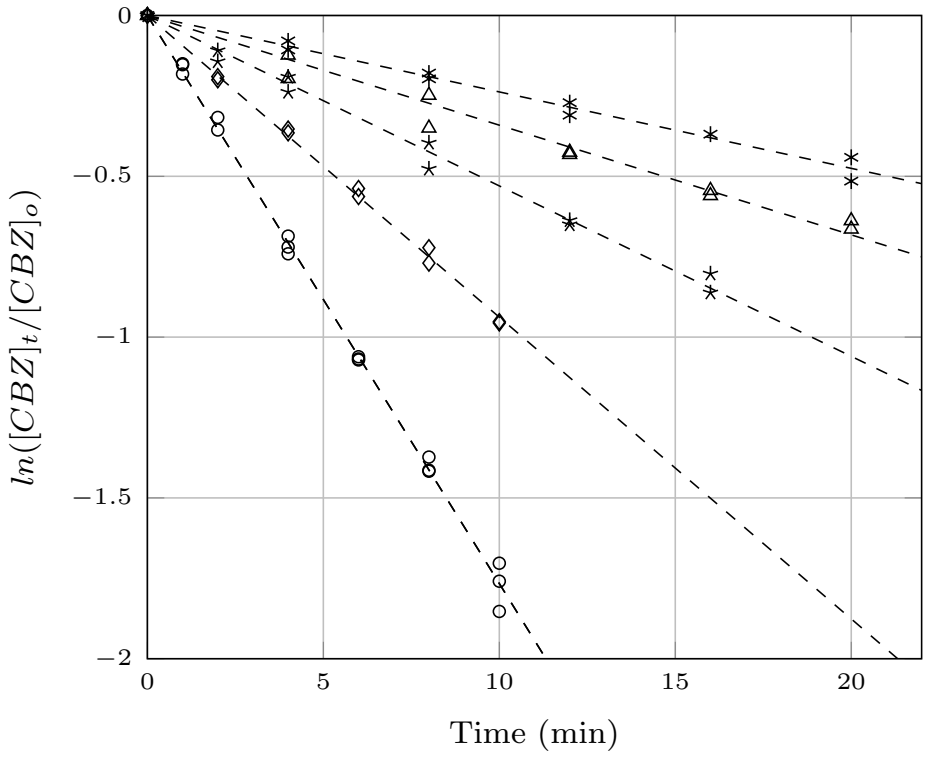

Figure 5.13: Kinetic method of determining ϵ_{185,Cl^-} using double cell. Lower 10.0 mm cell contains $[CBZ]_o \simeq 0.25\,\mu M$, $[(CH_3)_3COH] = 7\,mg\,L^{-1}$ as C. Upper 1.0 mm cell contains NaCl solutions or ultrapure water as a reference. Solutions of the upper cell: $[Cl^-] = 0\,mg\,L^{-1}$ (—○—), $[Cl^-] = 25\,mg\,L^{-1}$ (—◇—), $[Cl^-] = 50\,mg\,L^{-1}$ (—✶—), $[Cl^-] = 75\,mg\,L^{-1}$ (—△—), $[Cl^-] = 100\,mg\,L^{-1}$ (—✳—).

The value calculated for ϵ_{185} of chloride is $3540 \pm 150\,\mathrm{M^{-1}\,cm^{-1}}$, in excellent agreement with the value of $3800 \pm 300\,\mathrm{M^{-1}\,cm^{-1}}$ reported by Dainton and Fowles (1965) and the value of $\sim 3500\,\mathrm{M^{-1}\,cm^{-1}}$ estimated from a graph by Weeks et al. (1963) (see Table 1.1). It is important to note that these results were obtained by different methods. Dainton and Fowles (1965) used kinetic studies quantified by H_2 gas evolution and Weeks et al. (1963) used direct measurements of 185 nm absorbance by replacing the deuterium lamp with a low pressure mercury lamp in a nitrogen purged spectrophotometer. The current indirect methods using the double cell approach was also used to measure the value of ϵ_{185} for sulphate, bicarbonate and Suwannee River NOM, the values of which are presented in the following chapter.

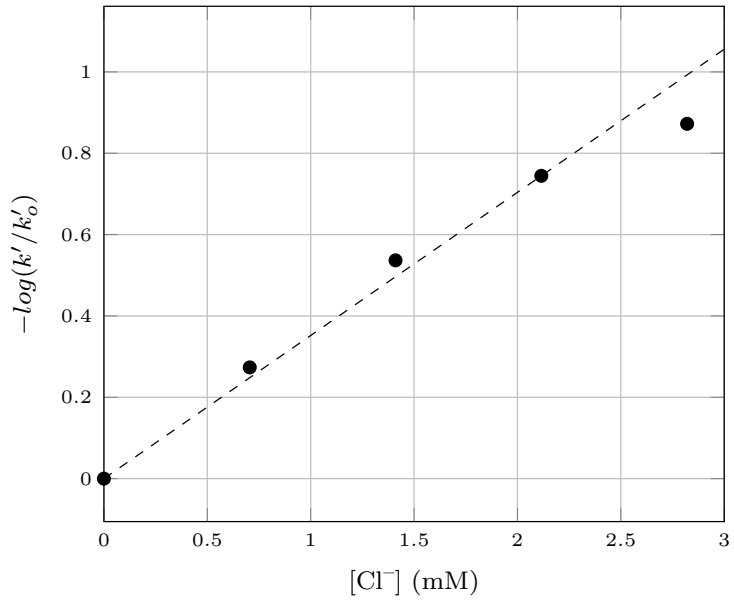

Figure 5.14: Calculation of $\boldsymbol{\epsilon_{185,Cl^-}}$ using double cell from kinetic data. Lower 10.0 mm cell contains $[CBZ]_o \simeq 0.25\,\mu\mathrm{M}$ and $[tBuOH] = 7\,\mathrm{mg\,L^{-1}}$ as C. Upper 1.0 mm cell contains NaCl solutions or ultrapure water as a reference.

5.11 Potential Cl• to •OH Interconversion

The determination of the molar absorption coefficient of chloride at 185 nm allows the evaluation of the model described by equations 5.6 and 5.7. This model implies that the photogeneration of both •OH and Cl• are independent and that any interconversion from one radical to the other is negligible.

If nitrobenzene is indeed of negligible reactivity with Cl• (i.e. $k_{\mathrm{Cl},NB} \ll k_{\mathrm{OH},NB}$), then the degradation of nitrobenzene observed in Figure 5.5, where tert-butanol is the organic scavenger, is a result of •OH alone. It would then be useful to compare the relative changes in k' and $f_{\mathrm{H_2O}}$ with increasing Cl^-. An additional assumption in this approach is that the Beer-Lambert law holds. These results are tabulated in Table 5.2.

Table 5.2: Model evaluation using the degradation of nitrobenzene with increasing Cl^- in the 185 nm regime

$[Cl^-]$ $(\mathrm{mg\,L^{-1}})$	k' $(\mathrm{min^{-1}})$	k'/k'_o	$f_{\mathrm{H_2O}}$	f_{Cl^-}
0	0.127 ± 0.002	1.00	1.00	0.00
25	0.105 ± 0.002	0.83	0.42	0.58
40	0.082 ± 0.002	0.64	0.31	0.69
100	0.068 ± 0.001	0.53	0.25	0.75

NB: Uncertainties are the standard errors calculated by linear regression of the aggregated rate data from triplicate runs.

It can be seen from Table 5.2 that $f_{\mathrm{H_2O}}$ decreases to a much greater extent with increased Cl^- than the relative decrease in the observed rate constant k'/k'_o. In fact, for each concentration of Cl^-, the resulting reduction in k' is approximately half the reduction in $f_{\mathrm{H_2O}}$. As discussed earlier, this would be explained if a portion of the photogenerated Cl• is converted to •OH. Attempts to account for such a conversion via reactions of Cl• and $Cl_2^{\bullet-}$ with water (Equations 5.4 and 5.5) have been unsuccessful. Additional research is required to understand this phenomena and permit the development of a more accurate kinetic model.

5.12 Summary

No previous literature reporting on the 185 nm AOP is known to have mentioned the role of chloride and of the $Cl^{\bullet}$ radical. Experimental evidence has been presented here to support the role of $Cl^{\bullet}$ as a major oxidant at environmentally relevant levels of both chloride and DOM. The evidence obtained is in agreement with the work reported from other fields such as radiation and atmospheric chemistry.

The chemistry related to Cl^{-} and $Cl^{\bullet}$ is complex. Many questions remain unanswered regarding such aspects as the extent to which equilibrium 5.3 is maintained, the mechanisms of $Cl^{\bullet}$ reactions, the reaction rate constants of $Cl^{\bullet}$ with compounds of interest, and the potential conversion of $Cl^{\bullet}$ to $^{\bullet}OH$.

Experimental evidence supports the explanation of several observations consistent with the work of others. No influence of Cl^{-} is observed for the 254 nm - H_2O_2 regime using either tert-butanol or Suwannee River NOM at circumneutral pH. Chloride is expected to exert a scavenging effect below pH 4, which is an unlikely condition in drinking water treatment. The explanation for this involves an intermediate reversible step between $^{\bullet}OH$ and $Cl^{\bullet}$ involving H^{+}, which is insufficiently available in the usual pH range of drinking water.

In contrast, the influence of chloride in the 185 nm regime is substantial. The postulated extent of $Cl^{\bullet}$ involvement relative to $^{\bullet}OH$, and the resulting degradation rate of the target contaminant produced depend on several factors. These include the concentration of chloride, the relative overall reactivities of $Cl^{\bullet}$ and $^{\bullet}OH$ with the mixture of organic matter present (i.e. scavengers), as well as the relative reactivities with target contaminants of interest.

Ionic strength effects observed support the existence of an equilibrium between the uncharged oxidant $Cl^{\bullet}$ and the relatively unreactive diradical anion $Cl_2^{\bullet-}$ via a secondary salt effect. The conditions under which such an equilibrium is maintained require further study, as this will effect the available oxidant when chloride concentrations are significant.

Product studies using phenol did not reveal any chlorinated phenols, excluding addition to an aromatic ring as a significant reaction mechanism in this case. The first generation daughter products observed when chloride was present were identical to those formed by $^{\bullet}OH$. Mechanistic explanation for this is provided by the formation of the phenoxyl radical, an intermediate theorized to form via both $^{\bullet}OH$ and $Cl^{\bullet}$.

The 185 nm regime with chloride at $100\,mg\,L^{-1}$ is interpreted to involve $Cl^{\bullet}$ as the dominant radical. Yet, under such conditions, no significant effect is observed on the measured absorbance of Suwannee River NOM solutions. Thus, the replacement of $^{\bullet}OH$ by $Cl^{\bullet}$ neither enhances nor diminishes the rate of bleaching of Suwannee River NOM under 254 nm irradiation.

Molar absorption coefficients can be accurately measured using an indirect kinetic technique involving two consecutive cells, with one used as the sample cell and a second the detecting cell used to measure the degradation rate of a probe compound. This method avoids the fundamental limitations inherent in using conventional spectrophotometers.

Further research is required to elucidate the role of $Cl^{\bullet}$ in the 185 nm AOP. It is likely that even when chloride is responsible for the majority of 185 nm photon absorption, the result is not a replacement of $^{\bullet}OH$ with $Cl^{\bullet}$, but a mixture of the two. The relative role these two radicals in contaminant degradation will depend on the concentrations of chloride and DOM, their relative reactivities, and the mechanisms involved in any conversion from $Cl^{\bullet}/Cl_2^{\bullet-}$ to $^{\bullet}OH$. In natural waters the situation is likely complicated further by the involvement of yet other species that absorb photons and generate

reactive radicals.

Chapter 6

Sulphate, Bicarbonate and Interactions of Major Solutes

6.1 The 185 nm AOP and Other Solutes

As with the UV/H_2O_2 and O_3/H_2O_2 AOPs, the 185 nm AOP is subject to the parasitic effects of $^{\bullet}$OH scavengers such as DOM and bicarbonate. Yet, it has been shown that a unique feature of the 185 nm AOP is the substantial sensitivity to the presence of chloride. Experimental evidence reported in Chapter 5 supports the interpretation of the chloride effect as being due to the involvement by $Cl^{\bullet}$ as a major oxidant, likely simultaneously with $^{\bullet}$OH. Thus, the presence of chloride in the 185 nm regime may result in the presence of a mixture of $^{\bullet}$OH and $Cl^{\bullet}$, both highly reactive oxidants, with the proportion of each dependent on their relative reactivities with major solutes. This has significant implications on the degradation rate of target contaminants, and possibly on the mixture of products formed. Yet, information regarding $Cl^{\bullet}$ reaction rates, reaction mechanisms, and end products are limited.

This situation is complicated further, as typical water matrices contain other major solutes that also contribute to the absorption of 185 nm photons and generation of radicals. Adequate elucidation of the details involved requires substantial experimental work and techniques beyond what is presented here. The current objective is to clearly demonstrate the importance of other solutes influencing the 185 nm AOP, which has not been reported to-date, indicate general trends in relevant reactivities, and provide guidance

to further detailed studies.

As mentioned in Chapter 1, the major inorganic ions in natural waters include Ca^{2+}, Mg^{2+}, Na^{+}, and K^{+} as cations, and Cl^{-}, SO_4^{2-}, HCO_3^{-}, and CO_3^{2-} as anions, with other ions occurring at concentrations typically less than $1\,mg\,L^{-1}$ (Wetzel, 2001).

A review of the literature provides no evidence that the major cationic species participate directly in any photochemical or radical reactions in the 185 nm regime. While it is likely that Mn^{2+} and Fe^{3+} may absorb photons, they are minor solutes (i.e. $\ll 1\,mg\,L^{-1}$). Nevertheless, the involvement of cationic species has not been rigorously tested and their lack of direct involvement should be experimentally confirmed under relevant conditions.

In contrast, all the major anionic species are expected to absorb 185 nm photons and generate radicals to varying extents. The involvement of Cl^{-} has been established in Chapter 5. In this chapter the focus is on SO_4^{2-} and HCO_3^{-} and some major interactions. The role of CO_3^{2-} has not been thoroughly tested. However, at pH 8 and below, its concentration is negligible. Thus, the pH dependent influence of the conjugate acid-base pair HCO_3^{-}/CO_3^{2-} should be included in future studies, particularly where treated waters exceed pH 8. As mentioned in Chapter 1, the molar absorption coefficient (ϵ_{185}) for CO_3^{2-} is estimated as approximately $10^3\,M^{-1}\,cm^{-1}$. No information is available on the value of ϵ_{185} or of the quantum yield (Φ) for HCO_3^{-}.

6.2 Sulphate

Sulphate is a major anion in natural waters present in rivers and lakes typically between 2.5 and $25\,mg\,L^{-1}$, though concentrations of $100\,mg\,L^{-1}$ or greater may occur depending on the dominant mineral rock type of the drainage region (Wetzel, 2001).

Before proceeding to investigate the role of SO_4^{2-} in the 185 nm regime, influence on the 254 nm-H_2O_2 regime is first investigated.

6.2.1 Sulphate in the 254 nm - H_2O_2 Regime

Experiments were conducted using the 254 nm collimated beam in the absence of 185 nm radiation. As before, carbamazepine was used as a probe compound. The scavenger used was either tert-butanol or Suwannee River NOM, in either case at a concentration of 7 mg L^{-1} as C. Solutions were brought to circumneutral pH by addition of NaOH. Though Na_2SO_4 is of sufficient aqueous solubility, due to difficulties in completely dissolving the solid, and in order to avoid colloidal remains even after filtration, a stock solution of Na_2SO_4 was prepared by neutralizing analytical grade H_2SO_4 with NaOH and verifying the dilutions by ion chromatography. Two levels of SO_4^{2-} were used, 0 and 100 mg L^{-1}.

In order to minimize the influence of H_2O_2 as a radical scavenger, it was desired to use a dose of H_2O_2 less than 10 mg L^{-1}, and a dose of 7 mg L^{-1} was found adequate. All irradiations were performed in triplicate, with samples taken at regular intervals. Residual H_2O_2 of samples was quenched with a 10 µL droplet of approximately 100 mg L^{-1} bovine catalase placed at the bottom of the HPLC vials, as discussed in Chapter 2.

Irradiations were conducted with exposure times sufficient to achieve at least 20% removal of the probe compound. The results are plotted in Figures 6.2 and 6.1 for tert-butanol and Suwannee River NOM as scavengers, respectively.

The calculated pseudo first-order rate constants k' for the degradation of the probe compound reveal no statistically significant difference between the levels of SO_4^{2-} used. The scatter in the data is substantial, increasing

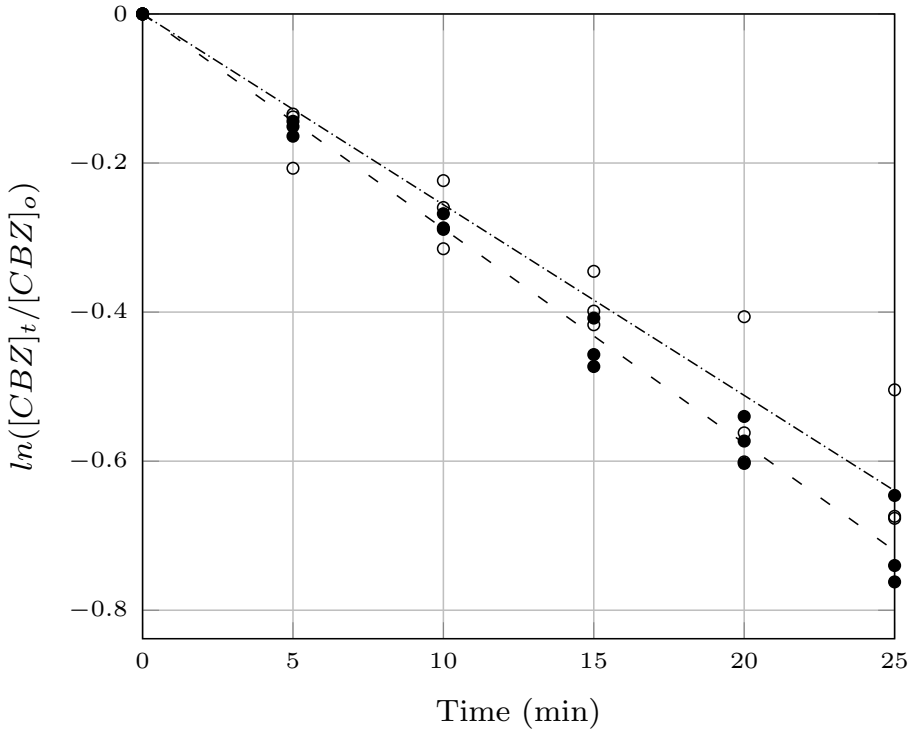

Figure 6.1: Tert-Butanol in the 254 nm - H_2O_2 regime and influence of sulphate. $[CBZ]_o \simeq 0.25\,\mu M$. $[(CH_3)_3COH] = 7\,mg\,L^{-1}$ as C. Solution of Na_2SO_4 at pH 7 used as source of sulphate. $[{SO_4}^{2-}] = 0\,mg\,L^{-1}$ (—○—),$100\,mg\,L^{-1}$ (—●—).

at the longer exposure times. This phenomena appears to be common to 254 nm-H_2O_2 experiments. In contrast, 185 nm experiments exhibit much greater repeatability and precision. It is possible that the observed scatter is due to slight differences in the dose of H_2O_2 delivered for each irradiation, despite the fact that the delivered dose of H_2O_2 was measured to vary by less than $\pm 0.1\,mg\,L^{-1}$ between runs. A verification of the quenching of H_2O_2 found this procedure to be adequate to reduce H_2O_2 to below detection ($0.01\,mg\,L^{-1}$) within a time of less than two minutes.

Regardless of the scatter of data and the failure to detect any effect of ${SO_4}^{2-}$

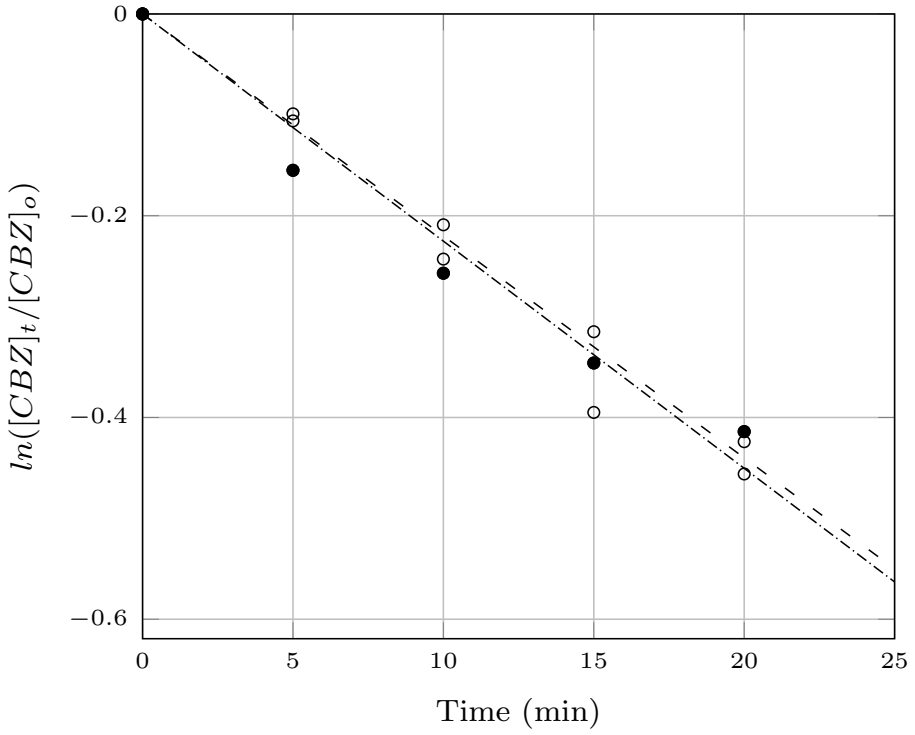

Figure 6.2: Swannee River NOM in the 254 nm - H_2O_2 regime and influence of sulphate. $[H_2O_2]$= 7 mg L^{-1} as C. $[CBZ]_o \simeq 0.25$ µM. $[DOC] = 7$ mg L^{-1} as C. Na_2SO_4 used as source of sulphate. All solutions prepared at pH 7. $[SO_4{}^{2-}] = 0$ mg L^{-1} (—○—),100 mg L^{-1} (—●—).

at the extremes of 0 and 100 mg L^{-1}, any effect that may exist is likely to be small and practically negligible.

At pH 7, the relevant one-electron reduction potentials include $E(SO_4^{\bullet-}/SO_4^{2-})$ $\simeq 2.4$ V and $E(^{\bullet}OH/OH^-) = 1.9$ V (Wardman, 1989). These values suggest that electron transfer from SO_4^{2-} to $^{\bullet}OH$ is unfavourable. This, and the experimental evidence support the assumption that SO_4^{2-} has a negligible influence in the 254 nm-H_2O_2 regime and therefore upon the UV/H_2O_2 AOP. Therefore, any effect observed in the 185 nm regime will not be due to presence of 254 nm radiation.

6.2.2 Sulphate in the 185 nm Regime

Experiments conducted under 185 nm irradiation found the impact of sulphate to be significant. These experiments used tert-butanol as the scavenger, with four concentrations of SO_4^{2-}. Results are plotted in Figure 6.3, where it can be seen that the increase in $[SO_4^{2-}]$ results in an increase in the degradation rate of the probe compound carbamazepine.

As discussed in Chapter 1, it is expected that SO_4^{2-} ions will absorb photons at 185 nm by a charge transfer to solvent mechanism, with electron ejection forming $SO_4^{\bullet-}$ with a quantum yield of ~ 0.65 (see Table 1.1 on page 22). The resulting $SO_4^{\bullet-}$ will react with the main scavenger tert-butanol with a second-order rate constant approximately three orders of magnitude less than the rate constant between $^{\bullet}OH$ and tert-butanol (Buxton et al., 2000). Thus, if the system consists of a mixture of both radicals $^{\bullet}OH$ and $SO_4^{\bullet-}$, a relatively small contribution of $SO_4^{\bullet-}$ is likely sufficient to induce a significant impact, provided the rate constants of both oxidants with the target contaminant (or probe) are similar (i.e $k_{SO_4^{\bullet-},CBZ} \sim k_{OH,CBZ}$), while the rate constant of $SO_4^{\bullet-}$ with the matrix is substantially lower (i.e. $k_{SO_4^{\bullet-},DOM} \ll k_{OH,DOM}$).

An expression for the pseudo-first order rate constant k' of the probe (or target) compound, based on a mixture of $^{\bullet}OH$ and $SO_4^{\bullet-}$, may be written as the sum of the two contributions:

$$k' = k'_{OH} + k'_{SO_4^-} \tag{6.1}$$

with each term on the right-hand side representing the contribution of the indicated radical. The expression may be further developed using equations 2.13 and 2.14 to give the $SO_4^{\bullet-}$ analog to equation 5.7:

$$k' = \left(\frac{k_{\mathrm{OH},C}}{k_{\mathrm{OH},S}} \Phi_{\mathrm{H_2O}} f_{\mathrm{H_2O}} + \frac{k_{\mathrm{SO_4^-},C}}{k_{\mathrm{SO_4^-},S}} \Phi_{\mathrm{SO_4^{2-}}} f_{\mathrm{SO_4^{2-}}} \right) \frac{I_a}{[S]} \tag{6.2}$$

where the k values of the right-hand side are the second-order reaction rate constants between the indicated subscripts, with C representing the probe compound and S the scavenger. $\Phi_{\mathrm{H_2O}}$ is the quantum yield for water photolysis and $\Phi_{\mathrm{SO_4^{2-}}}$ is the quantum yield for the ejection of an electron from $\mathrm{SO_4^{2-}}$, both at 185 nm. The values of $f_{\mathrm{H_2O}}$ and $f_{\mathrm{SO_4^{2-}}}$ are the fraction of 185 nm photons absorbed by water and $\mathrm{SO_4^{2-}}$, respectively, calculated using equation 2.15 ($f_i = \alpha_i/\alpha_{tot}$). I_a is the rate at of 185 nm photon absorption per unit volume, and $[S]$ is the concentration of the scavenger.

All the terms of the right-hand side of equation 6.2 are known or can be measured, with the exception of $k_{\mathrm{SO_4^{\bullet -},C}}$, the second-order rate constant of $\mathrm{SO_4^{\bullet -}}$ with the probe carbamazepine. With the experimental determinations of k', the value of $k_{\mathrm{SO_4^{\bullet -},C}}$ can be calculated. The quantities measured separately or quoted from the literature and used in these calculations are listed in Table 6.1. The experimentally determined values of k', the relative ratios of $k'_{\mathrm{^{\bullet}OH}}$ and $k'_{\mathrm{SO_4^{\bullet -}}}$, as well as the calculated values of $k_{\mathrm{SO_4^{\bullet -},C}}$ are tabulated in Table 6.2. From the measured value of k' with no $\mathrm{SO_4^{2-}}$, the term I_a was determined to be $2.70 \times 10^{-7}\,\mathrm{M\,s^{-1}}$, consistent with the values used for the determinations of 185 nm fluence rate presented in Chapter 4. This value of I_a was used here in subsequent calculations of $k_{\mathrm{SO_4^{2-},C}}$. Data using $[\mathrm{SO_4^{2-}}] = 50\,\mathrm{mg\,L^{-1}}$ were inconsistent, possibly due to contamination of samples, and were not used for these calculations but are included with the raw data in the Appendix.

Using the indirect kinetic technique discussed in Chapter 5 for $\mathrm{Cl^-}$, the molar absorption coefficient at 185 nm (ϵ) of $\mathrm{SO_4^{2-}}$ was determined by a separate experiment to measure $160 \pm 20\,\mathrm{M^{-1}\,cm^{-1}}$ (see Table A.43 on page 216 for

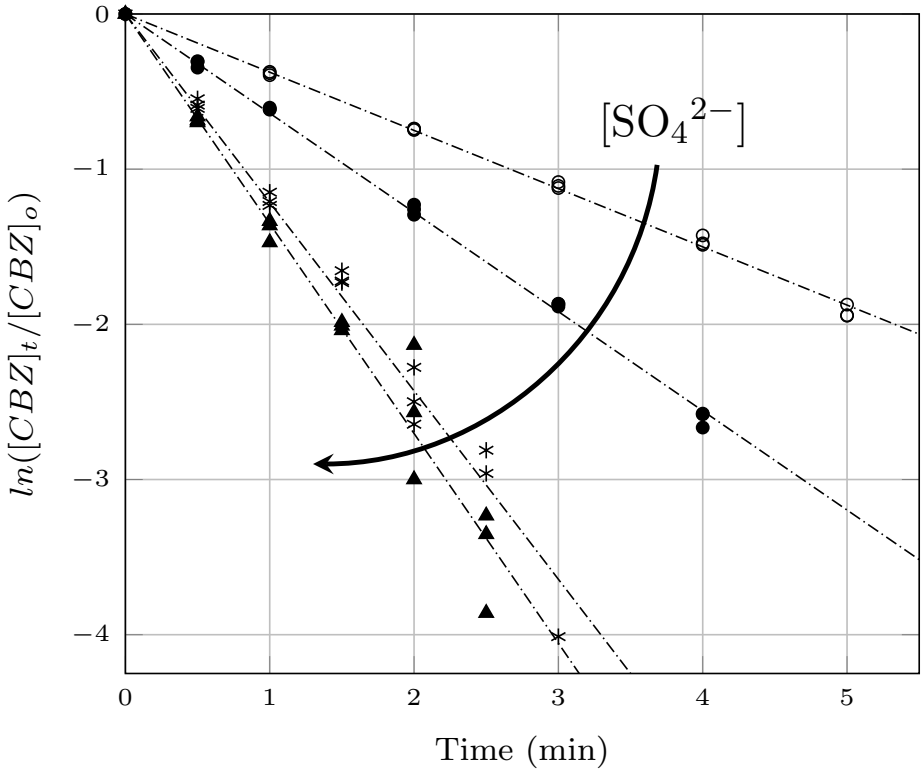

Figure 6.3: Influence of sulphate in the 185 nm regime with tert-butanol. $[tBuOH] = 7\,\mathrm{mg\,L^{-1}}$ as C. $[CBZ]_o \simeq 0.25\,\mu\mathrm{M}$. Na_2SO_4 used as source of sulphate. $[SO_4{}^{2-}] = 0\,\mathrm{mg\,L^{-1}}$ (—○—), $25\,\mathrm{mg\,L^{-1}}$ (—●—), $75\,\mathrm{mg\,L^{-1}}$ (—∗—), $100\,\mathrm{mg\,L^{-1}}$ (—▲—).

Table 6.1: Numerical values used in calculation of the second-order rate constant for the reaction of $SO_4^{\bullet-}$ with carbamazepine ($k_{SO_4^{\bullet-},CBZ}$) with equation 6.2

Value	Ref.
$k^{\bullet}_{OH,C} = 6.8 \times 10^9\,M^{-1}\,s^{-1}$	This work
$k^{\bullet}_{OH,S} = 6.0 \times 10^8\,M^{-1}\,s^{-1}$	Buxton et al. (2000)
$k_{SO_4^{\bullet-},S} = 8.4 \times 10^5\,M^{-1}\,s^{-1}$	Buxton et al. (2000)
$\alpha_{H_2O} = 1.80\,cm^{-1}$	Weeks et al. (1963)
$\epsilon_{SO_4^{2-}} = 160\,M^{-1}\,cm^{-1}$	This work
$\Phi_{H_2O} = 0.3$	Getoff and Schenck (1968)
$\Phi_{SO_4^{2-}} = 0.65$	Dainton and Fowles (1965), Barrett et al. (1965)

C = carbamazepine, S = tert-butanol, w = water.

Table 6.2: Experimental determination of the second-order rate constant for the reaction of $SO_4^{\bullet-}$ with carbamazepine ($k_{SO_4^{\bullet-},CBZ}$) with equation 6.2

$[SO_4^{2-}]$ (mM)	k' (s^{-1})	$k'_{^{\bullet}OH}/k'$	$k'_{SO_4^{\bullet-}}/k'$	$k_{SO_4^{\bullet-},C}$ $M^{-1}\,s^{-1}$
0.00	$6.31 \pm 0.09 \times 10^{-3}$	1.00	0.00	-
0.26	$1.08 \pm 0.01 \times 10^{-2}$	0.56	0.44	1.43×10^8
0.78	$2.09 \pm 0.07 \times 10^{-2}$	0.30	0.70	1.61×10^8
1.04	$2.26 \pm 0.12 \times 10^{-2}$	0.25	0.76	1.38×10^8
Average				$1.5 \pm 0.1 \times 10^8$

Uncertainty in average the standard deviation from the three determinations.

data)

Note from Table 6.2 that the contribution to k' from $SO_4^{\bullet-}$, relative to $^{\bullet}OH$, is substantial at $[SO_4^{2-}]$ values of 25, 75, and 100 mg L^{-1}, despite SO_4^{2-} contributing approximately 2, 6 and 8% of the total absorbance of the solution, respectively. The value of the rate constant for the reaction of sulphate radical and carbamazepine ($k_{SO_4^{\bullet-},C}$) was calculated to be 1.5×10^8 M^{-1} s^{-1}. The value 1.9×10^9 M^{-1} s^{-1} was reported by (Matta et al., 2011) whereby $SO_4^{\bullet-}$ was generated by the Fenton-like reaction of persulfate and cobalt ($S_2O_8^{2-}/Co^{2+}$). Since a nitrate salt of cobalt was used by that study, the higher value obtained may be due to unaccounted for effects of nitrate and the nitrate radical ($NO_3^{\bullet}$) or other matrix components. Reevaluation of this value may be accomplished by using the UV/$S_2O_3^{2-}$ AOP in a collimated beam in a competitive kinetics experiment with a convenient reference compound selected from the compilation of Ross and Neta (1979). In any case, the value obtained here is within the range of values expected based on the rate constants for other organic compounds (Neta et al., 1977; Ross and Neta, 1979). An important discovery, not previously reported in the literature, is that like chloride, sulphate present at environmentally relevant concentrations may have a profound influence on the 185 nm process, and that this AOP involves not only $^{\bullet}OH$, but a mixture of several highly reactive radical species.

6.3 Bicarbonate

In addition to Cl^- and SO_4^{2-}, the major anions in surface waters include the conjugate acid-base pair HCO_3^-/CO_3^{2-}. In surface waters exposed to the atmosphere, these two species form an equilibrium with each other and with dissolved carbon dioxide via its hydrolysis product carbonic acid (H_2CO_3). The pair HCO_3^-/CO_3^{2-} has a pK_a of 10.3 at 25 °C, with less than 1% change in this value between 5 and 35 °C (Butler, 1982). In the common pH range for surface waters of 6 to 8, the concentration of CO_3^{2-} is less than 1% that

of HCO_3^-, and thus can usually be considered negligible. The global average concentration of bicarbonate in river waters is approximately $60\,mg\,L^{-1}$ ($\sim 1\,mM$) with an upper range extending to $300\,mg\,L^{-1}$ (Stumm and Morgan, 1996; Wetzel, 2001). Depending on the underlying geology, some water bodies are naturally very low in HCO_3^-, with little buffer capacity against acidification. Such conditions are common in the granitic rock dominated regions of Eastern Canada and Northeastern United States (Bunce, 1990).

Both HCO_3^- and CO_3^{2-} react by electron transfer to $^{\bullet}OH$ with second-order reaction rate constants of 8.5×10^6 and $3.9 \times 10^8\,M^{-1}\,s^{-1}$, respectively (Buxton et al., 1988). Due to the carbonate radical being a strong acid ($pK_a < 0$), $CO_3^{\bullet-}$ is the common product of both reactions (Czapski et al., 1999). Unlike $^{\bullet}OH$ and $Cl^{\bullet}$, the species $CO_3^{\bullet-}$ is a highly selective reactant (Chen and Hoffman, 1973; Larson and Zepp, 1988), and with few exceptions will not significantly contribute to the degradation of trace organic contaminants. Thus, the pair HCO_3^-/CO_3^{2-} are considered $^{\bullet}OH$ scavengers, and together with DOM act to reduce the efficiency of AOPs. Furthermore, due to an approximate 50 fold increase in $^{\bullet}OH$ reactivity with CO_3^{2-} relative to HCO_3^-, the scavenging effect on AOPs due to the carbonate species increases dramatically above pH 8.

In addition to scavenging $^{\bullet}OH$, electron transfer reactions from HCO_3^-/CO_3^{2-} to $Cl^{\bullet}$ and $SO_4^{\bullet-}$ are also expected to occur based on the relative magnitude of the one-electron redox potential $E(CO_3^{\bullet-}/CO_3^{2-}) = 1.4\,V$ (Huie et al., 1991). The carbonate species therefore also serve as scavengers for the radicals $Cl^{\bullet}$ and $SO_4^{\bullet-}$, with the available literature values for rate constants tabulated in Table 1.2 on page 24. From these values, it can be seen that while the reactivities of $^{\bullet}OH$ and $SO_4^{\bullet-}$ with HCO_3^- are comparable, the reactivity of $Cl^{\bullet}$ with HCO_3^- is larger by one or two orders of magnitude. This may impose a substantial impact on the 185 nm AOP, depending on the water composition.

Photochemical reactions involving HCO_3^-/CO_3^{2-} are also expected to occur in the 185 nm regime via charge-transfer-to-solvent mechanisms, though as

mentioned in Chapter 1, virtually no information is available regarding molar absorption coefficients and quantum yields for electron photodissociation. If these quantities are significant, then HCO_3^-/CO_3^{2-} may be considered both scavengers of radicals as well as scavengers of 185 nm photons (i.e. inner filters), compounding the impact on 185 nm AOP efficiency.

Before considering the simultaneous presence of multiple anionic species under 185 nm irradiation, the influence of bicarbonate alone was investigated in a set of solutions using tert-butanol as a scavenger, carbamazepine as the probe compound, and four levels of HCO_3^- concentration. Aliquots of an $NaHCO_3$ stock were added to each solution. The pH of the solutions were approximately pH 6.1 in the case of no added HCO_3^- and pH 8.1 for solutions containing 60, 120, and 180 $mg\,L^{-1}$ of HCO_3^-. This was deemed sufficient to neglect the contribution of CO_3^{2-}, thus avoiding the depression of pH using any acids or buffer systems that would impart undesired species to the matrix. The results are plotted in Figure 6.4.

While the trend observed for the probe compound degradation rate k' decreases with increasing $[HCO_3^-]$ as expected, the scavenging of $^{\bullet}OH$ by HCO_3^- does not account for the entirety of the observed effect. Using the indirect kinetic technique discussed in Chapter 5 for Cl^-, the molar absorption coefficient at 185 nm (ϵ) of HCO_3^- was measured by a separate experiment and determined to be $290 \pm 40\,M^{-1}\,cm^{-1}$ (see Table A.43 on page 216 for data).

Using the known rate constants and concentrations for the probe carbamazepine, and the scavengers tert-butanol and HCO_3^-, a comparison of the calculated and observed values of k' was made to check for consistency of HCO_3^- acting by two independent processes. An expression relating the known quantities to the observed rate constant k' is obtained by elaborating Equation 2.11:

$$k' = \frac{k_{\mathrm{OH},C}\ \Phi_{\mathrm{H_2O}} f_{\mathrm{H_2O}} I_a}{k_{\mathrm{OH},S}\,[S]\ +\ k_{\mathrm{OH,HCO_3^-}}\,[\mathrm{HCO_3^-}]} \tag{6.3}$$

where all terms are as previously defined. If the above expression is valid and HCO_3^- does indeed absorb photons to generate nonreactive $CO_3^{\bullet -}$ at the expense of $^\bullet$OH generation, and the Beer-Lambert behaviour holds for HCO_3^- at 185 nm, then a correction of f_{H_2O} will yield better agreement between calculated and experimental results.

The value of I_a is required for calculations and can be obtained from the experimental results corresponding to the solution with no HCO_3^- addition, $\Phi_{H_2O} = 0.3$, and $f_{H_2O} = 1$. This yields a value of $I_a = 2.5 \times 10^{-7}\,\mathrm{M\,s^{-1}}$, in agreement with the values used for the fluence rate determinations reported in Chapter 4, and the calculations of the previous section. Using the nominal value of $\epsilon_{HCO_3^-} = 290\,\mathrm{M^{-1}\,cm^{-1}}$ allows the calculation of the absorbance coefficient $\alpha_{HCO_3^-} = \epsilon_{185} \cdot [HCO_3^-]$, which in turn permits the calculation of $\alpha_{tot} = \alpha_{H_2O} + \alpha_{HCO_3^-}$, and $f_{H_2O} = \alpha_{H_2O}/\alpha_{tot}$, where $\alpha_{H_2O} = 1.80\,\mathrm{cm^{-1}}$ is taken from (Weeks et al., 1963). This value of f_{H_2O} is then applied to the calculation of k'_{calc} and compared with experimental values k'_{exp}.

The values of the $^\bullet$OH rate constants are $6.8 \times 10^9\,\mathrm{M^{-1}\,s^{-1}}$ for carbamazepine, $6.0 \times 10^8\,\mathrm{M^{-1}\,s^{-1}}$ for tert-butanol, and $8.5 \times 10^6\,\mathrm{M^{-1}\,s^{-1}}$ for HCO_3^-. The concentrations of tert-butanol used was $7.0\,\mathrm{mg\,L^{-1}}$ as C or 1.35×10^{-4} M.

A comparison of the two processes involving HCO_3^- can be made by comparing the calculated rate values k'_{calc} when absorption of photons by HCO_3^- is not taken into account ($f_{H_2O} \equiv 1$) and when such absorption is taken into account ($f_{H_2O} < 1$). These are tabulated in Table 6.3.

The k' values of Table 6.3 are plotted in Figure 6.5. An inspection of Figure

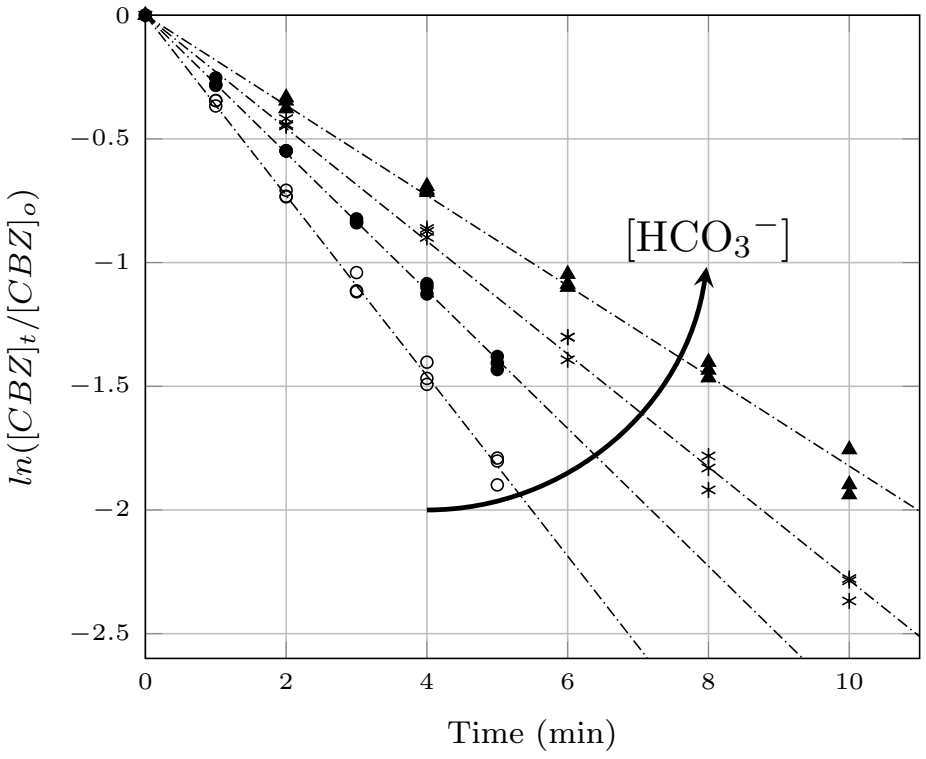

Figure 6.4: Influence of bicarbonate in the 185 nm regime with tert-butanol. $[tBuOH] = 7\,\mathrm{mg\,L^{-1}}$ as C. $[CBZ]_o \simeq 0.25\,\mu\mathrm{M}$. Solution of $NaHCO_3$ at pH 8 used as source of bicarbonate. $[HCO_3{}^-] = 0\,\mathrm{mg\,L^{-1}}$ (—○—), $60\,\mathrm{mg\,L^{-1}}$ (—●—), $120\,\mathrm{mg\,L^{-1}}$ (—∗—), $180\,\mathrm{mg\,L^{-1}}$ (—▲—).

Table 6.3: Comparison of the calculated and experimental rates due to HCO_3^- in the 185 nm regime

$[HCO_3^-]$ $(mg\,L^{-1})$	$\alpha_{HCO_3^-}$ (cm^{-1})	f_{H_2O}	k'_{calc} (min^{-1}) $f_w \equiv 1$	k'_{calc} (min^{-1}) $f_w < 1$	k'_{exp} (min^{-1})
0	0.00	1.000	-	-	0.367 ± 0.005
60	0.29	0.857	0.332	0.285	0.281 ± 0.003
120	0.58	0.750	0.303	0.227	0.234 ± 0.004
180	0.87	0.667	0.279	0.186	0.186 ± 0.004

NB: Uncertainties are the standard errors calculated by linear regression of the aggregated rate data from triplicate runs.

6.5 suggests that the two effects due to HCO_3^- in the 185 nm AOP are indeed independent. The black circles show the values of k'_{calc} corresponding to the condition where only the $^{\bullet}OH$ scavenging effect is considered. The grey circles show the values of k'_{calc} that take into account both $^{\bullet}OH$ scavenging and absorption of 185 nm photons due to HCO_3^-. Excellent agreement is found between the experimental values indicated by the asterisk and the latter calculated values that account for both phenomena. This result also supports the assumption that the reaction between $CO_3^{\bullet-}$ and carbamazepine is negligible. However, it should be noted that the inner filter effect of HCO_3^- may be negligible in a real water matrix with other solutes such as Cl^- and DOM that more strongly absorb at 185 nm.

At this point, it is now clear that the 185 nm regime involves not only $^{\bullet}OH$ as a reactive radical, but also potentially significant contributions from $Cl^{\bullet}$, $SO_4^{\bullet-}$, and that the major solutes Cl^-, SO_4^{2-}, HCO_3^-, and DOM significantly influence the involvement of these radicals. Aspects of the interactions between these major solutes are next considered.

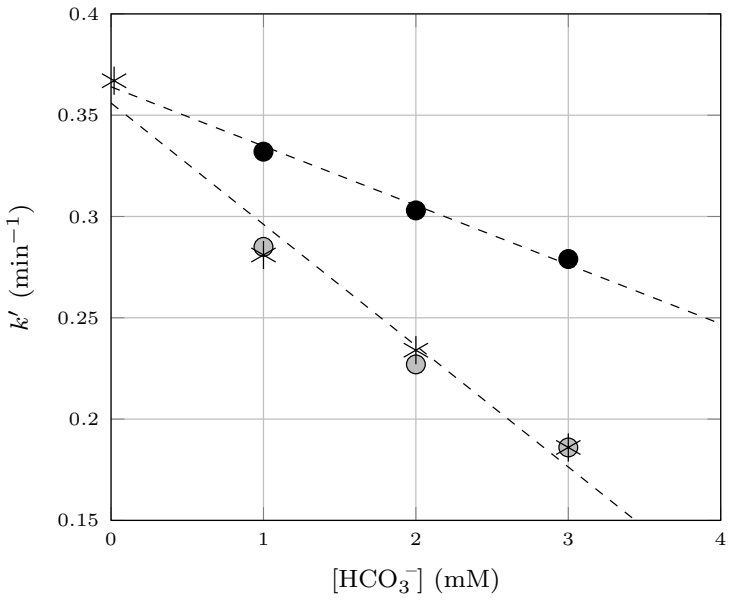

Figure 6.5: Comparison of calculated and experimentally observed rates due to HCO_3^- influence in the 185 nm regime, with $[CBZ]_o \simeq 0.25\,\mu M$ and $[tBuOH] = 7.0\,mg\,L^{-1}$ as C in all solutions. $NaHCO_3$ used as source of HCO_3^-. k'_{calc} with $f_w \equiv 1$ (●). k'_{calc} with $f_w < 1$ (◉). k'_{exp} (✳) from Figure 6.4. Best-fit lines shown for calculated values.

6.4 Interactions Among Major Solutes

Evidence has now been presented that 185 nm irradiation of aqueous solutions will generate the radicals $^{\bullet}OH$, $Cl^{\bullet}$, $SO_4^{\bullet-}$, and $CO_3^{\bullet-}$, which, save for the last species, will contribute by varying extents to the oxidative degradation of trace organic contaminants. The solutions studied represent simplified models of natural waters, and the available evidence indicates that these reactive species cannot be considered independently in general for actual natural waters.

The one-electron redox potentials of $E(^{\bullet}OH, OH^-) = 1.9\,V$ (pH > 2) and $E(Cl^{\bullet}, Cl^-) = 2.4 - 2.6\,V$ (Wardman, 1989) support the observations that Cl^- is not a scavenger of $^{\bullet}OH$. As discussed in the previous chapter, the

185 nm photogenerated $Cl^{\bullet}$ not only reacts with organic solutes, but also reacts reversibly with Cl^- to form the relatively nonreactive $Cl_2^{\bullet-}$ with an equilibrium constant ($K = 1.4 \times 10^5\,M^{-1}$) that heavily favours $Cl_2^{\bullet-}$ (Buxton et al., 1998). Both $Cl^{\bullet}$ and $Cl_2^{\bullet-}$ react with water itself, and via a mechanism not yet fully understood, may ultimately form $^{\bullet}OH$. Thus, unlike the case of $SO_4^{\bullet-}$ and $^{\bullet}OH$, the delineation between the contributions of $^{\bullet}OH$ and $Cl^{\bullet}$ to the observed degradation rate k' of a trace contaminant does not yield a simple relationship. The relative contributions of $^{\bullet}OH$ and $Cl^{\bullet}$ to k' is expected to be highly sensitive to the relative rates associated with the multiple sinks of $Cl^{\bullet}$, which depends on the matrix composition. A condition that also depends on the matrix composition is the possibility that significant deviations from equilibrium between $Cl^{\bullet}$ and $Cl_2^{\bullet-}$ may occur, as observed by Buxton et al. (1998).

As discussed earlier, the value of $E(SO_4^{\bullet-}, SO_4^{2-}) \simeq 2.6\,V$ also supports the observation that SO_4^{2-}, like Cl^-, is not a scavenger of $^{\bullet}OH$. The 185 nm molar absorption coefficient of Cl^- is over twenty times greater than that of SO_4^{2-} ($3540\,vs.\,160\,M^{-1}\,cm^{-1}$), which alone would suggest that SO_4^{2-} should have a negligible effect when Cl^- is also present at comparable concentrations. Yet, the redox potentials are approximately equal, and a reversible reaction occurs between these species with an equilibrium constant of approximately 1.2 at zero ionic strength (Buxton et al., 1999):

$$SO_4^{\bullet-} + Cl^- \rightleftharpoons Cl^{\bullet} + SO_4^{2-} \tag{6.4}$$

Thus, even when negligible 185 nm absorption occurs by SO_4^{2-}, resulting in negligible $SO_4^{\bullet-}$ photogeneration, $SO_4^{\bullet-}$ may still be a significant contributor to trace organic degradation as a result of the oxidation of SO_4^{2-} by $Cl^{\bullet}$.

To illustrate the potential sensitivity of the 185 nm AOP to the composition

of the water matrix, consider the model solution composed of tert-butanol, chloride, and sulphate at $7\,\mathrm{mg\,L^{-1}}$ as C, $25\,\mathrm{mg\,L^{-1}}$, and $50\,\mathrm{mg\,L^{-1}}$, respectively. The fractions of absorbed photons for water, Cl^-, and SO_4^{2-} are calculated to be 0.41, 0.57, and 0.02, respectively. Inclusion of HCO_3^- at $100\,\mathrm{mg\,L^{-1}}$ results in little change to the above values, with the fraction absorbed by HCO_3^- itself approximately 0.01. However, the relative contributions of the three radicals, $^{\bullet}OH$, $Cl^{\bullet}$, and $SO_4^{\bullet-}$, to the overall degradation rate of a trace organic contaminant (k') also depends strongly on the relative scavenging of the matrix and the relative rate constant with the target contaminant by the three radicals. Extending equation 6.1, a general expression for k' may be written as:

$$k' = k'_{OH} + k'_{Cl} + k'_{SO_4^-} \tag{6.5}$$

where

$$k'_{OH} = \frac{k_{OH,C}\ \Phi_{H_2O} f_{H_2O} I_a}{k_{OH,S}\,[S]\ +\ k_{OH,HCO_3^-}\,[HCO_3^-]} \tag{6.6}$$

$$k'_{Cl} = \frac{k_{Cl,C}\ \Phi_{Cl^-} f_{Cl^-} I_a}{k_{Cl,S}\,[S]\ +\ k_{Cl,HCO_3^-}\,[HCO_3^-]} \tag{6.7}$$

$$k'_{SO_4^{\bullet-}} = \frac{k_{SO_4^{\bullet-},C}\ \Phi_{SO_4^{2-}} f_{SO_4^{2-}} I_a}{k_{SO_4^{\bullet-},S}\,[S]\ +\ k_{SO_4^{\bullet-},HCO_3^-}\,[HCO_3^-]} \tag{6.8}$$

and where S represents tert-butanol, I_a is the rate of 185 nm photon absorption per unit volume of solution, and all other terms are as described previously. All terms in equations 6.6 to 6.8 are known or can be calculated, except for the second-order rate constant between $Cl^{\bullet}$ and carbamazepine (i.e. C) in equation 6.7. However, it has been deduced that this rate constant is likely to be comparable to that with $^{\bullet}OH$, if not slightly higher, and estimated to be on the order of $10^{10}\,M^{-1}\,s^{-1}$.

Continuing with the model solution from above, including bicarbonate, the sum of the denominators from equations 6.6 to 6.8 represent the scavenging terms for each respective radical and can be calculated using known reaction rate constants with tert-butanol (Buxton et al., 2000) and bicarbonate (see Table 1.2). The resulting scavenging terms for $^{\bullet}OH$, $Cl^{\bullet}$, and $SO_4^{\bullet-}$ are calculated as $8.2 \times 10^4\,s^{-1}$, $4.1 \times 10^5\,s^{-1}$, and $1.5 \times 10^3\,s^{-1}$, respectively. The contributions to k' from $^{\bullet}OH$, $Cl^{\bullet}$, and $SO_4^{\bullet-}$ are calculated to be 60%, 32%, and 8%, respectively. Note that this result is obtained assuming that interconversion between radicals is negligible.

6.4.1 Sulphate and Bicarbonate

The interaction of SO_4^{2-} and HCO_3^- was investigated with tert-butanol as the organic scavenger ($7\,mg\,L^{-1}$ as C), and carbamazepine ($\simeq 0.25\,\mu M$). Values of 0 to $50\,mg\,L^{-1}$ for SO_4^{2-}, and 0 to $180\,mg\,L^{-1}$ for HCO_3^-, formed the points of a 2×2 factorial design, including a centre point, used to detect interactions and curvature. Triplicate irradiations were performed for each of the five settings. The experimental values of k', the observed degradation rate of carbamazepine, were compared to the calculated values obtained by

using equations 6.5, 6.6, and 6.8. The experimental value of k' for no added sulphate or bicarbonate was used to determine the 185 nm photon absorption rate I_a, used in subsequent calculations. A value of $I_a = 2.5 \times 10^{-7}\,\mathrm{M\,s^{-1}}$ was found, in excellent agreement with previous determinations. Experimental and calculated values of k' are tabulated in Table 6.4.

Table 6.4: Comparison of calculated and experimental rates due to SO_4^{2-} and HCO_3^- in the 185 nm regime

$[SO_4^{2-}]$ $(\mathrm{mg\,L^{-1}})$	$[HCO_3^-]$ $(\mathrm{mg\,L^{-1}})$	f_{H_2O}	k'_{calc} $(\mathrm{min^{-1}})$	k'_{exp} $(\mathrm{min^{-1}})$
0	0	1.00	-	0.353 ± 0.006
50	0	0.96	0.870	0.824 ± 0.017
0	180	0.68	0.186	0.167 ± 0.002
25	90	0.79	0.247	0.371 ± 0.006
50	180	0.66	0.182	0.339 ± 0.007

NB: Uncertainties are the standard errors calculated by linear regression of the aggregated rate data from triplicate runs.

It can be seen from the plots of Figure 6.6 that, as before, SO_4^{2-} alone accelerates degradation, while HCO_3^- as a retarding effect. The combination of SO_4^{2-} and HCO_3^-, at the concentrations used, appears to induce little change in the degradation rate relative to the solution containing only tert-butanol as a major solute. For the solutions containing either SO_4^{2-} or HCO_3^-, a comparison of the values in Table 6.4 show close agreement between calculated and experimental k' values. However, for the case of interactions (bottom two rows), the calculated values of k' underestimate the experimental values. Rather than having a net decrease in the value of k', the experimental results appear as if the two effects cancel each other.

Several causes for the discrepancy can be ruled out from previous evidence. Firstly, it is unlikely that $CO_3^{\bullet -}$ is responsible for the unaccounted degradation of carbamazepine, since such an effect was not observed during studies of HCO_3^- alone (see Figure 6.5). It is also unlikely that a possible reaction of

$SO_4^{\bullet-}$ with water was sufficient to contribute significantly to the steady-state concentration of $^{\bullet}OH$, based on the success of equation 6.2 in estimating the second order reaction rate constant between $SO_4^{\bullet-}$ and carbamazepine (see Table 6.2). This phenomena may be due to radical interconversion and requires further study.

Note, the inclusion of centre points in the concentrations used allows the detection of curvature in the response, manifested as a significant difference between the average value of k' obtained from the centre points relative to the average value of k' of all the factorial points. The presence of curvature implies that a linear effects model is inappropriate and that the design must be augmented in order to investigate the nonlinearity. The present results serve to illustrate that the system is nonlinear using concentrations that bracket the environmentally relevant values. If one nevertheless proceeds with an Analysis of Variance (ANOVA), the required sum of squares of the error (SS_E) obtained will not represent the random error of pure noise, and any statistical tests that use it may produce spurious conclusions. Instead, SS_E will be composed of a contribution of pure noise and a contribution from the systematic error resulting from a lack of fit to a linear model. In the present case, the greatest contribution to SS_E is found to be that resulting from a lack of fit. How future investigations should augment the experimental design will depend on what type of nonlinearity is expected, which will require mechanistic information.

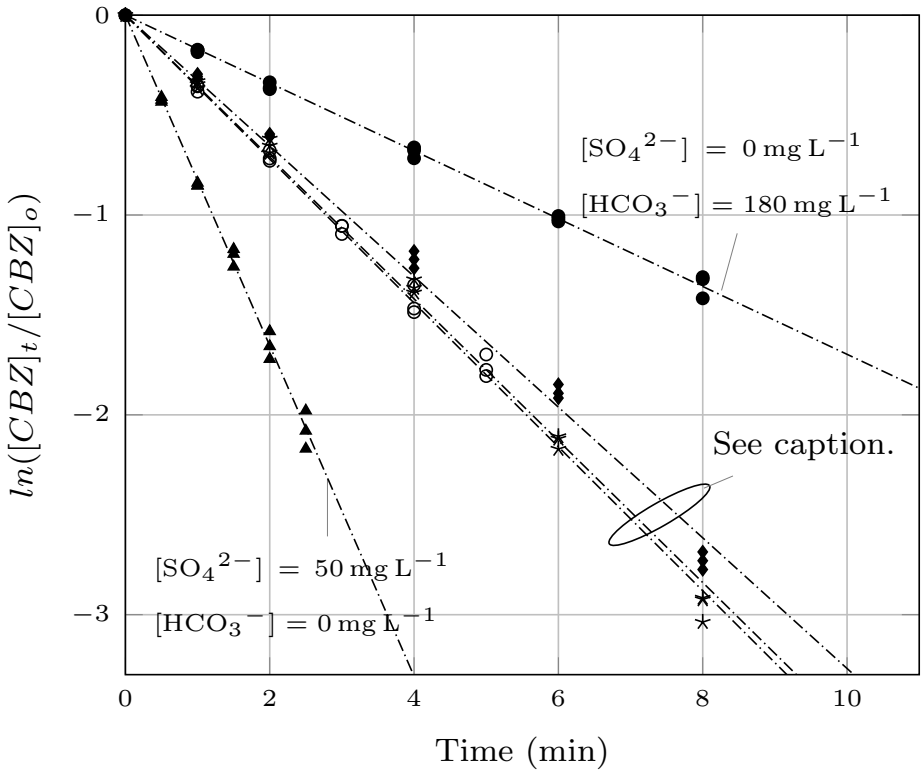

Figure 6.6: Interaction of sulphate and bicarbonate in the 185 nm regime with tert-butanol. $[tBuOH] = 7\,mg\,L^{-1}$ as C and $[CBZ]_o \simeq 0.25\,\mu M$. Na_2SO_4 and $NaHCO_3$ used as sources of sulphate and bicarbonate. $[SO_4{}^{2-}] = 0\,mg\,L^{-1}$, $[HCO_3{}^{-}] = 0\,mg\,L^{-1}$(—○—); $[SO_4{}^{2-}] = 0\,mg\,L^{-1}$,$[HCO_3{}^{-}] = 180\,mg\,L^{-1}$(—●—); $[SO_4{}^{2-}] = 25\,mg\,L^{-1}$, $[HCO_3{}^{-}] = 90\,mg\,L^{-1}$(—⋆—); $[SO_4{}^{2-}] = 50\,mg\,L^{-1}$, $[HCO_3{}^{-}] = 180\,mg\,L^{-1}$(—♦—). $[SO_4{}^{2-}] = 50\,mg\,L^{-1}$, $[HCO_3{}^{-}] = 0\,mg\,L^{-1}$(—▲—);

6.4.2 Chloride and Bicarbonate

The interaction between Cl^- and HCO_3^- was then studied using the same base system consisting of tert-butanol as organic scavenger and carbamazepine as probe, at $7\,mg\,L^{-1}$ as C, and $0.25\,\mu M$, respectively. As in the previous case, the concentrations used were 0 to $50\,mg\,L^{-1}$ for Cl^-, and 0 to $180\,mg\,L^{-1}$ for HCO_3^-. All five matrix conditions were irradiated in triplicate, from which the experimental values of k', the degradation rate of

carbamazepine, were determined. Both k'_{exp} and the calculated fractions of absorbed photons by water (f_{H_2O}) and Cl^- (f_{Cl^-}) are tabulated in Table 6.5.

Table 6.5: Experimental degradation rates of carbamazepine due to Cl^- and HCO_3^- in the 185 nm regime

$[Cl^-]$ $(mg\,L^{-1})$	$[HCO_3^-]$ $(mg\,L^{-1})$	f_{H_2O}	f_{Cl^-}	k'_{exp} (min^{-1})
0	0	1.00	-	0.372 ± 0.007
50	0	0.24	0.74	0.999 ± 0.024
0	180	0.68	0.00	0.169 ± 0.002
25	90	0.38	0.53	0.156 ± 0.003
50	180	0.24	0.65	0.107 ± 0.002

NB: Uncertainties are the standard errors calculated by linear regression of the aggregated rate data from triplicate runs.

As discussed in the previous chapter, the potential conversion of photogenerated $Cl^\bullet$ to $^\bullet OH$ via reactions with water itself, requires a more complex kinetic model than the one that has been used in this work. However, a few comments can nevertheless be made regarding the experimental observations. As previously seen, Cl^- alone accelerates the degradation rate, while HCO_3^- retards the degradation rate. When both Cl^- and HCO_3^-, the net influence is an even greater decrease in the degradation rate than that of HCO_3^- alone. This is consistent with the reactivity of HCO_3^- being greater with $Cl^\bullet$ than with $^\bullet OH$, as reported in the literature and summarized in Table 1.2.

Again, as in the last section, the experimental data indicates a substantial discrepancy between the average value of k' obtained from the centre points relative to the average of k' from the other factorial points. This curvature implies a lack of fit with a linear model. Further investigation of the nonlinearity will require an augmented experimental design chosen based on the type of nonlinearity that may be expected.

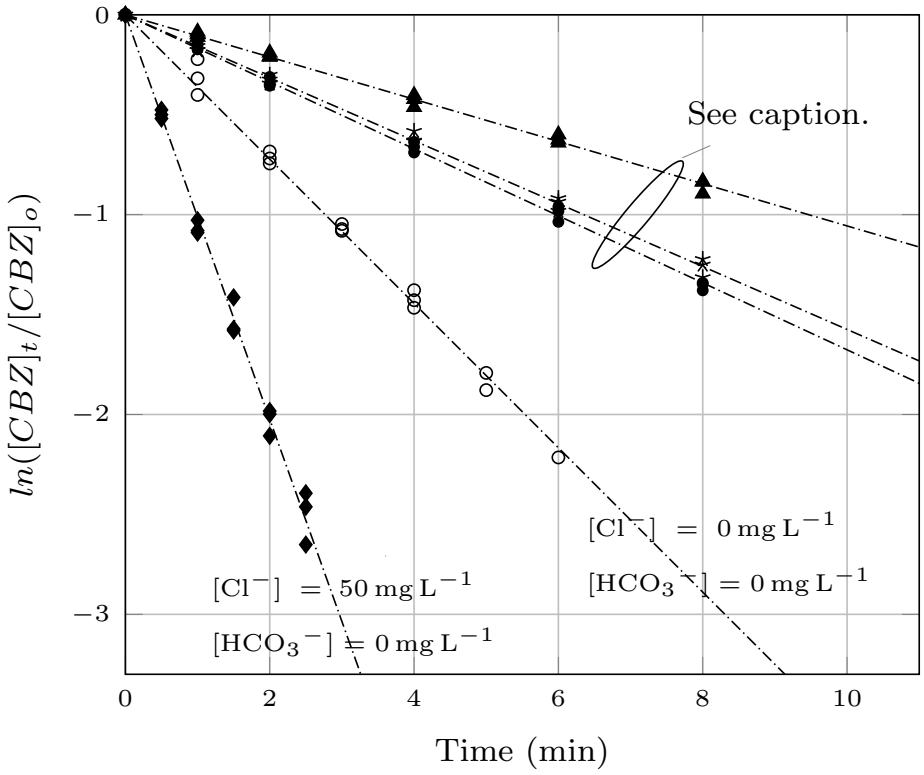

Figure 6.7: Interaction of chloride and bicarbonate in the 185 nm regime with text-butanol. $[tBuOH] = 7\,\mathrm{mg\,L^{-1}}$ as C and $[CBZ]_o \simeq 0.25\,\mu\mathrm{M}$. NaCl and $NaHCO_3$ used as sources of chloride and bicarbonate. $[Cl^-] = 0\,\mathrm{mg\,L^{-1}}$, $[HCO_3^-] = 0\,\mathrm{mg\,L^{-1}}$(—○—); $[Cl^-] = 0\,\mathrm{mg\,L^{-1}}$,$[HCO_3^-] = 180\,\mathrm{mg\,L^{-1}}$(—•—); $[Cl^-] = 25\,\mathrm{mg\,L^{-1}}$, $[HCO_3^-] = 90\,\mathrm{mg\,L^{-1}}$(—⋆—); $[Cl^-] = 50\,\mathrm{mg\,L^{-1}}$, $[HCO_3^-] = 0\,\mathrm{mg\,L^{-1}}$(—♦—); $[Cl^-] = 50\,\mathrm{mg\,L^{-1}}$, $[HCO_3^-] = 180\,\mathrm{mg\,L^{-1}}$(—▲—).

6.4.3 Chloride, Sulphate, and Bicarbonate

The interactions of Cl^-, SO_4^{2-}, and HCO_3^- are next considered with the presence of naturally occurring DOM, again using Suwannee River NOM from the IHSS. The influence on the observed degradation rate k' of the probe compound carbamazepine is investigated. Yet, before reviewing the results of those experiments, the 185 nm absorption of DOM must be considered.

Unlike tert-butanol, Suwannee River NOM absorption of 185 nm photons was suspected to be significant at environmentally relevant concentrations. While the optical properties of DOM have been well studied at 254 nm, no information to-date has been found relating to 185 nm. The Specific Ultraviolet Absorbance or SUVA at 254 nm, with units of $L\,mg^{-1}\,m^{-1}$, is a well used parameter in the field of water treatment, and typically ranges from 1 to $4\,L\,mg^{-1}\,m^{-1}$ in natural waters (APHA, 2012). The SUVA is essentially equivalent to the molar absorption coefficient expressed in different units. At 254 nm, SUVA correlates to the degree of unsaturated carbon-carbon bonds, with strong correlation to the amount of aromatic content in the DOM, the dominant chromophore at 254 nm. At 185 nm, photon absorption also occurs at unsaturated carbon-carbon bonds, as well as oxygen containing functional groups, and is thus expected to be strong.

As previously discussed, an indirect kinetic technique was developed to measure the absorptive properties of solutes at 185 nm, thus circumventing the limitations of conventional spectrophotometers operating at that wavelength. The 185 nm SUVA of Suwannee River NOM was found to be $6.2 \pm 0.5\,L\,mg^{-1}\,m^{-1}$. This value is higher than that observed at 254 nm confirming stronger absorption per unit mass at the shorter wavelength.

The experiments here used Suwannee River NOM in all solutions, at a concentration of $4\,mg\,L^{-1}$ as C, which represents an absorption coefficient of $0.25\,cm^{-1}$ at 185 nm. A set of solutions with Cl^-, SO_4^{2-}, and HCO_3^- formed at $2 \times 2 \times 2$ matrix with concentrations set at either at 0 or 50, 50, and

$180\,\mathrm{mg\,L^{-1}}$, respectively. All solutions were irradiated in triplicate, with the observed degradation rate of the probe carbamazepine calculated from the aggregate data. Results obtained in the absence of HCO_3^- are plotted in Figure 6.8. Results obtained with $180\,\mathrm{mg\,L^{-1}}$ of HCO_3^- are plotted in Figure 6.9. Table 6.6 shows the experimental settings used, calculated distribution of absorbed photons among the major solutes (i.e. f_i), experimental rates k', and relative rates k'/k'_o.

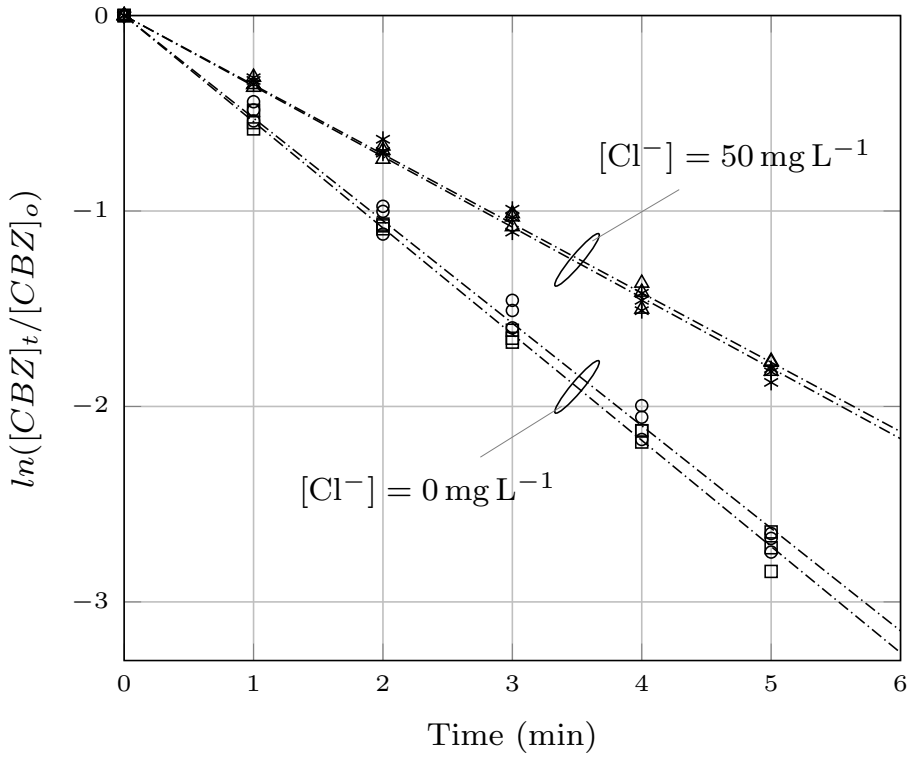

Figure 6.8: Interaction of chloride and sulphate in the 185 nm regime with Suwannee River NOM and without bicarbonate. $[DOM] = 4\,\mathrm{mg\,L^{-1}}$ as C and $[CBZ]_o \simeq 0.25\,\mu\mathrm{M}$. NaCl and Na_2SO_4 used as sources of chloride and sulphate. All solutions at pH 7. $[Cl^-] = 0\,\mathrm{mg\,L^{-1}}$, $[SO_4{}^{2-}] = 0\,\mathrm{mg\,L^{-1}}$(—○—); $[Cl^-] = 0\,\mathrm{mg\,L^{-1}}$,$[SO_4{}^{2-}] = 50\,\mathrm{mg\,L^{-1}}$(—□—); $[Cl^-] = 50\,\mathrm{mg\,L^{-1}}$, $[SO_4{}^{2-}] = 0\,\mathrm{mg\,L^{-1}}$(—△—); $[Cl^-] = 50\,\mathrm{mg\,L^{-1}}$, $[SO_4{}^{2-}] = 50\,\mathrm{mg\,L^{-1}}$(—✳—);

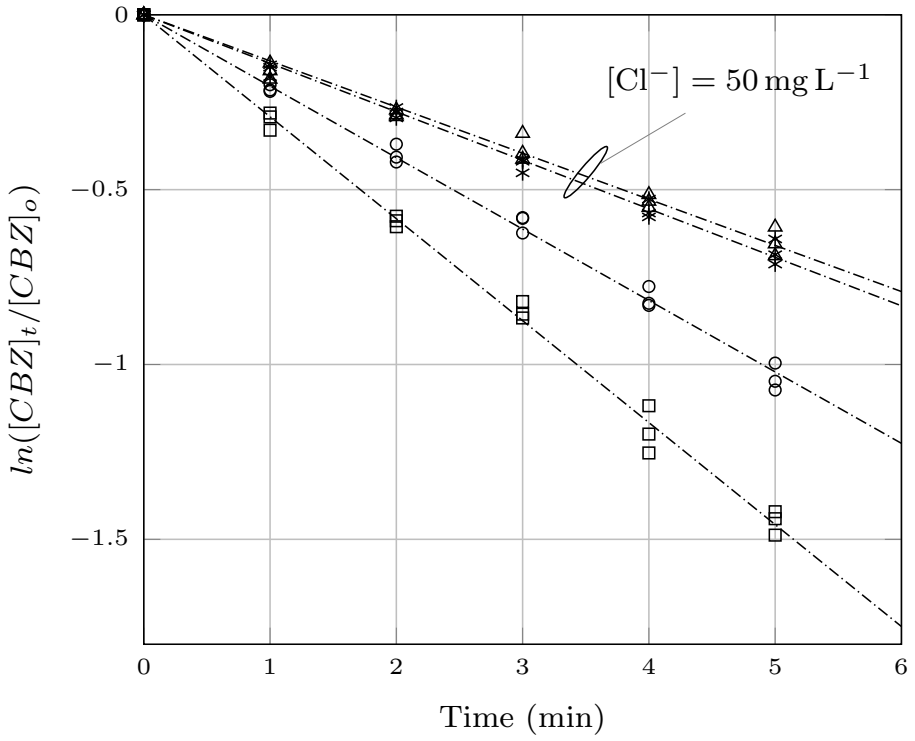

Figure 6.9: Interaction of chloride and sulphate in the 185 nm regime with Suwannee River NOM and with bicarbonate. $[DOM] = 4\,mg\,L^{-1}$ as C, $[HCO_3^-] = 180\,mg\,L^{-1}$ and $[CBZ]_o \simeq 0.25\,\mu M$. NaCl, Na_2SO_4, and $NaHCO_3$ used as sources of chloride, sulphate and bicarbonate. All solutions at pH 7. $[Cl^-] = 0\,mg\,L^{-1}$, $[SO_4{}^{2-}] = 0\,mg\,L^{-1}$(—○—); $[Cl^-] = 0\,mg\,L^{-1}$,$[SO_4{}^{2-}] = 50\,mg\,L^{-1}$(—□—); $[Cl^-] = 50\,mg\,L^{-1}$, $[SO_4{}^{2-}] = 0\,mg\,L^{-1}$(—△—); $[Cl^-] = 50\,mg\,L^{-1}$, $[SO_4{}^{2-}] = 50\,mg\,L^{-1}$(—✳—);

Several comments can now be made regarding degradation in the 185 nm regime based on the observations above. In the absence of HCO_3^-, the presence of Cl^- reduces the degradation rate. This can be explained by a higher reactivity of $Cl^\bullet$ than $^\bullet OH$ with DOM. In the absence of Cl^-, the presence of SO_4^{2-} has little effect on k', despite the fact that the second-order rate constant for carbamazepine and $SO_4^{\bullet-}$ was found to be lower than that of $^\bullet OH$ (i.e. $k_{SO_4^-,C} < k_{OH,C}$). This can be explained by a lower rate constant for $SO_4^{\bullet-}$ with DOM, than for $^\bullet OH$. From this information the relative reactivities for DOM may be deduced as follows:

$$k_{Cl,DOM} > k_{OH,DOM} > k_{SO_4^-,DOM} \tag{6.9}$$

In the presence of HCO_3^-, all degradation rates decrease further, with the lowest associated with the presence of Cl^-. In the absence of Cl^-, the presence of SO_4^{2-} induces a substantial increase in degradation rate. These observations are rationalized with the relative radical reactivities of HCO_3^- having the following pattern:

$$k_{Cl,HCO_3^-} > k_{OH,HCO_3^-} > k_{SO_4^-,HCO_3^-} \tag{6.10}$$

consistent with the $k_{SO_4^-,HCO_3^-}$ value of Mertens and von Sonntag (1995) of $3.5 \times 10^6\,M^{-1}\,s^{-1}$, quoted in Table 1.2, but not with that of Buxton et al. (2000) of $9.1 \times 10^6\,M^{-1}\,s^{-1}$, which is comparable to the widely cited value of $k_{OH,HCO_3^-} = 8.5 \times 10^6\,M^{-1}\,s^{-1}$ from the compilation of Buxton et al. (1988).

Table 6.6: Interactions of Cl^-, SO_4^{2-} and HCO_3^-, in the presence of Suwannee River NOM at $[DOC] = 4\,mg\,L^{-1}$ as C, in the 185 nm regime

	$[Cl^-]$	$[SO_4^{2-}]$	$f_i = \alpha_i/\alpha_{tot}$					k'	k'/k'_o
			H_2O	Cl^-	SO_4^{2-}	HCO_3^-	DOM		
	$(mg\,L^{-1})$	$(mg\,L^{-1})$						(min^{-1})	
$[HCO_3^-] = 0\,mg\,L^{-1}$	0	0	0.88	0	0	0	0.12	0.539 ± 0.011	1.00
	0	50	0.84	0	0.04	0	0.12	0.546 ± 0.008	1.01
	50	0	0.26	0.71	0	0	0.04	0.360 ± 0.006	0.67
	50	50	0.25	0.70	0.01	0	0.03	0.374 ± 0.007	0.69
$[HCO_3^-] = 180\,mg\,L^{-1}$	0	0	0.62	0	0	0.29	0.09	0.206 ± 0.004	0.38
	0	50	0.60	0	0.03	0.29	0.08	0.290 ± 0.006	0.54
	50	0	0.23	0.63	0	0.11	0.03	0.125 ± 0.004	0.23
	50	50	0.23	0.63	0.01	0.11	0.03	0.134 ± 0.004	0.25

NB: Uncertainties are the standard errors calculated by linear regression of the aggregated rate data from triplicate runs. The fractions of photons f_i absorbed by species i are calculated from the experimentally measured molar absorption coefficients. Carbamazepine used as the probe compound with $[CBZ]_o \simeq 0.25\,\mu M$. The observed rate k'_o corresponds to a solution with DOM as the only major solute.

Regarding the distribution of absorbed photons, it can be seen that the three anions and the DOM are significant compared to water, and that all these species should be considered in an actual water matrix. These observations demonstrate the sensitivity of the degradation kinetics on the composition of the water matrix.

Other species that may also be significant are nitrate (NO_3^-) and ferric iron (Fe^{3+}), and possibly manganese (Mn^{2+}). While these species are generally present at concentrations much less than $1\,mg\,L^{-1}$, there are cases where the concentration may be elevated significantly above typical levels. In such cases, these species may induce signifiant photochemical and radical effects in 185 nm regime and merit study.

6.5 Summary

The UV/H_2O_2 was found to be insensitive to the presence of SO_4^{2-}. In the 185 nm regime, SO_4^{2-} was found to have a significant impact. Experimental data was used to calculate the second-order reaction rate of $SO_4^{\bullet-}$ with carbamazepine, estimated to be $1.5 \pm 0.1 \times 10^8\,M^{-1}\,s^{-1}$.

The influence of HCO_3^- was found to manifest by two separate phenomena, including the known scavenging of $^\bullet OH$, as well as by the absorption of 185 nm. The latter inner filter or "photon scavenger" mechanism, previously unreported, should be considered in general as the associated fraction of absorbed photons may be substantial in some waters.

When considering the interaction of HCO_3^- with either SO_4^{2-} or Cl^-, the model used with success in simpler cases proves inadequate in predicting degradation rates. It is suspected that the discrepancies observed are due to the interconversion of radicals not taken into account by the current model. Such interconversions merit further investigation.

The three major anions Cl^-, SO_4^{2-}, and HCO_3^-, as well as Suwannee River NOM reference material, have been analyzed for their optical absorption constants at 185 nm using the indirect kinetic method discussed in Chapter 5. The molar absorption coefficients are: $\epsilon_{Cl^-} = 3540 \pm 150\,M^{-1}\,cm^{-1}$, $\epsilon_{SO_4^{2-}} = 160 \pm 20\,M^{-1}\,cm^{-1}$, $\epsilon_{HCO_3^-} = 290 \pm 40\,M^{-1}\,cm^{-1}$. The $SUVA_{185}$ of Suwannee River NOM is $6.2 \pm 0.2\,L\,mg^{-1}\,m^{-1}$.

Experiments investigating the interactions of the three major anions in the presence of Suwannee River NOM allowed the deduction of relative reactivities for the three radical species with both Suwannee River NOM and HCO_3^-. In both cases, it was found that reactivity follows the order of $Cl^\bullet > {}^\bullet OH > SO_4^{\bullet-}$.

These investigations indicate that the 185 nm removal kinetics are highly sensitive to the presence of the major anions and DOM, and that multiple radicals are likely to be involved in trace organic contaminant degradation.

Chapter 7

Conclusions and Recommendations

7.1 Conclusions

The conventional low pressure mercury lamp used in UV disinfection has become a mature technology and a method of choice for disinfection of chlorine resistant pathogens. UV technology, developed for disinfection, has allowed the expanded use of UV treatment to the advanced oxidation process (AOP).

The UV AOP, using low pressure lamps, uses $^{\bullet}OH$ generated by the 254 nm photolysis of H_2O_2 to destroy trace organic contaminants. However, H_2O_2 is a poor absorber of photons, and its addition involves increased process complexity that scales poorly to small systems. An alternative method of generating $^{\bullet}OH$ exploits the second major emission line of the low pressure mercury lamp at 185 nm to generate $^{\bullet}OH$ from the photolysis of water itself. Fundamental aspects of the 185 nm photochemistry relevant to natural waters have been investigated and reported by this work for the first time.

Experimental techniques have been developed to investigate the 185 nm AOP on a bench scale. A N_2 purged collimated beam was designed for use with commercially available fused silica cells. Carbamazepine was found to be an ideal probe compound due to negligible direct photolysis at 254 nm and ease of quantification. Tert-Butanol was found to be an ideal model of dissolved organic carbon, due to its well characterized radical chemistry, availability in pure form, complete miscibility with water, and lack of sig-

nificant absorbance at either 254 or 185 nm. Its use allowed better study of major inorganic solutes. Phosphate buffers were found to be inappropriate, as they are not photochemically inert at 185 nm and result in reactive radical formation.

Temperature effects were studied quantitatively and by comparison between the 254 nm-H_2O_2 and 185 nm processes. Of the two processes, it was found that the 185 nm AOP is less temperature sensitive under the conditions tested, implying that the change in 185 nm absorbance of water with temperature imparts a negligible effect. The calculated activation energy for water photolysis supports a fundamental model of liquid water that includes a small minority of non-hydrogen bonded interstitial monomers. Major solutes, particularly Cl^-, were not included in the temperature studies, and merit additional study.

The study of Dissolved Organic Matter (DOM), using pure compounds and humic reference materials, revealed that DOM acts in two independent ways to impede the efficiency of the 185 nm AOP, acting both as a radical scavenger and an absorber of photons. Furthermore, the use of transparent pure compounds allowed the estimation of 185 nm fluence rates, which are particularly useful in the absence of convenient actinometers and reliable radiometers. By using tert-butanol and methanol, it was found that the 185 nm fluence rate is approximately 16% of that at 254 nm determined by KI-KIO_3 actinometry. This is a useful parameter since the amount of 185 nm radiation produced by a low pressure mercury lamp is a critically important quantity, yet poorly documented and difficult to measure accurately.

The role of chloride in water under 185 nm irradiation is perhaps the most significant of all major inorganic solutes. Using a new measurement technique, the molar absorption coefficient of chloride at 185 nm was determined to be $\epsilon_{185,Cl^-} = 3540 \pm 150\,M^{-1}\,cm^{-1}$. When chloride exceeds approximately $20\,mg\,L^{-1}$, then chloride, and not water, will be the dominant absorber of 185 nm photons. Subsequent to photon absorption, the generated chlorine

radical, $Cl^{\bullet}$, with a quantum yield of approximately 0.4, is capable of reacting with many trace organics with second-order rate constants comparable to those of $^{\bullet}OH$. In addition to differences in kinetics as compared to purely $^{\bullet}OH$ driven processes, differences in reaction mechanisms likely result in different distributions of products in the resulting mixtures, if not different products themselves. The simultaneous generation of the two radicals $Cl^{\bullet}$ and $^{\bullet}OH$, and the postulated conversion of the former to the latter via reactions with water, result in a mixture of oxidative species. The importance of each one to the oxidation degradation of trace organic contaminants will depend on both the composition of the water matrix and the relative reactivities of the target contaminant.

Sulphate was also found to be a significant contributor to degradation via 185 nm irradiation. Its molar absorption coefficient was determined to be $\epsilon_{185,SO_4^{2-}} = 160 \pm 20\,M^{-1}\,cm^{-1}$. Photon absorption followed by generation of the sulphate radical, $SO_4^{\bullet-}$, with a quantum yield of approximately 0.65, is similarly able to oxidize many organic molecules with elevated rate constants. However, despite the relatively low absorption of SO_4^{2-}, the presence of Cl^- allows the generation of $SO_4^{\bullet-}$ by electron transfer to $Cl^{\bullet}$ and vice-versa. An equilibrium constant close to unity for the reaction $Cl^{\bullet} + SO_4^{2-} \rightleftharpoons Cl^- + SO_4^{\bullet-}$ provides an additional link between $SO_4^{\bullet-}$ and $Cl^{\bullet}$, and therefore $^{\bullet}OH$. The mixture of the three radicals further complicates the resulting degradation kinetics and mechanistic pathways. Even when $SO_4^{\bullet-}$ may be much smaller than the other two, its significance may be amplified if its reactivity with the dominant scavengers is relatively low.

Bicarbonate was studied and found to impart not only the usual parasitic effect of radical scavenging, but also via 185 nm photon absorption. Its molar absorption coefficient was determined to be $\epsilon_{185,HCO_3^-} = 290 \pm 40\,M^{-1}\,cm^{-1}$.

An investigation of the influence of more than two major solutes at a time reveals that significant interactions exist. The overall kinetics depend therefore, not only on the concentrations of the major solutes, but also on their

relative absorption coefficients, and relative reactivities with the water matrix and target contaminants. The kinetic model used successfully for individual matrix components fails to properly predict observed degradation rates when more than one major inorganic solute is present. More accurate predictions of reaction kinetics may be obtained upon improved understanding of radical interconversion mechanisms. The information presented here should serve as an aide in planning additional experiments.

Lastly, for the reader interested in the practical application of the 185 nm AOP, a few comments can be made. As mentioned, one of the greatest benefits of the 185 nm AOP is the elimination of the need for storage, addition, and quenching of H_2O_2. This fact alone may be sufficiently desirable in some contexts to favour its use. In other cases, a more detailed comparison of the 185 nm and 254 nm-H_2O_2 AOPs requires information on reactor geometry, water composition, target contaminants, and treatment objectives. Such a comparison could incorporate the figure of merit known as the electrical energy per order (EE_O) to express the energy required, in units of kW h m^{-3}, to reduce the concentration of a given contaminant by an order of magnitude under the conditions used. Electrical and chemical costs of H_2O_2 addition and quenching would assist operating cost comparisons. Ultimately, any calculated estimates need to be confirmed by pilot and full scale testing. Such a rigorous analysis is beyond the scope of this work, yet it is hoped that fundamental information presented here will assist such an endeavour.

7.2 Recommendations

Research on the 185 nm AOP should report the identity and concentrations of all major anions present in the studied water matrix when specifying the experimental conditions. A dedicated instrument for accurate measurement of optical absorption at 185 nm will facilitate routine analysis.

While the temperature sensitivity of the 185 nm AOP was found to be small,

this was determined in the absence of major inorganic solutes. The absorbances and quantum yields of the charge-transfer-to-solvent absorption bands are reported to be sensitive to temperature. Thus, temperature sensitivity should be reinvestigated in the presence of such solutes.

A convenient chemical actinometer should be developed to allow expression of the extent of treatment specified not by exposure time, but by fluence or dose of photons. Such an actinometer would ideally employ a simple method of analysis of the photochemical products, such as by UV-VIS spectrophotometry. Such an actinometer could allow the fluence delivered by a flow through reactor to be quantified by a reduction equivalent dose correlated with a collimated beam experiment.

Laser flash photolysis studies would allow the evaluation of the relative involvement of $^{\bullet}OH$, $Cl^{\bullet}$, and $SO_4^{\bullet-}$ during oxidative degradation in various water matrices. Such studies would also facilitate the determination of rate constants by competitive kinetics for a list of relevant organic contaminants and the elucidation of radical interconversion mechanisms.

Product studies of 185 nm treatment would facilitate the identification of product ratios, as well as the existence of unique products associated with the three main reactive radicals. If unique products are found, the parent compounds could serve as useful probes for determining the contribution of each radical degradation pathway.

A numerical model could be developed with sufficient kinetic information that would allow the exact rate expression to be evaluated. Such a model would predict the extent of removal for a particular target contaminant given the 185 nm photon absorption rate and water matrix composition. Coupling such a kinetic model with radiation and hydrodynamics models would serve the ultimate goal of reactor design.

Bibliography

J L Acero and U Von Gunten. Characterization of oxidation processes: Ozonation and the AOP O_3/H_2O_2. *Journal - American Water Works Association*, 93(10):90–100, 2001.

J L Acero, K Stemmler, and U Von Gunten. Degradation kinetics of atrazine and its degradation products with ozone and OH radicals: A predictive tool for drinking water treatment. *Environmental Science and Technology*, 34(4):591–597, 2000.

J E Amoore and E Hautala. Odor as an aid to chemical safety: Odor thresholds compared with threshold limit values and volatilities for 214 industrial chemicals in air and water dilution. *Journal of Applied Toxicology*, 3(6): 272–290, 1983.

M Anbar and J K Thomas. Pulse radiolysis studies of aqueous sodium chloride solutions. *The Journal of Physical Chemistry*, 68(12):3829–3835, 1964.

APHA. *Standard Methods for the Examination of Water and Wastewater*. American Public Health Association, American Water Works Association, Water Environment Federation, 22nd edition, 2012.

AWWA ASCE. *Water Treatment Plant Design*. McGraw-Hill, 2nd edition, 1990.

CSSE ASCE, AWWA. *Water Treatment Plant Design*. American Water Works Association, Inc., New York, N.Y., 1969.

ASCE AWWA. *Water Treatment Plant Design*. McGraw-Hill, 3rd edition, 1998.

ASCE AWWA. *Water Treatment Plant Design*. McGraw-Hill, 5th edition, 2012.

M N Baker and M J Taras. *The Quest for Pure Water: A History of the Twentieth Century*. American Water Works Association, 1981.

P Ball. Water: An enduring mystery. *Nature*, 452(7185):291–292, 2008.

B T Barnes. Intensities of λ1850 and λ2537 in low-pressure mercury vapor lamps with rare gas present. *Journal of Applied Physics*, 31(5):852–854, 1960.

J Barrett and A L Mansell. Ultraviolet absorption spectra of the molecules H_2O, HDO and D_2O. *Nature*, 187:138, 1960.

J Barrett, M F Fox, and A L Mansell. The photochemistry of aqueous sulfate ion. *The Journal of Physical Chemistry*, 69(9):2996–3000, 1965.

J H Baxendale and J A Wilson. The photolysis of hydrogen peroxide at high light intensities. *Transactions of the Faraday Society*, 53:344–356, 1957.

T A Bellar and J J Lichtenberg. Determining volatile organics at microgram-per-litre levels by gas chromatography. *Journal - American Water Works Association*, pages 739–744, 1974.

T A Bellar, J J Lichtenberg, and R C Kroner. The occurrence of organohalides in chlorinated drinking waters. *Journal - American Water Works Association*, pages 703–706, 1974.

M J Benotti, R A Trenholm, B J Vanderford, J C Holady, B D Stanford, and S A Snyder. Pharmaceuticals and endocrine disrupting compounds in US drinking water. *Environmental Science and Technology*, 43(3):597–603, 2009.

B Bielski, D Cabelli, R Arudi, and A B Ross. Reactivity of $HO_2^{\bullet}/O_2^{\bullet-}$ radicals in aqueous solution. *Journal of Physical and Chemical Reference Data*, 14(4):1041–1100, 1985.

M J Blandamer and M F Fox. Theory and applications of charge-transfer-to-solvent spectra. *Chemical Reviews*, 70(1):59–93, 1970.

J R Bolton and C Cotton. *The Ultraviolet Disinfection Handbook*. American Water Works Association, 2011.

J R Bolton and M I Stefan. Fundamental photochemical approach to the concepts of fluence (UV dose) and electrical energy efficiency in photochemical degradation reactions. *Research on Chemical Intermediates*, 28 (7):857–870, 2002.

J R Bolton, K G Bircher, W Tumas, and C A Tolman. Figures-of-merit for the technical development and application of advanced oxidation processes. *Journal of Advanced Oxidation Technologies*, 1:13–17, 1996.

J R Bolton, M I Stefan, P Shaw, and K R Lykke. Determination of the quantum yields of the potassium ferrioxalate and potassium iodide - iodate actinometers and a method for the calibration of radiometer detectors. *Journal of Photochemistry and Photobiology A: Chemistry*, 222(1):166–169, 2011.

M Born and E Wolf. *Principles of Optics: Electromagnetic Theory of Propagation, Interference and Diffraction of Light*. Cambridge University Press, 7th edition, 1999.

N V Brodtmann Jr and P J Russo. The use of chloramine for reduction of trihalomethanes and disinfection of drinking water. *Journal - American Water Works Association*, pages 40–42, 1979.

Z Bukhari, T M Hargy, J R Bolton, B Dussert, and J L Clancy. Medium-pressure UV for oocyst inactivation. *Journal - American Water Works Association*, 91(3):86, 1999.

N J Bunce. *Environmental Chemistry*. Wuerz Pub., 1990.

C Burgess and T Frost, editors. *Standards and Best Practice in Absorption Spectrometry*. Blackwell Science, 1999.

J Butler. *Ionic Equilibrium: A Mathematical Approach*. Addison-Wesley, MA, 1964.

J Butler. *Carbon Dioxide Equilibria and their Applications*. Addison-Wesley, 1982.

G V Buxton, C L Greenstock, W P Helman, and A B Ross. Critical review of rate constants for reactions of hydrated electrons, hydrogen atoms and hydroxyl radicals $^{\bullet}OH$ and $O^{\bullet-}$ in aqueous solution. *Journal of Physical and Chemical Reference Data*, 17(2):513–886, 1988.

G V Buxton, M Bydder, and G A Salmon. Reactivity of chlorine atoms in aqueous solution: Part 1 The equilibrium $Cl^{\bullet} + Cl^{-} = Cl_2^{\bullet-}$. *Journal of the Chemical Society, Faraday Transactions*, 94(5):653–657, 1998.

G V Buxton, M Bydder, and G A Salmon. The reactivity of chlorine atoms in aqueous solution: Part II The equilibrium $SO_4^{\bullet-} + Cl^{-} = Cl^{\bullet} + SO_4^{2-}$. *Physical Chemistry Chemical Physics*, 1(2):269–273, 1999.

G V Buxton, M Bydder, G A Salmon, and J E Williams. The reactivity of chlorine atoms in aqueous solution: Part III The reactions of $Cl^{\bullet}$ with solutes. *Physical Chemistry Chemical Physics*, 2(2):237–245, 2000.

J G Calvert and J N Pitts. *Photochemistry*. Wiley, 1966.

A T Campbell, L J Robertson, M R Snowball, and H V Smith. Inactivation of oocysts of Cryptosporidium parvum by ultraviolet irradiation. *Water Research*, 29(11):2583–2586, 1995.

S Chen and M Z Hoffman. Rate constants for the reaction of the carbonate radical with compounds of biochemical interest in neutral aqueous solution. *Radiation Research*, 56(1):40–47, 1973.

S Chen, M Z Hoffman, and G H Parsons Jr. Reactivity of the carbonate radical toward aromatic compounds in aqueous solution. *The Journal of Physical Chemistry*, 79(18):1911–1912, 1975.

Z K Chowdhury, R S Summers, G P Westerhoff, B J Leto, K O Nowack, and C J Corwin. *Activated Carbon: Solutions for Improving Water Quality.* American Water Works Association, 2013.

J L Clancy, T M Hargy, M M Marshall, and J E Dyksen. UV light inactivation of Cryptosporidium oocysts. *Journal - American Water Works Association*, 90(9):92, 1998.

J L Clancy, Z Bukhari, T M Hargy, J R Bolton, B W Dussert, and M M Marshall. Using UV to inactivate Cryptosporidium. *Journal - American Water Works Association*, 92(9):97, 2000.

M Clara, B Strenn, and N Kreuzinger. Carbamazepine as a possible anthropogenic marker in the aquatic environment: Investigations on the behaviour of carbamazepine in wastewater treatment and during groundwater infiltration. *Water Research*, 38(4):947–954, 2004.

J T Cookson Jr. Virus and water supply. *Journal - American Water Works Association*, pages 707–711, 1974.

J A Cotruvo and C Wu. Controlling organics: Why Now? *Journal-American Water Works Association*, 70(11):590–594, 1978.

S A Craik, G R Finch, J R Bolton, and M Belosevic. Inactivation of Giardia muris cysts using medium-pressure ultraviolet radiation in filtered drinking water. *Water Research*, 34(18):4325–4332, 2000.

G F Craun, L J McCabe, and J M Hughes. Waterborne disease outbreaks in the US 1971-1974. *Journal - American Water Works Association*, 68 (8):420–424, 1976.

J C Crittenden, S Hu, D W Hand, and S A Green. A kinetic model for H_2O_2/UV process in a completely mixed batch reactor. *Water Research*, 33(10):2315–2328, 1999.

G Crozes, P White, and M Marshall. Enhanced coagulation. *Journal - American Water Works Association*, 87:78–89, 1995.

G Czapski, S V Lymar, and H A Schwarz. Acidity of the carbonate radical. *The Journal of Physical Chemistry A*, 103(18):3447–3450, 1999.

F S Dainton and P Fowles. The photolysis of aqueous systems at 1849 å II. solutions containing Cl^-, Br^-, SO_4^{2-}, or OH^- ions. In *Proc. R. SOC. London A*, volume 287, page 3, 1965.

B. Darwent. Bond dissociation energies in simple molecules. *NIST Special Publication*, 1(1), 1970.

C P Dionigi, T E Lawlor, J E McFarland, and P B Johnsen. Evaluation of geosmin and 2-methylisoborneol on the histidine dependence of TA98 and TA100 Salmonella typhimurium tester strains. *Water Research*, 27 (11):1615–1618, 1993.

A D Dotson, C E Rodriguez, and K G Linden. UV disinfection implementation status in US water treatment plants. *Journal - American Water Works Association*, 104(5):77–78, 2012.

J I Drever. *The Geochemistry of Natural Waters*. Prentice Hall Englewood Cliffs, 1988.

P L Du Pisani. Direct reclamation of potable water at Windhoek's Goreangab reclamation plant. *Desalination*, 188(1):79–88, 2006.

H L DuPont, C L Chappell, C R Sterling, P C Okhuysen, J B Rose, and W Jakubowski. The infectivity of cryptosporidium parvum in healthy volunteers. *New England Journal of Medicine*, 332(13):855–859, 1995.

M S Elovitz and U von Gunten. Hydroxyl radical/ozone ratios during ozonation processes. I. The Rct concept. *Ozone Science and Engineering*, 1999.

B Ervens, S Gligorovski, and H Herrmann. Temperature-dependent rate constants for hydroxyl radical reactions with organic compounds in aqueous solutions. *Physical Chemistry Chemical Physics*, 5(9):1811–1824, 2003.

Y Feng, D W Smith, and J R Bolton. Photolysis of aqueous free chlorine species (HOCl and OCl^-) with 254 nm ultraviolet light. *Journal of Environmental Engineering and Science*, 6(3):277–284, 2007.

L Forni, D Bahnemann, and E J Hart. Mechanism of the hydroxide ion-initiated decomposition of ozone in aqueous solution. *The Journal of Physical Chemistry*, 86(2):255–259, 1982.

K R Fox and D A Lytle. Milwaukee's Crypto outbreak: Investigation and recommendations. *Journal - American Water Works Association*, 88(9): 87, 1996.

M F Fox. The photolysis of simple inorganic anions in solution. *Quarterly Reviews, Chemical Society*, 24(4):565–584, 1970.

M F Fox, B E Barker, and E Hayon. Far-ultraviolet solution spectroscopy of chloride ion. *Journal of the Chemical Society, Faraday Transactions 1: Physical Chemistry in Condensed Phases*, 74:1776–1785, 1978.

H. S. Frank. Structural models. In F Franks, editor, *Water a Comprehensive Treatise: Volume 1: The Physics and Physical Chemistry of Water*, chapter 14. Plenum Press, 1972.

F Franks. *Water: A Matrix of Life*. Royal Society of Chemistry, 2000.

N Getoff and G O Schenck. Primary products of liquid water photolysis at 1236, 1470 and 1849 å. *Photochemistry and Photobiology*, 8(3):167–178, 1968.

B C Gilbert, J K Stell, W J Peet, and K J Radford. Generation and reactions of the chlorine atom in aqueous solution. *Journal of the Chemical Society, Faraday Transactions 1: Physical Chemistry in Condensed Phases*, 84 (10):3319–3330, 1988.

W H Glaze, J Kang, and D H Chapin. The chemistry of water treatment processes involving ozone, hydrogen peroxide and ultraviolet radiation. *Ozone Science and Engineering*, 9:335–352, 1987.

W H Glaze, R Schep, W Chauncey, E C Ruth, J J Zarnoch, E M Aieta, C H Tate, and M J McGuire. Evaluating oxidants for the removal of model taste and odor compounds from a municipal water supply. *Journal - American Water Works Association)*, pages 79–84, 1990.

C Gleeson and N Gray. *The Coliform Index and Waterborne Disease: Problems of microbial drinking water assessment*. CRC Press, 1997.

J V Goldstone, M J Pullin, S Bertilsson, and B M Voelker. Reactions of hydroxyl radical with humic substances: Bleaching, mineralization, and production of bioavailable carbon substrates. *Environmental Science and Technology*, 36(3):364–372, 2002.

W R Haag and J Hoigné. Ozonation of bromide-containing waters: Kinetics of formation of hypobromous acid and bromate. *Environmental Science and Technology*, 17(5):261–267, 1983.

W R Haag and C C Yao. Rate constants for reaction of hydroxyl radicals with several drinking water contaminants. *Environmental Science and Technology*, 26(5):1005–1013, 1992.

T Hargy. Status of UV disinfection of municipal drinking water systems in North America. *Water Conditioning and Purification International*, pages 30–35, 2002.

W Harm. *Biological Effects of Ultraviolet Radiation*. Cambridge University Press, 1980.

D C Harris. *Quantitative Chemical Analysis*. Macmillan, 2010.

K Hasegawa and P Neta. Rate constants and mechanisms of reaction of $Cl_2^{\bullet -}$ radicals. *The Journal of Physical Chemistry*, 82(8):854–857, 1978.

E Hayon and J J McGarvey. Flash photolysis in the vacuum ultraviolet region of sulfate, carbonate, and hydroxyl ions in aqueous solutions. *The Journal of Physical Chemistry*, 71(5):1472–1477, 1967.

O S Heavens. *Optical Properties of Thin Solid Films*. Courier Corporation, 1991.

E Heilker. The Mülheim process for treating Ruhr River water. *Journal-American Water Works Association*, 71(11):623–627, 1979.

Charles P Hibler. *Inactivation of Giardia Cysts with Chlorine at 0.50 to 5.00 °C*. American Water Works Association, 1987.

J Hoigné. Inter-calibration of OH radical sources and water quality parameters. *Water Science and Technology*, 35(4):1–8, 1997.

K J Howe, D W Hand, J C Crittenden, R R Trussell, and G Tchobanoglous. *Principles of Water Treatment*. John Wiley and Sons, 2012.

S E Hrudey and J W A Charrois. *Disinfection By-products and Human Health*. IWA Publishing, 2012.

S E Hrudey and E J Hrudey. *Safe Drinking Water: Lessons from recent outbreaks in affluent nations*. IWA publishing, 2004.

R E Huie, C L Clifton, and P Neta. Electron transfer reaction rates and equilibria of the carbonate and sulfate radical anions. *International Journal of Radiation Applications and Instrumentation. Part C. Radiation Physics and Chemistry*, 38(5):477–481, 1991.

J P Hunt and H Taube. The photochemical decomposition of hydrogen peroxide. Quantum yields, tracer and fractionation effects. *Journal of the American Chemical Society*, 74(23):5999–6002, 1952.

J Jagger. *Introduction to Research in Ultraviolet Photobiology*. Prentice-Hall, 1967.

G G Jayson, B J Parsons, and A J Swallow. Some simple, highly reactive, inorganic chlorine derivatives in aqueous solution. their formation using pulses of radiation and their role in the mechanism of the Fricke dosimeter. *Journal of the Chemical Society, Faraday Transactions 1: Physical Chemistry in Condensed Phases*, 69:1597–1607, 1973.

J Jin, M G El-Din, and J R Bolton. Assessment of the UV/chlorine process as an advanced oxidation process. *Water Research*, 45(4):1890–1896, 2011.

P D Johnson. Mercury resonance radiation in the high-current, low-pressure discharge. *Journal of the Optical Society of America*, 61(11):1451–1454, 1971.

J Jortner, M Ottolenghi, and G Stein. On the photochemistry of aqueous solutions of chloride, bromide, and iodide ions. *The Journal of Physical Chemistry*, 68(2):247–255, 1964.

R Kitamura, L Pilon, and M Jonasz. Optical constants of silica glass from extreme ultraviolet to far infrared at near room temperature. *Applied optics*, 46(33):8118–8133, 2007.

U K Kläning and T Wolff. Laser flash photolysis of HClO, ClO^-, HBrO, and BrO^- in aqueous solution. Reactions of Cl and Br atoms. *Berichte der Bunsengesellschaft für Physikalische Chemie*, 89(3):243–245, 1985.

N V Klassen, D Marchington, and H C E McGowan. H_2O_2 determination by the I_3^- method and by $KMnO_4$ titration. *Analytical Chemistry*, 66(18): 2921–2925, 1994.

P L Knoppert, G Oskam, and E G H Vreenbenburgh. Overview of European water treatment practice. *Journal - American Water Works Association*, 72(11):592–9, 1980.

L R Koller. *Ultraviolet Radiation*. J. Wiley, 1965.

D G Korich, J R Mead, M S Madore, N A Sinclair, and C R Sterling. Effects of ozone, chlorine dioxide, chlorine, and monochloramine on Cryptosporidium parvum oocyst viability. *Applied and Environmental Microbiology*, 56 (5):1423–8, May 1990.

I Kristiana, J Charrois, and S E Hrudey. Research overview, regulatory history and current worldwide status of DBP regulations and guidelines. In S E Hrudey and J Charrois, editors, *Disinfection By-Products and*

Human Health, chapter 2, pages 11–39. International Water Association, 2012.

L Kröckel and M A Schmidt. Extinction properties of ultrapure water down to deep ultraviolet wavelengths. *Optical Materials Express*, 4(9):1932–1942, 2014.

J C Kruithof, R Van der Leer, and W Hijnen. Practical experiences with UV disinfection in the Netherlands. *Journal of Water Supply: Research and Technology - Aqua*, 41(2):88–94, 1992.

H J Kuhn, S E Braslavsky, and R Schmidt. Chemical Actinometry (IUPAC Technical Report). *Pure and Applied Chemistry*, 76(12):2105–2146, 2004.

W Kühn, H Sontheimer, L Steiglitz, D Maier, and R Kurz. Use of ozone and chlorine in water utilities in the Federal Republic of Germany. *Journal - American Water Works Association*, pages 326–331, 1978.

J L Kurz. Hydration of acetaldehyde. I. Equilibrium thermodynamic parameters. *Journal of the American Chemical Society*, 89(14):3524–3528, 1967.

K J Laidler. *Chemical Kinetics*. Harper & Row, New York, 3rd edition, 1987.

S Lalezary, M Pirbazari, and M J McGuire. Oxidation of five earthy-musty taste and odor compounds. *Journal - American Water Works Association)*, pages 62–69, 1986.

B Langlais, D A Reckhow, and D R Brink. *Ozone in Water Treatment: Application and Engineering*. CRC Press, 1991.

R A Larson and R G Zepp. Reactivity of the carbonate radical with aniline derivatives. *Environmental Toxicology and Chemistry*, 7(4):265–274, 1988.

M W LeChevallier and G Di Giovanni. *Source Water Assessment: Variability of Pathogen Concentrations*. American Water Works Association, 2002.

M W LeChevallier and W D Norton. Giarda and Cryptosporidium in raw and finished water. *Journal-American Water Works Association*, 87(9): 54–68, 1995.

M W LeChevallier, William D Norton, and R G Lee. Occurrence of Giardia and Cryptosporidium spp. in surface water supplies. *Applied and Environmental Microbiology*, 57(9):2610–2616, 1991.

O Legrini, E Oliveros, and A M Braun. Photochemical processes for water treatment. *Chemical Reviews*, 93(2):671–698, 1993.

W L LePage. The anatomy of an ozone plant. *Journal - American Water Works Association*, pages 105–111, 1981.

K G Linden, G Shin, G Faubert, W Cairns, and M D Sobsey. UV disinfection of Giardia lamblia cysts in water. *Environmental Science and Technology*, 36(11):2519–2522, 2002.

R D Lingg, R G Melton, F C Kopfler, W E Coleman, and D E Mitchell. Quantitative analysis of volatile organic compounds by GC-MS. *Journal - American Water Works Association*, pages 605–612, 1977.

W Liu, S A Andrews, J R Bolton, K G Linden, C Sharpless, and M Stefan. Comparison of disinfection byproduct (DBP) formation from different UV technologies at bench scale. *Water Science and Technology: Water Supply*, 2(5-6):515–521, 2002.

D A Livingstone. *Chemical Composition of Rivers and Lakes*. US Government Printing Office, 1963.

G S Logsdon and E C Lippy. The role of filtration in preventing waterborne disease. *Journal-American Water Works Association*, pages 649–655, 1982.

W R MacKenzie, N J Hoxie, M E Proctor, M S Gradus, K A Blair, D E Peterson, J J Kazmierczak, D G Addiss, K R Fox, and J B Rose. A massive outbreak in Milwaukee of Cryptosporidium infection transmitted

through the public water supply. *New England Journal of Medicine*, 331 (3):161–167, 1994.

J P Malley, J P Shaw, and J R Ropp. *Evaluation of By-Products Produced by Treatment of Groundwaters with Ultraviolet Irradiation.* AWWAR, 1996.

P Maruthamuthu and P Neta. Reactions of phosphate radicals with organic compounds. *The Journal of Physical Chemistry*, 81(17):1622–1625, 1977.

W J Masschelein and R G Rice. *Ultraviolet Light in Water and Wastewater Sanitation.* Lewis Publishers, 2002.

R Matta, S Tlili, S Chiron, and S Barbati. Removal of carbamazepine from urban wastewater by sulfate radical oxidation. *Environmental Chemistry Letters*, 9(3):347–353, 2011.

M J McGuire. Off-flavor as the consumer's measure of drinking water safety. *Water Science and Technology*, 31(11):1–8, 1995.

J McMurry. *Organic Chemistry.* Brooks/Cole, 1996.

R Mertens and C von Sonntag. Photolysis (λ= 354 nm) of tetrachloroethene in aqueous solutions. *Journal of Photochemistry and Photobiology A: Chemistry*, 85(1):1–9, 1995.

J P Mieure. A rapid and sensitive method for determining volatile organohalides in water. *Journal - American Water Works Association*, pages 60–62, 1977.

J W Moore and R G Pearson. *Kinetics and Mechanism.* John Wiley and Sons, 3rd edition, 1981.

E Mvula, M N Schuchmann, and C von Sonntag. Reactions of phenol-OH-adduct radicals. Phenoxyl radical formation by water elimination vs. oxidation by dioxygen. *Journal of the Chemical Society, Perkin Transactions 2*, (3):264–268, 2001.

V Nagarajan and R W Fessenden. Flash photolysis of transient radicals. 1. X_2^- with X = Cl, Br, I, and SCN. *The Journal of Physical Chemistry*, 89 (11):2330–2335, 1985.

P Neta and L M Dorfman. Pulse radiolysis studies. XIII. Rate constants for the reaction of hydroxyl radicals with aromatic compounds in aqueous solutions. Technical report, Ohio State University, Columbus, 1968.

P Neta, V Madhavan, H Zemel, and R W Fessenden. Rate constants and mechanism of reaction of sulfate radical anion with aromatic compounds. *Journal of the American Chemical Society*, 99(1):163–164, 1977.

T S Norman, L L Harms, and R W Looyenga. The use of chloramines to prevent trihalomethane formation. *Journal - American Water Works Association*, pages 176–180, 1980.

L H Nowell and J Hoigné. Photolysis of aqueous chlorine at sunlight and ultraviolet wavelengths—II. Hydroxyl radical production. *Water Research*, 26(5):599–605, 1992.

N P Page. *Report on carcinogenesis bioassay of chloroform*. US Dept. of Health, Education, and Welfare, Public Health Service, National Institutes of Health], National Cancer Institute, Division of Cancer Cause and Prevention, Carcinogenesis Program, Carcinogen Bioassay and Program Resources Branch, 1976.

G W Pendygraft, Fred E Schlegel, and Michael J Huston. Organics in drinking water: A health perspective. *Journal - American Water Works Association*, 71(3):118–126, 1979.

P Persson. Sensory properties and analysis of two muddy odour compounds, geosmin and 2-methylisoborneol, in water and fish. *Water Research*, 14 (8):1113–1118, 1980.

A Peter and U Von Gunten. Oxidation kinetics of selected taste and odor compounds during ozonation of drinking water. *Environmental Science and Technology*, 41(2):626–631, 2007.

B Pett, F Smith, D Stendahl, and R Welker. Cryptosporidiosis outbreak from an operations point of view: Kitchener—Waterloo, Ontario, spring 1993. In *Proceedings of the Water Quality Technology Conference 1993, Miami*, 1993.

R Phillips. *Sources and Applications of Ultraviolet Radiation.* Academic Press, 1983.

T I Quickenden and J A Irvin. The ultraviolet absorption spectrum of liquid water. *The Journal of Chemical Physics*, 72(8):4416–4428, 1980.

R O Rahn. Potassium iodide as a chemical actinometer for 254 nm radiation: use of iodate as an electron scavenger. *Photochemistry and Photobiology*, 66(4):450–455, 1997.

R O Rahn, M I Stefan, J R Bolton, E Goren, P Shaw, and K R Lykke. Quantum yield of the iodide - iodate chemical actinometer: dependence on wavelength and concentration. *Photochemistry and Photobiology*, 78 (2):146–152, 2003.

K L Rakness. *Ozone in Drinking Water Treatment: Process design, operation, and optimization.* American Water Works Association, 2011.

M Rapinat. Recent developments in water treatment in France. *Journal - American Water Works Association*, 74(12):610–7, 1982.

D A Reckhow, K G Linden, J Kim, H Shemer, and G Makdissy. Effect of UV treatment on DBP formation. *Journal - American Water Works Association*, 102(6):100, 2010.

R C Rendtorff. The experimental transmission of human intestinal protozoan parasites. II. Giardia lamblia cysts given in capsules. *American Journal of Hygiene*, 59(2):209–20, 1954.

R G Rice and J A Cotruvo. Introductory Comments. In Rip G Rice and Joseph A Cotruvo, editors, *Ozone/Chlorine Dioxide Oxidation Products of Organic Materials. Proceedings of a conference held in Cincinnati, Ohio, November 17-19, 1976.* Ozone Press International, 1978.

R G Rice and C M Robson, editors. *Biological Activated Carbon– Enhanced Aerobic Biological Activity in GAC Systems.* Ann Arbor Science, 1982.

R G Rice, C M Robson, G W Miller, and A G Hill. Uses of ozone in drinking water treatment. *Journal - American Water Works Association*, pages 44–57, 1981.

P A Roefer, J T Monscvitz, and D J Rexing. The Las Vegas cryptosporidiosis outbreak. *Journal - American Water Works Association*, 88(9):95, 1996.

J J Rook. Formation of haloforms during chlorination of natural waters. *Journal of Water Treatment Examination*, 23:234–243, 1974.

A A Rosen. Foundations of organic pollutant analysis. In L H Keith, editor, *Identification and Analysis of Organic Pollutants in Water*, chapter 1. Ann Arbor Science, 1976.

E J Rosenfeldt, K G Linden, S Canonica, and U Von Gunten. Comparison of the efficiency of OH radical formation during ozonation and the advanced oxidation processes O_3/H_2O_2 and UV/H_2O_2. *Water Research*, 40(20): 3695–3704, 2006.

A B Ross and P Neta. *Rate Constants for Reactions of Inorganic Radicals in Aqueous Solution.* US Department of Commerce, National Bureau of Standards Washington D. C, 1979.

I M Sayre. International standards for drinking water. *Journal-American Water Works Association*, 80(1):53–60, 1988.

M Schalekamp. The use of GAC filtration to ensure quality in drinking water from surface sources. *Journal-American Water Works Association*, 71(11):638–647, 1979.

M N Schuchmann and C Von Sonntag. Hydroxyl radical-induced oxidation of 2-methyl-2-propanol in oxygenated aqueous solution. a product and pulse radiolysis study. *Journal of Physical Chemistry*, 83(7):780–784, 1979.

P Schulhof. An evolutionary approach to activated carbon treatment. *Journal-American Water Works Association*, 71(11):648–659, 1979.

S M Serkiz and E M Perdue. Isolation of dissolved organic matter from the Suwannee River using reverse osmosis. *Water Research*, 24(7):911–916, 1990.

L Sommer. *Analytical Absorption Spectrophotometry in the Visible and Ultraviolet: The Principles*, volume 8. Elsevier, 1989.

H Sontheimer, E Heilker, M R Jekel, H Nolte, and F H Vollmer. The Mülheim process. *Journal - American Water Works Association*, pages 393–396, 1978.

J Staehelin and J Hoigné. Decomposition of ozone in water: Rate of initiation by hydroxide ions and hydrogen peroxide. *Environmental Science and Technology*, 16(10):676–681, 1982.

M I Stefan and J R Bolton. Reinvestigation of the acetone degradation mechanism in dilute aqueous solution by the UV/H_2O_2 process. *Environmental Science and Technology*, 33(6):870–873, 1999.

M I Stefan, A R Hoy, and J R Bolton. Kinetics and mechanism of the degradation and mineralization of acetone in dilute aqueous solution sensitized by the UV photolysis of hydrogen peroxide. *Environmental Science & Technology*, 30(7):2382–2390, 1996.

D P Stevenson. On the monomer concentration in liquid water. *The Journal of Physical Chemistry*, 69(7):2145–2152, 1965.

W Stumm and J Morgan. *Aquatic Chemistry: Chemical Equilibria and Rates in Natural Waters*. Wiley-Interscience, 3rd edition, 1996.

W Stumm, R Schwarzenbach, and L Sigg. From environmental analytical chemistry to ecotoxicology—a plea for more concepts and less monitoring and testing. *Angewandte Chemie International Edition in English*, 22(5): 380–389, 1983.

I H Suffet. An evaluation of activated carbon for drinking water treatment: a national academy of science report. *Journal - American Water Works Association*, pages 41–50, 1980.

I H Suffet, editor. *Advances in Taste-and-Odor Treatment and Control*. American Water Works Association, 1995.

L Sun, E M Perdue, and J F McCarthy. Using reverse osmosis to obtain organic matter from surface and ground waters. *Water Research*, 29(6): 1471–1477, 1995.

J M Symons. A history of the attempted federal regulation requiring GAC adsorption for water treatment. *Journal - American Water Works Association*, pages 34–43, 1984.

J M Symons, T A Bellar, J K Carswell, J DeMarco, K L Kropp, G G Robeck, D R Seeger, C J Slocum, B L Smith, and A A Stevens. National organics reconnaissance survey for halogenated organics. *Journal-American Water Works Association*, pages 634–647, 1975.

G Tchobanoglous, J Cotruvo, J Crook, E McDonald, A Olivieri, A Salveson, S Trussell, J Mattingly, J Mosher, and G Vartanian. Development of Framework for Direct Potable Reuse Guidelines, Results of the NWRI/WateReuse Association Expert Panel. In *Proceedings of the Water Environment Federation*, number 5, pages 4943–4946. Water Environment Federation, 2015.

E M Thurman. *Organic Geochemistry of Natural Waters*. Martinus Nijhoff/Dr W. Junk Publishers, 1985.

C Tixier, H P Singer, S Oellers, and S R Müller. Occurrence and fate of carbamazepine, clofibric acid, diclofenac, ibuprofen, ketoprofen, and naproxen in surface waters. *Environmental Science and Technology*, 37 (6):1061–1068, 2003.

A Treinin and E Hayon. Charge transfer spectra of halogen atoms in water - Correlation of the electronic transition energies of iodine, bromine,

chlorine, hydroxyl, and hydrogen radicals with their electron affinities. *Journal of the American Chemical Society*, 97(7):1716–1721, 1975.

USEPA. Industrial Pollution of the Lower Mississippi River in Louisiana. (as cited by Symons 1984), 1972.

USEPA. National Organics Monitoring Survey (NOMS). Technical report, Technical Support Division, Office of Drinking Water, 1978.

D H Volman and J C Chen. The photochemical decomposition of hydrogen peroxide in aqueous solutions of allyl alcohol at 2537 å. 1. *Journal of the American Chemical Society*, 81(16):4141–4144, 1959.

U Von Gunten. Ozonation of drinking water: Part I. Oxidation kinetics and product formation. *Water Research*, 37(7):1443–1467, 2003.

D Wang, J R Bolton, and R Hofmann. Medium pressure UV combined with chlorine advanced oxidation for trichloroethylene destruction in a model water. *Water Research*, 46(15):4677–4686, 2012.

P Wardman. Reduction potentials of one-electron couples involving free radicals in aqueous solution. *Journal of Physical and Chemical Reference Data*, 18(4):1637–1755, 1989.

K Watanabe and M Zelikoff. Absorption coefficients of water vapor in the vacuum ultraviolet. *Journal of the Optical Society of America*, 43(9): 753–754, 1953.

M J Watts and K G Linden. Chlorine photolysis and subsequent OH radical production during UV treatment of chlorinated water. *Water Research*, 41(13):2871–2878, 2007.

M J Watts, E J Rosenfeldt, and K G Linden. Comparative OH radical oxidation using UV-Cl_2 and UV-H_2O_2 processes. *Journal of Water Supply: Research and Technology-AQUA*, 56(8):469–477, 2007.

R P Wayne. *Principles and Applications of Photochemistry*. Oxford University Press, 1988.

J L Weeks, G Meaburn, and S Gordon. Absorption coefficients of liquid water and aqueous solutions in the far ultraviolet. *Radiation Research*, 19 (3):559–567, 1963.

P Westerhoff, G Aiken, G Amy, and J Debroux. Relationships between the structure of natural organic matter and its reactivity towards molecular ozone and hydroxyl radicals. *Water Research*, 33(10):2265–2276, 1999.

P Westerhoff, S P Mezyk, W J Cooper, and D Minakata. Electron pulse radiolysis determination of hydroxyl radical rate constants with Suwannee River fulvic acid and other dissolved organic matter isolates. *Environmental Science and Technology*, 41(13):4640–4646, 2007.

R G Wetzel. *Limnology: Lake and River Ecosystems*. Academic Press, 3rd edition, 2001.

WHO. *Guidelines for Drinking Water Quality: Recommendations*. World Health Organization, 2004.

A Wolman. 200 years of water service. *Journal-American Water Works Association*, 68(8):A13–A18, 1976.

A Wolman and A E Gorman. The significance of waterborne typhoid fever outbreaks, 1920-1930. *Journal-American Water Works Association*, 23 (2):160–201, 1931.

H Wright, D Gaithuma, M Heath, C Schulz, T Bogan, A Cabaj, M Schmalweiser, Aand Schmelzer, and J Finegan-Kelly. UV Disinfection Knowledge Base. Technical report, Water Research Foundation, 2012.

W F Young, H Horth, R Crane, T Ogden, and M Arnott. Taste and odour threshold concentrations of potential potable water contaminants. *Water Research*, 30(2):331–340, 1996.

J Zorbist and W Stumm. Chemical dynamics of the Rhine catchment area in Switzerland - Extrapolation to the "pristine" Rhine River input to the ocean. In *Proceedings of Review and Workshop on River Inputs to Ocean Systems, Food and Agricultural Organization, Rome.*, 1981.

K Zoschke, H Börnick, and E Worch. Vacuum-uv radiation at 185 nm in water treatment - A review. *Water research*, 52:131–145, 2014.

Appendix A

Experimental Data and Calculations

Table A.1: Raw data and calculations for linearity and precision of Carbamazepine quantification by HPLC.

Standard	Peak Area - A					
(μM)	Injection 1	Injection 2	Injection 3	Avg	σ	%RSD
0.01	0.0653	0.0684	0.0677	0.0671	0.0016	2.4
0.02	0.1215	0.1238	0.1237	0.1230	0.0013	1.1
0.05	0.3113	0.3276	0.3225	0.3205	0.0083	2.6
0.10	0.6171	0.6171	0.6138	0.6160	0.0019	0.3
0.15	0.9172	0.9312	0.9239	0.9241	0.0070	0.8
0.20	1.2344	1.2354	1.2291	1.2330	0.0034	0.3
0.40	2.4675	2.4721	2.4677	2.4691	0.0026	0.1
0.60	3.7176	3.6885	3.6919	3.6993	0.0159	0.4
0.80	4.8992	4.9044	4.9001	4.9012	0.0028	0.1
1.00	6.0803	6.0930	6.0672	6.0802	0.0129	0.2

Table A.2: The concentration dependent absorbance of three compounds at 254 nm in 1.00 cm cell.

$[pCBA]$	A_{254}			$[CBZ]$	A_{254}			$[NB]$	A_{254}		
$(\times 10^{-4}M)$	Run 1	Run 2	Run 3	$(\times 10^{-4}M)$	Run 1	Run 2	Run 3	$(\times 10^{-4}M)$	Run 1	Run 2	Run 3
0.60	0.238	0.247	0.249	0.378	0.248	0.244	0.250	0.465	0.258	0.258	0.257
0.90	0.347	0.339	0.356	0.756	0.487	0.490	0.505	0.698	0.434	0.434	0.434
1.20	0.452	0.462	0.448	1.130	0.724	0.729	0.739	0.931	0.567	0.565	0.565
1.50	0.555	0.571	0.575	1.510	0.995	0.994	0.977	1.160	0.713	0.714	0.712
1.80	0.664	0.649	0.666	1.890	1.257	1.301	1.269	1.400	0.865	0.871	0.868
								1.860	1.134	1.134	1.133

Table A.3: Raw data for direct photolysis of para-chlorobenzoic acid at 254 nm.

Time	Peak Area A_t					
	Run 1		Run 2		Run 3	
(min)	Light	Dark	Light	Dark	Light	Dark
0	1.6215	1.5844	1.6416	1.6554	1.7010	1.7181
10	1.5762		1.5865	1.6542	1.6316	1.7040
20	1.5455	1.6084	1.5466	1.6528	1.5925	1.7090
30	1.4900	1.5055	1.5057	1.6626	1.5433	1.7173
40	1.4459	1.6225	1.4627	1.6597	1.5045	1.7215
50	1.4078	1.6074	1.4170	1.6752	1.4563	1.7174
60	1.3704	1.6239			1.4285	1.7246

These are some notes for this part about direct photolysis of para-chlorobenzoic acid. The fluence rate for this data is 0.0493 plus or minus 0.0006 mW per cm2.

Table A.4: Calculated data for direct photolysis of para-chlorobenzoic acid at 254 nm.

Time	$\ln(A_t/A_o)$					
	Run 1		Run 2		Run 3	
(min)	Light	Dark	Light	Dark	Light	Dark
0	0.0000	0.0000	0.0000	0.0000	0.0000	0.0000
10	-0.0283		-0.0341	-0.0007	-0.0417	-0.0082
20	-0.0480	0.0150	-0.0596	-0.0016	-0.0659	-0.0053
30	-0.0846	-0.0511	-0.0864	0.0043	-0.0973	-0.0005
40	-0.1146	0.0238	-0.1154	0.0026	-0.1228	0.0020
50	-0.1413	0.0144	-0.1471	0.0119	-0.1553	-0.0004
60	-0.1682	0.0246			-0.1746	0.0038

These are some notes for this part about direct photolysis of para-chlorobenzoic acid.

Table A.5: Raw data for direct photolysis of nitrobenzene at 254 nm.

Time	Peak Area A_t Run 1		Run 2		Run 3	
(min)	Light	Dark	Light	Dark	Light	Dark
0	0.6492	0.6492	0.6469	0.6469	0.6567	0.6567
10	0.5889	0.6114	0.5918	0.6333	0.5883	0.6285
20	0.5396	0.5969	0.5342	0.6040	0.5258	0.5279
30	0.4917	0.5765	0.4868	0.5968	0.4791	0.5820
40	0.4656	0.5602	0.4423	0.5773	0.4341	0.5634
50	0.4236	0.5410	0.4112	0.5555	0.3863	0.5467

Note that nitrobenzene dark reaction is significant due to volatilization from open dish during the course of the irradiations.

Table A.6: Calculations for direct photolysis of nitrobenzene at 254 nm.

Time	$\ln(A_t/A_o)$ Run 1		Run 2		Run 3	
(min)	Light	Dark	Light	Dark	Light	Dark
0	0.0000	0.0000	0.0000	0.0000	0.0000	0.0000
10	-0.0975	-0.0600	-0.0890	-0.0212	-0.1100	-0.0439
20	-0.1849	-0.0840	-0.1914	-0.0686	-0.2223	
30	-0.2779	-0.1188	-0.2843	-0.0806	-0.3153	-0.1208
40	-0.3324	-0.1474	-0.3802	-0.1138	-0.4140	-0.1532
50	-0.4270	-0.1823	-0.4531	-0.1523	-0.5306	-0.1833

A correction for the rate of volatilization is obtained from the dark reaction and applied to light reaction for determination of the photolysis rate constant.

Table A.7: Raw and calculated data for direct photolysis of carbamazepine acid at 254 nm.

Time (min)	Fluence ($mJ\,cm^{-2}$)	A_t	$\ln(A_t/A_o)$
0	0	5.700	0.0000
60	1031	5.534	-0.0296
60	1031	5.537	-0.0290
120	2062	5.281	-0.0763
120	2062	5.453	-0.0443
180	3094	5.303	-0.0721
180	3094	5.345	-0.0642
240	4125	5.197	-0.0923
300	5156	4.809	-0.1699
420	7218	4.650	-0.2037
480	8249	4.848	-0.1618
540	9281	4.470	-0.2431
600	10312	4.649	-0.2038

These are some notes for this part about carbamazepine photolysis quantum yield at 254 nm if needed. For example the fluence rate was 0.286 +/- 0.001 mW/cm2.

Table A.8: Raw data for indirect photolysis of para-chlorobenzoic acid at 254 nm with H_2O_2.

Time	Peak Area A_t Run 1		Run 2		Run 3	
(min)	Light	Dark	Light	Dark	Light	Dark
0	1.6059	1.6097	1.6496	1.6476	1.6326	1.6283
10	1.2699	1.6162	1.3245	1.6414	1.2931	1.6349
20	1.0764	1.6113	1.0726	1.6500	1.0396	1.6280
30	0.8992	1.6156	0.8729	1.6631	0.8214	1.6434
40	0.7593	1.6261	0.7134	1.6585	0.6627	1.6333
50	0.6539	1.6215	0.5788	1.6648	0.5313	1.6516
60	0.5579	1.6266	0.4685	1.6632		1.6464

Table A.9: Calculations for indirect photolysis of para-chlorobenzoic acid at 254 nm with H_2O_2.

Time	$\ln(A_t/A_o)$ Run 1		Run 2		Run 3	
(min)	Light	Dark	Light	Dark	Light	Dark
0	0.0000	0.0000	0.0000	0.0000	0.0000	0.0000
10	-0.2347	0.0040	-0.2195	-0.0038	-0.2331	0.0040
20	-0.4001	0.0010	-0.4304	0.0015	-0.4513	-0.0002
30	-0.5799	0.0037	-0.6365	0.0094	-0.6869	0.0092
40	-0.7490	0.0101	-0.8382	0.0066	-0.9016	0.0031
50	-0.8985	0.0073	-1.0473	0.0104	-1.1226	0.0142
60	-1.0573	0.0104	-1.2588	0.0094		0.0111

Table A.10: Raw data for indirect photolysis of carbamazepine at 254 nm with H_2O_2.

Time	Peak Area A_t					
	Run 1		Run 2		Run 3	
(min)	Light	Dark	Light	Dark	Light	Dark
0	1.6411	1.6496	1.6737	1.6754	1.6461	1.6426
10	1.2421	1.6419	1.2994	1.6732	1.2646	1.6583
20	1.0319	1.6622	1.0211	1.6734	0.9876	1.6591
30	0.8421	1.6665	0.8009	1.6798	0.7608	1.6636
40	0.6928	1.6663	0.6294	1.6826	0.5825	1.6536
50	0.5774	1.6557	0.4895	1.6853	0.4423	1.6655
60	0.4895	1.6719	0.3906	1.6904		1.6710

Table A.11: Calculations for indirect photolysis of carbamazepine at 254 nm with H_2O_2.

Time	$\ln(A_t/A_o)$					
	Run 1		Run 2		Run 3	
(min)	Light	Dark	Light	Dark	Light	Dark
0	0.0000	0.0000	0.0000	0.0000	0.0000	0.0000
10	-0.2786	-0.0047	-0.2531	-0.0013	-0.2637	0.0095
20	-0.4640	0.0076	-0.4942	-0.0012	-0.5109	0.0100
30	-0.6672	0.0102	-0.7371	0.0026	-0.7718	0.0127
40	-0.8624	0.0101	-0.9780	0.0043	-1.0388	0.0067
50	-1.0446	0.0037	-1.2294	0.0059	-1.3142	0.0138
60	-1.2097	0.0134	-1.4551	0.0089		0.0171

Table A.12: Raw data and calculations for phosphate buffer (10 mM) at 185 nm using Carbamazepine.

Time	Phosphate Buffer (10 mM)					
	pH 6.0		pH 7.0		pH 8.0	
(min)	A_t	$\ln(A_t/A_o)$	A_t	$\ln(A_t/A_o)$	A_t	$\ln(A_t/A_o)$
0	1.8221	0.0000	1.8263	0.0000	1.8697	0.0000
2	0.8871	-0.7198	0.8159	-0.7855	0.6999	-0.9826
4	0.4933	-1.3066	0.4219	-1.5033	0.3161	-1.7775
6	0.2759	-1.8877	0.2292	-2.1642	0.1650	-2.4276

These are some notes for this part.

Table A.13: Influence of phosphate buffer strength at pH 7 at 185 nm using carbamazepine as probe.

Time	pH 7.0							
	0 mM*		1 mM		10 mM		100 mM	
(min)	A_t	$\ln(A_t/A_o)$	A_t	$\ln(A_t/A_o)$	A_t	$\ln(A_t/A_o)$	A_t	$\ln(A_t/A_o)$
0	1.9324	0.0000	1.8504	0.0000	1.8263	0.0000	1.8426	0.0000
2	1.3569	-0.3536	1.2211	-0.4156	0.8159	-0.8058	0.8400	-0.7855
4	0.9282	-0.7333	0.8140	-0.8212	0.4219	-1.4653	0.4098	-1.5033
6	0.6764	-1.0497	0.5353	-1.2403	0.2292	-2.0755	0.2116	-2.1642

* Ultrapure water pH 5.4.

Table A.14: Influence of fluoride in 185 nm regime

$[F^-]$	Time	A_t			$ln(A_t/A_o)$		
(mg/L)	(min)	Run 1	Run 2	Run 3	Run 1	Run 2	Run 3
1	0	2.8736	2.8631	2.8933	0.000	0.000	0.000
	2	1.3600	1.3221	1.3349	-0.748	-0.773	-0.774
	4	0.6643	0.5743	0.6079	-1.465	-1.607	-1.560
	6	0.3207	0.2788	0.2580	-2.193	-2.329	-2.417
	8	0.1392	0.1125	0.1179	-3.027	-3.237	-3.200
	10	0.1038	0.0573	0.0553	-3.321	-3.911	-3.957
10	0	2.9734	2.9612	2.9923	0.000	0.000	0.000
	2	1.5725	1.3576	1.3556	-0.637	-0.780	-0.792
	4	0.6700	0.5779	0.5935	-1.490	-1.634	-1.618
	6	0.3383	0.2842	0.2749	-2.174	-2.344	-2.387
	8	0.1395	0.1193	0.1330	-3.059	-3.212	-3.113
	10	0.0811	0.0567	0.0567	-3.602	-3.956	-3.966
100	0	2.5477	2.5391	2.5281	0.000	0.000	0.000
	2	1.2020	1.1278	1.1811	-0.751	-0.812	-0.761
	4	0.5639	0.5299	0.5261	-1.508	-1.567	-1.570
	6	0.2640	0.2257	0.2268	-2.267	-2.420	-2.411
	8	0.1094	0.1027	0.1049	-3.148	-3.208	-3.182
	10	0.0592	0.0508	0.0450	-3.762	-3.912	-4.029

NaF used as source of F^-. Tert-Butanol used as a radical scavenger ($7.0\,mg\,L^{-1}$ as C) and carbamazepine as probe compound ($[CBZ]_i = 0.5\,\mu M$).

Table A.15: Demonstration of high absorbance of water at 185 nm.

	1.00 cm cell (Volume = 3.097 mL)			2.00 cm cell (Volume = 5.617 mL)		
Time (min)	Time/Volume (min/mL)	A_t	$\ln(A_t/A_o)$	Time/Volume (min/mL)	A_t	$\ln(A_t/A_o)$
0	0.00	6.0856	0.000	0.00	6.0856	0.000
2	0.65	2.0962	-1.066	0.36	4.8199	-0.233
4	1.29	0.8695	-1.946	0.71	2.0839	-1.072
6	1.94	0.5578	-2.390	1.07	1.2716	-1.566
8	2.58	0.1663	-3.600	1.42	0.8126	-2.013
10	3.23	0.1023	-4.086	1.78	0.5520	-2.400

This demonstrations involves the assumption that the number of photons absorbed by the sample is proportional to the exposure time and that both the 1 and 2 cm cells are sufficiently mixed. Thus the quantity Time/Volume is proportional to the fluence. Plotting using the Time/Volume not Time as the abscissa will thus show agreement between both the 1 and 2 cm cells.

Table A.16: Raw data and calculations of I^-- $IO_3{}^-$ actinometry study applied to 254 nm.

Run	A_{352} (cm^{-1})	I_o ($mW\,cm^{-2}$)	A_{352} (cm^{-1})	I_t ($mW\,cm^{-2}$)
1	0.888	0.518	0.821	0.478
2	0.854	0.498	0.844	0.492
3	0.879	0.512	0.854	0.498
4	0.873	0.509	0.853	0.497
5	0.890	0.519	0.818	0.476
6	0.830	0.483	0.826	0.481
7	0.854	0.498	0.836	0.487
8	0.865	0.504	0.828	0.482
9	0.836	0.487	0.824	0.480
10	0.831	0.484	0.832	0.485

Table A.17: Raw data and calculations of I^-- $IO_3{}^-$ actinometry applied to 185 and 254 nm.

Run	A_{352} (cm^{-1})	I_o ($mW\,cm^{-2}$)	A_{352} (cm^{-1})	I_t ($mW\,cm^{-2}$)
1	0.856	0.907	0.819	0.8672
2	0.831	0.880	0.775	0.8199
3	0.808	0.855	0.794	0.8403
4	0.827	0.876	0.795	0.8414
5	0.793	0.839	0.793	0.8392

Table A.18: Influence of temperature in 254 nm - H_2O_2 regime

T	Time	A_t			$ln(A_t/A_o)$		
(°C)	(min)	Run 1	Run 2	Run 3	Run 1	Run 2	Run 3
5	0	0.9022	0.9041	0.8973	0.000	0.000	0.000
	10	0.8597	0.8760	0.8452	-0.048	-0.032	-0.060
	20	0.7937	0.8087	0.8147	-0.128	-0.112	-0.097
	30	0.7667	0.7340	0.7318	-0.163	-0.208	-0.204
	40	0.7021	0.6999	0.6687	-0.251	-0.256	-0.294
	50	0.6537	0.6466	0.6030	-0.322	-0.335	-0.397
	60	0.5858	0.6076	0.5699	-0.432	-0.397	-0.454
20	0	0.9259	0.9124	0.9109	0.000	0.000	0.000
	10	0.8369	0.8130	0.8341	-0.101	-0.115	-0.088
	20	0.7636	0.7281	0.7244	-0.193	-0.226	-0.229
	30	0.6517	0.6603	0.6453	-0.351	-0.323	-0.345
	40	0.5868	0.5824	0.5616	-0.456	-0.449	-0.484
	50	0.5392	0.5324	0.5132	-0.541	-0.539	-0.574
	60	0.4705	0.4562	0.4621	-0.677	-0.693	-0.679
35	0	0.9208	0.9238	0.9229	0.000	0.000	0.000
	10	0.7915	0.8014	0.8414	-0.151	-0.142	-0.092
	20	0.6914	0.7021	0.7142	-0.287	-0.274	-0.256
	30	0.5999	0.5900	0.6480	-0.428	-0.448	-0.354
	40	0.5072	0.4870	0.5377	-0.596	-0.640	-0.540
	50	0.4259	0.3966	0.4420	-0.771	-0.846	-0.736
	60	0.3552	0.3383	0.3710	-0.953	-1.005	-0.911

Notes regarding temperature study at 254 nm. Tert-Butanol used as a radical scavenger ($7.0\,mg\,L^{-1}$ as C) and carbamazepine as probe compound ($[CBZ]_i = 0.5\,\mu M$) with detection at 267 nm.

Table A.19: Influence of temperature in 185 nm regime

T	Time	A_t			$ln(A_t/A_o)$		
(°C)	(min)	Run 1	Run 2	Run 3	Run 1	Run 2	Run 3
5	0	0.9385	0.9515	0.9397	0.000	0.000	0.000
	2	0.5680	0.5578	0.5619	-0.502	-0.534	-0.514
	4	0.3478	0.3669	0.3483	-0.993	-0.953	-0.992
	6	0.2057	0.2251	0.2121	-1.518	-1.441	-1.489
	8	0.1254	0.1266	0.1335	-2.013	-2.017	-1.951
	10	0.0817	0.0752	0.0816	-2.441	-2.538	-2.444
20	0	0.9415	0.9334	0.9272	0.000	0.000	0.000
	2	0.5149	0.4749	0.5043	-0.604	-0.676	-0.609
	4	0.3007	0.2901	0.2754	-1.141	-1.169	-1.214
	6	0.1479	0.1492	0.1698	-1.851	-1.834	-1.698
	8	0.0745	0.0760	0.0837	-2.537	-2.508	-2.405
	10			0.0452			-3.021
35	0	0.9602	0.9109	0.9364	0.000	0.000	0.000
	2	0.4755	0.4611	0.4818	-0.703	-0.681	-0.665
	4	0.2472	0.2194	0.2433	-1.357	-1.424	-1.348
	6	0.1163	0.1019	0.1224	-2.111	-2.190	-2.035
	8	0.0585	0.0603	0.0547	-2.798	-2.715	-2.840
	10		0.0238	0.0124		-3.645	-4.324

Notes regarding temperature study. Tert-Butanol used as a radical scavenger ($7.0\,\mathrm{mg\,L^{-1}}$ as C) and carbamazepine as probe compound ($[CBZ]_i = 0.5\,\mu\mathrm{M}$) and detection at 267 nm.

Table A.20: Influence of Suwannee River NOM in 185 nm regime

$[DOC]$	Time	A_t			$ln(A_t/A_o)$		
(mg L^{-1} as C)	(min)	Run 1	Run 2	Run 3	Run 1	Run 2	Run 3
3.0	0	3.0227	3.0488	3.0278	0.000	0.000	0.000
	1	1.4541	1.4178	1.4747	-0.732	-0.766	-0.719
	2	0.7175	0.6777	0.6741	-1.438	-1.504	-1.502
	3	0.2676	0.3012	0.3204	-2.424	-2.315	-2.246
	4	0.1173	0.1154	0.1235	-3.249	-3.274	-3.199
	5	0.0863	0.0401	0.0507	-3.556	-4.331	-4.090
5.0	0	1.4844	1.4936	1.4783	0.000	0.000	0.000
	1	0.8926	0.8895	0.8893	-0.509	-0.518	-0.508
	2	0.5184	0.5168	0.5139	-1.052	-1.061	-1.057
	3	0.2914	0.3157	0.2985	-1.628	-1.554	-1.600
	4	0.1626	0.1793	0.1695	-2.211	-2.120	-2.166
	5	0.0978	0.0863	0.0992	-2.720	-2.851	-2.702
7.5	0	1.4602	1.4846	1.4520	0.000	0.000	0.000
	1	1.0553	1.0607	1.0361	-0.325	-0.336	-0.337
	2	0.7594	0.7394	0.7425	-0.654	-0.697	-0.671
	3	0.4935	0.5143	0.5272	-1.085	-1.060	-1.013
	4	0.3687	0.3589	0.3522	-1.376	-1.420	-1.416
	5	0.2528	0.2607	0.2426	-1.754	-1.740	-1.789
10.0	0	1.4541	1.4646	1.4499	0.000	0.000	0.000
	1	1.1266	1.1762	1.1590	-0.255	-0.219	-0.224
	2	0.8972	0.9049	0.9009	-0.483	-0.482	-0.476
	3	0.6940	0.6994	0.6964	-0.740	-0.739	-0.733
	4	0.5599	0.5442	0.5491	-0.954	-0.990	-0.971
	5	0.4448	0.4175	0.3994	-1.185	-1.255	-1.289

Carbamazepine as probe compound ($[CBZ]_o \simeq 0.5\,\mu M$) with detection at 211 nm. Solutions irradiated at pH 7.0.

Table A.21: Influence of Nordic NOM in 185 nm regime

$[DOC]$	Time	A_t			$ln(A_t/A_o)$		
(mg L^{-1} as C)	(min)	Run 1	Run 2	Run 3	Run 1	Run 2	Run 3
1.8	0	2.9128	2.8966	2.9313	0.000	0.000	0.000
	1	1.1507	1.1362	1.0993	-0.929	-0.936	-0.981
	2	0.3306	0.3467	0.3768	-2.176	-2.123	-2.051
2.7	0	2.8865	2.8914	2.8838	0.000	0.000	0.000
	1	1.3443	1.3751	1.4256	-0.764	-0.743	-0.705
	2	0.6755	0.6676	0.6973	-1.452	-1.466	-1.420
	3	0.2937	0.2620	0.2953	-2.285	-2.401	-2.279
	4	0.0921	0.1308	0.1198	-3.445	-3.096	-3.181
5.2	0	2.9134	2.8901	2.8930	0.000	0.000	0.000
	1	1.9718	1.9752	1.9533	-0.390	-0.381	-0.393
	2	1.3019	1.3528	1.3326	-0.805	-0.759	-0.775
	3	0.8936	0.8839	0.8489	-1.182	-1.185	-1.226
	4	0.5786	0.5262	0.5534	-1.616	-1.703	-1.654
	5	0.4180	0.3561	0.3573	-1.942	-2.094	-2.091
9.8	0	2.8935	2.8968	2.8878	0.000	0.000	0.000
	1	2.3711	2.3838	2.3705	-0.199	-0.195	-0.197
	2	1.9334	1.9556	1.9425	-0.403	-0.393	-0.397
	3	1.5938	1.5683	1.5770	-0.596	-0.614	-0.605
	4	1.3123	1.3016	1.3085	-0.791	-0.800	-0.792
	5	1.0559	1.0663	1.0377	-1.008	-0.999	-1.023

Carbamazepine as probe compound ($[CBZ]_o \simeq 0.5\,\mu M$) with detection at 211 nm. Solutions irradiated at pH 7.0.

Table A.22: Influence of tert-butanol in 185 nm regime

$[(CH_3)_3COH]$	Time	A_t			$ln(A_t/A_o)$		
(mg L^{-1} as C)	(min)	Run 1	Run 2	Run 3	Run 1	Run 2	Run 3
5	0	2.9737	2.9641	2.9671	0.000	0.000	0.000
	2	1.1674	1.1704	1.2115	-0.935	-0.929	-0.896
	4	0.4522	0.4366	0.4593	-1.883	-1.915	-1.866
	6	0.1691	0.1768	0.1877	-2.867	-2.819	-2.760
	8		0.0621			-3.866	
10	0	2.9135	2.9171	2.8943	0.000	0.000	0.000
	2	1.7099	1.7079	1.7197	-0.533	-0.535	-0.521
	4	1.0165	0.9984	1.0223	-1.053	-1.072	-1.041
	6	0.5927	0.6228	0.6059	-1.592	-1.544	-1.564
	8	0.3463	0.3484	0.3443	-2.130	-2.125	-2.129
	10	0.2007	0.2095	0.1816	-2.675	-2.634	-2.769
15	0	2.9266	2.9187	2.9355	0.000	0.000	0.000
	2	2.0576	1.9928	2.0291	-0.352	-0.382	-0.369
	4	1.4345	1.4447	1.4563	-0.713	-0.703	-0.701
	6	0.9931	1.0220	1.0054	-1.081	-1.049	-1.071
	8	0.6780	0.7022	0.6933	-1.462	-1.425	-1.443
	10	0.4702	0.4997	0.4690	-1.828	-1.765	-1.834
20	0	2.9182	2.9332	2.9485	0.000	0.000	0.000
	2	2.212	2.2059	2.2089	-0.277	-0.285	-0.289
	4	1.6493	1.6881	1.7212	-0.571	-0.552	-0.538
	6	1.2439	1.3	1.2902	-0.853	-0.814	-0.826
	8	0.9564	0.9898	0.976	-1.116	-1.086	-1.106
	10	0.7237	0.7366	0.7449	-1.394	-1.382	-1.376
25	0	2.8522	2.8601	2.8757	0.000	0.000	0.000
	2	2.2437	2.2532	2.2763	-0.240	-0.239	-0.234
	4	1.8091	1.7793	1.7675	-0.455	-0.475	-0.487
	6	1.4376	1.3782	1.3926	-0.685	-0.730	-0.725
	8	1.1257	1.1002	1.0885	-0.930	-0.955	-0.971
	10	0.8590	0.8523	0.8812	-1.200	-1.211	-1.183

Carbamazepine as probe compound ($[CBZ]_o \simeq 0.5\,\mu M$) with detection at 211 nm.

Table A.23: Influence of methanol in 185 nm regime

$[CH_3OH]$	Time	A_t			$ln(A_t/A_o)$		
(mg L^{-1} as C)	(min)	Run 1	Run 2	Run 3	Run 1	Run 2	Run 3
1.0	0	1.9369	1.9463	1.9471	0.000	0.000	0.000
	2	1.0033	1.0301	0.9827	-0.658	-0.636	-0.684
	4	0.4701	0.4902	0.4947	-1.416	-1.379	-1.370
	6	0.2145	0.2297	0.2274	-2.201	-2.137	-2.147
	8			0.1191			-2.794
2.0	0	1.9274	1.9095	1.9278	0.000	0.000	0.000
	2	1.2889	1.3061	1.2967	-0.402	-0.380	-0.397
	4	0.8866	0.8736	0.8339	-0.777	-0.782	-0.838
	6	0.5538	0.5925	0.5821	-1.247	-1.170	-1.197
	8	0.392	0.3933	0.3618	-1.593	-1.580	-1.673
	10	0.2591	0.2502	0.2649	-2.007	-2.032	-1.985
3.0	0	1.9346	1.9250	1.9408	0.000	0.000	0.000
	2	1.4608	1.4466	1.4550	-0.281	-0.286	-0.288
	4	1.1076	1.0918	1.1130	-0.558	-0.567	-0.556
	6	0.8130	0.8310	0.8273	-0.867	-0.840	-0.853
	8	0.6295	0.5661	0.5965	-1.123	-1.224	-1.180
	10	0.4560	0.4713	0.4429	-1.445	-1.407	-1.478
4.0	0	1.9229	1.9063	1.9086	0.000	0.000	0.000
	2	1.5254	1.5283	1.5098	-0.232	-0.221	-0.234
	4	1.2212	1.2028	1.1973	-0.454	-0.461	-0.466
	6	0.9683	0.9537	0.9517	-0.686	-0.693	-0.696
	8	0.7546	0.7415	0.7679	-0.935	-0.944	-0.910
	10	0.6043	0.6001	0.6010	-1.158	-1.156	-1.156
5.0	0	1.9223	1.9189	1.9170	0.000	0.000	0.000
	2	1.5704	1.5890	1.6170	-0.202	-0.189	-0.170
	4	1.3257	1.3336	1.3030	-0.372	-0.364	-0.386
	6	1.0965	1.0871	1.1035	-0.561	-0.568	-0.552
	8	0.9189	0.9167	0.9311	-0.738	-0.739	-0.722
	10	0.7528	0.7529	0.7480	-0.937	-0.936	-0.941

Carbamazepine as probe compound ($[CBZ]_o \simeq 0.3\,\mu M$) with detection at 211 nm.

Table A.24: Influence of acetone in 185 nm regime

$[(CH_3)_2CO]$	Time	A_t			$ln(A_t/A_o)$		
(mg L^{-1} as C)	(min)	Run 1	Run 2	Run 3	Run 1	Run 2	Run 3
60	0.0	1.5395	1.5135	1.4911	0.000	0.000	0.000
	0.5	0.9816	0.9826	0.9594	-0.450	-0.432	-0.441
	1.0	0.6849	0.6570	0.6329	-0.810	-0.834	-0.857
	1.5	0.4315	0.4342	0.4239	-1.272	-1.249	-1.258
	2.0	0.2886	0.2881	0.2706	-1.674	-1.659	-1.707
	2.5	0.1793	0.2061	0.2413	-2.150	-1.994	-1.821
	3.0	0.1148	0.1247	0.1341	-2.596	-2.496	-2.409
125	0.0	1.4909	1.4893	1.5034	0.000	0.000	0.000
	1.0	0.8842	0.8873	0.8836	-0.522	-0.518	-0.531
	2.0	0.5236	0.5050	0.5394	-1.046	-1.082	-1.025
	3.0	0.3155	0.3353	0.3241	-1.553	-1.491	-1.534
	4.0	0.1942	0.2133	0.1970	-2.038	-1.943	-2.032
	5.0	0.1070	0.1189	0.1112	-2.634	-2.528	-2.604
	6.0	0.0595	0.0730	0.0902	-3.221	-3.016	-2.813
240	0.0	1.3255	1.3421	1.3374	0.000	0.000	0.000
	1.0	0.9629	0.9524	0.9473	-0.320	-0.343	-0.345
	2.0	0.6916	0.6986	0.6785	-0.651	-0.653	-0.679
	3.0	0.4899	0.5036	0.5066	-0.995	-0.980	-0.971
	4.0	0.3639	0.3741	0.3804	-1.293	-1.277	-1.257
	6.0	0.1907	0.1982	0.1890	-1.939	-1.913	-1.957
	8.0	0.0960	0.1018	0.1102	-2.625	-2.579	-2.496
480	0.0	1.4296	1.4203	1.4181	0.000	0.000	0.000
	1.0	1.1511	1.1365	1.1411	-0.217	-0.223	-0.217
	2.0	0.9395	0.9423	0.9556	-0.420	-0.410	-0.395
	3.0	0.7779	0.7883	0.7801	-0.609	-0.589	-0.598
	4.0	0.6480	0.6469	0.6249	-0.791	-0.786	-0.819
	6.0	0.4464	0.4412	0.4437	-1.164	-1.169	-1.162
	8.0	0.3075	0.3093	0.3027	-1.537	-1.524	-1.544
1025	0.0	1.3899	1.3977	1.4063	0.000	0.000	0.000
	1.0	1.2097	1.2155	1.2241	-0.139	-0.140	-0.139
	2.0	1.0826	1.0570	1.0700	-0.250	-0.279	-0.273
	3.0	0.9648	0.9341	0.9639	-0.365	-0.403	-0.378
	4.0	0.8394	0.8585	0.8486	-0.504	-0.487	-0.505
	6.0	0.6572	0.6715	0.6797	-0.749	-0.733	-0.727
	8.0	0.5134	0.5367	0.5509	-0.996	-0.957	-0.937

Carbamazepine as probe compound ($[CBZ]_o \simeq 0.25\,\mu M$) with detection at 211 nm.

Table A.25: Decrease in 1.0 cm absorbance at 254 nm (A_0) for a solution of Suwannee River NOM following exposure by 185 and 254 nm radiation (A_t).

$[Cl^-]$	Time	Run 1			Run 2			Run 3		
($mg\,L^{-1}$)	(min)	A_0	A_t	A_t/A_o	A_0	A_t	A_t/A_o	A_0	A_t	A_t/A_o
< 1	5	0.123	0.102	0.829	0.123	0.104	0.846	0.126	0.102	0.810
	10	0.122	0.085	0.697	0.129	0.090	0.698	0.123	0.087	0.707
	20	0.122	0.057	0.467	0.125	0.060	0.480	0.123	0.062	0.504
100	5	0.126	0.105	0.833	0.125	0.106	0.848	0.125	0.107	0.856
	10	0.124	0.090	0.726	0.124	0.090	0.726	0.126	0.090	0.714
	20	0.126	0.063	0.500	0.125	0.063	0.504	0.125	0.060	0.480

Solution concentration of Suwannee River NOM is $3.5\,mg\,L^{-1}$ as C.

Table A.26: Influence of chloride in 254 nm - H_2O_2 regime with Suwannee River NOM and using carbamazepine as probe

$[Cl^-]$	Time	A_t					$ln(A_t/A_o)$				
($mg\,L^{-1}$)	(min)	Run 1	Run 2	Run 3	Run 4	Run 5	Run 1	Run 2	Run 3	Run 4	Run 5
< 1	0	1.3528	1.3584	1.4248	1.4007	1.4283	0.0000	0.0000	0.0000	0.0000	0.0000
	5	1.2392	1.1675	1.2770	1.2739	1.2716	-0.0877		-0.1095	-0.0949	-0.1162
	10	1.1675	1.1264	1.1541	1.1747	1.1447	-0.1473	-0.1873	-0.2107	-0.1760	-0.2213
	15	1.0600	1.0686	1.0459	1.0701	1.0586	-0.2439	-0.2400	-0.3092	-0.2692	-0.2995
	20	0.9527	0.9829	0.9528	0.9793	0.9747	-0.3506	-0.3236	-0.4024	-0.3579	-0.3821
	25	0.8902	0.9150	0.8496	0.8855	0.8836	-0.4185	-0.3951	-0.5170	-0.4586	-0.4802
	30	0.8403	0.8375	0.7799	0.8095	0.7860	-0.4762	-0.4836	-0.6026	-0.5483	-0.5973
100	0	1.4299	1.4221	1.4104	1.3953	1.4404	0.0000	0.0000	0.0000	0.0000	0.0000
	5	1.2935	1.2844	1.2785	1.2809	1.2847	-0.1003	-0.1018	-0.0982	-0.0855	-0.1144
	10	1.1672	1.1723	1.1616	1.1795	1.1670	-0.2030	-0.1932	-0.1941	-0.1680	-0.2105
	15	1.0689	1.0808	1.0590	1.0534	1.0633	-0.2910	-0.2744	-0.2865	-0.2811	-0.3035
	20	0.9871	1.0212	0.9655	0.9900	0.9729	-0.3706	-0.3312	-0.3790	-0.3432	-0.3924
	25	0.8728	0.9588	0.8907	0.8760	0.8856	-0.4937	-0.3942	-0.4596	-0.4655	-0.4864
	30	0.8285	0.9037	0.8057	0.8319	0.8226	-0.5457	-0.4534	-0.5599	-0.5172	-0.5602

$[CBZ]_o \simeq 0.25\,\mu M$ with detection at 211 nm. Suwannee River NOM concentration $7.0\,mg\,L^{-1}$ as C. H_2O_2 dose of $3.0\,mg\,L^{-1}$. Fluence rate at 254 nm of $1\,mW\,cm^{-2}$. Solutions at pH 7.0.

Table A.27: Influence of chloride in 254 nm - H_2O_2 regime with tert-butanol and using carbamazepine as probe

$[Cl^-]$	Time	A_t			$ln(A_t/A_o)$		
($mg\,L^{-1}$)	(min)	Run 1	Run 2	Run 3	Run 1	Run 2	Run 3
< 1	0	1.3971	1.4067	1.3986	0.0000	0.0000	0.0000
	5	1.2330	1.2601	1.2075	-0.1249	-0.1101	-0.1469
	10	1.0983	1.1246	1.0795	-0.2406	-0.2238	-0.2590
	15	0.9855	0.9990	0.9376	-0.3490	-0.3422	-0.3999
	20	0.8487	0.9137	0.8351	-0.4984	-0.4315	-0.5157
	25		0.8160	0.7244		-0.5446	-0.6579
	30		0.7214	0.6453		-0.6678	-0.7735
25	0	1.3983	1.4067	1.3991	0.0000	0.0000	0.0000
	5	1.2376	1.2453	1.2256	-0.1221	-0.1219	-0.1324
	10	1.0952	1.1165	1.0890	-0.2443	-0.2310	-0.2506
	15	0.9672	1.0007	0.9517	-0.3686	-0.3405	-0.3853
	20	0.8414	0.8851	0.8330	-0.5079	-0.4633	-0.5186
	25	0.7507	0.7815	0.7098	-0.6220	-0.5878	-0.6786
	30	0.6440	0.7098	0.6637	-0.7753	-0.6840	-0.7458
40	0	1.4118	1.4024	1.3926	0.0000	0.0000	0.0000
	5	1.2498	1.2302	1.2420	-0.1219	-0.1310	-0.1144
	10	1.0931	1.0827	1.1089	-0.2558	-0.2587	-0.2278
	15	0.9654	0.9730	0.9695	-0.3801	-0.3656	-0.3621
	20	0.8743	0.8358	0.8564	-0.4792	-0.5176	-0.4862
	25	0.7564	0.7317	0.7625	-0.6241	-0.6506	-0.6023
	30	0.6739	0.6396	0.6751	-0.7395	-0.7851	-0.7241
100	0	1.3887	1.3984	1.4060	0.0000	0.0000	0.0000
	5	1.2293	1.2705	1.2274	-0.1219	-0.0959	-0.1359
	10	1.0931	1.1182	1.1007	-0.2394	-0.2236	-0.2448
	15	0.9525	0.9806	0.9757	-0.3770	-0.3549	-0.3653
	20	0.8615	0.9071	0.8713	-0.4774	-0.4328	-0.4785
	25	0.7631	0.7808	0.7622	-0.5987	-0.5828	-0.6123
	30	0.6574	0.6946	0.6759	-0.7478	-0.6997	-0.7325

$[CBZ]_o \simeq 0.25\,\mu M$ with detection at 211 nm. Tert-butanol concentration $7.0\,mg\,L^{-1}$ as C. H_2O_2 dose of $3.0\,mg\,L^{-1}$. Fluence rate at 254 nm of $1\,mW\,cm^{-2}$.

Table A.28: Influence of chloride in 185 nm regime with Suwannee River NOM and using carbamazepine as probe

$[Cl^-]$	Time	A_t			$ln(A_t/A_o)$		
($mg\,L^{-1}$)	(min)	Run 1	Run 2	Run 3	Run 1	Run 2	Run 3
< 1	0	1.3568	1.3814	1.3661	0.0000	0.0000	0.0000
	1	1.0033	1.0064	1.0022	-0.3018	-0.3167	-0.3098
	2	0.7448	0.7531	0.7549	-0.5998	-0.6067	-0.5931
	3	0.5720	0.5441	0.5351	-0.8637	-0.9317	-0.9373
	4	0.3857	0.3822	0.3803	-1.2578	-1.2849	-1.2788
	5	0.2871	0.2894	0.2747	-1.5531	-1.5630	-1.6040
25	0	1.4443	1.4346	1.4460	0.0000	0.0000	0.0000
	0.5	1.2453	1.2355	1.2541	-0.1482	-0.1494	-0.1424
	1	1.0987	1.1041	1.0931	-0.2735	-0.2619	-0.2798
	2	0.8095	0.8057	0.8187	-0.5790	-0.5769	-0.5688
	3	0.6055	0.6036	0.6111	-0.8693	-0.8657	-0.8613
	4	0.4626	0.4518	0.4198	-1.1385	-1.1554	-1.2368
	5	0.3443	0.3213	0.3218	-1.4339	-1.4963	-1.5026
40	0	1.3006	1.3088	1.2948	0.0000	0.0000	0.0000
	1	1.0267	1.0331	1.0266	-0.2365	-0.2365	-0.2321
	2	0.7877	0.7929	0.8109	-0.5015	-0.5012	-0.4680
	3	0.5959	0.5915	0.6257	-0.7805	-0.7942	-0.7272
	4	0.4423	0.4755	0.4937	-1.0786	-1.0125	-0.9642
	5	0.3480	0.3539	0.3362	-1.3184	-1.3079	-1.3484
100	0	1.4500	1.4639	1.4766	0.0000	0.0000	0.0000
	0.5	1.3524	1.3321	1.3545	-0.0697	-0.0943	-0.0863
	1	1.2196	1.2045	1.2079	-0.1730	-0.1950	-0.2009
	2	0.9831	0.9639	1.0144	-0.3886	-0.4179	-0.3754
	3	0.8043	0.7814	0.7772	-0.5893	-0.6278	-0.6418
	4	0.6534	0.5964	0.6122	-0.7971	-0.8979	-0.8804
	5	0.4993	0.4985	0.4860	-1.0661	-1.0773	-1.1113

$[CBZ]_o \simeq 0.25\,\mu M$ with detection at 211 nm. Suwannee River NOM concentration $7.0\,mg\,L^{-1}$ as C. Irradiated solutions at pH 7.0.

Table A.29: Influence of chloride in 185 nm regime with tert-butanol and using carbamazepine as probe

$[Cl^-]$	Time	A_t			$ln(A_t/A_o)$		
($mg\,L^{-1}$)	(min)	Run 1	Run 2	Run 3	Run 1	Run 2	Run 3
< 1	0	1.4651	1.4607	1.4732	0.000	0.000	0.000
	1	0.9688	0.9812	0.9809	-0.414	-0.398	-0.407
	2	0.6681	0.6688	0.6469	-0.785	-0.781	-0.823
	3	0.4499	0.4571	0.4229	-1.181	-1.162	-1.248
	4	0.3184	0.3063	0.3060	-1.526	-1.562	-1.572
	6	0.1349	0.1370	0.1286	-2.385	-2.367	-2.438
	8	0.0764	0.0439	0.0618	-2.954	-3.505	-3.171
10	0	1.4325	1.4437	1.4422	0.000	0.000	0.000
	1	0.9020	0.8937	0.9182	-0.463	-0.480	-0.452
	2	0.5912	0.5894	0.5841	-0.885	-0.896	-0.904
	3	0.3923	0.3868	0.3943	-1.295	-1.317	-1.297
	4	0.2660	0.2662	0.2600	-1.684	-1.691	-1.713
	6	0.0941	0.1160	0.1072	-2.723	-2.521	-2.599
	8	0.0616	0.0534	0.0481	-3.147	-3.297	-3.401
25	0	1.1207	1.1258	1.1463	0.000	0.000	0.000
	1	0.5849	0.5988	0.5944	-0.650	-0.631	-0.657
	2	0.3262		0.3310	-1.234		-1.242
	3	0.1971	0.1876	0.1869	-1.738	-1.792	-1.814
	4	0.1067	0.0972	0.1105	-2.352	-2.449	-2.339
	6	0.0410	0.0319	0.0333	-3.308	-3.564	-3.539
40	0	1.4520	1.4593	1.4658	0.000	0.000	0.000
	0.5	0.8815	0.8978	0.9045	-0.499	-0.486	-0.483
	1	0.5806	0.5803	0.5712	-0.917	-0.922	-0.942
	2	0.2532	0.2574	0.2418	-1.747	-1.735	-1.802
	3	0.1121	0.1288	0.1102	-2.561	-2.427	-2.588
	4	0.0466	0.0570	0.0551	-3.439	-3.243	-3.281
100	0.0	1.4145	1.4237	1.4271	0.000	0.000	0.000
	0.5	0.6502	0.6712	0.6859	-0.777	-0.752	-0.733
	1.0	0.2998	0.3278	0.3354	-1.551	-1.469	-1.448
	1.5	0.1332	0.1495	0.1406	-2.363	-2.254	-2.317
	2.0	0.0596	0.0667		-3.167	-3.061	
	2.5	0.0290	0.0236	0.0220	-3.887	-4.100	-4.172

$[CBZ]_o \simeq 0.25\,\mu M$ with detection at 211 nm. Tert-butanol concentration $7.0\,mg\,L^{-1}$ as C.

Table A.30: Influence of chloride in 185 nm regime with Suwannee River NOM and using nitrobenzene as probe

$[Cl^-]$	Time	A_t			$ln(A_t/A_o)$		
($mg\,L^{-1}$)	(min)	Run 1	Run 2	Run 3	Run 1	Run 2	Run 3
< 1	0	0.8883	0.8927	0.9061	0.0000	0.0000	0.0000
	2	0.6845	0.7092	0.6993	-0.2606	-0.2301	-0.2591
	4	0.5459	0.5587	0.5249	-0.4869	-0.4686	-0.5459
	6	0.4029	0.4165	0.4082	-0.7906	-0.7624	-0.7974
	8	0.3165	0.3282	0.3170	-1.0320	-1.0006	-1.0502
	10	0.2609	0.2538	0.2476	-1.2252	-1.2577	-1.2973
	12	0.1888	0.1889	0.1711	-1.5486	-1.5530	-1.6669
25	0	0.8924	0.8907	0.9147	0.0000	0.0000	0.0000
	2	0.7222	0.7230	0.7141	-0.2116	-0.2086	-0.2476
	4	0.5931	0.6039	0.5914	-0.4086	-0.3886	-0.4361
	6	0.4697	0.4686	0.4804	-0.6418	-0.6423	-0.6440
	8	0.3750	0.3794	0.3843	-0.8670	-0.8534	-0.8672
	10	0.3025	0.2949	0.3041	-1.0818	-1.1054	-1.1012
	12	0.2700	0.2491	0.2489	-1.1955	-1.2742	-1.3015
50	0	0.8850	0.8476	0.8684	0.0000	0.0000	0.0000
	2	0.7161	0.7272	0.7377	-0.2118	-0.1532	-0.1631
	4	0.5538	0.5742	0.5786	-0.4688	-0.3894	-0.4060
	6	0.4447	0.4850	0.4805	-0.6882	-0.5583	-0.5918
	8	0.3677	0.3825	0.3982	-0.8783	-0.7957	-0.7797
	10	0.2907	0.3135	0.3351	-1.1133	-0.9946	-0.9522
	12	0.2527	0.2541	0.2575	-1.2534	-1.2047	-1.2156
100	0	0.8902	0.8860	0.8999	0.0000	0.0000	0.0000
	2	0.7913	0.7617	0.7757	-0.1178	-0.1512	-0.1485
	4	0.6665	0.6660	0.6610	-0.2894	-0.2854	-0.3085
	6	0.5771	0.5646	0.5637	-0.4334	-0.4506	-0.4678
	8	0.4780	0.4525	0.4593	-0.6218	-0.6719	-0.6726
	10	0.3760	0.3800	0.3707	-0.8619	-0.8465	-0.8869
	12	0.3343	0.3267	0.3436	-0.9794	-0.9977	-0.9628

$[NB]_o \simeq 1\,\mu M$ with detection at 267 nm. Suwannee River NOM concentration $7.0\,mg\,L^{-1}$ as C. Irradiated solutions at pH 7.0.

Table A.31: Influence of chloride in 185 nm regime with tert-butanol and using nitrobenzene as probe

$[Cl^-]$	Time	A_t			$ln(A_t/A_o)$		
($mg\,L^{-1}$)	(min)	Run 1	Run 2	Run 3	Run 1	Run 2	Run 3
< 1	0	0.9068	0.9031	0.9012	0.0000	0.0000	0.0000
	2	0.6777	0.6917	0.7138	-0.2912	-0.2667	-0.2331
	4	0.5296	0.5345	0.5376	-0.5378	-0.5245	-0.5166
	6	0.4329	0.4224	0.4012	-0.7394	-0.7599	-0.8093
	8	0.3268	0.3271	0.3159	-1.0206	-1.0156	-1.0483
	10	0.2560	0.2729	0.2579	-1.2647	-1.1967	-1.2512
	12	0.2022	0.1883	0.1821	-1.5007	-1.5678	-1.5992
25	0	0.9062	0.8993	0.9191	0.0000	0.0000	0.0000
	2	0.7228	0.7385	0.7396	-0.2261	-0.1970	-0.2173
	4	0.6026	0.6024	0.6214	-0.4080	-0.4007	-0.3914
	6	0.4932	0.4592	0.4812	-0.6083	-0.6721	-0.6471
	8	0.3856	0.3839	0.3821	-0.8545	-0.8512	-0.8777
	10	0.3069	0.3156	0.3124	-1.0827	-1.0471	-1.0791
	12	0.2727	0.2572	0.2570	-1.2009	-1.2518	-1.2743
50	0	0.9277	0.8991	0.9218	0.0000	0.0000	0.0000
	2	0.7540	0.7767	0.7751	-0.2073	-0.1463	-0.1733
	4	0.6431	0.6574	0.6523	-0.3664	-0.3131	-0.3458
	6	0.5475	0.5507	0.5403	-0.5273	-0.4902	-0.5342
	8	0.4720	0.4898	0.4663	-0.6757	-0.6074	-0.6815
	10	0.3897	0.4106	0.4074	-0.8673	-0.7838	-0.8165
	12	0.3323	0.3348	0.3473	-1.0267	-0.9879	-0.9761
100	0	0.9151	0.9154	0.9131	0.0000	0.0000	0.0000
	2	0.8117	0.8008	0.8006	-0.1199	-0.1337	-0.1315
	4	0.6999	0.6887	0.6972	-0.2681	-0.2846	-0.2698
	6	0.6019	0.6084	0.6149	-0.4189	-0.4085	-0.3954
	8	0.5333	0.5232	0.5499	-0.5399	-0.5594	-0.5071
	10	0.4730	0.4488	0.4617	-0.6599	-0.7128	-0.6819
	12	0.3973	0.4262	0.4033	-0.8343	-0.7645	-0.8172

$[NB]_o \simeq 1\,\mu M$ with detection at 267 nm. Tert-butanol concentration $7.0\,mg\,L^{-1}$ as C.

Table A.32: Acetate system in 185 nm regime with carbamazepine and nitrobenzene as probes

Probe	$[Cl^-]$	Time	A_t			$ln(A_t/A_o)$		
	($mg\,L^{-1}$)	(min)	Run 1	Run 2	Run 3	Run 1	Run 2	Run 3
CBZ	< 1	0	1.4767	1.4757	1.5093	0.000	0.000	0.000
		0.5	1.1231	1.1300	1.1517	-0.274	-0.267	-0.270
		1.0	0.8422	0.8602	0.8860	-0.562	-0.540	-0.533
		2.0	0.5404	0.4970	0.5099	-1.005	-1.088	-1.085
		3.0	0.2794	0.2716	0.2916	-1.665	-1.693	-1.644
		4.0	0.1660	0.1524	0.1654	-2.186	-2.270	-2.211
		5.0	0.0834	0.0937	0.1048	-2.874	-2.757	-2.667
	100	0	1.5351	1.5085	1.5093	0.000	0.000	0.000
		0.5	1.1982	1.1782	1.1580	-0.248	-0.247	-0.265
		1.0	0.9171	0.8941	0.8738	-0.515	-0.523	-0.547
		2.0	0.5935	0.5787	0.5807	-0.950	-0.958	-0.955
		3.0	0.3923	0.3808	0.3716	-1.364	-1.377	-1.402
		4.0	0.2576	0.2662	0.2483	-1.785	-1.735	-1.805
		5.0	0.1803	0.1648	0.1672	-2.142	-2.214	-2.200
NB	< 1	0	1.0910	1.0992	1.0665	0.000	0.000	0.000
		0.5	0.9596	0.9557	1.0037	-0.128	-0.140	-0.061
		1.0	0.9190	0.9055	0.9271	-0.172	-0.194	-0.140
		2.0	0.7890	0.7986	0.7798	-0.324	-0.319	-0.313
		3.0	0.6725	0.6464	0.6524	-0.484	-0.531	-0.491
		4.0	0.5976	0.5483	0.5818	-0.602	-0.696	-0.606
		5.0	0.4849	0.5070	0.4591	-0.811	-0.774	-0.843
	100	0	1.1150	1.0965	1.0718	0.000	0.000	0.000
		0.5	1.0412	1.0121	1.0231	-0.068	-0.080	-0.047
		1.0	1.0426	0.9817	1.0007	-0.067	-0.111	-0.069
		2.0	0.9276	0.9484	0.9306	-0.184	-0.145	-0.141
		3.0	0.9024	0.8402	0.8741	-0.212	-0.266	-0.204
		4.0	0.8301	0.8019	0.8016	-0.295	-0.313	-0.290
		5.0	0.7406	0.7639	0.7482	-0.409	-0.361	-0.359

$[CBZ]_o \simeq 0.25\,\mu M$ with detection at 211 nm. $[NB]_o \simeq 1\,\mu M$ with detection at 267 nm. Solutions contained $8.2\,mg\,L^{-1}$ as C of acetate at pH 6.0.

Table A.33: Acetone system in 185 nm regime with carbamazepine and nitrobenzene as probes

Probe	$[Cl^-]$	Time	A_t			$ln(A_t/A_o)$		
	($mg\,L^{-1}$)	(min)	Run 1	Run 2	Run 3	Run 1	Run 2	Run 3
CBZ	< 1	0	1.3899	1.3977	1.4063	0.0000	0.0000	0.0000
		1.0	1.2097	1.2155	1.2241	-0.1389	-0.1397	-0.1388
		2.0	1.0826	1.0570	1.0700	-0.2499	-0.2794	-0.2733
		3.0	0.9648	0.9341	0.9639	-0.3651	-0.4030	-0.3777
		4.0	0.8394	0.8585	0.8486	-0.5043	-0.4874	-0.5051
		6.0	0.6572	0.6715	0.6797	-0.7490	-0.7331	-0.7271
		8.0	0.5134	0.5367	0.5509	-0.9959	-0.9571	-0.9372
	100	0	1.4212	1.4263	1.4330	0.0000	0.0000	0.0000
		0.25	0.9466	1.0487	1.0060	-0.4064	-0.3075	-0.3538
		0.50	0.6715	0.6469	0.6611	-0.7497	-0.7906	-0.7736
		0.75	0.4394	0.6326	0.5352	-1.1738	-0.8130	-0.9849
		1.00	0.2725	0.2907	0.2749	-1.6516	-1.5905	-1.6511
		1.50	0.1059	0.1155	0.1307	-2.5968	-2.5136	-2.3946
		2.00	0.0391	0.0566	0.0658	-3.5931	-3.2268	-3.0809
NB	< 1	0	1.0944	1.0660	1.0588	0.0000	0.0000	0.0000
		1.0	1.0305	1.0388	1.0182	-0.0602	-0.0258	-0.0391
		2.0	1.0143	0.9788	1.0069	-0.0760	-0.0853	-0.0503
		3.0	0.9744	0.9721	0.9657	-0.1161	-0.0922	-0.0920
		4.0	0.9459	0.9552	0.9201	-0.1458	-0.1097	-0.1404
		6.0	0.8692	0.8645	0.8701	-0.2304	-0.2095	-0.1963
		8.0	0.8147	0.8294	0.8163	-0.2951	-0.2510	-0.2601
	100	0	1.0757	1.0429	1.0658	0.0000	0.0000	0.0000
		0.25	1.0095	1.0530	1.1015	-0.0635	0.0096	0.0329
		0.50	1.0673	1.0625	1.0494	-0.0078	0.0186	-0.0155
		0.75	1.0503	1.0503	1.0529	-0.0239	0.0071	-0.0122
		1.0	1.0432	1.0576	1.0524	-0.0307	0.0140	-0.0127
		1.5	1.0536	1.0303	1.0478	-0.0208	-0.0122	-0.0170
		2.0	1.0345	1.0379	0.9964	-0.0391	-0.0048	-0.0673
		2.5	1.0100	1.0447	1.0452	-0.0630	0.0017	-0.0195
		3.0	1.0075	0.9792	0.9879	-0.0655	-0.0630	-0.0759
		4.0	0.9852	0.9542	0.9476	-0.0879	-0.0889	-0.1175
		6.0	0.9534	0.9492	0.9112	-0.1207	-0.0941	-0.1567
		8.0	0.8619	0.9121	0.8856	-0.2216	-0.1340	-0.1852

$[CBZ]_o \simeq 0.25\,\mu M$ with detection at 211 nm. $[NB]_o \simeq 1\,\mu M$ with detection at 267 nm. Solutions contained $10.2\,mg\,L^{-1}$ as C of acetone.

Table A.34: Influence of ionic strength and chloride in 185 nm regime with carbamazepine as probe

$[Cl^-]$	Ionic Strength	Time	A_t			$ln(A_t/A_o)$		
($mg\,L^{-1}$)	(M)	(min)	Run 1	Run 2	Run 3	Run 1	Run 2	Run 3
0	0.00	0	1.4391	1.4202	1.4200	0.000	0.000	0.000
		1	0.9875	0.9821	0.9948	-0.377	-0.369	-0.356
		2	0.6971	0.6753	0.6879	-0.725	-0.743	-0.725
		3	0.4744	0.4520	0.4780	-1.110	-1.145	-1.089
		4	0.3135	0.3354	0.3218	-1.524	-1.443	-1.484
		6	0.1593	0.1276	0.1340	-2.201	-2.410	-2.361
	0.08	0	1.4589	1.4378	1.4449	0.000	0.000	0.000
		1	1.0502	1.0295	1.0018	-0.329	-0.334	-0.366
		2	0.7128	0.7359	0.7315	-0.716	-0.670	-0.681
		3	0.5257	0.5177	0.5221	-1.021	-1.021	-1.018
		4	0.3721	0.3843	0.3773	-1.366	-1.319	-1.343
		6	0.1772	0.1908	0.1933	-2.108	-2.020	-2.012
	0.16	0	1.4462	1.4352	1.4257	0.000	0.000	0.000
		1	1.0876	1.0620	1.0963	-0.285	-0.301	-0.263
		2	0.8202	0.7981	0.8026	-0.567	-0.587	-0.575
		3	0.6195	0.6180	0.6185	-0.848	-0.843	-0.835
		4	0.4638	0.4712	0.4533	-1.137	-1.114	-1.146
		6	0.2870	0.2764	0.2418	-1.617	-1.647	-1.774
100	0.00	0.0	1.4250	1.4032	1.4452	0.000	0.000	0.000
		0.5	0.5726	0.5285	0.5828	-0.912	-0.976	-0.908
		1.0	0.2234	0.1840	0.2077	-1.853	-2.032	-1.940
		1.5	0.0952	0.0626	0.0819	-2.706	-3.110	-2.871
	0.08	0.0	1.4444	1.4404	1.4427	0.000	0.000	0.000
		0.5	0.9432	0.9254	0.9145	-0.426	-0.442	-0.456
		1.0	0.6458	0.6516	0.6232	-0.805	-0.793	-0.839
		1.5	0.4506	0.4270	0.4554	-1.165	-1.216	-1.153
		2.0	0.3197	0.2970	0.3007	-1.508	-1.579	-1.568
		2.5	0.2037	0.2110	0.2264	-1.959	-1.921	-1.852
	0.16	0.0	1.4435	1.4286	1.4230	0.000	0.000	0.000
		0.5	1.0905	1.0703	1.0859	-0.280	-0.289	-0.270
		1.0	0.7880	0.7867	0.8267	-0.605	-0.597	-0.543
		1.5	0.6016	0.5892	0.6573	-0.875	-0.886	-0.772
		2.0	0.4526	0.4751	0.4766	-1.160	-1.101	-1.094
		2.5	0.3455	0.3422	0.3214	-1.430	-1.429	-1.488

$[CBZ]_o \simeq 0.25\,\mu M$ with detection at 211 nm. Tert-butanol concentration $7.0\,mg\,L^{-1}$ as C. Ionic strength adjusted using NaF. Chloride adjusted using NaCl.

Table A.35: Quantification of molar absorption coefficient of chloride at 185 nm using a kinetic method

$[Cl^-]$	Time	A_t			$ln(A_t/A_o)$		
($mg\,L^{-1}$)	(min)	Run 1	Run 2	Run 3	Run 1	Run 2	Run 3
0	0	1.3595	1.3458	1.3760	0.000	0.000	0.000
	1	1.1669	1.1589	1.1469	-0.153	-0.150	-0.182
	2	0.9519	0.9803		-0.356	-0.317	
	4	0.6479	0.6778	0.6701	-0.741	-0.686	-0.720
	6	0.4705	0.4612	0.4731	-1.061	-1.071	-1.068
	8	0.3297	0.3410	0.3345	-1.417	-1.373	-1.414
	10	0.2342	0.2450	0.2158	-1.759	-1.703	-1.853
25	0	1.3781	1.3856		0.000	0.000	
	2	1.1393	1.1346		-0.190	-0.200	
	4	0.9570	0.9737		-0.365	-0.353	
	6	0.8049	0.7890		-0.538	-0.563	
	8	0.6381	0.6734		-0.770	-0.722	
	10	0.5317	0.5324		-0.952	-0.956	
50	0	1.4115	1.3548		0.000	0.000	
	2	1.2229	1.2148		-0.143	-0.109	
	4	1.1131	1.1195		-0.238	-0.191	
	8	0.8759	0.9114		-0.477	-0.396	
	12	0.7465	0.7072		-0.637	-0.650	
	16	0.5962	0.6068		-0.862	-0.803	
75	0	1.4032	1.3866		0.000	0.000	
	4	1.2412	1.1396		-0.123	-0.196	
	8	1.0955	0.9774		-0.248	-0.350	
	12	0.9173	0.9002		-0.425	-0.432	
	16	0.8019	0.8049		-0.560	-0.544	
	20	0.7225	0.7327		-0.664	-0.638	
100	0	1.3632	1.4057		0.000	0.000	
	4	1.2598	1.2629		-0.079	-0.107	
	8	1.1402	1.1544		-0.179	-0.197	
	12	1.0397	1.0312		-0.271	-0.310	
	16	0.9424			-0.369		
	20	0.8771	0.8401		-0.441	-0.515	

Lower 1.0 cm cell contains $[CBZ]_o \simeq 0.25\,\mu M$ with detection at 211 nm, and tert-butanol concentration $7.0\,mg\,L^{-1}$ as C. Upper 1.0 mm cell contains varying chloride concentration adjusted using NaCl.

Table A.36: Influence of sulphate in 254 nm - H_2O_2 regime with Suwannee River NOM and using carbamazepine as probe

$[SO_4{}^{2-}]$	Time	A_t		$ln(A_t/A_o)$	
($mg\,L^{-1}$)	(min)	Run 1	Run 2	Run 1	Run 2
< 1	0	1.3408	1.2895	0.000	0.000
	5	1.2146	1.1594	-0.099	-0.106
	10	1.0512	1.0460	-0.243	-0.209
	15	0.9783	0.8686	-0.315	-0.395
	20	0.8775	0.8176	-0.424	-0.456
100	0	1.3472	1.2546	0.000	0.000
	5	1.1534	1.1730	-0.155	-0.067
	10	1.0424		-0.257	
	15	0.9533	0.9554	-0.346	-0.272
	20	0.8908	0.8643	-0.414	-0.373

$[CBZ]_o \simeq 0.25\,\mu M$ with detection at 211 nm. Suwannee River NOM concentration $7.0\,mg\,L^{-1}$ as C. H_2O_2 dose of $7.0\,mg\,L^{-1}$. Fluence rate at 254 nm of $1\,mW\,cm^{-2}$. Solutions at pH 7.0.

Table A.37: Influence of sulphate in 254 nm - H_2O_2 regime with tert-butanol and using carbamazepine as probe

$[SO_4{}^{2-}]$	Time	A_t			$ln(A_t/A_o)$		
($mg\,L^{-1}$)	(min)	Run 1	Run 2	Run 3	Run 1	Run 2	Run 3
< 1	0	1.3630	1.3657	1.3581	0.0000	0.0000	0.000
	5	1.1872	1.1941	1.1038	-0.1381	-0.1343	-0.207
	10	1.0513	1.0921	0.9909	-0.2597	-0.2236	-0.315
	15	0.9148	0.9669	0.8953	-0.3987	-0.3453	-0.417
	20	0.7770	0.9098	0.7446	-0.5620	-0.4062	-0.601
	25	0.6928	0.8248	0.6923	-0.6767	-0.5043	-0.674
100	0	1.3766	1.4052	1.3469	0.000	0.000	0.000
	5	1.1920	1.2080	1.1433	-0.144	-0.151	-0.164
	10	1.0310	1.0748	1.0113	-0.289	-0.268	-0.287
	15	0.8578	0.9348	0.8529	-0.473	-0.408	-0.457
	20	0.7530	0.8185	0.7598	-0.603	-0.540	-0.573
	25	0.6422	0.7367	0.6429	-0.762	-0.646	-0.740

$[CBZ]_o \simeq 0.25\,\mu M$ with detection at 211 nm. Tert-butanol concentration $7.0\,mg\,L^{-1}$ as C. H_2O_2 dose of $7.0\,mg\,L^{-1}$. Fluence rate at 254 nm of $1\,mW\,cm^{-2}$.

Table A.38: Influence of sulphate in 185 nm regime with tert-butanol and using carbamazepine as probe

$[SO_4{}^{2-}]$	Time	A_t			$ln(A_t/A_o)$		
($mg\,L^{-1}$)	(min)	Run 1	Run 2	Run 3	Run 1	Run 2	Run 3
< 1	0.0	1.4806	1.4633	1.4524	0.000	0.000	0.000
	1.0	0.9983	0.9992	1.0004	-0.394	-0.381	-0.373
	2.0	0.7012	0.6988	0.6934	-0.747	-0.739	-0.739
	3.0	0.5012	0.4767	0.4797	-1.083	-1.122	-1.108
	4.0	0.3345	0.3337	0.3486	-1.488	-1.478	-1.427
	5.0	0.2125	0.2249	0.2078	-1.941	-1.873	-1.944
25	0.0	1.4396	1.4287	1.4492	0.000	0.000	0.000
	0.5	1.0617	1.0501	1.0258	-0.304	-0.308	-0.346
	1.0	0.7772	0.7810	0.7853	-0.616	-0.604	-0.613
	2.0	0.3949	0.4180	0.4116	-1.293	-1.229	-1.259
	3.0	0.2185	0.2208	0.2235	-1.885	-1.867	-1.869
	4.0	0.1002	0.1083	0.1103	-2.665	-2.580	-2.576
50	0.0	1.4657	1.4237	1.4360	0.000	0.000	0.000
	0.5	0.9174	0.9231	0.9157	-0.469	-0.433	-0.450
	1.0	0.5494	0.5916	0.5995	-0.981	-0.878	-0.874
	2.0	0.2319	0.2490	0.2480	-1.844	-1.744	-1.756
	3.0	0.0620	0.0887	0.1071	-3.163	-2.776	-2.596
	4.0	0.0226	0.0338	0.0445	-4.172	-3.741	-3.474
75	0.0	1.4982	1.4928	1.4920	0.000	0.000	0.000
	0.5	0.8329	0.8126	0.8638	-0.587	-0.608	-0.547
	1.0	0.4363	0.4458	0.4731	-1.234	-1.209	-1.149
	1.5	0.2653	0.2671	0.2853	-1.731	-1.721	-1.654
	2.0	0.1065	0.1227	0.1530	-2.644	-2.499	-2.277
	2.5		0.0773	0.0897		-2.961	-2.811
	3.0	0.0271			-4.012		
100	0.0	1.4475	1.4488	1.4577	0.000	0.000	0.000
	0.5	0.7200	0.7296	0.7529	-0.698	-0.686	-0.661
	1.0	0.3322	0.3708	0.3837	-1.472	-1.363	-1.335
	1.5	0.1941	0.1887	0.2001	-2.009	-2.038	-1.986
	2.0	0.0721	0.1716	0.1119	-3.000	-2.133	-2.567
	2.5	0.0571	0.0507	0.0307	-3.233	-3.353	-3.860

$[CBZ]_o \simeq 0.25\,\mu M$ with detection at 211 nm. Tert-butanol concentration $7.0\,mg\,L^{-1}$ as C.

Table A.39: Influence of bicarbonate in 185 nm regime with tert-butanol and using carbamazepine as probe

$[HCO_3^-]$	Time	A_t			$ln(A_t/A_o)$		
($mg\,L^{-1}$)	(min)	Run 1	Run 2	Run 3	Run 1	Run 2	Run 3
< 1	0	1.4328	1.4234	1.4295	0.000	0.000	0.000
	1	1.0150	0.9861	1.0118	-0.345	-0.367	-0.346
	2	0.6876	0.7015	0.6877	-0.734	-0.708	-0.732
	3	0.4702	0.4653	0.5051	-1.114	-1.118	-1.040
	4	0.3222	0.3279	0.3516	-1.492	-1.468	-1.403
	5	0.2364	0.2376	0.2141	-1.802	-1.790	-1.899
60	0	1.5035	1.4866	1.4832	0.000	0.000	0.000
	1	1.1365	1.1194	1.1512	-0.280	-0.284	-0.253
	2	0.8692	0.8593	0.8566	-0.548	-0.548	-0.549
	3	0.6495	0.6525	0.6435	-0.839	-0.823	-0.835
	4	0.4872	0.5022	0.4938	-1.127	-1.085	-1.100
	5	0.3687	0.3549	0.3733	-1.406	-1.432	-1.380
120	0	1.4084	1.4105	1.4205	0.000	0.000	0.000
	2	0.9270	0.9071	0.9080	-0.418	-0.441	-0.448
	4	0.5947	0.5745	0.5930	-0.862	-0.898	-0.874
	6	0.3831	0.3840	0.3528	-1.302	-1.301	-1.393
	8	0.2371	0.2262	0.2085	-1.782	-1.830	-1.919
	10	0.1445	0.1434	0.1331	-2.277	-2.286	-2.368
180	0	1.4250	1.4350	1.4150	0.000	0.000	0.000
	2	1.0082	0.9838	1.0143	-0.346	-0.377	-0.333
	4	0.6968	0.7082	0.7089	-0.715	-0.706	-0.691
	6	0.5003	0.4781	0.4773	-1.047	-1.099	-1.087
	8	0.3506	0.3316	0.3373	-1.402	-1.465	-1.434
	10	0.2053	0.2153	0.2445	-1.937	-1.897	-1.756

$[CBZ]_o \simeq 0.25\,\mu M$ with detection at 211 nm. Tert-butanol concentration $7.0\,mg\,L^{-1}$ as C. Solutions at pH 8.3.

Table A.40: Interaction study for influence of bicarbonate and sulphate in 185 nm regime with tert-butanol and using carbamazepine as probe

$[SO_4{}^{2-}]$	$[HCO_3{}^{-}]$	Time	A_t			$ln(A_t/A_o)$		
($mg\,L^{-1}$)	($mg\,L^{-1}$)	(min)	Run 1	Run 2	Run 3	Run 1	Run 2	Run 3
0	0	0	1.4016	1.4000	1.4255	0.000	0.000	0.000
		1	0.9815	0.9549	1.0026	-0.356	-0.383	-0.352
		2	0.6844	0.7114	0.6876	-0.717	-0.677	-0.729
		3	0.4689	0.4880	0.4964	-1.095	-1.054	-1.055
		4	0.3171	0.3226	0.3697	-1.486	-1.468	-1.350
		5	0.2566	0.2300	0.2417	-1.698	-1.806	-1.775
50	0	0.0	1.3994	1.3967	1.3892	0.000	0.000	0.000
		0.5	0.9287	0.9136	0.8999	-0.410	-0.424	-0.434
		1.0	0.5967	0.6036	0.5913	-0.852	-0.839	-0.854
		1.5	0.4337	0.3967	0.4204	-1.171	-1.259	-1.195
		2.0	0.2669	0.2498	0.2856	-1.657	-1.721	-1.582
		2.5	0.1935	0.1594	0.1736	-1.979	-2.170	-2.080
25	90	0	1.4129	1.4068	1.4000	0.000	0.000	0.000
		1	0.9992	0.9767	1.0054	-0.346	-0.365	-0.331
		2	0.7347	0.7066	0.7535	-0.654	-0.689	-0.619
		4	0.3521	0.3592	0.3728	-1.389	-1.365	-1.323
		6	0.1717	0.1604	0.1680	-2.108	-2.171	-2.120
		8	0.0759	0.0762	0.0672	-2.924	-2.916	-3.037
0	180	0	1.4188	1.4540	1.4470	0.000	0.000	0.000
		1	1.1938	1.2191	1.2023	-0.173	-0.176	-0.185
		2	1.0138	1.0045	1.0069	-0.336	-0.370	-0.363
		4	0.7216	0.7501	0.7071	-0.676	-0.662	-0.716
		6	0.5121	0.5324	0.5157	-1.019	-1.005	-1.032
		8	0.3825	0.3526	0.3863	-1.311	-1.417	-1.321
50	180	0	1.3975	1.4098	1.4129	0.000	0.000	0.000
		1	1.0407	1.0266	1.0396	-0.295	-0.317	-0.307
		2	0.7711	0.7680	0.7703	-0.595	-0.607	-0.607
		4	0.4117	0.4327	0.3982	-1.222	-1.181	-1.266
		6	0.2106	0.2075	0.2227	-1.892	-1.916	-1.848
		8	0.0911	0.0961	0.0882	-2.730	-2.686	-2.774

$[CBZ]_o \simeq 0.25\,\mu M$ with detection at 211 nm. Tert-butanol concentration $7.0\,mg\,L^{-1}$ as C. Solutions at pH 7-8.

Table A.41: Interaction study for influence of bicarbonate and chloride in 185 nm regime with tert-butanol and using carbamazepine as probe

$[Cl^-]$	$[HCO_3^-]$	Time	A_t			$ln(A_t/A_o)$		
($mg\,L^{-1}$)	($mg\,L^{-1}$)	(min)	Run 1	Run 2	Run 3	Run 1	Run 2	Run 3
0	0	0	1.4467	1.4005	1.4616	0.000	0.000	0.000
		1	0.9689	1.0193	1.1706	-0.401	-0.318	-0.222
		2	0.7299	0.6824	0.6949	-0.684	-0.719	-0.744
		3	0.4906	0.4795	0.5132	-1.081	-1.072	-1.047
		4	0.3338	0.3532	0.3505	-1.466	-1.378	-1.428
		5		0.2142	0.2436		-1.878	-1.792
		6	0.1579			-2.215		
50	0	0	1.4353	1.4418	1.4099	0.000	0.000	0.000
		0.5	0.8913	0.8748	0.8394	-0.476	-0.500	-0.519
		1.0	0.4826	0.4894	0.5046	-1.090	-1.080	-1.028
		1.5	0.2957	0.2995	0.3427	-1.580	-1.572	-1.414
		2.0	0.1745	0.1956	0.1940	-2.107	-1.998	-1.983
		2.5	0.1013	0.1229	0.1287	-2.651	-2.462	-2.394
25	90	0	1.4269	1.3671	1.4091	0.000	0.000	0.000
		1	1.1950	1.1683	1.1803	-0.177	-0.157	-0.177
		2	1.0311	1.0119	0.9983	-0.325	-0.301	-0.345
		4	0.7592	0.7641	0.7474	-0.631	-0.582	-0.634
		6	0.5345	0.5362	0.5629	-0.982	-0.936	-0.918
		8	0.3836	0.4022	0.4035	-1.314	-1.223	-1.251
0	180	0	1.4150	1.3786	1.4369	0.000	0.000	0.000
		1	1.1908	1.1967	1.2326	-0.173	-0.142	-0.153
		2	1.0367	0.9668	1.0161	-0.311	-0.355	-0.347
		4	0.7105	0.7299	0.7418	-0.689	-0.636	-0.661
		6	0.5411	0.5159	0.5101	-0.961	-0.983	-1.036
		8	0.3562	0.3606	0.3737	-1.379	-1.341	-1.347
50	180	0	1.3932	1.3939	1.4002	0.000	0.000	0.000
		1	1.2802	1.2473	1.2692	-0.085	-0.111	-0.098
		2	1.1286	1.1527	1.1396	-0.211	-0.190	-0.206
		4	0.9136	0.9327	0.8820	-0.422	-0.402	-0.462
		6	0.7345	0.7661	0.7497	-0.640	-0.599	-0.625
		8	0.5691	0.6057	0.6068	-0.895	-0.833	-0.836

$[CBZ]_o \simeq 0.25\,\mu M$ with detection at 211 nm. Tert-butanol concentration $7.0\,mg\,L^{-1}$ as C. Solutions at pH 7-8.

Table A.42: Interaction study for influence of bicarbonate, chloride and sulphate in 185 nm regime with Suwannee River NOM and using carbamazepine as probe

$[HCO_3^-]$	$[Cl^-]$	$[SO_4{}^{2-}]$	Time	A_t			$ln(A_t/A_o)$		
($mg\,L^{-1}$)	($mg\,L^{-1}$)	($mg\,L^{-1}$)	(min)	Run 1	Run 2	Run 3	Run 1	Run 2	Run 3
0	0	0	0	1.3812	1.3681	1.3993	0.000	0.000	0.000
			1	0.8061	0.8804	0.8631	-0.539	-0.441	-0.483
			2	0.5204	0.5021	0.4573	-0.976	-1.002	-1.118
			3	0.3054	0.3188	0.2830	-1.509	-1.457	-1.598
			4	0.1579	0.1859	0.1792	-2.169	-1.996	-2.055
			5	0.0887	0.0967	0.0964	-2.745	-2.650	-2.675
0	0	50	0	1.3992	1.4194	1.4406	0.000	0.000	0.000
			1	0.8619	0.8206	0.8068	-0.485	-0.548	-0.580
			2	0.4812	0.4769	0.4913	-1.067	-1.091	-1.076
			3	0.2685	0.2836	0.2709	-1.651	-1.610	-1.671
			4	0.1671	0.1697	0.1626	-2.125	-2.124	-2.182
			5	0.0996	0.0826	0.0946	-2.642	-2.844	-2.723
0	50	0	0	1.3962	1.3781	1.3605	0.000	0.000	0.000
			1	0.9809	1.0057	0.9429	-0.353	-0.315	-0.367
			2	0.7001	0.6611	0.6980	-0.690	-0.735	-0.667
			3	0.4740	0.5005	0.4858	-1.080	-1.013	-1.030
			4	0.3109	0.3349	0.3461	-1.502	-1.415	-1.369
			5	0.2263	0.2337	0.2323	-1.820	-1.774	-1.768
0	50	50	0	1.3798	1.3685	1.3661	0.000	0.000	0.000
			1	1.0042	0.9823	0.9613	-0.318	-0.332	-0.351
			2	0.6823	0.6832	0.7253	-0.704	-0.695	-0.633
			3	0.4555	0.4878	0.5072	-1.108	-1.032	-0.991
			4	0.3049	0.3306	0.3183	-1.510	-1.421	-1.457
			5	0.2111	0.2211	0.2244	-1.877	-1.823	-1.806
180	0	0	0	1.4138	1.3921	1.3842	0.000	0.000	0.000
			1	1.1360	1.1226	1.1331	-0.219	-0.215	-0.200
			2	0.9276	0.9269	0.9561	-0.421	-0.407	-0.370
			3	0.7912	0.7779	0.7417	-0.580	-0.582	-0.624
			4	0.6498	0.6103	0.6030	-0.777	-0.825	-0.831
			5	0.4958	0.5144	0.4735	-1.048	-0.996	-1.073
180	0	50	0	1.4155	1.3979	1.3581	0.000	0.000	0.000
			1	1.0175	1.0439	1.0252	-0.330	-0.292	-0.281
			2	0.7961	0.7628	0.7539	-0.576	-0.606	-0.589
			3	0.5946	0.6155	0.5768	-0.867	-0.820	-0.856
			4	0.4268	0.3992	0.4440	-1.199	-1.253	-1.118
			5	0.3352	0.3375	0.3066	-1.441	-1.421	-1.488
180	50	0	0	1.4279	1.4211	1.3797	0.000	0.000	0.000
			1	1.1874	1.2105	1.2019	-0.184	-0.160	-0.138
			2	1.0679	1.0828	1.0368	-0.291	-0.272	-0.286

Continued on next page

Table A.42: (continued)

$[HCO_3^-]$	$[Cl^-]$	$[SO_4{}^{2-}]$	Time	A_t			$ln(A_t/A_o)$		
($mg\,L^{-1}$)	($mg\,L^{-1}$)	($mg\,L^{-1}$)	(min)	Run 1	Run 2	Run 3	Run 1	Run 2	Run 3
			3	0.9606	0.9407	0.9827	-0.396	-0.413	-0.339
			4	0.8229	0.8503	0.8096	-0.551	-0.514	-0.533
			5	0.7172	0.7385	0.7522	-0.689	-0.655	-0.607
180	50	50	0	1.3946	1.3760	1.4102	0.000	0.000	0.000
			1	1.1689	1.1928	1.2136	-0.177	-0.143	-0.150
			2	1.0387	1.0561	1.0678	-0.295	-0.265	-0.278
			3	0.9170	0.9092	0.8975	-0.419	-0.414	-0.452
			4	0.7827	0.8124	0.7997	-0.578	-0.527	-0.567
			5	0.6833	0.7250	0.7105	-0.713	-0.641	-0.686

$[CBZ]_o \simeq 0.25\,\mu M$ with detection at 211 nm. Suwannee River NOM concentration $7.0\,mg\,L^{-1}$ as C. Solutions at pH 7-8.

Table A.43: Quantification of molar absorption coefficient of sulphate, bicarbonate, and Suwannee River NOM at 185 nm using a kinetic method**.

Solute	$[S]$	Time	A_t		$ln(A_t/A_o)$	
	($mg\,L^{-1}$)	(min)	Run 1	Run 2	Run 1	Run 2
$SO_4{}^{2-}$	500	0	1.3780	1.3680	0.000	0.000
		1	1.2120	1.1977	-0.128	-0.133
		2	1.0454	1.0146	-0.276	-0.299
		4	0.7702	0.7701	-0.582	-0.575
		6	0.5832	0.5673	-0.860	-0.880
		8	0.4203	0.4323	-1.187	-1.152
$HCO_3{}^{-}$	180	0	1.3802	1.3938	0.000	0.000
		1	1.1850	1.1643	-0.152	-0.180
		2	1.0362	1.0160	-0.287	-0.316
		4	0.7571	0.7379	-0.600	-0.636
		6	0.5657	0.5720	-0.892	-0.891
		8	0.4290	0.4139	-1.169	-1.214
		10	0.3217		-1.456	
SR NOM	43*	0	1.3703	1.3948	0.000	0.000
		1	1.2706	1.2469	-0.076	-0.112
		2	1.1719	1.1239	-0.156	-0.216
		4	0.9502	0.9481	-0.366	-0.386
		6	0.7869	0.7867	-0.555	-0.573
		8	0.6599	0.6172	-0.731	-0.815

Lower 1.0 cm cell contains $[CBZ]_o \simeq 0.25\,\mu M$ with detection at 211 nm, and tert-butanol concentration $7.0\,mg\,L^{-1}$ as C. Upper 1.0 mm cell contains solute under test of known concentration ($[S]$)
*SR NOM in units of $mg\,L^{-1}$ as C.
** See TableA.35 on 208 for data of 1.0 mm blank using ultrapure water .